*Titan, Geomorphologie, fluviale Täler, Methan, Cassini, VIMS, RADAR-SAR*

Mirjam LANGHANS
Institut für Planetengeologie des DLR, Berlin-Adlershof

**Erosion auf dem Saturnmond Titan – Analysen der Verteilung, Morphologie und Spektraleigenschaften von fluvialen Tälern des Titan**

*DLR-Forschungsbericht 2011-07, 2011, 178 Seiten, 60 Bilder, 5 Tabellen, 295 Literaturstellen, XX,XX € zzgl. MwSt.*

Diese Arbeit liefert eine umfassende Analyse fluvialer Täler des Titan, basierend auf Bilddaten des Cassini-Radar-SAR Sensors (Synthetic Aperture Radar) sowie auf Daten des abbildenden Spektrometers Cassini-VIMS (Visible and Infrared Mapping Spectrometer). Dendritische Flussnetze mit Tallängen von bis zu 1200 km konzentrieren sich auf wenige Gebiete, während vereinzelte Täler über alle geographischen Breiten verteilt sind. Die äquatornahen Dünenfelder und Ebenen der mittleren Breiten zeigen dagegen keine oder nur wenige Zeichen fluvialer Erosion. Basierend auf Radar-SAR-Daten wurden verschiedene morphologische Taltypen unterschieden. Dendritische Talsysteme weisen auf eine Entstehung durch Niederschlag hin. Die Morphologie anderer Täler ähnelt der terrestrischer Trockentäler, was als Anzeichen für überwiegend aride klimatische Verhältnisse auf dem Titan in heutiger Zeit interpretiert wird. Hinsichtlich ihrer Spektraleigenschaften wurde festgestellt, dass Talregionen mit den hellen 'Kontinenten' als auch mit einer spektralen Oberflächenklasse korreliert werden können, die in RGB-Falschfarb-Kompositen mit der Spezifikation R: 1.59/1.27 µm, G: 2.03/1.27 µm und B: 1.27/1.08 µm blau erscheint. Der Methankreislauf auf dem Titan verläuft vermutlich langsamer verglichen mit dem terrestrischen Wasserkreislauf. Es handelt sich dennoch mit hoher Wahrscheinlichkeit um einen Prozess, der weit in die Vergangenheit des Titan zurückreicht.

*Titan, geomorphology, fluvial valleys, methane, Cassini, VIMS, RADAR-SAR*

*(Veröffentlicht in englischer Sprache)*

Mirjam LANGHANS
Institut für Planetengeologie des DLR, Berlin-Adlershof

**Erosion on Saturn's Moon Titan – Analyses of the Distribution, Morphology, and Spectral Properties of Titan's Fluvial Valleys**

*DLR-Forschungsbericht 2011-07, 2011, 178 pages, 60 figs., 5 tabs., 295 refs., XX.XX €*

This work presents a comprehensive analysis of fluvial valleys on Titan, based on data obtained by the Synthetic Aperture Radar (SAR) instrument and the Visible and Infrared Mapping Spectrometer (VIMS) onboard the Cassini spacecraft. Dendritic networks, with channel lengths of up to 1,200 km, are concentrated only at a few locations, whereas individual valleys are scattered over all latitudes. Equatorial dunefields and undifferentiated plains at mid-latitudes are almost entirely free of valleys. Several distinct morphologic types of fluvial valleys can be discerned based on SAR-images. Dendritic valleys clearly indicate an origin from rainfall. The morphology of many other valleys resembles terrestrial wadis and indicates dry climatic conditions in recent times. In spectral terms, fluvial terrains are often associated with Titan's bright 'continents' as well as with a surface unit appearing blue in VIMS false-color RGB composites with R: 1.59/1.27 µm, G: 2.03/1.27 µm, and B: 1.27/1.08 µm. The proceeding of Titan's methane cycle is likely to be very slow compared to Earth' water cycle; however, the long-term action of the methane cycle is certain.

**Forschungsbericht 2011-07**

# Erosion on Saturn’s Moon Titan - Analyses of the Distribution, Morphology, and Spectral Properties of Titan's Fluvial Valleys

Mirjam Langhans

Deutsches Zentrum für Luft- und Raumfahrt
Institut für Planetenforschung
Berlin Adlershof

178 Seiten
60 Bilder
5 Tabellen
295 Literaturstellen

DLR Deutsches Zentrum für Luft- und Raumfahrt e.V.
in der Helmholtz-Gemeinschaft

# Erosion on Saturn's Moon Titan

## Analyses of the Distribution, Morphology, and Spectral Properties of Titan's Fluvial Valleys

Dissertation zur Erlangung des akademischen Grades
"doctor rerum naturalium"
(Dr. rer. nat.)

**Eingereicht am Fachbereich Geowissenschaften**
**der Freien Universität Berlin**

von

Dipl. Geogr. Mirjam Langhans
Berlin, Februar 2011

**Erstgutachter:** Prof. Dr. Ralf Jaumann
Freie Universität Berlin
Institut für Geologische Wissenschaften
Fachrichtung Planetologie und Fernerkundung
sowie
Deutsches Zentrum für Luft- und Raumfahrt
Institut für Planetenforschung, Abt. Planetengeologie

**Zweitgutachter:** Prof. Dr. Gerhard Neukum
Freie Universität Berlin
Institut für Geologische Wissenschaften
Fachrichtung Planetologie und Fernerkundung

**Tag der Disputation: 23.06.2011**

## Eidesstattliche Erklärung

Hiermit versichere ich, die vorliegende Arbeit selbständig und nur mit den angegebenen Hilfsmitteln angefertigt, sowie an keiner anderen Hochschule eingereicht habe.

Mirjam Langhans Berlin, den 15. Februar 2011

# Danksagung

Die vorliegende Arbeit wurde am Institut für Planetenforschung des Deutschen Zentrums für Luft- und Raumfahrt e.V. (DLR) in Berlin-Adlershof erstellt. Diese Arbeit wurde zum Teil finanziert durch die Helmholtz Allianz im Rahmen der Forschungsgemeinschaft 'Planetary Evolution and Life'. Ich danke dem Cassini-Radar-Team für die Bereitstellung der Radar-SAR Datenbasis als auch dem Cassini-VIMS Team, ohne dessen Arbeit die spektrale Analyse in der vorliegenden Arbeit nicht möglich gewesen wäre.

Mein besonderer Dank geht an Prof. Dr. R. Jaumann, der diese Arbeit ermöglicht hat, für die Motivation, Betreuung, wertvolle Anregungen und Diskussionen zu dieser Arbeit sowie für die Ermöglichung der Teilnahme an zahlreichen internationalen Konferenzen und die Bereitstellung erstklassiger technischer Gerätschaften.

Herrn Prof. Dr. G. Neukum vom Institut für Geologische Wissenschaften der Freien Universität Berlin danke ich sehr herzlich für die Übernahme des Koreferats.

Frau Dr. K. Stephan möchte ich danken für die geduldige Unterstützung, beginnend mit der Einführung in die Programme und Thematik bis hin zu zahlreichen fachlichen Diskussionen.

Außerdem danke ich den Kollegen am DLR und an der FUB für die angenehme Arbeitsatmosphäre, für zahlreiche fachliche Anregungen und Diskussionen, besonders Dr. M. Sowe, Dipl.-Inf. F. Trauthan, Dipl. Geol. E. Hauber, Dipl.-Phys. M. Wählisch, Dipl.-Ing. F. Preusker, Dr. T. Roatsch, Dipl. Geogr. T. Kneissl, Dipl.-Math. K. D. Matz, Dipl. Geol. M. Al-Samir, I. Vogt und A. Rexin. Allen weiteren Kollegen, die durch ihre Unterstützung zum Gelingen dieser Arbeit beitrugen, sei hier ebenfalls gedankt.

Meiner Zimmerkollegin Dipl.-Ing A. Naß danke ich für die kritische Durchsicht vieler Passagen, die zuverlässige Hilfe bei kartographische Belangen und nicht zuletzt für die moralische Unterstützung während der Arbeit. Ein großer Dank geht an meine Kollegin und Freundin Dr. D. Tirsch, die mir über die Arbeitszeit und die Türen des DLR hinaus mit Rat und Tat zur Seite stand. Auch möchte ich mich bei meinen Freunden und meiner Familie bedanken, die mich unterstützt, bestärkt und mir den Rücken frei gehalten haben.

# Summary

The surface of Titan, Saturn's largest moon, is shaped by many fluvial valleys due to the action of a volatile cycle, which is based on liquid methane. The aim of this work is to present a comprehensive analysis of these valleys. Titan's channels are investigated based on data obtained by the Synthetic Aperture Radar (SAR) instrument, the Visible and Infrared Mapping Spectrometer (VIMS) onboard the Cassini spacecraft, and by the Descent Imager/Spectral Radiometer (DISR) carried by the Huygens Landing Probe. To gain a deeper understanding of Titan's geology, a database of fluvial features is created based on radar-SAR data to reveal the distribution, morphology, and spectral characteristics of its valleys on a global scale. This study further explores the ways in which fluvial valleys are spatially related to other geologic landforms and spectral surface units, which are now accessible thanks to Cassini-VIMS data. Highly developed dendritic networks, with channel lengths of up to 1,200 km and widths of up to 10 km, are concentrated only at a few locations, whereas individual valleys are scattered over all latitudes. The geometric dimensions of Titan's valleys are comparable to major streams on Earth and Mars. Fluvial valleys are frequently found close to impact craters and in mountainous areas. Some terrains, such as equatorial dunefields and undifferentiated plains at mid-latitudes, are almost entirely free of valleys. Several distinct morphologic types of fluvial valleys can be discerned based on SAR-images. Extended networks of dendritic valleys occur near the equator as well as close to the north pole. Dendritic valleys clearly indicate an origin from rainfall. The morphology of some valley types, such as putative canyons, cannot uniquely be explained by rainfall but could equally be attributable to volcanic or tectonic action or groundwater sapping. The morphology of many valleys at low and mid-latitudes resembles terrestrial wadis and indicates dry climatic conditions in recent times. Regarding their spectral properties, fluvial terrains are often characterized by a high reflectance in each of Titan's atmospheric windows, as most of them are located on Titan's bright 'continents' and 'islands'. Many valleys are spatially associated with a surface unit appearing blue in VIMS false-color RGB composites with R: 1.59/1.27 µm, G: 2.03/1.27 µm, and B: 1.27/1.08 µm, due to its higher reflection at 1.3 µm. This observation could have two explanations: either the channels dissect pure bluish surface units, or they are carved into terrain with a mixed spectral signature between bright and bluish surface materials. Recent fluvial activity is very likely in the north polar region, which stands in contrast to the more arid con-

ditions at lower and mid-latitudes and at the south pole of Titan. This divergence is a possible indication but not a conclusive proof of seasonal climatic asymmetries between the hemispheres. A general disparity in the distribution of clouds and valleys is observed, since some areas, such as the south polar region, do not possess a high density of active channels despite of their dense cloud coverage. This disagreement might be explained by a non-conclusive relation of clouds and channels or by climatic differences at the time when the channels developed. However, traces of previous fluvial activity are scattered over all latitudes of Titan, indicative of previous climatic conditions with at least episodic rainfall. The high prevalence of valleys in mountains point to orographic rainfall shaping these valleys, although this cannot be the single origin of Titan's valleys. The proceeding of Titan's methane cycle is likely to be very slow compared to Earth' water cycle; however, the long-term action of the methane cycle is certain. The global picture of fluvial flows clearly indicates a high significance and a large diversity of liquid-related processes acting near the surface, and provides information about the controlling parameters of fluvial erosion, such as rainfall regimes in space and time, and surface and bedrock types.

# Zusammenfassung

Die Oberfläche des größten Saturnmonds Titan ist geformt durch eine Vielzahl von Flusstälern, infolge eines Flüssigkeitskreislaufes basierend auf Methan. Die vorliegende Arbeit liefert eine umfassende Analyse dieser Täler. Die Untersuchung der Talstrukturen basiert auf Bilddaten des Radar-SAR Sensors (Synthetic Aperture Radar), sowie auf abbildenden Spektrometerdaten der VIMS-Kamera (Visible and Infrared Mapping Spectrometer) an Bord des Cassini-Orbiters und auf Daten des Descent Imager/Spectral Radiometer (DISR) an Bord der Huygens-Sonde. Eine Datenbank fluvialer Täler wurde mithilfe von Radar-SAR-Daten erstellt, welche eine genaue geologische Charakterisierung der Täler, deren globaler Verbreitung sowie deren morphologischer und spektraler Eigenschaften ermöglicht. Weiterhin wurden die räumlichen, geologischen, spektralen und stratigraphischen Zusammenhänge zwischen Titans Tälern und anderen geologischen und spektralen Einheiten untersucht. Weit verzweigte dendritische Flussnetze, deren Hauptflüsse Längen von bis zu 1200 km und maximale Breiten von 10 km erreichen, konzentrieren sich auf wenige Gebiete, während vereinzelte Täler über alle geographischen Breiten verteilt sind. Titans Täler sind in ihrer geometrische Ausdehnung vergleichbar mit Hauptflüssen auf der Erde und auf dem Mars. Fluviale Täler treten häufig in der Nähe von Impaktkratern und in bergigen Gegenden auf. Die äquatornahen Dünenfelder und Ebenen der mittleren Breiten zeigen keine oder nur wenige Zeichen fluvialer Erosion. Basierend auf Radar-SAR-Daten wurden verschiedene morphologische Taltypen unterschieden. Ausgedehnte dendritische Talsysteme treten nahe des Äquators sowie in den hohen nördlichen Breiten auf und weisen eindeutig auf eine Entstehung durch Niederschlag hin. Andere Taltypen, wie die Canyons der mittleren Breiten, können auf Basis ihrer Morphologie nicht eindeutig mit einem Ursprung durch Niederschlag in Verbindung gebracht werden. Eine Entstehung durch vulkanische oder tektonische Aktivität oder durch Erosion durch austretendes Grundwasser kann hier nicht ausgeschlossen werden. Die Morphologie vieler Täler der niederen und mittleren Breiten ähnelt der terrestrischer Trockentäler, was als Anzeichen für aride klimatische Verhältnisse auf dem Titan in heutiger Zeit interpretiert wird. Hinsichtlich ihrer Spektraleigenschaften kann festgestellt werden, dass fluviale Regionen mit den hellen 'Kontinenten' oder 'Inseln' als auch mit einer spektralen Oberflächenklasse, die in RGB-Falschfarb-Kompositen mit der Spezifikation R: 1.59/1.27 µm, G: 2.03/1.27 µm und B: 1.27/1.08 µm blau erscheint, korreliert werden können. Es konnte gezeigt

werden, dass die Täler entweder in reine blaue Oberflächen eingeschnitten sind oder dass sie Gebiete mit einer spektralen Mischsignatur heller und blauer Oberflächen durchfließen. Die Beobachtungen dieser Arbeit zeigen, dass fluviale Erosion in heutiger Zeit nur nahe des Nordpols aktiv stattfindet. Die klimatischen Gegebenheiten in dieser Region stehen im Gegensatz zu den ariden Bedingungen in den mittleren und niederen Breiten sowie am Südpol des Titan. Dieser Unterschied könnte ein Anzeichen für saisonale klimatische Unterschiede zwischen den Hemisphären sein. Es konnte keine Übereinstimmung zwischen der räumlichen Verteilung von Tälern und Wolken nachgewiesen werden. In manchen Gebieten, wie z.B. der südlichen Polarregion, konnte, trotz einer hohen Wolkendichte, die zu erwartende hohe Taldichte nicht nachgewiesen werden. Diese Abweichungen sind vermutlich auf einen nicht-eindeutigen Zusammenhang zwischen Wolken und Flusstälern oder durch abweichende klimatische Bedingungen zum Zeitpunkt der Talentstehung im Vergleich zu heute zurückzuführen. Dennoch sind fluviale Prozesse über alle Breiten des Titan belegt, was auf ein feuchteres Klima in der Vergangenheit hindeutet, das sich zumindest durch episodische Niederschlagsereignisse auszeichnete. Eine hohe Dichte von Tälern in höher gelegenen oder bergigen Regionen deutet auf orographisch bedingte Niederschlagsereignisse hin. Allerdings ist die alleinige Entstehung aller Täler durch orographischen Niederschlag unwahrscheinlich, da viele Täler außerhalb bergiger Regionen vorkommen. Der Methankreislauf auf dem Titan verläuft vermutlich langsamer verglichen mit dem terrestrischen Wasserkreislauf. Es handelt sich dennoch mit hoher Wahrscheinlichkeit um einen Prozess, der weit in die Vergangenheit des Titan zurückreicht. Die globale Verteilung der fluvialen Täler liefert Erkenntnisse auf die Einflussgrößen fluvialer Erosion, wie z.B. das Niederschlagsregime und Eigenschaften des zugrundeliegenden Bodens oder Gesteins. Die Ergebnisse dieser Arbeit deuten auf eine hohe Bedeutung, aber auch auf eine ausgesprochene Diversität fluvialer Prozesse an der Oberfläche hin.

# Contents

# List of Figures

# List of Tables

# List of Abbreviations

| | |
|---|---|
| ACP | Aerosol Collector Pyrolyser |
| ADONIS | Adaptive Optics Near Infrared System |
| AO | Adaptive Optics |
| ASI | Agenzia Spaziale Italiana |
| AU | Astronomical Unit |
| CAPS | Cassini Plasma Spectrometer |
| CCD | Charged Coupled Device |
| CDA | Cosmic Dust Analyzer |
| CFHT | Canada-France-Hawaii-Telescope |
| CIRS | Composite Infrared Spectrometer |
| DISR | Descent Imager/Spectral Radiometer |
| DISR | Descent Imager/Spectral Radiometer |
| DLR | Deutsches Zentrum für Luft- und Raumfahrt |
| DN | Digital Number |
| DWE | Doppler Wind Experiment |
| ENVI | ENvironment for Visualizing Images |
| ESA | European Space Agency |
| ESO | European Southern Observatory |
| ESRI | Environmental Systems Research Institute |
| FOV | Field of View |
| GCM | Global Circulation Model |
| GCMS | Gas Chromatograph/Mass Spectrometer |
| GIS | Geographical Information System |
| HASI | Huygens Atmospheric Structure Instrument |
| HLS | Huygens Landing Site |
| HST | Hubble Space Telescope |
| INMS | Ion and Neutral Mass Spectrometer |
| IRIS | Voyager Infrared Interferometric Spectrometer |
| LCM | Longitude of Central Meridian |
| MAG | Dual Technique Magnetometer |
| MIMI | Magnetospheric Imaging Instrument |
| MOC | Mars Orbiter Camera |
| NASA | National Aeronautics and Space Administration |

| | |
|---|---|
| NICMOS | Near Infrared Camera and Multi-Object Spectrometer |
| NIR | Near Infrared Radiation |
| PDS | Planetary Data System |
| RSS | Radio Science Subsystem |
| RWPS | Radio and Plasma Wave Science |
| SPICE | Spacecraft Planet Instrument C-matrix Events |
| SSP | Surface Science Package |
| USGS | United States Geological Survey |
| UV | ultraviolet light |
| UVIS | Ultraviolet Imaging Spectrograph |
| VLA | Very Large Array |

# Chapter 1

# Introduction and Motivation

Saturn's largest moon, Titan, is one of the most attractive and challenging targets for planetary scientists. Due to its enormous distance from the Sun, environmental conditions significantly differ from those of the Earth, especially with regard to the very low temperatures at its surface. Despite this, many fascinating analogies to our home planet make the distant moon an interesting object of study, often designated as an analog of the early Earth (*Coustenis*, 1995; *Lunine and McKay*, 1995). In contrast to many other bodies within our Solar System, Titan exhibits a close geological similarity to the Earth with its abundance of landforms, such as dunes, mountains, lakes, and channels (e.g. *Lorenz et al.*, 2006; *Lopes et al.*, 2007a; *Radebaugh et al.*, 2007; *Jaumann et al.*, 2008; *Lorenz et al.*, 2008a; *Jaumann et al.*, 2009; *Lopes et al.*, 2010). The high level of scientific interest in this remote world is driven by many unsolved questions about processes within its interior, atmosphere, and surface that motivated not least the Cassini mission, which serves as the major data supplier for this work.

Titan's surface has long been concealed from view owing to the presence of its dense and absorbing atmosphere. It is only since the arrival of the Cassini spacecraft in the Saturnian system in 2004 that a wealth of data has become available, providing information about the atmosphere, the interior structure, and also about the surface of Saturn's largest moon. However, Titan's atmosphere has a significant distorting effect on image data, so that what the images reproduce is often the atmosphere rather than the surface. Thus, analyzing and interpreting image data of the surface remains challenging.

Due to its advantageous size and location, Titan is the only body besides Earth currently known to host liquids that are mobile within the atmosphere and near the surface (*Flasar*, 1983; *Lunine et al.*, 1983; *Raulin*, 1987; *Lunine and McKay*, 1995; *Lorenz et al.*, 2002; *Lorenz and Lunine*, 2005). Liquid methane enables the action of a volatile cycle, most likely involving processes such as evaporation, the formation of clouds, and even rainfall (*Tomasko et al.*, 2005; *Atreya et al.*, 2006; *Hueso and Sánchez-Lavega*, 2006; *Jaumann et al.*, 2008; *Burr et al.*, 2009; *Jaumann et al.*, 2009). On Earth, the hydrological cycle and erosion by water are important processes that have given its surface its distinct shape. Liquid water was once active at the surface of Mars, too, and left its

unmistakable traces. In contrast to Mars, the action of liquids on Titan and Earth is a much more recent process.

Titan's very dense atmosphere with nitrogen as a main component, its versatile organic chemistry, and an active volatile cycle constitutes the most obvious analogy between Titan and Earth. Despite Titan's location far away from the habitable zone of our Solar System, many characteristics suggest a certain potential for the evolution of life (e.g. *Lorenz et al.*, 2005a; *Lunine et al.*, 2008a; *Coustenis et al.*, 2009a). Taking the evolution of life on Earth as a basis, which is inconceivable without the mobility of water at the surface and within the atmosphere, together with the presence of different organic molecules, Titan's methane cycle is a compelling aspect that supports a certain potential for harboring life (e.g. *McKay and Smith*, 2005).

Evidence of a volatile cycle is apparent at the surfaces of Titan and Earth, given the presence of fluvial valleys on both of them. Fluvial activity is an important process that can determine the physiography of landscapes in a unique way. Erosion by flowing liquids at Titan's surface was already proposed by *Lunine and McKay* (1995) and confirmed during the survey of Cassini imagery (e.g. *Tomasko et al.*, 2005; *Jaumann et al.*, 2008; *Lorenz et al.*, 2008a; *Jaumann et al.*, 2009). Fluvial erosion on Titan appears to have a significant impact since extensive areas on Titan show unambiguous traces of flowing liquids. Morphologically, Titan's valleys reveal many similarities to terrestrial valleys. Their origin from rainfall is backed up by morphological recognition features, visible from current image data (*Tomasko et al.*, 2005; *Perron et al.*, 2006; *Jaumann et al.*, 2009). Furthermore, resurfacing through fluid-flow erosion is assumed to have been very effective as can be seen from a substantial rate of erosion and many other geological indicators that underline the relatively young age of landforms on Titan (*Collins*, 2005; *Barnes et al.*, 2006; *Coustenis*, 2006; *Lorenz et al.*, 2007).

However, many questions regarding that volatile cycle and its effect on the surface are still unsolved. One of the most important matters still to be resolved is the source of atmospheric methane on Titan (*Lewis*, 1971; *Strobel*, 1982). Other controversies concern the relationship between the methane cycle and fluvial erosion: at first, it is Titan's rainfall regime that raises questions, and it is still debated what process(es) account for precipitation (e.g. *Hueso and Sánchez-Lavega*, 2006; *Tokano et al.*, 2006). Furthermore, a global and comprehensive survey and the description of fluvial valleys incorporating the most recent Cassini data is still outstanding, although individual fluvial features have already been investigated (e.g. *Jaumann et al.*, 2008; *Lorenz et al.*, 2008a). The description of the global distribution of fluvial features is of high value in order to analyze the global variability of rainfall on Titan in space and time. The origin, development as well as the age of fluvial systems are also the subject of discussion (e.g. *Lorenz et al.*, 2008a; *Lopes et al.*, 2010), demanding a thorough investigation. What is also lacking is a detailed morphologic description of fluvial features, including their geological background, as well as a comparison of different channels and channel systems. Determining the spectral properties of fluvial terrains

and their relationship to other stratigraphic units might be helpful in characterizing Titan's fluvial processes further.

Within the scope of this work, light will be shed on the characteristics of fluvial valleys from different perspectives. To accomplish this, various image datasets of the Cassini mission were evaluated. The morphology of valleys is investigated to obtain qualitative, quantitative, and comparative characteristics of fluvial erosion, e.g. about the geology of the underlying substrate, the climatic conditions, and the amount of liquids and sediments transported. Moreover, it is considered essential to correlate the spatial distribution of fluvial features with spectral data in order to reveal their overall spectral properties and to deduce how and to what extent the surface is altered chemically by liquid-related processes. Moreover, studying the spectral properties of fluvial terrains is relevant to gain insights into topographic relations between different spectral units on a regional scale. Furthermore, this thesis analyzes the interactions of fluvial terrains with the remaining geological landforms, such as craters and mountains, to understand the relationship and interactions between geologically different landforms. Additionally, stratigraphic relationships between different features and surface units as well as the relative age of different landforms are outlined. Another aim of this work is to explore spatial relations between clouds and fluvial valleys in order to verify the origin of the valleys from rainfall and to determine whether the current climatic situation corresponds to the climate at the formation of the valleys. Locating and analyzing fluvial features on Titan provides indirect insights into the climatic conditions at the time of their formation up to the present day. Finally, the results of this research are interpreted, drawing further conclusions on the origin and development of Titan's valleys, and characterizing Titan's climate, its seasonal dynamics, and the mechanisms underlying the methane cycle.

The survey of fluvial valleys on Titan includes a comparison with a number of Martian and terrestrial valleys, to draw analogies between landforms and, by inference, decide what processes might have occurred on Titan that are known to be responsible for the formation of such landforms elsewhere. A detailed study of the questions listed above will be possible thanks to the huge amount of data delivered by the Cassini mission which has been running since 2004, and is extended until 2017 (*NASA*, 2010a).

Structurally, this work begins with a brief summary of existing basic knowledge about Saturn's largest moon. Chapter 2 is an introduction into Titan's fundamental astronomical and physical characteristics, its geological history and its climatic conditions, providing a general idea of Titan within the Saturnian System. This Section is based on knowledge acquired during several space missions to the Saturnian System and includes references to more detailed examinations. Specifications of the Cassini instruments and datasets used in this thesis can be found in the subsequent Section 3. Chapter 4 presents Titan's overall geological setting. Beyond the landscapes shaped by liquid-related processes, manifold geologic units, such as dunes, mountains, craters,

and cryovolcanoes, are introduced. These features and their geographic distribution are correlated with the spatial pattern of fluvial valleys in the following Section 5. In this main Section the questions raised above are addressed in detail, using the datasets and methods outlined before. Parts of this Chapter are based on the publication 'Titan's fluvial valleys: Morphology distribution, and spectral properties', which is accepted for publication by *Planetary and Space Science*. In Chapter 6 the results of this work are summarized and discussed. Finally, Chapter 7 lists a number of open questions and offers suggestions for future work and missions.

# Chapter 2

# Background

Saturn's largest moon, Titan, has been attracting the attention of scientists far beyond the confines of the planetary sciences due to its many astonishing similarities to the Earth. However, Titan has a number of singularities resulting from its location in the outer Solar System and its different astronomical characteristics. This Chapter is a basic introduction to Titan. It provides some brief insights into its physical and astronomical properties (Section 2.1) followed by a synopsis of Earth- and space-based observation of Saturn's moon up to and including the Cassini-Huygens mission (Section 2.2). Finally, the current state of knowledge about its physical, geological, and climatic background is briefly summarized in Section 2.3 of this Chapter.

## 2.1 Titan in the Saturnian System

Titan is the largest of currently 53 officially named moons of Saturn (September 2010, (*NASA/JPL*, 2010)). A comprehensive listing of Titan's physical and astronomical characteristics is given in Table 2.1. Titan is the second largest moon and the only satellite in the Solar System surrounded by a dense atmosphere (*Hunten et al.*, 1984) with an enormous vertical dimension of 1,500 km, accounting for a 50% higher atmospheric pressure at Titan's surface than at the surface the Earth (*Coustenis and Taylor*, 2008). The moon itself lacks an intrinsic magnetic field but it is influenced by Saturn's magnetosphere (*Coustenis and Taylor*, 2008). With a diameter of 5,150 km, Titan is smaller than the Earth (diameter: 12,742 km) but larger than Earth's moon (diameter: 3,474 km). Titan's gravity of 1.35 $m/s^{-2}$ is weak compared to the terrestrial value (see Table 2.1). Titan rotates slowly and synchronously around Saturn, which means that it always faces Saturn with the same side (*Lemmon et al.*, 1995; *Muhleman et al.*, 1995; *Richardson et al.*, 2004). Owing to its long distance from the Sun of 9.5 AU, Titan receives 100 times less energy from the Sun compared to Earth (*Hunten et al.*, 1984) and its mean temperature of 94 K is thus very low. As a result of Saturn's obliquity of 26.7° Titan has a distinct seasonality (*Lorenz et al.*, 2002, 2009). Currently, Titan's southern hemisphere is switching from summer to autumn while spring in the northern hemisphere started at the vernal equinox in August 2009 (see Figure 2.1).

**Table 2.1:** Physical and astronomical parameters of Titan, from *Hunten et al.* (1984) and *Coustenis and Taylor* (2008).

| Property | Dimension |
|---|---|
| Orbit (Mean distance from the Sun) | $1.422 \times 10^9$ km (9.546 AU) |
| Mean distance from Saturn | $1.222 \times 10^6$ km |
| Obliquity | 26.7° |
| Equatorial Radius | 2,575 km (0.202 of Earth's) |
| Mass | $1.346 \times 10^{23}$ kg (0.0226 of Earth's) |
| Mean Density | 1.88 gm $cm^{-2}$ |
| Surface Gravity | 135 cm $s^{-2}$ |
| Rock/Ice Ratio (by mass) | $\sim 52:48$ |
| Sunfall | 1.1% of Earth's |
| Visual geometric albedo | 0.21 |
| Magnitude ($V_o$) | 8.28 |
| Orbital Period (Rotational Period) | 15.945 Earth days |
| Orbital Period (Rotation around Sun) | 29.46 Earth years |
| Orbital Eccentricity | 0.0292 |
| Orbital Inclination | 0.33° |
| Escape Velocity | 2.65 km $s^{-1}$ |
| Mean Orbital Velocity | 5.58 km $s^{-1}$ |
| Mean Surface Temperature | 94 K (-179°C) |
| Atmospheric Pressure at Surface | $1496 \pm 20$ mbar (1.5 of Earth's) |

Given Titan's physical conditions, some hydrocarbons are present in their liquid and partly even in their gaseous state, namely methane ($CH_4$), ethane ($C_2H_6$), and propane ($C_3H_8$) (*Flasar*, 1983; *Lunine et al.*, 1983; *Raulin*, 1987; *Lunine and McKay*, 1995; *Lorenz et al.*, 2002; *Lorenz and Lunine*, 2005; *Brown et al.*, 2008; *Lorenz et al.*, 2008a). This physical situation results in a volatile cycle that bears interesting geological parallels between Earth and Titan and has even triggered a discussion about the potential habitability of the distant moon (e.g. *McKay and Smith*, 2005).

## 2.2 Historical Overview on the Observation of Titan

The Dutch astronomer Christiaan Huygens discovered Saturn's largest moon on March 25th, 1655 (*Huygens*, 1659). He detected Titan with a self-made telescope during his study of the Saturnian rings. Due to its extended atmosphere, the size of the moon was initially overestimated. Its real diameter was measured much later, during the Voyager mission (see Table 2.1 and Section 2.2.3). Titan was named in 1847 by the English astronomer John Frederick William Herschel after a dynasty in Greek mythology, inspired by the enormous size of the moon (*Herschel*, 1847).

### 2.2.1 Early Investigations

A first mention of a possible atmosphere around Titan was made by José Comas Solá in 1908, based on his observation of limb darkening, i.e. the continuous decrease of brightness at the edge of the disk (*de Pater et al.*, 2004). In 1944, Gerard Peter Kuiper confirmed the existence of Titan's atmosphere with methane as its main constituent by means of spectral measurements (*Kuiper*, 1944; *Coustenis et al.*, 2009b).

Other constituents, many of them hydrocarbons, such as acetylene ($C_2H_2$), ethane ($C_2H_6$), ethylene ($C_2H_4$), hydrogen ($H_2$), and nitrogen ($N_2$), were already suggested prior to the Voyager encounters, inferred from spectroscopic observations (*Trafton*, 1972; *Hunten*, 1974; *Bar-Nun and Podolak*, 1979). During the time of these observations, Titan's surface was completely shielded from view due to the opacity of its atmosphere.

In the early 1970ies, the idea of photochemical destruction of atmospheric $CH_4$ was established (*Strobel*, 1974) (see Section 2.2.1). Photodissociation (or photolysis) is responsible for the irreversible destruction of $CH_4$, in analogy to processes in the Jovian atmosphere. The process takes place in Titan's stratosphere and is induced by solar ultraviolet radiation (*Strobel*, 1974). The bulk photochemical end products of photolysis are $C_2H_6$ and $C_2H_2$. It was also found that the chemical disequilibrium caused by photolysis results in a total decomposition of $CH_4$ within about $10^7$ years (*Lewis*, 1971). To maintain the methane inventory, a source of $CH_4$ is required that replenishes the atmosphere and makes up for the photolytic loss. The observation of photolytic destruction prompted many studies to unveil that source of $CH_4$, and research continues to this day. *Hunten* (1974) suspected that the surface of Titan is covered by a layer of dark end products of photolysis. Outgassing and the escape of $H_2$, associated with photolytic processes, were proposed by *Trafton* (1972).

The process of photodissociation was reproduced in the laboratory by *Sagan and Khare* (1979). As a result, oily and tarry molecules were generated which were of a brown-orange color, akin to the color of Titan's atmosphere in images at visible wavelengths (*Sagan and Khare*, 1979). The term *tholin* was introduced to describe the physical properties of that substance. Tholins have spectral properties similar to Titan's aerosols at VIS and near-infrared wavelengths, characterized by a flat spectrum (*Khare et al.*, 1984).

However, prior to the Pioneer and Voyager missions to the Saturnian System it was controversial whether methane or nitrogen is the major constituent of Titan's atmosphere. Furthermore, knowledge about Titan's physical conditions, i.e. its radius, the temperature and pressure regime, and the exact amount of atmospheric methane was still vague or even missing altogether. Information about Titan's surface, its composition, and geology was entirely unavailable.

### 2.2.2 Pioneer 11

Pioneer 11 was the first spacecraft to explore the Saturnian system. The small, unmanned spacecraft passed Saturn on September 1$^{st}$, 1979, and obtained data of Titan at a distance of 363,000 km (*Coustenis and Taylor*, 2008; *Coustenis et al.*, 2009b). Pioneer images confirmed the presence of a dense atmosphere around the moon. The instrument captured maps of the brightness of the disk and enabled the measurement of the linear polarization in red and blue light at different phase angles (*Tomasko*, 1980; *Tomasko and Smith*, 1982). The data obtained provided information about the

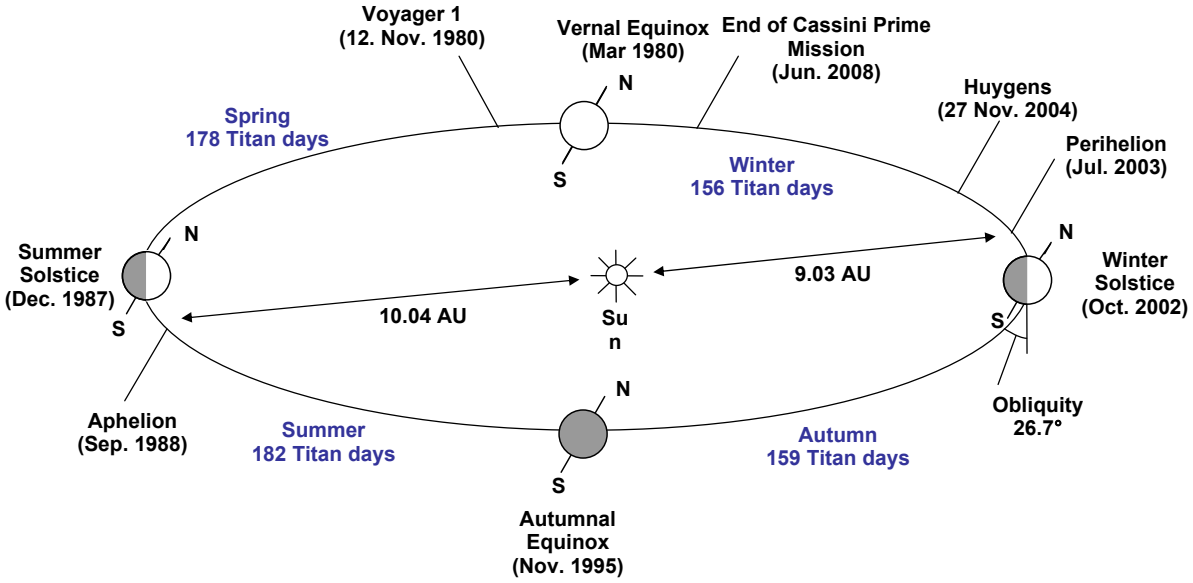


**Figure 2.1:** Titan's seasons and epochs of Voyager and Cassini encounters (from *Lorenz et al.* (2009), modified).

properties and composition of aerosols at the top of Titan's atmosphere but failed to bring out features of the surface owing to the long distance to the target and due to the limited spectral sensitivity of the camera. The scattering atmospheric haze layer still prevented a definite determination of Titan's radius. Titan's radius was expected to amount to either 2845 $\pm$ 25 km (based on observations at 0.64 µm) or 2880 $\pm$ 22 km (based on observations at 0.44 µm) (*Smith*, 1980).

### 2.2.3 Voyager 1 and 2

Launched in 1977, both Voyager spacecraft were dedicated to exploring the Jovian and the Saturnian systems as well as other objects of the outer Solar System. Voyager 1 arrived at the Saturnian System in November 1980, whereas Voyager 2 encountered Titan in August 1981. On November 12$^{th}$, 1980, Voyager 1 had its closest approach to Titan at a distance of 4,400 km (*Coustenis and Taylor*, 2008). The Voyager spacecraft were equipped with eleven scientific instruments, such as medium and high-resolution imaging cameras, spectrometers, radio receivers, and a high-precision Earth/spacecraft radio link for data transmission and navigation (*Kohlhase and Penzo*, 1977). Voyager 1 data were more valuable due to the shorter distance at closest approach compared to Voyager 2 imagery (*Coustenis and Taylor*, 2008). Yet, Voyager's optical sensors were only sensitive at optical wavelengths, similar to the sensitivity of the human eye. Owing to extreme scattering and absorption in the atmosphere, Titan's surface was shielded at optical wavelengths and surface features could still not be recognized from Voyager image data (*Smith et al.*, 1981) (see Figure 2.2). Re-examination of Voyager data was initiated in recent years and compared to maps taken at visible and near-infrared wavelengths by telescopes (see Sections 2.2.4.2 and 2.2.5) (*Richardson et al.*, 2004). Even Voyager images were found to exhibit a certain

sensitivity to the surface albedo at optical wavelengths. Given the advantage of their comparatively high spatial resolution due to the relatively short distance between camera and target, Voyager images provided valuable complementary information for the investigation of surface features (*Richardson et al.*, 2004), particularly compared to Earth-based imaging devices.

Generally, Voyager constrained Titan's basic physical and astronomical characteristics (see Table 2.1), such as the exact radius of the moon, its temperature of 94 K $\pm$ 1.5 K, and pressure of 1.6 bar at surface level (*Tyler et al.*, 1981; *Coustenis and Taylor*, 2008). The mean density of 1.881 $\pm$ 0.002 $g/cm^3$ determined by Voyager led to the finding that the moon is composed of an icy and a rocky component in quasi equal fractions; most likely arranged as an icy mantle of water-ammonia and water-methane-ice over a rocky core (*Tyler et al.*, 1981; *Sagan and Dermott*, 1982; *Clarke and Ferris*, 1997). An atmospheric temperature-pressure profile was obtained based on the radio-occultation experiment (*Tyler et al.*, 1981; *Lindal et al.*, 1983). The main atmospheric constituent was identified to be nitrogen (*Tyler et al.*, 1981), and a $CH_4$-abundance at the surface of up to 6% was determined with a gradual decrease of the $CH_4$-mixing ratio within the troposphere (*Samuelson et al.*, 1981).

By means of the Voyager Infrared Interferometric Spectrometer (IRIS), the composition, structure, and dynamics of Titan's atmosphere as well as the physical properties of its aerosols were constrained. Particularly the atmospheric conditions regarding methane condensation and cloud formation were a subject of research with respect to a possible 'methanological cycle' (*Toon et al.*, 1988) (see Section 2.3.4.2). Near-infrared spectra confirmed the presence of a wealth of organics in the atmosphere (*Hanel et al.*, 1981). Moreover, details about the horizontal and vertical structure of the atmosphere and the arrangement of different haze layers were provided by Voyager data (*Smith et al.*, 1981, 1982). Voyager measurements were used to constrain models simulating processes in the atmosphere, e.g. to deduce the quantities of hydrocarbons generated by photolysis (e.g. *Lara et al.*, 1994; *Tokano et al.*, 2001).

Voyager data on the atmospheric methane mixing ratio suggested the presence of a global ocean filled with liquid ethane and methane (e.g. *Flasar*, 1983; *Lunine et al.*, 1983). This ocean was suspected to serve both as a source for the continuous depletion of methane and as a sink for the photolytic end products and it relativized the contradiction between the measured methane content and its photolytic destruction (e.g. *Sagan and Dermott*, 1982; *Flasar*, 1983; *Lunine et al.*, 1983). This idea was later disproved by radar measurements and near-infrared-data (see Sections 2.2.4.2 and 2.2.4.3).

### 2.2.4 Earth-Based Imaging

In the 1980s and 1990s ground-based telescopes became significantly more powerful, which made this technique suitable even for the observation of targets as remote as Titan. Major disadvantages of this imaging technique result from Titan's long distance to the Earth and its small angular diameter of $\sim$0.8 arcsec (*Coustenis et al.*, 2001)

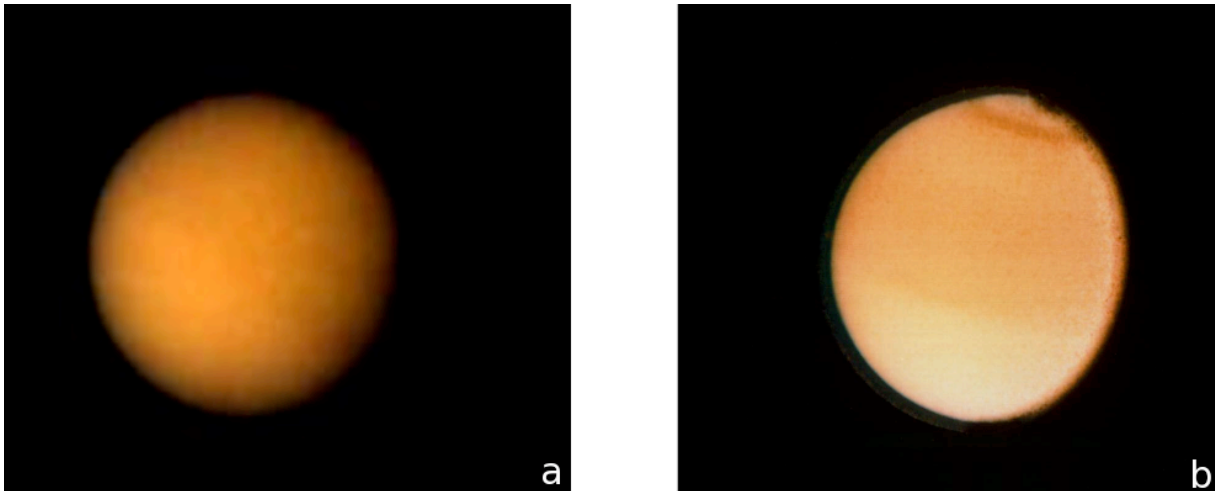


**Figure 2.2:** Voyager images of Titan. Both images fail to show the surface, which is shielded from view by a thick orange haze. (a) Voyager-1 image of Titan (November 4, 1980). Titan's southern hemisphere appears slightly brighter than its northern hemisphere (Courtesy NASA/JPL-Caltech). (b) Voyager-2 image of Titan (August 23, 1981). The brightness gradient between the northern and the southern hemisphere is clearly visible (Courtesy NASA/JPL-Caltech).

and the influence of Earth's and Titan's atmospheres with their indefinite, dynamic condition and composition. Despite this, knowledge on surface features of Saturn's largest moon increased dramatically (see Section 2.2.4.2).

Titan's atmosphere obstructs the view on the surface owing to molecular absorption mainly by $CH_4$ and other hydrocarbons as well as through backscattering by aerosols (*Combes et al.*, 1997; *Rodriguez et al.*, 2006). Absorption affects several different wavelength intervals while scattering influences more or less the entire spectrum, with a lower effect at longer wavelengths. The fact that the absorption by methane and thus the opacity of Titan's atmosphere is reduced in a few *atmospheric windows* in the near-infrared part of the electromagnetic spectrum has been established some years after the Voyager encounters (*Griffith et al.*, 1991; *Lemmon et al.*, 1993). Thanks to this discovery, the identification of surface features became possible within wavelength intervals outside the strong molecular $CH_4$ absorption bands (*Brown et al.*, 2004; *Barnes et al.*, 2007a; *Clark et al.*, 2010). The signal detected in the transparent windows was expected to reflect the albedo of the the upper mm or cm of the surface, to return topographic effects or even features below the tropopause, e.g. clouds of the lower atmosphere (*Lemmon et al.*, 1993; *Saint-Pé et al.*, 1993).

Another way to obtain images of planetary surfaces despite the presence of dense absorbing atmospheres is the radar technique (Radio Detection and Ranging). Radar is an active remote sensing technique that is largely unaffected by potential distorting effects of the atmosphere and clouds (see Section 2.2.4.3).

#### 2.2.4.1 Rotational Lightcurves

Rotational lightcurves, obtained at different telescope facilities, indicate the reflectance of individual wavelength intervals, recorded over the course of the target's rotation. Lightcurves reveal brightness differences of a body as a function of time, thus constraining the orbital and rotational period of the respective planetary object (*NASA*, 2010b). Titan's lightcurves represent its near-infrared reflectance around the equator.

At the beginning of the 1990s, lightcurves obtained at the Steward Observatory (Arizona) and at NASA's Infrared Telescope Facility on Mauna Kea (Hawaii) revealed brightness differences between Titan's leading side, centered at 80°W, and its trailing side, centered at 260°W, at 1.6 and 2 µm, respectively (e.g. *Griffith*, 1993; *Lemmon et al.*, 1993, 1995). The interpretation of lightcurves confirmed the assumption that Titan is in synchronous rotation (*Lemmon et al.*, 1993).

#### 2.2.4.2 Telescopes and Ground-Based Spectrometry

Telescopes such as the Infrared Telescope Facility (Hawaii), the Keck telescope (Hawaii) and the European Southern Observatory (ESO) telescope in Chile have been used since the 1990s for large-scale spectral investigations of Titan's surface (e.g. *Combes et al.*, 1997; *Roe et al.*, 2002; *Coustenis and Taylor*, 2008). Surface maps are captured using the speckle imaging technique and adaptive optic systems (AO), which improve the image quality and reduce distortions caused by (Earth's) atmosphere (e.g. *Saint-Pé et al.*, 1993; *Coustenis and Taylor*, 2008). It was particularly the technical breakthrough in adaptive optics that yielded great qualitative improvements of the near-infrared images (*Saint-Pé et al.*, 1993). Imaging of Titan's surface by telescopes is mainly carried out at 1.3, 1.6, and 2 µm (*Griffith et al.*, 1991; *Coustenis et al.*, 2001).

An early study of this kind was performed by *Saint-Pé et al.* (1993) based on data from the ESO. Images of the 1.96 to 2.14 µm band revealed a higher reflectance at the center of Titan's disk compared to its margins, which is indicative of substantial surface heterogeneities. Furthermore, the existence of a global ocean of liquid hydrocarbons was rejected based on observations by ground-based telescopes since Titan's comparably high near-infrared reflectance was found to be more consistent with a surface composed of dirty water ice (e.g. *Griffith et al.*, 1991). Moreover, candidate (solid) constituents of Titan's surface, such as acetylene ($C_2H_2$), tholins (see Section 2.2.1), and haze particles, were suggested (*Griffith et al.*, 1991; *Combes et al.*, 1997).

Later, *Coustenis et al.* (2001) interpreted data delivered by the Canada-France-Hawaii-Telescope (CFHT) at 1.29 and 1.6 µm with the Adaptive Optics Bonette, and related the results to earlier knowledge obtained from radar observations, Hubble and Keck images. The major question focused on the origin and the characteristics of albedo differences near the equator, which were detected at different wavelengths, affirmed by several instruments and at different points in time (e.g. *Smith et al.*, 1996; *Gibbard et al.*, 1999) (see also Section 2.3.2).

The spectral detection of transient clouds was first carried out successfully in 1998 by *Griffith et al.* (1998) using the United Kingdom Infrared Telescope and the CGS4 spectrometer (see Section 2.3.3.2). Since then, Titan's clouds have been identified and analyzed by telescope images and spectra obtained from the Gemini and Keck telescopes (e.g. *Roe et al.*, 2002).

#### 2.2.4.3 Radar Observations

The radar technique is an active method to obtain data of remote targets. Unlike optical and near-infrared radiation, the radar signal is largely unaffected even by thick atmospheres. Several Earth and space-based instruments, such as the joint Goldstone/Very Large Array (VLA) planetary radar (New Mexico/California) and the Arecibo telescope (Puerto Rico), deliver surface data from Titan (e.g. *Muhleman et al.*, 1990). Radar data reflect the physical properties of the observed material, such as its texture, roughness, and composition. It penetrates the upper layers of the surface down to depths of about 10 wavelengths, e.g. up to 35 cm depth in the case of the Goldstone/VLA with 3.5 cm wavelength (*Muhleman et al.*, 1995). High radar reflectance or cross-sections are obtained from rough and clean icy surfaces.

The most important discovery made by means of radar measurements using the Goldstone/VLA was the ruling out of the existence of a global hydrocarbon ocean by *Muhleman et al.* (1990). Moreover, radar data were used to examine the composition of the surface as well as the characteristics of the albedo dichotomy (*Campbell et al.*, 2003) (see Section 2.3.2).

### 2.2.5 Hubble Space Telescope (HST)

Set into space in 1990, the Hubble Space Telescope (HST) enables the detailed imaging of distant objects owing to its orbit far from the atmosphere of the Earth ($\sim$ 600 km distance from Earth's surface) (*Coustenis and Taylor*, 2008). HST is equipped with several cameras and spectrographs covering wavelengths from ultraviolet to near infrared.

The Wide-Field Planetary Camera on the HST, operating at wavelengths within Titan's atmospheric windows, resolved surface features and enabled the creation of global albedo maps for the first time in 1994 (*Smith et al.*, 1996). Methane windows at 0.67, 0.94, and at 1.08 µm were sampled through F850LP and F1042M filters. HST-images disclosed a bright continent at the leading face of the moon (see Figure 2.3 and Section 2.3.2). The bright feature was detected again in 1997 and 1998 on images of the Near Infrared Camera and Multi-Object Spectrometer (NICMOS) on HST by *Meier et al.* (2000). Therefore, HST-data confirmed the permanence of the bright region previously detected by rotational light-curves (*Lemmon et al.*, 1993), telescopes (*Saint-Pé et al.*, 1993), and radar instruments (*Muhleman et al.*, 1990). Hubble maps failed to reveal clouds, possibly due to their low spatial resolution of 295 km/pixel (*Meier et al.*, 2000).

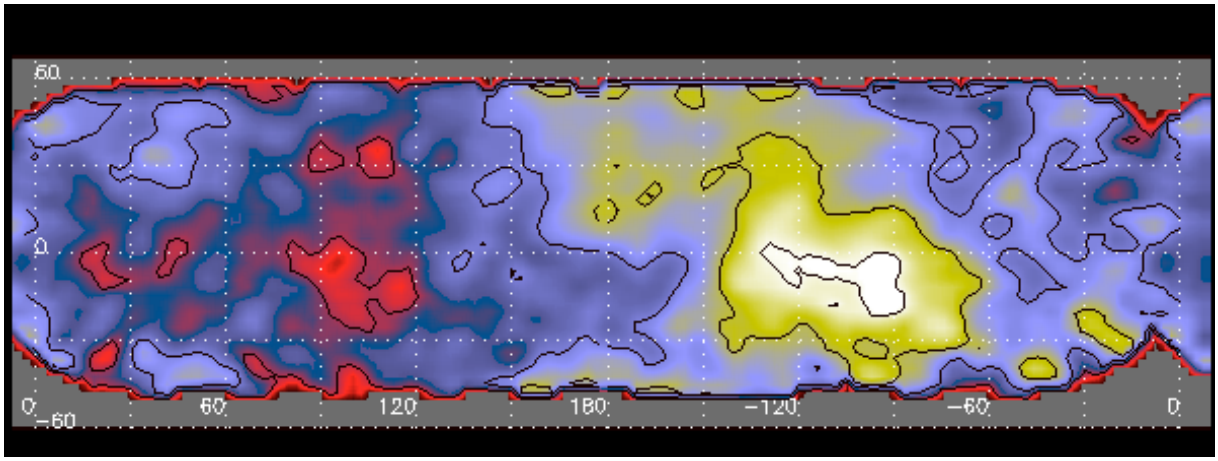


**Figure 2.3:** Hubble Space Telescope Map of Titan's surface, F850LP filter image (reflectance at 0.94 µm). Image is centered at 180°W, 0°N. Color coding: Yellow/white is bright terrain, and red is dark terrain. The gray areas and red boundaries were not imaged (Source: http://www.lpl.arizona.edu/~lemmon/titan/850c.html).

Hubble images as well as near-infrared observations and light curves are primarily sensitive to Titan's reflectance near its equator up to mid-latitudes owing to their particular observing geometry (cf. HST maps in *Smith et al.* (1996)). Therefore, images covering the higher latitudes and the poles were unavailable until the Cassini mission.

### 2.2.6 Cassini-Huygens Mission

#### 2.2.6.1 Cassini-Huygens Mission Profile

Cassini-Huygens is a joint mission of ESA, NASA, and ASI, dedicated to studying Saturn, its atmosphere, magnetosphere, rings, and its icy moons (*Coustenis*, 2006). Not only because of the long distance to the Saturnian System, this US/European mission is one of the most challenging space missions and attracts worldwide scientific and public attention.

Cassini-Huygens, launched on October 15$^{th}$, 1997, arrived in the Saturnian System more than 6 years later, on July 1$^{st}$, 2004 (*Lebreton and Matson*, 2007). Since then, the mothership Cassini has been gathering a wealth of data about its targets including large quantities of image and spectral data (e.g. *Brown et al.*, 2004; *Porco et al.*, 2005; *Brown et al.*, 2006; *Lunine et al.*, 2008a; *Barnes et al.*, 2009a). The most remarkable event was when the Huygens descent probe that had been carried by Cassini into the Saturnian System was released to make its descent to the surface of Titan in December 2004 (e.g. *Lebreton et al.*, 2005). The descent and landing of the probe allowed exploring of the vertical structure of the atmosphere and obtaining high-resolution images of the surface (*Tomasko et al.*, 2005; *Lebreton and Matson*, 2007). The direct sampling on Titan by a landing probe equipped with six science instruments highlights that Saturn's largest moon was always considered a priority target throughout the Cassini mission (*Coustenis and Taylor*, 2008).

**Figure 2.4:** Cassini-Huygens spacecraft (Courtesy NASA/JPL, Source: http://cassini-huygens.jpl.nasa.gov/spacecraft/index.cfm).

During Cassini's prime or nominal mission (from July 2004 until July 2008) 45 targeted encounters with Titan were realized. NASA announced a two-year extension of the mission (called Extended Mission, 'XM' or Equinox Mission), yielding another 26 Titan flybys (*NASA*, 2010c). Another extension of the Cassini mission until late 2017 was approved recently (*NASA*, 2010a).

*Science Objectives:* From the first conception of the mission in 1982, the decision to launch Cassini-Huygens was motivated by a number of unsolved questions regarding the Saturnian System and Titan. The main objectives concerning Titan were to study the moon's interior, surface, and its atmosphere as well as their dynamics and interactions (e.g. *Lorenz et al.*, 2003; *Lorenz and Lunine*, 2005; *Tobie et al.*, 2005; *Coustenis and Taylor*, 2008; *Barnes et al.*, 2009a; *Coustenis et al.*, 2009b). From the atmospheric perspective, data were required to understand its global, seasonal, and local dynamics as well as its complex photochemistry (e.g. *Lunine et al.*, 1998; *Barth and Toon*, 2003; *Coustenis et al.*, 2009b). Basic atmospheric characteristics, such as cloud properties, the temperature and wind field were to provide a valuable background for advanced studies of Titan's atmosphere. The abundance and distribution of organics, aerosols, trace gases, and noble gases were considered important to characterize the atmosphere's spatial structure (e.g. *Lunine et al.*, 1998; *Brown et al.*, 2004; *Coustenis and Taylor*, 2008; *Coustenis et al.*, 2009b). Titan's surface aroused great interest since before Cassini-Huygens only its large-scale features had been observed. The unique spatial resolution offered by the Cassini imaging instruments, particularly those on the Huygens Landing Probe, was expected to yield a wealth of information about small and medium-scale geologic features (*Lorenz et al.*, 2002). Furthermore, information about the topography, spectral characteristics, and composition of the surface was in demand (e.g. *Brown et al.*, 2004; *Lorenz and Lunine*, 2005; *Coustenis and Taylor*, 2008; *Coustenis et al.*, 2009a).

#### 2.2.6.2 Cassini Orbiter and Payload

The Cassini orbiter and its descent probe consist of 18 science instruments and two low-gain antennas for communication. Cassini is equipped with four remote sensing instruments, three of which enable spectral imaging. The Imaging Science Subsystem (ISS) allows monochromatic imaging through several spectral filters between 0.2 and 1.1 µm (*Porco et al.*, 2004) (see Section 3.2). An advanced version of Voyager's IRIS is provided through the Composite Infrared Spectrometer (CIRS) onboard Cassini. This instrument measures the infrared emission in the spectral range between 7 and 1,000 µm and is designed to explore the composition of the atmosphere (e.g. *Vinatier et al.*, 2007; *Coustenis and Taylor*, 2008). The Ultraviolet Imaging Spectrograph (UVIS) investigates atmospheres and surfaces of bodies in the Saturnian System at wavelengths from 55 to 190 nm (e.g. *Hendrix and Hansen*, 2008). A third spectrometer, dedicated to obtaining information about the surface and the atmosphere, is the Visual and Infrared Mapping Spectrometer (VIMS), which is sensitive to reflected light between 0.3 and 5.1 µm (*Capaccioni et al.*, 1998; *Brown et al.*, 2004). Detailed specifications of this sensor are given in Section 3.1.

The Radio Detection and Ranging (RADAR) instrument with its different imaging modes expands Cassini's imaging capabilities. Data obtained from the radar sensor often come in a better quality due to the instrument's high spatial resolution and since the signal is not distorted by Titan's hazy atmosphere. Further, data obtained by the radar instrument allow to derive the relative elevation and topography, and to measure the brightness temperature and other physical properties of the surface (*Elachi et al.*, 2004) (see Section 3.3).

The precise tracking of the spacecraft is carried out by the Radio Science Subsystem (RSS). The RSS also receives gravitational data and delivers details on the internal structure of Saturn and its satellites (e.g. *Perrot and Giordani*, 1998; *NASA*, 2009).

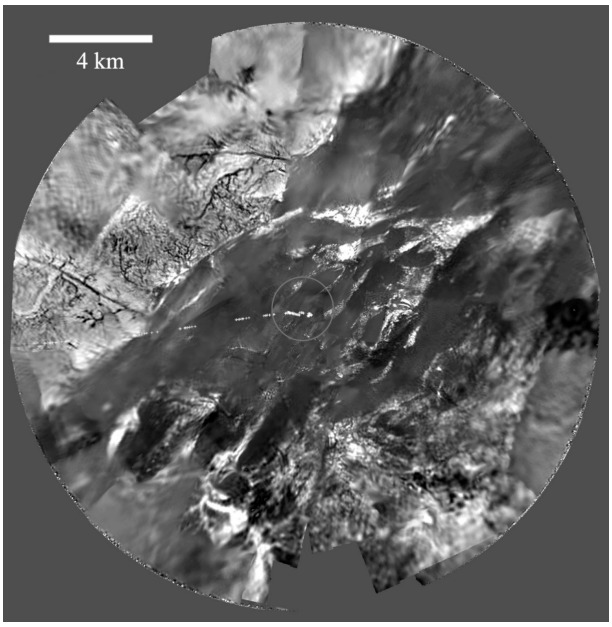


**Figure 2.5:** View of Titan from 8 km above its surface. Medium-altitude panoramic image, obtained by the Descent Imager/Spectral Radiometer (DISR). The image was acquired on January 14, 2005 (Courtesy NASA/JPL).

A number of instruments are primarily dedicated to the investigation of Saturn's magnetosphere but also to studying its interaction with Titan and characterizing the moon's upper atmosphere, namely the Ion and Neutral Mass Spectrometer (INMS) (e.g. *Cui et al.*, 2009), the Cassini Plasma Spectrometer (CAPS) (e.g. *Hartle et al.*, 2006), the Dual Technique Magnetometer (MAG) (e.g. *Dunlop et al.*, 1999), the Magnetospheric Imaging Instrument (MIMI) (e.g. *Krupp et al.*, 2009), Radio and Plasma Wave Science (RWPS) (e.g. *Wang et al.*, 2006), and the Cosmic Dust Analyzer (CDA) (e.g. *Hillier et al.*, 2007).

The Huygens landing probe carried an Aerosol Collector Pyrolyser (ACP) (e.g. *Nguyen et al.*, 2007) coupled with a Gas Chromatograph/Mass Spectrometer (GCMS) (e.g. *Niemann et al.*, 2005), which enabled atmospheric sampling and the determination of the aerosol composition during descent (*Lebreton and Matson*, 2007). Also onboard the probe was the Descent Imager/Spectral Radiometer (DISR) that collected sensational panoramic views as it approached the surface, providing valuable clues on the topography and composition of the terrain (e.g. *Tomasko et al.*, 2005; *Soderblom et al.*, 2007a). In order to measure energy fluxes by solar radiation and to determine aerosol properties, DISR could focus both in an upward and downward direction. The DISR-instrument also determined the methane mole fraction as a function of altitude (*Niemann et al.*, 2005; *Tomasko et al.*, 2005). Extending previous knowledge on atmospheric dynamics, the Doppler Wind Experiment (DWE) (e.g. *Kazeminejad et al.*, 2007) yielded data about the wind velocity and -direction up to altitudes of 160 km above the surface. Profiles of temperature, pressure, density, and conductivity were deduced from measurements of the Huygens Atmospheric Structure Instrument (HASI) (e.g. *Fulchignoni et al.*, 2002; *Lebreton and Matson*, 2007). Finally, the Surface Science Package (SSP) determined mechanical properties of the surface after the landing of the probe (*Zarnecki et al.*, 2005).

#### 2.2.6.3 Huygens Launch

The descent and landing of the Huygens probe on Titan's surface provided a multitude of valuable in-situ data, such as images, spectra, as well as atmospheric temperature, pressure, and density profiles (e.g. *Niemann et al.*, 2005; *Tomasko et al.*, 2005). This probe, the most distant one deployed so far in the Solar System, was released from Cassini on December 25$^{th}$, 2004, and remained dormant until its entry into the atmosphere (*Coustenis*, 2006; *Lebreton and Matson*, 2007). The probe entered Titan's atmosphere on January 14$^{th}$, 2005, and arrived at Titan's surface about two and a half hours later (*Lebreton et al.*, 2005; *Coustenis and Taylor*, 2008). Its descent was stabilized and decelerated by several parachutes. Due to a programming error, only one of the two nearly redundant transmission channels operated. A loss of data was finally avoided thanks to the radio reception of the Huygens signals by a network of Earth-based radio telescopes (*Lebreton and Matson*, 2007). Titan's landscape became visible soon after the probe's entry into the atmosphere by the transmission of DISR data

**Figure 2.6:** Color view of Titan's surface returned from the Huygens Probe. Rounded pebble-sized rocks are indicative of fluvial erosion. The image was acquired on January 14, 2005 (Courtesy NASA/JPL).

(e.g. *Tomasko et al.*, 2005) (see Figure 2.5). To measure the reflectivity of the surface before landing, a descent lamp of the imaging instrument was switched on (*Lebreton et al.*, 2005; *Tomasko et al.*, 2005).

The surface on which the probe landed was found to be soft and solid, with characteristics similar to wet sand (*Zarnecki et al.*, 2005; *Lebreton and Matson*, 2007). Interestingly, the surface was covered by a number of rounded pebbles and rocks (see Figure 2.6), resembling fluvial sediments deposited in terrestrial valleys, which is interpreted as a strong argument for erosion by flowing liquids (*Tomasko et al.*, 2005). Exceeding all expectations, the probe operated another hour and 12 minutes after landing, obtaining further data of the surface (*Coustenis*, 2006; *Lebreton and Matson*, 2007). The landing site of the probe was estimated to be located at southern latitudes near a bright continent and was finally specified to be located at 192.3°W, 10.3°S (*Tomasko et al.*, 2005).

## 2.3 Background: Titan's Characteristics

This Section briefly outlines the current state of knowledge on the formation, climatic conditions, and the geology of Titan. This background is essential in order to investigate fluvial erosion and processes associated with the methane cycle, which is mainly determined by the processes and dynamics of the atmosphere. Finally, many questions regarding Titan's background still remain unsolved. These questions are summarized in Section 2.3.5.

### 2.3.1 Titan's Formation

The accretion of Titan occurred in the outer Saturnian sub-nebula, at temperatures below 60 K (*Coustenis and Taylor*, 2008). Due to its formation at a long distance from the Sun, Titan contains a high fraction of lighter material and ice, with roughly 0.3 to 0.5 mass fraction being water ice (e.g. *Stevenson*, 1992; *Lunine et al.*, 2009). Silicates, water, ammonia, methane, nitrogen, carbon monoxide, and argon were involved in the formation of Saturn's moon (e.g. *Coustenis and Taylor*, 2008; *Lunine et al.*, 2009).

Thermal energy was supplied by impacts of incoming planetesimals and through the decay of radiogenic elements, leading to an overall increase in Titan's gravity (e.g. *Coustenis and Taylor*, 2008). Melting and mixing followed, coupled with outgassing and internal stratification (see Figure 2.7). Consequently, ices were arranged at the surface and heavier compounds were concentrated near the core of the moon (*Lunine and Stevenson*, 1987; *Lunine et al.*, 2009). Depending on the composition of the primal planetesimals, which is largely unknown, several scenarios for the evolution of Titan and its internal differentiation are conceivable. Whether the core itself is composed of silicate or if it is divided into an inner iron core and an outer silicate layer is yet unsolved (*Grasset et al.*, 2000).

Different scenarios about the origin of the atmosphere are debated: The simple capturing or trapping of gases from the surrounding nebula or from impacting comets is an unlikely hypothesis owing to a deficit of noble gases in the atmosphere ($^{38}$Ar, Kr, and Xe) (*Niemann et al.*, 2005). What also makes it unlikely is the D/H ratio of Titan's methane, which is rather consistent with outgassing of volatiles and methane from clathrate hydrates (*Mousis et al.*, 2002). The idea of outgassing of volatiles from Titan's icy shell is a more favorable scenario as it accounts for the enormous density of the atmosphere. It is assumed that $N_2$, $NH_3$ $CH_4$, and Ar were released from the ice during the accretion and stratification of the satellite (*Owen*, 1982; *Niemann et al.*, 2005). The previous trapping of gases in ices is reasonable owing to low temperatures in the Saturn subnebula (*Owen*, 2000). Furthermore, the current low abundances of noble gases suggests the formation of molecular nitrogen, the main compound of Titan's atmosphere, from ammonia ($NH_3$), which, in turn, originates from the solar nebula (*Niemann et al.*, 2005; *Lunine et al.*, 2009). Alternatively, a subsurface water-ammonia ocean might have released methane and caused the dominance of atmospheric nitrogen through extrusion of ammonia-water magma (*Lunine and Stevenson*, 1987). The conversion of ammonia into nitrogen is suggested to have occurred via photolysis or by shockheating in the primordial atmosphere (*Owen*, 1982; *Courtin et al.*, 1995). Regarding the origin of methane, it is most likely that it formed subsequent to the accretion rather than originating from methane clathrate from the subnebula. Depending on the temperature during the formation of the planetesimals, either $CH_4$, or $NH_3$ and $CO_2$ (T>75 K) were captured (*Niemann et al.*, 2005). A second plausible explanation attempt suggests methane to have been formed through a reduction of various forms of carbon in a hydrogen-rich environment (*Owen*, 2000).

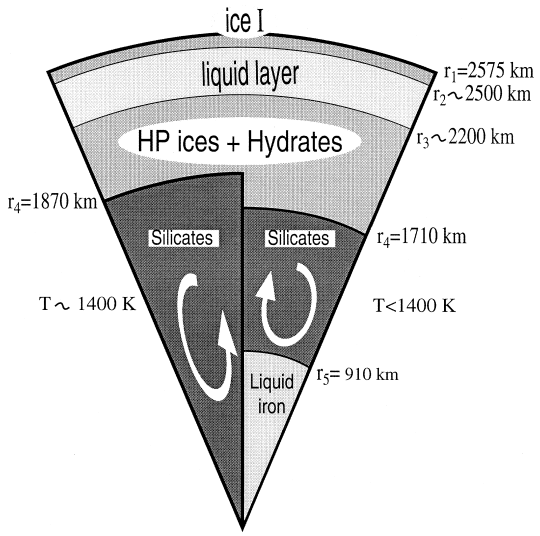


**Figure 2.7:** Possible present internal structure of Titan (from *Grasset et al.* (2000)).

In order to understand the methane delivery mechanism that seems to be replenishing the atmosphere counteracting photodissociation, it is essential to know more about Titan's history and internal structure. As an example, the release of methane from clathrate hydrates within the outer icy shell might play a part in this delivery (e.g. *Stevenson*, 1992; *Mitri et al.*, 2008) (see Section 2.3.4.1). Moreover, knowledge about the interior, its origin, and composition provides insights into Titan's geologic history and vice versa (*Tobie et al.*, 2006).

### 2.3.2 Surface

Titan's surface became visible in moderate resolutions through near-infrared imaging after the Voyager encounters. Following the rejection of the global-ocean concept by scientists in the early 1990s (see Section 2.2.4.2 and 2.2.4.3), Titan's surface was now expected to be mainly solid, presumably composed of different ices (e.g. *Griffith et al.*, 1991). An accumulation of organics at the surface, originating from photolytic reactions in the atmosphere, was considered possible (e.g. *Strobel*, 1974). Indeed, even pre-Cassini near-infrared imaging yielded a broad subdivision of the terrain in terms of albedo. Cassini imagery greatly contributed to the knowledge on the spectral properties of the surface, particularly through revealing a wealth of medium and small-scale surface features.

#### Albedo Dichotomy

Near-infrared imaging of Titan's surface disclosed brightness heterogeneities with a brighter leading hemisphere compared to the trailing hemisphere. This brightness pattern was highly reproducible with different sensors and at several points in time, e.g. through rotational lightcurves (*Lemmon et al.*, 1993), HST-images (*Smith et al.*, 1996), radar observations (*Campbell et al.*, 2003), and telescope observations (*Saint-Pé et al.*, 1993) (see Figure 2.3 and Figure 2.8). Thus, the albedo dichotomy was

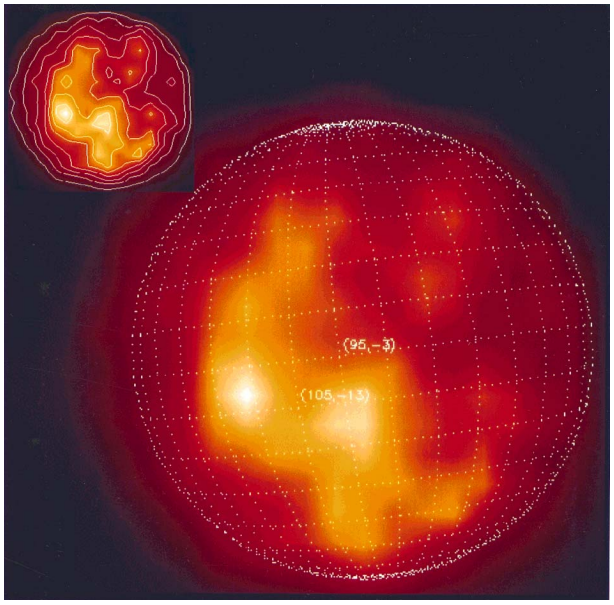


**Figure 2.8:** Titan's leading face at 2 µm, acquired with the ADONIS adaptive optics system installed at the ESO telescope (September 16, 1994). The bright surface feature (centered at 114°W, 13°S) with two distinct peaks as well as several smaller bright features can be discerned (from *Combes et al.* (1997)). Note also the correlations of this image and the HST map in Figure 2.3.

thought to be attributable to albedo differences of the surface or to persisting, possibly orographic, clouds. Moreover, a correlation between the reflectance of several near-infrared wavelength bands was observed, resulting in similar brightness patterns in images of different wavelength intervals (*Lemmon et al.*, 1993, 1995; *Lellouch et al.*, 2004). Despite this, the brightness difference was found to be most pronounced at 2 µm (*Lemmon et al.*, 1995).

Figure 2.3 shows the first global map of Titan's surface at mid- and lower latitudes which also roughly depicts the shape and spatial extent of the albedo features. The bright continent-sized feature, later named 'Xanadu' (see global map with Titan's nomenclature, Figure A.1, Appendix) was found to be centered at 110°W, 10°S[1] with a size of roughly 30° in latitude and 60° in longitude (*Smith et al.*, 1996; *Coustenis et al.*, 2001) (see Figure 2.8). Within the bright area, other albedo variations were identified (*Combes et al.*, 1997; *Gibbard et al.*, 1999; *Coustenis et al.*, 2001), e.g. at least two individual albedo peaks (*Meier et al.*, 2000). Moreover, Hubble maps revealed another distinct bright region at 10°W, 25°S (*Smith et al.*, 1996).

The remaining dark surface including the trailing hemisphere was found to be heterogeneous, too, since other fainter bright features and inhomogeneities within the dark terrains were detected (*Combes et al.*, 1997; *Gibbard et al.*, 1999; *Coustenis et al.*, 2001). The existence of those reflectance features was later confirmed by near-infrared images of the Near Infrared Camera and Multi-Object Spectrometer (NICMOS) observations of the Hubble Space Telescope (*Meier et al.*, 2000). Thanks to the Cassini ISS and VIMS sensors, very detailed maps (in a spatial and spectral sense) are available that bear out pre-Cassini observations and reveal the albedo dichotomy in great detail.

[1]Longitude of Central Meridian (LCM) convention, or cartographic/geographic convention. The present work uses the astronomical ('IAU' planetographic) system, with positive west longitudes, for reasons of comparability to recent studies.

Prior to Cassini it was suspected that bright terrains are elevated with respect to the dark terrains. Height differences were expected to be within a maximal range of 10 km (*Smith et al.*, 1996). However, mountain heights determined by Cassini radar data were found to be below 2 km (*Radebaugh et al.*, 2007). Moreover, recent surface height estimates based on Cassini's radar-SAR swaths argue against the proposed correlation between surface height and albedo since parts of the large bright continent at the leading hemisphere - initially interpreted to be elevated - have a lower surface height compared to their low-albedo surroundings (*Stiles et al.*, 2009) (see Section 4.3.2).

The most likely explanation for the presence of different-albedo materials is a different composition of these surface units, possibly due to an accumulation of dark organic compounds, such as tholins or dark carbonaceous components, which formed in the atmosphere and subsequently settled down on the surface (e.g. *Griffith et al.*, 1991; *Smith et al.*, 1996; *Meier et al.*, 2000). Rain and weathering might have cleaned elevated terrain and removed dark superficial layers, exposing bright continents and islands. The concept of methane rainfall was first proposed by (*Toon et al.*, 1988) and later taken on by (*Griffith et al.*, 1991; *Lorenz and Lunine*, 1996, 1997; *Barnes et al.*, 2007b).

**Composition of the Surface**

Titan's low density of 1.88 g/$cm^2$ and its location in the outer Solar System points to a high abundance of comparably light water ice (*Griffith et al.*, 1991; *Smith et al.*, 1996), which presumably settled in the outer layers or near the surface during the differentiation of the body. The presence of water ice at Titan's surface was supported by radar observations at the Arecibo Observatory. *Campbell et al.* (2003) attributes the comparably high radar reflectivity of the bright region at the leading hemisphere to volume scattering. This effect might be induced by fractions of water ice which are transparent at radar wavelengths (*Campbell et al.*, 2003). In contradiction to this, a spectral mismatch to the expected water ice-rich surface was discovered, since pure water ice strongly absorbs at 2 µm (*Griffith et al.*, 1991; *Lemmon et al.*, 1995) which is not the case for the high-albedo features at Titan's surface. To explain the spectral mismatch it was suggested that the substance under consideration might be a mixture of water ice with another unknown organic and dark component, such as mixtures of benzene ($C_2H_6$), acetylene ($C_2H_2$), and perhaps solid acetonitrile ($CH_3CN$) (*Yung et al.*, 1984; *Clark et al.*, 2006). An alternative conjecture for the unknown substance was to consist of tholins and/or other organic compounds (*Griffith et al.*, 1991; *Coustenis et al.*, 1995; *Combes et al.*, 1997).

Other candidate compounds are $CO_2$ ice (*Griffith et al.*, 1991), methane/ethane ice, and ammonia hydrate (*Coustenis et al.*, 2001). Although their spectral properties match those of the compound in question, methane and ethane ice were ruled out due to the extreme temperature and pressure conditions required to explain their formation and maintenance (*Lorenz and Lunine*, 2002). Titan's environmental conditions also rule

out the precipitation and accumulation of $CO_2$ (*Griffith et al.*, 1991; *Lorenz and Lunine*, 2005). Ammonia hydrate ice is not consistent, either, in terms of its spectral properties or regarding its radar reflectivity (*Campbell et al.*, 2003; *Lorenz and Lunine*, 2005).

*Griffith et al.* (1991) further considered isolated shallow lakes of methane or ethane to exist at Titan's surface which lower Titan's reflectance at 2 µm. This could, indeed, be true for the bright areas, but the reflectance of the dark areas is nonetheless too high to be explained by the presence of reservoirs of liquid ethane or methane since those constituents strongly absorb at 2.1 µm (*Combes et al.*, 1997). The spectral fingerprint of the dark hemisphere is not indicative of pure water ice either because of its low overall reflectance. Again, a mixture of water ice with silicates, tholins, or other organic solids has been suggested (*Combes et al.*, 1997; *Gibbard et al.*, 1999). In summary, even before the start of the Cassini-mission, a consensus was achieved that water ice combined with another yet unknown dark component in unknown fractions make up the surface of Titan, rather than a global ocean of liquids (*Griffith et al.*, 1991). The possibility of smaller open reservoirs of liquid hydrocarbons still remained conceivable.

**VIMS Surface Units**

Cassini images greatly enhanced our knowledge about the stratification and spectral properties of Titan's surface. ISS data precisely disclosed the contours of bright- and dark -albedo features (*Porco et al.*, 2005). Through VIMS data, a detailed spectral analysis of the terrains in question became possible at a favorable spatial resolution (e.g. *Brown et al.*, 2006; *Barnes et al.*, 2007a).

Generally, images of both sensors confirmed the brightness variations within the bright terrains already recognized earlier on (*Porco et al.*, 2005; *Brown et al.*, 2006; *Barnes et al.*, 2007a). Furthermore, the boundaries of the continents were found to be frayed. Distinct bright small-sized features ('islands') became visible within the dark terrain (*Porco et al.*, 2005). Although the shape and extent of the different spectral units can be easily discerned and a further subdivision of the dark surface was revealed by images made by the VIMS instrument (see Section 4.2), the exact composition of Titan's various terrains is still controversial.

### 2.3.3 Atmosphere

Since the Voyager observations at the beginning of the 1980s, a wealth of data and models describing the atmosphere had become available that helped to deduce information about Titan's structure and dynamics (see Figure 2.9). Aside from deriving basic knowledge about the atmosphere, its composition and structure, Voyager's findings engendered speculations about the weather on Titan, the greenhouse effect, and the formation of clouds (*Kondratev and Moskalenko*, 1985; *Lunine*, 1990; *Coustenis*, 1991; *Tokano et al.*, 2001). Cassini data - particularly the measurements obtained during the descent of the Huygens probe - greatly deepened our knowledge on atmospheric

properties and processes, such as temperature distribution and the abundances and relative humidity of condensable constituents.

Titan's atmosphere is a secondary atmosphere that undoubtedly originates from devolatilization of solid icy components and has most likely not been captured from the solar nebula (*Owen*, 1982; *Coustenis*, 1991) (see Section 2.3.1). Titan's atmosphere is maintained by the moon's gravity, which is sufficient to retain most of the gases (*Coustenis*, 1991). The atmosphere is chemically reducing - in contrast to the oxidizing atmospheres of Earth and Mars (*Yung et al.*, 1984; *Raulin and Owen*, 2002). Presumably, similar reducing conditions prevailed in the atmosphere of the early Earth (*Tyler et al.*, 1981).

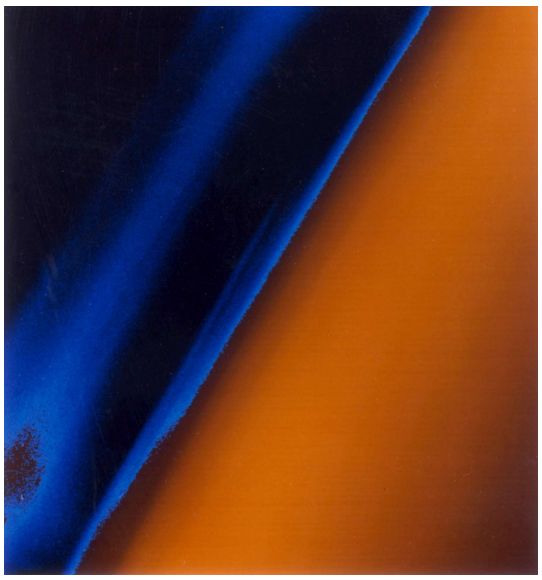

**Figure 2.9:** False-color Voyager 1 image (November 12, 1980). Haze layer appears in blue colors and shows subdivisions at 200, 375, and 500 m. The orange sphere is equivalent to the upper level of a thick aerosol layer above the limb (Courtesy NASA/JPL).

#### 2.3.3.1 Composition and Stratification of the Atmosphere

Methane was spectrally detected as an atmospheric constituent by *Kuiper* (1944), whereas $N_2$ as the principal constituent of Titan's atmosphere was successfully identified by the Radio Science Experiment onboard the Voyager-spacecraft (*Tyler et al.*, 1981). Assuming an atmosphere consisting of 100% $N_2$, the surface pressure and temperature were determined to be 1,6 bars and 93 K, very close to the real values (*Tyler et al.*, 1981) (cf. Table 2.1). Recent Cassini meaurements yielded a $CH_4$-content of up to 5% near the surface (*Tobie et al.*, 2006).

Aside from $N_2$ and $CH_4$, numerous other atmospheric hydrocarbons were detected at the time of the Voyager encounters. Besides the already identified molecules $C_2H_6$, Ar, $C_2H_2$, $C_2H_4$, H, and $H_2$, other more or less minor elements were detected, such as benzene ($C_6H_6$), hydrogen cyanide (HCN), carbon dioxide ($CO_2$), carbon monoxide (CO), cyanoacetylene ($HC_3N$), and cyanogen ($C_2N_2$) (*Gillett et al.*, 1973; *Gillett*, 1975; *Hanel et al.*, 1981; *Lindal et al.*, 1983; *Yung et al.*, 1984; *Clark et al.*, 2006).

Voyager disclosed a north-south brightness-gradient of Titan's disk at visible wavelengths. The northern hemisphere appeared darker and redder than the

southern hemisphere. Additionally, a dark north polar hood was discovered with a dark ring located at about 70°N (*Smith et al.*, 1981; *Sromovsky et al.*, 1981; *Smith et al.*, 1982). Both effects were suggested to be caused by seasonal variations in solar illumination (*Smith et al.*, 1981; *Clarke and Ferris*, 1997). The brightness asymmetry between the two hemispheres was found to be reversed in Hubble images taken at visible wavelengths obtained about 20 years later, which confirmed the seasonal origin of that effect (*Caldwell et al.*, 1992). Another seasonal effect derived from Voyager data was a temperature gradient between equator and pole in the upper stratosphere. The range of that gradient comprehended 15-20 K (*Hanel et al.*, 1981). In the lower atmosphere the temperature difference between the equator and the poles was determined to amount to 3 K (*Flasar et al.*, 1981), a fact recently confirmed by Cassini-CIRS data (*Coustenis and Taylor*, 2008; *Jennings et al.*, 2009). Further, Voyager data demonstrated the lack of diurnal or longitudinal thermal differences. Nevertheless, seasons have an effect on the latitudinal temperature gradients and on the fractions of minor atmospheric constituents (*Coustenis and Taylor*, 2008), although seasonal effects seem to be less pronounced than on Earth.

Data obtained during the Voyager encounters made it possible to determine the vertical structure of the atmosphere, i.e. the vertical temperature profile and its mean molecular weight (*Hanel et al.*, 1981; *Tyler et al.*, 1981). Thermal inversion due to the absorption of solar radiation in the stratosphere was verified (*Danielson et al.*, 1973; *Samuelson*, 1983). Additionally, various distinct haze layers have since been identified (see Figure 2.9). Condensation and the formation of clouds were predicted to occur at about 70 km altitude (*Lara et al.*, 1994).

The Huygens descent provided direct and very precise in-situ measurements of each atmospheric constituent, most interestingly $CH_4$, as well as delivering an atmospheric temperature profile (see Figure 2.10) recorded by the Huygens GCMS (*Niemann et al.*, 2005). The measurement of the methane mole fraction revealed a strong increase of the methane concentration with decreasing altitude. The relative humidity of $CH_4$ near the surface amounts to 45% (*Niemann et al.*, 2005; *Atreya et al.*, 2006).

#### 2.3.3.2 Atmospheric Methane, Clouds, and Rain

Methane condensation and cloud formation are essential for a methane cycle to function. Theoretical reflection on Voyager data already suggested the presence of clouds, knowing that clouds are common phenomena on the outer gas planets, e.g. Saturn and Jupiter (e.g. *Hanel et al.*, 1981; *Courtin*, 1982).

The formation of clouds depends on the abundance of methane, the temperature, and the availability of condensation nuclei in the atmosphere. Given saturated conditions in the atmosphere, decreasing temperatures result in a transfer of methane vapor into the liquid or even solid phase. Consequently, condensation in Earth's and Titan's atmosphere mainly occurs at a substantial distance to the surface within the

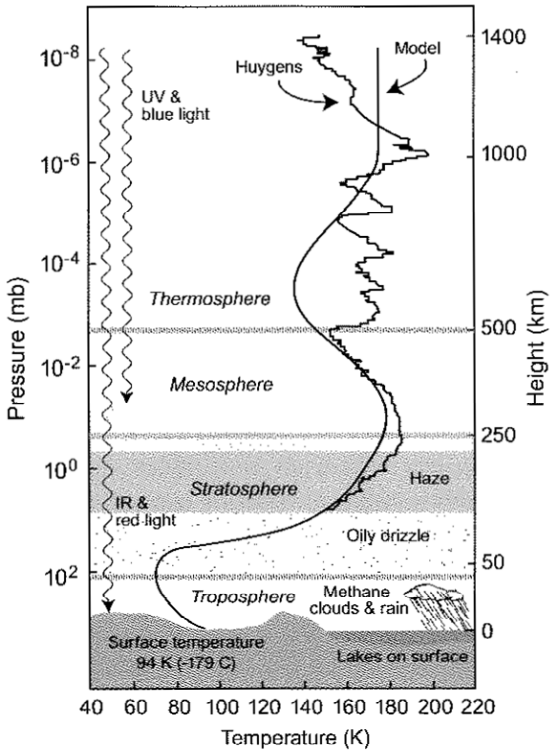


**Figure 2.10:** Temperature-Pressure-Altitude Profile of Titan's atmosphere. The smooth curve indicates the temperature profile expected prior to Cassini; the jagged curve is the measured temperature profile from the Huygens Probe. Atmospheric and surface features (clouds, haze, and drizzle) are added (from *Coustenis and Taylor* (2008) p. 131.)

troposphere. Prior to Cassini, supersaturation of methane in the troposphere was assumed (*Courtin et al.*, 1995; *Tokano et al.*, 2001). It was expected that condensation of methane is inhibited by the low wettability of aerosols and by a lack of condensation nuclei, such as haze or tholins, resulting in large particle sizes and a rapid particle growth (*Toon et al.*, 1988; *Courtin et al.*, 1995). Therefore, the formation of clouds, precipitation events, and the vanishing of clouds were expected to be faster compared to Earth (*Toon et al.*, 1988; *Griffith et al.*, 1998). The idea of supersaturated methane was ruled out soon after the Huygens descent. Observational data suggested relative methane humidities well below 100% (*Niemann et al.*, 2005). Furthermore, a sufficient number condensation nuclei is in fact present in the form of tropospheric haze and ethane (*Barth and Toon*, 2003; *Graves et al.*, 2008).

Candidate cloud forming molecules were assumed to be $CH_4$, $C_2H_6$, and $N_2$, whereas nitrogen was soon ruled out since its condensation temperature is lower than the effective atmospheric temperature (*Tyler et al.*, 1981; *Samuelson*, 1983). Nevertheless, $N_2$ might be involved in the cloud formation process, influencing the vapor pressure of $CH_4$ (*Thompson et al.*, 1992; *Lorenz*, 1993). Despite this finding, $CH_4$ and $C_2H_6$ were suggested to be the major constituents of clouds in the troposphere, which is still the prevailing opinion (*Hanel et al.*, 1981; *Eshleman et al.*, 1983; *Barth and Toon*, 2003).

The first detection of clouds near the equator succeeded in a survey by telescopes at near-infrared wavelengths, which showed an anomalous brightening in different atmospheric windows (at 1.3, 1.6, 2.0, and 2.9 µm) during two nights in 1995, relative to data of a reference period (*Griffith et al.*, 1998). Later, Gemini and Keck adaptive-optics

images disclosed clouds at high southern latitudes, i.e. south of 50°S (*Roe et al.*, 2002) and south of 70°S (*Brown et al.*, 2002; *Roe et al.*, 2005). Finally, the Huygens GCMS- and HASI-instruments measured the relative humidity as a function of altitude during the descent. In fact, the relative methane humidity obtained allows condensation and cloud formation above 8 km altitude given that the relative humidity of methane at this level is 100% (*Niemann et al.*, 2005; *Tokano et al.*, 2006). Furthermore, even subsaturated conditions are expected to permit condensation (*Atreya et al.*, 2006).

Stable clouds at both poles and at southern mid-latitudes were observed over the entire course of the Cassini mission (e.g. *Roe et al.*, 2002; *Griffith et al.*, 2005; *Rannou et al.*, 2006; *Schaller et al.*, 2006; *Rodriguez et al.*, 2009a). Apart from that, the near-infrared observations indicate a sporadic and ephemeral rather than ubiquitous distribution of mid-latitude clouds (e.g. *Rodriguez et al.*, 2009a). Clusters of clouds at the southern hemisphere led to speculations about their possible seasonal origin (*Brown et al.*, 2002).

Global circulation models (GCM's) of Titan's atmosphere predict a circulation pattern similar to Earth's Hadley circulation, which is typical for atmospheres of slowly rotating planets (*Hourdin et al.*, 1995; *Tokano et al.*, 2001). Temperature gradients between equator and pole persist due to the overbalancing of solar radiance around the equator relative to the poles and owing to a latitudinal variation of the atmospheric opacity (*Tokano et al.*, 2001). The Hadley circulation tends to compensate gradients of temperature and pressure. As a result, motion rises in the summer hemisphere and descents around the winter pole. The global circulation has thus a strong influence on cloud activity (*Tokano et al.*, 2001; *Tokano*, 2009).

GCM's predict the formation of widespread and persistent clouds at both poles, clouds due to convection near the equator and in the respective summer/autumn hemisphere, particularly near the summer pole, as is confirmed by near-infrared observations. Sporadic clouds should also appear at mid-latitudes (*Rannou et al.*, 2006). Clouds are expected to be stable around the winter pole and could also occur at 40° in the winter hemisphere; the latter is not confirmed by observational data. Due to the coupling of the cloud distribution with the seasons, the global pattern should change in a timescale of 15 terrestrial years (*Tokano et al.*, 2001; *Brown et al.*, 2002; *Rannou et al.*, 2006; *Rodriguez et al.*, 2009a). However, it seems that the global cloud distribution lags behind the insolation constraints, as the predicted inversion of the cloud pattern has not been observed yet (*Rodriguez et al.*, 2009a).

The life cycle of a raindrop on Titan is described in a model by *Lorenz* (1993), which suggests that Titan's low gravity results in large particles, descending slowly to the surface. Others considered it possible that precipitation does not even reach the surface due to re-evaporation on the way down (*Flasar*, 1983; *Lorenz*, 1993; *Lorenz and Lunine*, 2005). However, it has not yet been proven by Cassini-Huygens whether raindrops finally reach the surface or if they evaporate again when entering a layer with undersaturated conditions and whether a hydrological cycle on Titan is primarily

a process limited to the atmosphere (*Tokano et al.*, 2001). Falling raindrops or hailstones might serve as condensation nuclei themselves and could even intensify a rainfall event (*Tokano et al.*, 2001). Furthermore, a stabilizing effect of ethane and the effect of cooling by evaporation might protect methane from re-evaporating in the lower atmosphere (*Graves et al.*, 2008).

The rate of evaporation as well as the strength and duration of rainfall events, which determine the intensity of erosional processes, are presumably lower on Titan than those on Earth (*Lorenz and Lunine*, 1996; *Lorenz et al.*, 2008a). It was assumed that Titan's low gravity and temperature, its faint solar illumination, and the enormous atmospheric density slow down atmospheric exchange processes, entail slow fall velocities of Titan's raindrops and reduce the erosional forces of fluvial processes (*Lorenz*, 1993; *Lorenz and Lunine*, 1996). Titan's raindrops only attain velocities of 1.5 m/s with diameters of up to 9.5 mm in contrast to terrestrial velocities of 10 m/s (*Lorenz et al.*, 2008a).

The fact that Titan's volatile cycle proceeds much more slowly despite the wealth of fluvial features at the surface led to the idea of infrequent violent storms followed by long droughts (*Lorenz*, 2000; *Lorenz and Lunine*, 2005; *Hueso and Sánchez-Lavega*, 2006). The apparent erosional potential can only be explained by heavy storms triggered by convection (*Jaumann et al.*, 2008), instead of steady rainfall with moderate rainfall rates as in temperate climates on Earth. Episodic storms allow high rainfall rates, subsequent runoff, and fluvial incision even if the undersaturated lower altitudes have to be saturated by the first drops (*Lorenz*, 1993; *Mitri et al.*, 2007).

### 2.3.4 Models of Titan's Geology

During the exploration of Titan by Cassini, several concepts and models evolved, intended to explain the complex processes occurring at the surface and in the atmosphere of Saturn's moon. Although not all of these concepts are approved, these models provide an approach to understanding the nature of this alien world. The major points of discussion, relevant for the geological analysis and for understanding Titan's methane cycle, are listed in this Section.

#### 2.3.4.1 Resupply of Atmospheric Methane

The most controversial debate is caused by the question about the source of the atmospheric methane. Due to its continuous depletion in the atmosphere, the substantial amount of methane requires a convincing explanation. Several studies addressed the problem of the continuously destroyed methane and its supposed delivery. Since no intrinsic atmospheric source could be found for $CH_4$, its source was suspected to be located near or beneath Titan's surface. The recent concepts are listed in the following:

**1. Storage and release of methane through a subsurface regolith:** Atmospheric methane might be supplied by a subsurface reservoir, as proposed by *Stevenson* (1992).

Large amounts of methane (and ethane) might be stored in the enormous pore volume of an icy regolith, composed of water ice, other ices, silicates, tholins, and/or methane clathrates, extending into great depths (*Lara et al.*, 1994; *Kossacki and Lorenz*, 1996). This regolith operates similarly to terrestrial aquifers which store liquids in their pore volume. Release of subsurface methane is conceivable through cryovolcanic activity, convection, geysers, hot springs, and mud volcanoes (*Kossacki and Lorenz*, 1996; *Lorenz*, 1996; *Fortes and Grindrod*, 2006; *Czechowski and Kossacki*, 2009). Lakes or seas filled with liquid hydrocarbons at surface level might be in contact with the regolith below the surface (*Lara et al.*, 1994; *Lorenz*, 1994; *Dermott and Sagan*, 1995).

**2. Cryovolcanism and outgassing from the interior:** Connected with the idea of a subsurface regolith or ocean is the concept of methane being resupplied by episodic cryovolcanic or outgassing events (*Lorenz*, 1996; *Atreya et al.*, 2006; *Fortes et al.*, 2007). Methane gas might be generated and delivered by serpentinization that takes place in a hydrogeochemical source in the interior of the moon (*Atreya et al.*, 2006; *Lunine and Atreya*, 2008). A similar process led to the formation of methane hydrates and clathrates in Earth's oceans. The formation of clathrate hydrates from different forms of carbon conceivably occurred in the early history of Titan by water-rock reactions (*Lunine and Atreya*, 2008), or even today within a subsurface water-ammonia ocean (*Atreya et al.*, 2006). Methane might be stored as a stable clathrate hydrate layer above a water-ammonia ocean (*Tobie et al.*, 2006). Due to the low solubility of methane in the expected subsurface ocean, a substantial contribution of volcanic events to the atmospheric abundance of methane is questionable (*Lorenz*, 1996; *Jaumann et al.*, 2009). However, calculations of the resurfacing rate yielded a total amount of 24 cm per million years, about 4 cm of which correspond to liquid methane (*Baines et al.*, 2006; *Atreya et al.*, 2006). Although this number is small compared to resurfacing rates on Earth and Venus, it might compensate the loss of methane due to photodissociation. The idea of subsurface reservoirs is very prominent since Cassini-Huygens data failed to show wide-spread pools, lakes, or oceans of hydrocarbons at the surface. A brief description of cryovolcanic and tectonic activity on Titan with respect to its geological outcome is given in Section 2.3.4.3.

**3. Methane evaporation from lakes:** Radar observations prior to Cassini suggested another explanation attempt. The strong absorption of the radar signal and the nearly Lambertian radar scattering excluded the presence of a widespread hydrocarbon ocean but still allowed the presence of localized lakes or seas (*Muhleman et al.*, 1995; *Lorenz and Lunine*, 2005). In fact, lakes of liquid hydrocarbons were brought out by Cassini's radar data (see Section 5.8). Particularly, Titan's north polar region exhibits numerous and extended lakes (*Stofan et al.*, 2007). *Mitri et al.* (2007) argues that although the lakes cover only 0.2 - 2% of the surface, they are able to act as a buffer against photolytic losses of $CH_4$. Whether it is these lakes that account for the methane abundance remains unclear but most likely they act as a sink for the photochemical end products of photolysis (*Lorenz and Lunine*, 2005).

**4. Production of $CH_4$ by microorganisms:** The fact that Titan holds such a rich organic repository has been giving rise to speculations about a biologically induced release of $CH_4$. Chemical energy, which is a prerequisite for life on Earth, is available on Titan through $C_2H_2$ molecules (*McKay and Smith*, 2005). In theory, $C_2H_2$ and $C_2H_6$ can be converted into $CH_4$ by biological activity. Nevertheless, a bacterial production of methane is doubtful, because of the very low solubility of organics in liquid methane and Titan's low temperatures that would significantly slow down chemical reactions and biological processes (*McKay and Smith*, 2005).

**5. No resupply of methane, decreasing methane content:** For the sake of completeness it has to be remarked that the possibility of a total depletion of methane remains (*Grasset et al.*, 2000). This concept does not explain the past and recent methane content of the atmosphere, which restrains its credibility, but it predicts the loss of methane in the near future. As a result, the atmospheric temperature would most likely drop, chemical processes would die down and Titan's atmosphere would presumably collapse due to condensation of nitrogen (*Lorenz et al.*, 1997).

#### 2.3.4.2 Volatile Cycle

The idea of a volatile cycle on Titan goes back to a publication by *Tyler et al.* (1981) and is based on the fact that methane is near its triple point at the surface temperature of Titan of 94 K (*Sagan and Dermott*, 1982), where physical conditions allow in principle the presence of methane in its gaseous, liquid, and solid form. Methane is liquid between its melting point at 90.6 K and its boiling point at 118 K (*Sagan and Dermott*, 1982). Pure methane has its triple point at 90.7 K and 117 mbar (*Tyler et al.*, 1981).

The 'methalogical cycle' (*Atreya et al.*, 2006) is often compared to the water-based hydrological cycle on Earth. Evaporation on Earth occurs primarily over ocean surfaces; the rising and cooling of the air induces saturation and subsequent condensation. The formation of clouds and precipitation are the consequence, responsible for typical fluvial morphologies on the (land) surfaces. Titan's methane abundance and its relative humidity in the lower troposphere, as measured by Huygens' GCMS, affirms the idea of an active methane cycle with evaporation, condensation, cloud formation, and rainfall (*Niemann et al.*, 2005; *Atreya et al.*, 2006). Titan's methalogical cycle is considered to be a closed cycle, too, where sources and sinks of methane are balanced although not all details on this cycle are explained (*Atreya et al.*, 2006).

The major precondition for the presence of a volatile cycle is that the boundary environmental conditions of a planet or moon allow a certain element or molecule to occur at least in its liquid aggregate state. Phase changes between the liquid, gaseous, and solid state and the mobility of the liquid allow the circulation of matter within the lower atmosphere and near the surface and enable the transport of thermal energy between the spheres, since evaporation consumes and condensation releases energy. Given the present situation on Earth, an energy source and the presence and persistence of an atmosphere seem to be essential requirements for the action of a

volatile cycle. The atmosphere acts as a medium for evaporation and condensation, and the wide-spread transport and mixing with other compounds. Solar energy is the main impulse responsible for many material and volatile cycles. A more locally limited energy supply is offered by volcanism, which might be a possible explanation for the development of local clouds on Titan (*Owen*, 2000).

Differences and similarities between the methane cycle on Titan and the hydrological cycle on Earth become obvious if one takes the components and phenomena associated with the methalogical cycle into account (from *Tokano et al.* (2001)):

- photolytic destruction of methane (sink)
- transport in the atmosphere (diffusion, advection)
- phase change (condensation, evaporation, latent heat exchange)
- transport in liquid/solid phase (precipitation, rivers)
- greenhouse effect (heating of the atmosphere)
- release of methane (surface or subsurface)
- subsurface methane cycle

One of the elements of Titan's volatile cycle that is accepted as a fact is the process of methane decomposition, established even before the Voyager encounters (*Strobel*, 1974) (see Section 2.2.1). The presence of an atmospheric greenhouse effect based on methane is also confirmed. Atmospheric heating is caused by $CH_4$, $N_2$, and $H_2$ (*McKay et al.*, 1989, 1997; *Tokano et al.*, 2001), similarly to the terrestrial greenhouse effect, which is based on $H_2O$, $CO_2$, and $CH_4$. On Titan, this greenhouse effect is essential for the persistence of the atmosphere, since a drop in temperature would cause a depletion in $H_2$, resulting in the condensation and finally the total breakdown of the atmosphere (*Lorenz et al.*, 1997).

Until now, there has been no direct confirmation of rainfall, drizzle, dew, or even thunderstorm events (*Karkoschka and Tomasko*, 2009). There are further inconsistencies due to the relatively high atmospheric aerosol abundance which, in principle, argues against any precipitation in the recent past since drizzle or rain would have cleared the troposphere from these solid constituents (*Karkoschka and Tomasko*, 2009). Despite this, many indirect indications of rainfall that has, in fact, reached the surface are provided by images of the Huygens probe and other recent imagery by the Cassini instruments. Images of the Huygens Decent Imager unveiled a complex network of fluvial valleys (*Tomasko et al.*, 2005). The geometry of this network is indicative of an origin from a distributed source, such as rainfall (see Section 5.1.1 and Figure 5.4) (*Mangold et al.*, 2004; *Tomasko et al.*, 2005; *Perron et al.*, 2006; *Soderblom et al.*, 2007b; *Jaumann et al.*, 2008; *Lorenz et al.*, 2008a; *Jaumann et al.*, 2009). Furthermore, the high relative methane humidity at the surface, measured by the Huygens Landing Probe,

is suggestive of condensation and at least occasional rainfall (*Karkoschka and Tomasko*, 2009). Another indication of fluvial processes at the surface of Titan comes from the Huygens Landing Site, where a number of rounded cobbles confirm the alluvial character of this area (*Tomasko et al.*, 2005). Supporting the origin of the valleys from rainfall, Titan's dearth of craters with diameters between 20 and 100 km is evidence for intense resurfacing processes (*Porco et al.*, 2005; *Elachi et al.*, 2006; *Jaumann et al.*, 2008, 2009; *Wood et al.*, 2010). The activity of liquid-related processes at the surface is additionally confirmed by the albedo dichotomy of Titan's surface, which is possibly due to fluvial transport of dark material into topographic depressions (*Perron et al.*, 2006; *Jaumann et al.*, 2008).

Certainly, there are many differences between volatile cycles on Titan and Earth aside from those caused by their different chemical composition, such as the slower proceeding of the methane cycle due to the weaker insolation (e.g. *Lorenz et al.*, 2008a) (see Section 2.3.3.2). The nearly uniform latitudinal distribution of temperatures at Titan's surface indicates a compensation of energy gradients by wind both in a vertical and a meridional direction (*Griffith et al.*, 1998). Conversely, small global temperature gradients might indicate small latitudinal differences of insolation, which means that not much compensation of energy gradients by motion and transport of energy and mass is required in the first place.

Unfortunately, many details about the methane cycle remain unknown up to now. Besides the unknown source or delivery of the atmospheric methane, any quantitative information, e.g. about the amount of evaporated or precipitated liquids, if anything, are only estimates. Even some of the major aspects of that cycle still remain questionable or uncertain. In all probability, the subsurface methane cycle will remain an enigma for the present.

#### 2.3.4.3 Volcanism and Tectonics

Cassini image data recently disclosed several candidate mountain chains, putative cryovolcanic domes, and associated landforms, such as lava flows, calderas, etc. (e.g. *Lopes et al.*, 2007a; *Radebaugh et al.*, 2007; *Jaumann et al.*, 2009; *Le Corre et al.*, 2009; *Lopes et al.*, 2010). In general, volcanism presupposes the presence of a subsurface layer of liquids and an internal heat source. Several models consider liquid water-ammonia in a subsurface ocean that represents a potential magma source (*Lorenz*, 1996; *Mitri et al.*, 2008) (see Section 2.3.4.1). Internal heating, which is another precondition of tectonic activity, is suspected to be primarily due to radiogenic decay of radioactive elements in the silicate component of the body as well as due to residual accretional heat (*Lorenz*, 1996). Titan's low eccentricity and its great distance to Saturn results in weak tidal forces which cannot contribute very much to volcanic processes (*Sohl et al.*, 1995). However, internal heat sources are assumed to be weak compared to those of the Earth, making any major tectonic activity unlikely (*Lorenz and Lunine*, 2005).

In spite of this, image data revealed many extended ridges resembling mountain chains whose ages were determined to be between 20 and 100 million years (*Radebaugh et al.*, 2007). The often west-to-east oriented ridges possibly represent faults, or blocks of faulted crust. These features are highly consistent with a development from lateral crustal compression (*Radebaugh et al.*, 2007) (see Section 4.3.2).

The amount of radiogenic argon ($^{40}$Ar) in the atmosphere, as a decay product of potassium ($^{40}$K), is used as an indication for volcanic activity in planetary research. A substantial fraction of $^{40}$Ar, measured by the Huygens GCMS, indicates tectonic and outgassing activity (*Niemann et al.*, 2005), confirming the interpretation of Cassini imagery.

Despite the plausibility and obviousness of recent cryovolcanic activity, explosive volcanism can be ruled out. The high atmospheric pressure would prevent explosive eruptions and the formation of ash clouds (*Lorenz*, 1996). Furthermore, the low solubility of gases in a candidate methane-ammonia magma inhibits cryoplastic volcanism (*Meier et al.*, 2000), although volatiles within the melt, such as methane, nitrogen, and carbon monoxide, or from an external source (e.g. from dikes) may promote large explosive eruptions (*Fortes et al.*, 2007). Eruptions of this kind are rather unlikely under present-day conditions but can't be excluded for Titan's past. For the more recent period, effusive volcanism is the only probable alternative (*Lorenz*, 1996; *Smith et al.*, 1996). *Nelson et al.* (2009) proposed episodic effusive volcanic events that deliver ammonia to the surface in recent times, based on multitemporal spectral observations.

In order to understand Titan's volcanic activity, it is necessary to establish reasonable models of its interior structure. Recent studies describe Titan's volcanism based on a model of a differentiated, multilayer interior structure (see Figure 2.7) (*Tobie et al.*, 2006; *Mitri et al.*, 2008). An ammonia-water ocean is probably located in a liquid layer underneath an outer ice-shell (*Tobie et al.*, 2006). Tidal stresses, topography, or thermal convection could initiate effusive volcanism that delivers ammonia-water. Ammonia lowers the freezing temperature of water and the density of the mixture and is therefore considered a likely cryolava (*Mitri et al.*, 2008; *Jaumann et al.*, 2009). According to *Mitri et al.* (2008) the problem is not to explain cryovolcanism on Titan but explaining why it is still ongoing and to find out why the system has not already achieved thermal/chemical equilibrium.

Tectonic and volcanic processes most likely occur on Titan, although localized and weak (*Baines et al.*, 2006). Whether volcanism alone compensates the loss of atmospheric methane or if other sources are required to replenish the atmosphere is to be determined.

#### 2.3.4.4 Chemical Evolution

Titan's nitrogen-based atmosphere contains numerous organic constituents, stimulating the discussion about its potential habitability. Chemical evolution and the formation of organic compounds are regarded as the precursors of the evolution of life on

Earth. Supporting the concept of a possible chemical and biological evolution is the continuous conversion of molecules, often in the direction of increasing complexity (*Strobel*, 1982; *Yung et al.*, 1984; *Raulin and Owen*, 2002). As an example, atmospheric $N_2$ and $CH_4$ are converted by photolysis into hydrocarbons, nitriles, and aerosols. Further energy providers and contributors to a possible chemical evolution are solar UV light and electrons from Saturn's magnetosphere (*Raulin and Owen*, 2002). Insolation, although being very weak, might play a part in activating chemical reactions on Titan since many of those reactions are temperature-dependent. Temperature gradients in the atmosphere (vertical, horizontal, and seasonal) might result in the acceleration or deceleration of chemical reactions (*Clarke and Ferris*, 1997). A high global variability of environmental conditions and seasonal dynamics support Titan's potential for a chemical or even biological evolution. Photochemical processes in Titan's atmosphere lead to a high diversity of trace species, possibly similar to the prebiotic chemistry on Earth. Although not quantifiable, Titan's evolutionary potential is certainly greater than that of most other bodies in the Solar System.

### 2.3.5 Open Questions

Regardless of intensive research efforts, particularly by the Cassini-Huygens-mission, many important questions still remain open. As shown in Section 2.3.4.2, substantial differences between the hydrological cycle on Earth and the methane cycle on Titan make it difficult to explain Titan's volatile cycle. The dynamics of Titan's atmosphere, including processes like condensation and evaporation, are not sufficiently constrained, which complicates the modeling of atmospheric processes. It is not known whether precipitation takes place in form of steady rain, thunderstorms, or drizzle (or combinations of all three) and whether it really reaches the ground (*Lorenz*, 1993; *Tokano et al.*, 2001) although Cassini imagery unveiled many indirect indications of rainfall. While information on the dynamics, interrelations, and spatial distribution of those processes is now available, e.g. through the observation of clouds and the measurements by the Huygens Probe, the specific interplay within the entire atmospheric-climatic system, including mutual interactions between atmosphere, surface and interior, and seasonal and global dynamics are not yet fully understood.

The source of atmospheric methane has been addressed by numerous studies, and several different concepts are currently being debated (see Section 2.3.4.1). However, this problem has not yet been entirely resolved, and neither has the closely related question as to what constitutes the sink for the photolytic end products. Solid compounds are suspected to accumulate at the surface, building a layer of several hundred meters in thickness (e.g. *Lara et al.*, 1994), whereas liquid decomposition products presumably erode the surface, form fluvial valleys and coalesce in lakes. It is still open today whether the lakes resupply atmospheric methane (*Mitri et al.*, 2007), or if they act as a sink for the end products of photolysis, or both (*Rodriguez et al.*, 2003; *Lorenz and Lunine*, 2005).

Moreover, the reason for the stratification of the surface into several types with different spectral properties is still subject of speculation. Also, the exact composition of bright and dark surfaces and the reason for the albedo differences are not well understood. Another open question in that context is the partly uncertain origin of Titan's diverse geologic landforms as well as their interaction and stratigraphic relationships. Particularly the origin of cryovolcanic and tectonic processes is still debated.

The present thesis aims to fill at least some of the mentioned knowledge gaps, mainly focusing on the methane cycle and its interrelations with the surface. The approach chosen is to interpret the traces of that volatile cycle and investigate fluvial valleys in a global frame. The analysis is also intended to study the connections between the spectral properties of different terrains and their geomorphological context.

# Chapter 3

# Database and Methodology

The database for the present work is provided by Cassini image data. Basic information about the relevant imaging instruments, the datasets used, and the methodology of this work are given in this Section.

## 3.1 Visible and Infrared Mapping Spectrometer (VIMS)

Titan is considered one of the principle science objectives of the Cassini Visual and Infrared Mapping Spectrometer Mission (*Brown et al.*, 2004), although the instrument was not initially designed for imaging the surface (*Barnes et al.*, 2009a). Besides its capability to explore the atmospheric structure, composition, and dynamics, the instrument is perfectly suitable for imaging the surface, e.g. identifying small-scale geologic features and surface units with similar spectral properties, investigating the distribution of surface constituents, and thus creating geological maps (*Capaccioni et al.*, 1998; *Brown et al.*, 2004). To this day, VIMS data obtained during Cassini's prime mission are being analyzed to identify and interpret small-scale surface features (e.g. *Jaumann et al.*, 2008; *Soderblom et al.*, 2010a) as well as for studying geological, stratigraphic, and compositional issues on a global scale (e.g. *Barnes et al.*, 2007a; *Clark et al.*, 2010). A detailed summary of all findings concerning Titan's surface based on VIMS data during Cassini's prime mission can be found in *Barnes et al.* (2009a).

The Cassini Visual and Infrared Mapping Spectrometer (VIMS) is a powerful remote sensing instrument operating at a broad range of visible and near-infrared wavelengths, thus falling into the category of imaging spectrometers (*Brown et al.*, 2004). Basically, VIMS obtains image-data in two spatial dimensions that can be displayed as a monochromatic map, representing the surface as a gray-scale map. Furthermore, every individual pixel in the image contains information about the reflectance in each of 352 short spectral intervals, thus adding another spectral dimension to the classic cartographic 2D representation of the surface, producing an 'image cube' (*Brown et al.*, 2004). VIMS covers a broad wavelength range as it measures the radiance, reflected off the surface between 0.35 and 5.1 µm

(*Capaccioni et al.*, 1998; *Brown et al.*, 2004; *McCord et al.*, 2004). Thus, VIMS data allow both mapping of surface features and spectroscopic analyses.

The VIMS camera consists of two separate spectrometers covering the visual wavelength range (VIMS-VIS, from 0.35 to 1.05 µm) and the near-infrared spectral region (VIMS-IR, from 0.8 to 5.1 µm) (*Capaccioni et al.*, 1998; *Brown et al.*, 2004; *McCord et al.*, 2004; *Jaumann et al.*, 2006). Due to different configurations of the two subsystems, calibrating the data involves a different workflow (*Brown et al.*, 2004; *McCord et al.*, 2004; *Jaumann et al.*, 2006).

VIMS-VIS contains a telescope mirror that is capable to point at or scan targets. Scanning the surface is done in pushbroom mode in which the surface is imaged line by line. Each spectral channel of one line of pixels is detected in a single exposure. VIMS-VIS comprises a spectrometer slit and a diffraction grating to disperse incoming radiation by wavelength. Spatial and spectral data are recorded and stored on a CCD matrix simultaneously. VIMS-VIS has a spectral resolution of 7.3 nm, resulting in 96 spectral channels. Two spatial modes are available, with spatial resolutions of 167 $\times$ 167 µrad (high-resolution mode) and 500 $\times$ 500 µrad (nominal-resolution mode), respectively (*Jaumann et al.*, 2006). The total field of view (FOV) of the instrument is 32 $\times$ 32 mrad, leading to image sizes of 64 $\times$ 64 pixel (*Brown et al.*, 2004; *McCord et al.*, 2004).

VIMS-IR is a one-dimensional focal plane detector, which operates in whiskbroom mode, i.e. it detects the entire spectrum of one spatial pixel per exposure and scans the surface in both spatial directions, supported by a secondary mirror. The infrared subsystem samples in spectral intervals of 16.6 nm, thus providing 256 wavelength bands. The instrument also supports two spatial resolution modes of 250 $\times$ 500 µrad (high-resolution mode) and 500 $\times$ 500 µrad (nominal-resolution mode) (*Jaumann et al.*, 2006). The generated images consist of 64 $\times$ 64 pixels determined by a FOV of 32 $\times$ 32 mrad (*Brown et al.*, 2004; *McCord et al.*, 2004).

Depending on the distance to Titan as well as on the selected spatial resolution mode, different ground resolutions are achieved (*Brown et al.*, 2004). High spatially resolved images of some individual targets allow the distinction of very small-scale surface features. Some areas on Titan are covered by VIMS data with ground resolutions down to a few hundred meters per pixel, e.g. Chusuk Planitia (*Jaumann et al.*, 2008). On the other hand, comprehensive regional and global views are obtainable from moderate-resolution data as illustrated e.g. by *Barnes et al.* (2007a). Those images offer the opportunity to analyze Titan's spectral properties at a global level at the remarkably high spectral resolution of the VIMS sensor.

Imaging spectroscopy enables the identification of surface materials and partly even determining their particular physical states by interpretation of their characteristic reflectance spectrum (e.g. *Bell et al.*, 1975; *Hunt*, 1977; *Brown and Cruikshank*, 1997). Spectral profiles depict the reflectance of a material, which is the fraction of incident to reflected or emitted radiation as a function of wavelength. The overall

shape of this spectrum at ultraviolet, visible, and infrared wavelengths as well as the location, depth, and width of absorption bands serve as a fingerprint by which many materials can be identified. Diagnostic features evolve particularly in the visible and near-infrared part of the solar spectrum, between 0.3 and 3.0 µm, due to crystal field effects, vibrational overtones, electronic transitions, charge transfer, and conduction processes (*Bell et al.*, 1975; *Hunt*, 1977; *Clark et al.*, 1990; *Gaffey et al.*, 1993).

The interpretation of reflectance spectra however is more complex due to the various factors affecting the spectrum, such as the grain size, viewing conditions and -geometry, and non-linear effects in material mixtures (*Clark and Roush*, 1984; *Clark et al.*, 1990). Further, it is important to consider that spectral data - and consequently also VIMS data - only reflect the compositional properties from the upper tens of microns (*Le Mouélic et al.*, 2008) up to a few mm or cm of the surface (*Clark et al.*, 2010). Spectral images generally do not return the properties of the deeper subsurface.

Imaging spectroscopy, as a remote sensing technique, only allows indirect conclusions about the composition of the surface material since its composition is derived through typical reflection and absorption patterns of compounds, molecules, or mixtures of them. However, one and the same spectral profile can be generated by different materials. Thus, spectroscopy provides valuable knowledge about the composition of the surface but is not unambiguously diagnostic.

**Table 3.1:** Specifications of the VIMS observations used in this study (from *Barnes et al.* (2009a) and *Hansen et al.* (2009).

| Flyby/ Event | Orbit | Date | Lat (at closest approach) | Lon (at closest approach) | Phase angle (°) | Best spatial sampling (km) |
|---|---|---|---|---|---|---|
| TA | A | October 26, 2004 | 38.8 | 88.5 | 90.9 | 2.6 |
| TB | B | December 13, 2004 | 59.1 | 84.2 | 101.5 | 1.35 |
| T4 | 5 | March 31, 2005 | 33.4 | 118.7 | 66.4 | 1.2 |
| T5 | 6 | April 16, 2005 | 74.0 | 272.3 | 127.2 | 5 |
| T8 | 17 | October 28, 2005 | 1.2 | 246.1 | 104.8 | 42 |
| T9 | 19 | December 26, 2005 | -0.2 | 110.4 | 67.1 | 2.9 |
| T10 | 20 | January 15, 2006 | 0.1 | 250.8 | 120.5 | 3.9 |
| T11 | 21 | February 27, 2006 | 0 | 107.4 | 92.5 | 18 |
| T12 | 22 | March 18, 2006 | 0.1 | 250.6 | 148.0 | 7 |
| T13 | 23 | April 30, 2006 | 0.1 | 106.3 | 120.7 | 10 |
| T17 | 28 | September 7, 2006 | 23 | 56.74 | 44.7 | 7.5 |
| T20 | 31 | October 25, 2006 | 7.5 | 44.34 | 25.3 | 0.49 |
| T28 | 42 | April 10, 2007 | 50.4 | 358.1 | 137.2 | 11 |
| T31 | 45 | May 28, 2007 | 76.8 | 360 | 114.3 | 11 |
| T32 | 46 | June 13, 2007 | 84.5 | 0.9 | 106.9 | 12 |
| T33 | 47 | June 29, 2007 | 8.1 | 294.9 | 95.6 | 12 |
| T34 | 48 | July 19, 2007 | 1.3 | 244.7 | 34.0 | 8 |
| T35 | 49 | August 31, 2007 | 63.5 | 110.6 | 87.0 | 10 |
| T38 | 53 | December 5, 2007 | -78.9 | 175.1 | 69.7 | 0.33 |
| T40 | 55 | January 8, 2008 | -12.2 | 130.4 | 37.1 | 1.95 |
| T42 | 62 | March 25, 2008 | -27.1 | 156.4 | 21.3 | 10 |
| T48 | 95 | Dec. 5, 2008 | -10.28 | 178.78 | 25.01 | 14.2 |

A major concern when studying and analyzing spectral data of Titan is its dense atmosphere. The dominance of the atmospheric signal is a challenge to image processing because absorption by and scattering within the atmosphere significantly affect the detected signal. A small but substantial amount of atmospheric methane of ~5% (*Atreya*, 2007; *Schröder and Keller*, 2008) dominates the spectrum of Titan (see Figure 3.1). Strong molecular absorption prevents the direct detection of surface reflectance within broad wavelength regions (*Combes et al.*, 1997). Imaging of the surface is only possible outside those wavelength ranges, where the transmission is increased. These are referred to as 'atmospheric windows', marked by the blue vertical bars in Figure 3.1. Atmospheric windows with different widths are centered at 0.76, 0.83, 0.94, 1.08, 1.28, 1.6, 2.0, 2.8, and 5.0 µm (*Griffith et al.*, 2003; *Brown et al.*, 2004; *Sotin et al.*, 2005; *Barnes et al.*, 2007a; *Clark et al.*, 2010). Owing to the dominant atmospheric signal within the spectrum and the narrow size of most of the atmospheric windows, characteristic absorption bands of candidate surface compounds can hardly be recognized. Thus, VIMS-imaging would be more suitably labeled a multispectral technique (*Jaumann et al.*, 2008). However, compared to 'conventional' imaging with its two spatial dimensions and just one or only very few spectral dimensions, the significance of VIMS data remains high.

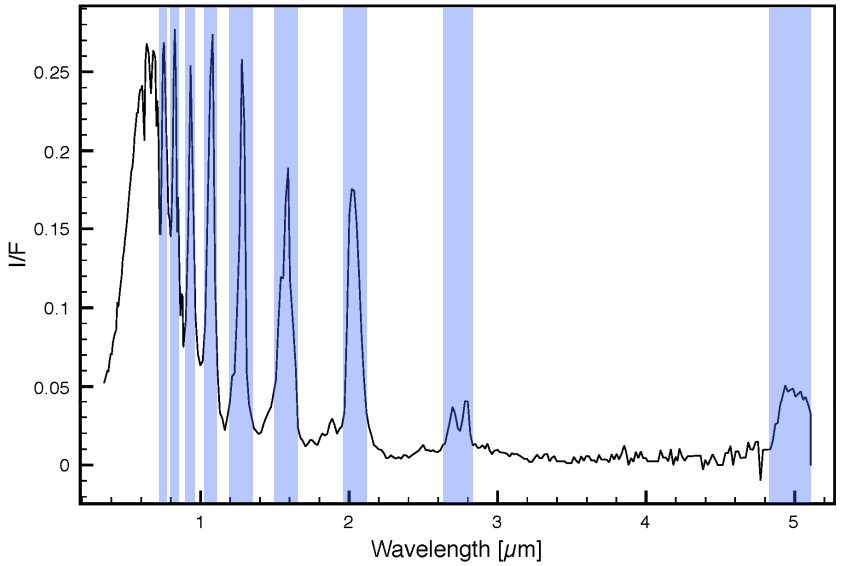


**Figure 3.1:** Exemplary average spectrum of the bright spectral unit (VIMS observation T5, April 16, 2005). Atmospheric windows are highlighted in blue.

Besides a high level of methane absorption, another factor to compromise spectral imaging on Titan is backscattering by atmospheric particles (*Combes et al.*, 1997). The scattered component of the detected signal does not interact with the surface, which makes it a serious source of image distortion. Scattering brightens up the image and reduces its contrast (*Lillesand et al.*, 2003). Scattering particles, such as haze and aerosols, account for Titan's orange-brown color at visible wavelengths

(*Sagan and Khare*, 1979). The influence of scattering is variable within the broad wavelength range covered by VIMS. It is most severe at shorter wavelengths, and mainly within the range of the visible light, with decreasing intensity toward greater wavelengths (*Lillesand et al.*, 2003; *Richardson et al.*, 2004; *Barnes et al.*, 2007a,b).

Besides the wavelength-dependent variation of atmospheric scattering and absorption, the magnitude of these distortions can additionally vary within one image, e.g. as a function of the phase angle (*Rodriguez et al.*, 2009a). Eliminating or even reducing atmospheric effects in order to isolate the surface signal is a complex task due to highly variable additive and multiplicative effects by the atmosphere on the spectra (*Le Mouélic et al.*, 2010). This high variability and the unknown composition of Titan's atmosphere cause difficulties in the implementation of empirical models or even radiative transfer modeling (*Le Mouélic et al.*, 2010). Omitting the removal of atmospheric effects altogether and assuming the effect of the atmosphere on different observations or even within one image to be equal is a simplification that could handicap the interpretation of the data and influence the results of image analysis.

## 3.2 Imaging Science Subsystem (ISS)

The Imaging Science Subsystem (ISS) onboard Cassini obtains 2D-images of a very high spatial resolution and is therefore highly relevant in revealing and identifying surface features on Titan (*Porco et al.*, 2004; *Coustenis and Taylor*, 2008). Other scientific objectives that motivated the ISS survey are to investigate the atmospheres of both Saturn and Titan (*Porco et al.*, 2004; *Perry et al.*, 2005).

The system consists of a wide-angle television camera (FOV: $3.5^\circ \times 3.5^\circ$) and a narrow-angle telescope (FOV: $0.35^\circ \times 0.35^\circ$) (*Coustenis and Taylor*, 2008). Both cameras detect and store data on CCD arrays (*Porco et al.*, 2004; *Coustenis and Taylor*, 2008). The spectral range between 0.2 and 1.1 µm is covered by several spectral filters integrated in the system. Despite considerable haze scattering at shorter wavelengths, the detection of surface features is possible. Filter CB3 (at 0.938 µm) is dedicated to surveying Titan through its dense atmosphere as it is situated in the middle of a methane window (*Porco et al.*, 2004). The preprocessing of ISS-data comprises flatfield calibration, noise removal, and band arithmetics in order to normalize images and remove scattering and phase-angle effects, and finally the geometric projection of the images (*Porco et al.*, 2004; *Perry et al.*, 2005; *Stephan et al.*, 2009). ISS obtains images at different spatial resolutions in order to provide global, comprehensive data as well as regional and local close-ups. ISS-data also permit the investigation of temporal dynamics of surface features due to repeated sensing of the same target.

During the Cassini prime mission, pixel scales down to a few hundred meters were achieved (*Porco et al.*, 2005). Up to now, global mosaics[1] have been created and

[1] http://ciclops.org/maps/maps.php

supplied by NASA/JPL/Space Science Institute with pixel scales up to 1 km and at an almost complete surface coverage (*Turtle et al.*, 2009) (see Figure A.1 and Figure A.4, Appendix).

Actually, both the ISS and the VIMS instrument imaged the leading hemisphere of Titan since the beginning of the Cassini mission and gradually completed the coverage. Even the trailing hemisphere, the mapping of which began in February 2007, is now satisfactorily resolved (e.g. *Perry et al.*, 2007). Due to the fainter sunlight at high northern latitudes in winter, both near-infrared sensors did not begin to observe the north-polar area until August 2009, when Titan attained its spring equinox (*Stephan et al.*, 2009).

## 3.3 Radar-SAR

Cassini RADAR (Radio Detection and Ranging) is a multimode microwave Ku-band-instrument operating at 13,8 GHz, $\lambda$ 2.17 cm, developed and designed at JPL/NASA and ASI (*Elachi et al.*, 2004). In contrast to the other near-infrared imaging facilities onboard Cassini, this active remote sensing instrument is not influenced by Titan's opaque atmosphere or by solar illumination. The Cassini Radar experiment was mainly motivated to determine the physical state, topography, and composition of Titan's surface, to measure global temperatures as well as the general circulation (*Elachi et al.*, 2004). Imaging-mode observations of the radar instrument are devoted to the detection and mapping of small-scale features, such as cryovolcanic domes and craters, as well as to comprehensive imaging of the polar regions (*Elachi et al.*, 2004).

Radar offers four operational modes to gain data on Titan's surface (*Elachi et al.*, 2004; *Coustenis and Taylor*, 2008): Elevation profiles of the surface are obtained with the radar instrument in altimeter mode. This mode operates at a statistical height accuracy of around 35 to 50 m (*Zebker et al.*, 2009). In scatterometer mode the instrument yields large-scale information on the surface slope, the density, and the electrical properties of the upper surface layer (*Elachi et al.*, 2004; *Wye et al.*, 2007). Brightness temperature maps and information about the thermal emission are acquired in the passive radiometric mode (*Elachi et al.*, 2004; *Janssen et al.*, 2009), whereas thermal emission is associated with the density and dielectric constant of the target material. In active SAR-mode (Synthetic Aperture Radar), the instrument is sensitive to the physical properties of the surface, such as material composition, and volume scattering properties (*Elachi et al.*, 2006). The detected radar-SAR signal is also affected by the local topography, i.e. the slope and orientation of the terrain relating to the illumination angle, and the roughness of the surface at a wavelength scale of 2.17 cm (*Elachi et al.*, 2006). High radar backscatter indicates a high surface roughness but could also be caused by surfaces directly facing the sensor and/or highly conductive materials (*Burr et al.*, 2009). Surface data obtained in this mode are particularly relevant to the present work.

The SAR instrument maps the surface of Titan in the form of long thin strips (swaths) reaching ground resolutions of up to 300 m/pixel, which exceeds the spatial capabilities of the other radar modes since the operation at closest approach (i.e. at spacecraft altitudes of 1,000 to 4,000 km) is reserved for SAR (*Elachi et al.*, 2006; *Coustenis and Taylor*, 2008). Thus, radar-SAR swaths have a width of 120 up to 450 km and lengths of several thousand kilometers (*Elachi et al.*, 2004) (see Table 3.2). The best ground resolution is achieved at the center of each swath and decreases toward the edges. Overlapping SAR data even offer the opportunity to determine surface heights (e.g. *Stiles et al.*, 2009).

Given the high spatial resolution, radar-SAR provides a useful complement to near-infrared imagery, which offers a more global view. Small-scale regions of interest such as the Huygens Landing Site, and the Sinlap and Selk craters (see nomenclature in Figure A.1, Appendix) have even been investigated on the basis of both VIMS and radar data in combined studies (e.g. *Soderblom et al.*, 2007a; *Le Mouélic et al.*, 2008; *Soderblom et al.*, 2010a).

Because of its particular geometry and recording conditions, radar-SAR still does not cover the entire surface of the moon. At the end of Cassini's prime mission in 2008, the long and thin radar swaths covered about one-third of Titan's surface. The radar swaths dealt with in the present study add up to a coverage of about 40% (swaths TA to T57, see Table 3.2, Figure A.2, and Figure A.2, Appendix). Since the radar-SAR sensor is independent of specific illumination conditions, Titan's entire surface

**Table 3.2:** Characteristics of the radar-SAR swaths used in this work.

| Orbit | Date | Altitude (km) | Latitude range (°) | Longitude range (°) | Incidence angle (°) |
|---|---|---|---|---|---|
| TA | 2004 Oct 26 | 1200 | 32-53N | 130-10W | 2-46 |
| T3 | 2005 Feb 15 | 950 | 2S-22.5N | 0.4-133W | 1-30 |
| T7 | 2005 Sept 07 | 950 | 25-75S | 23-350W | 7-35 |
| T8 | 2005 Oct 28 | 450 | 7-11S | 186-314W | 1-31 |
| T13 | 2006 Apr 30 | 1850 | 3-18S | 60-172W | 10-29 |
| T16 | 2006 Jul 22 | 950 | 13-90N | 138-358W | 9-40 |
| T17 | 2006 Sept 07 | 950 | 5-14N | 33-68W | 29-45 |
| T18 | 2006 Sept 23 | 950 | 15-65N | 105-346W | 19-45 |
| T19 | 2006 Oct 09 | 950 | 2S-42N | 160-318W | 9-39 |
| T21 | 2006 Dec 12 | 950 | 25S-50N | 195-290W | 9-57 |
| T23 | 2007 Jan 13 | 950 | 35S-53N | 95-335W | 9-39 |
| T25 | 2007 Feb 22 | 953 | 33S-62N | 215-55W | 8-39 |
| T28 | 2007 Apr 10 | 951 | 18S-62N | 5-37W | 6-36 |
| T29 | 2007 Apr 26 | 951 | 4S-90N | 195-360W | 0-38 |
| T30 | 2007 May 12 | 950 | 35-68N | 225-325W | 9-48 |
| T36 | 2007 Oct 02 | 950 | 35-77S | 24-196W | 30-61 |
| T39 | 2007 Dec 20 | 953 | 26-89S | 13-220W | 9-55 |
| T41 | 2008 Feb 22 | 959 | 16N-45S | 53-220W | 2-41 |
| T43 | 2008 May 12 | 950 | 32N-37S | 73-219W | 8-41 |
| T44 | 2008 May 28 | 1320 | 25N-35S | 93-225W | 8-26 |
| T48 | 2008 Dec 05 | 3575 | 53N-34S | 94-239W | 11-75 |
| T49 | 2008 Dec 21 | 3575 | 31N-72S | 207-280W | 8-39 |
| T50 | 2009 Feb 07 | 3575 | 18N-61S | 293-17W | 30-59 |
| T55 | 2009 May 21 | 965 | 39N-76S | 120-285W | 10-39 |
| T56 | 2009 June 6 | 965 | 31N-73S | 129-319W | 9-39 |
| T57 | 2009 June 22 | 955.5 | 19N-85S | 127-330W | 30-75 |

is imaged roughly in equal proportions. Titan's north-polar region as well as the area around its equator have received the best radar coverage with many SAR swaths even overlapping (see Figure A.8, Appendix).

## 3.4 Software and Preprocessing of Data

Geodata preprocessing comprises the entire workflow that is necessary to enable the combined analysis of image data from different sources. Through radiometric calibration the signal recorded by the particular sensor is adjusted for distorting signals and is translated into a physical value (e.g. radiance or reflectance) (*Schowengerdt*, 1997). Geometric referencing, i.e. creating a spatial link between different datasets, is another important step preceding any further work with geographic data from different sources (*Schowengerdt*, 1997; *Jaumann et al.*, 2006).

**VIMS**

Preprocessing of VIMS data includes their conversion into raw image cubes, which is conducted by NASA/JPL. Subsequently, the data are supplied to the VIMS team (*Jaumann et al.*, 2006). Before the launch of the spacecraft a spectral calibration was performed, in which each spectral channel was assigned to a certain wavelength interval by specification of the center wavelength and the spectral width (*Capaccioni et al.*, 1998; *Brown et al.*, 2004). Subsequent to each VIMS observation, any disturbing signals, such as dark current and thermal background signals, are subtracted (*Capaccioni et al.*, 1998; *Brown et al.*, 2004). To account for the instrument response and to transfer the measured values (digital numbers, DN's) into physical units, such as radiance or reflectance, each pixel is then multiplied by a radiometric response function, which is continuously updated over the course of the Cassini mission (*Brown et al.*, 2004; *McCord et al.*, 2004). To obtain reflectance data (or the radiance factor, I/F), the radiance is then divided by the incident solar radiation, for each wavelength band separately. Compatibility between VIMS-VIS and VIMS-IR data is ensured through integration to a spatial resolution of $500 \times 500$ µrad and by adjustment of the exposure times of both instruments (*Brown et al.*, 2004; *McCord et al.*, 2004). In order to process and analyze the data, VIMS cubes are converted into the VICAR-format (Video Image Communication and Retrieval) by the user. VICAR was developed at the JPL for the purpose of processing multidimensional imaging data (*Duxbury and Jensen*, 1994).

VIMS datasets were geometrically corrected and map-projected based on positional data of the spacecraft and pointing data of each flyby, provided as SPICE-kernels (Spacecraft Planet Instrument C-matrix Events) (*Jaumann et al.*, 2006). A suitable reference body for the particular planetary object is available that is gradually being improved over the course of the Cassini mission (*Jaumann et al.*, 2006). Through map-projecting, VIMS-VIS and VIMS-IR-images are co-registered, which is essential for data acquired in high-resolution mode.

A global VIMS mosaic was created for the present comprehensive global analysis to facilitate the mapping of spectral units and their combination with radar data. VIMS data obtained between October 2004 and May 2008 (see Table 3.1) are the basis for each global VIMS map in this work. The VIMS cubes were projected using simple cylindrical projection (centered at 180°W, 0°N) with a spatial resolution of 10 km per pixel. Resampling was done using the nearest-neighbor algorithm in order to transfer the original data to a new coordinate system while maintaining the original spectral information (*Jaumann et al.*, 2006; *Stephan et al.*, 2009). In order to combine different VIMS cubes within one comprehensive map, the data were mosaiced. Geometric referencing as well as mosaicing were performed using the VICAR development environment. VIMS mosaics with deficient ground resolution, low signal-to-noise-ratios, short exposure times, and unfavorable illumination conditions were rejected following *Stephan et al.* (2009). Beyond the equatorial region (latitudes outside $\pm$ 30°), the VIMS coverage and/or ground resolution is currently not adequate for a comprehensive spectral analysis, thus mapping of spectral units was confined to latitudes between $\pm$ 30°.

For regional and local analyses of spectral data in combination with radar-SAR, both datasets were transferred into an orthographic projection, with a higher spatial resolution according to the particular original ground resolution of the best-resolved dataset. In this case, oversampling of the pixel ground resolution was applied to maintain both the spatial and spectral information in the resulting map (*Jaumann et al.*, 2006). Spectral analysis of VIMS data was conducted using the ENVI software (ENvironment for Visualizing Images) which offers basic and advanced spectral analysis techniques, such as the display of spectral remote sensing data, the extraction of spectra, and the application of more sophisticated analysis and classification algorithms.

**Radar**

Radar-SAR swaths utilized in this work were retrieved from the website of the Planetary Data System (PDS)[2]. The radar swaths used here were acquired between October 2004 and June 2009 (T00A to T057, see Table 3.2). The preprocessing and calibration of Cassini's radar imagery is described in *Stiles et al.* (2006). SAR data of the lower and mid-latitudes were processed and reprojected into a simple cylindrical (equidistant) projection, using the nearest-neighbor technique for resampling. Geometric preprocessing is performed within the USGS image processing environment ISIS3 (Integrated Software for Imagers and Spectrometers). The global map thus generated is centered at 180°W, 0°N, and allows the joint analysis with the VIMS and ISS database. Polar maps were created following the same preprocessing steps and applying a polarstereographic projection.

[2]http://pdsimg.jpl.nasa.gov/

**ISS**
A global high-resolution monochromatic ISS map is included in this study for spatial reference (see Figure A.4, Appendix). This ISS map supplied by the NASA/JPL/Space Science Institute[3] is already radiometrically preprocessed and geometrically projected into the simple cylindrical projection with the above-mentioned specifications, which is required for compatibility with the VIMS and radar database.

## 3.5 Methodology

**Combination of image datasets**
Joint analyses of Cassini imaging data supply additional information about the target under investigation. In this work, the whole set of data available was combined, aiming to gain comprehensive insights into the characteristics of the fluvial terrain. Taken together, Cassini image data help to enlighten interrelations between different surface types and geologic phenomena. A combined analysis of geodata requires using a common map projection based on identical specifications (spatial resolution, central coordinates). The simple cylindrical projection for the global views is chosen for reasons of comparability with other studies, (cf. *Barnes et al.*, 2007a; *Stephan et al.*, 2009). The global views generated cover the area between 60°N and 60°S. Simple cylindrical global maps are equidistant at the equator with increasing distortion toward higher latitudes. This projection is neither an equal-area nor a conformal map projection. Data covering higher latitudes were converted and displayed in polarstereographic projection to avoid any major spatial distortions.

The entire image database was integrated into the ArcGIS software provided by ESRI[4], which enables exploring and analyzing spatial raster and vector data. The subsequent mapping of VIMS units and fluvial valleys was conducted in the same software environment.

When comparing spectral VIMS and radar data, it is important to consider that the two sensors are sensitive to different characteristics of the surface. VIMS data shed light on the composition of the upper cm or mm of the surface (*Clark et al.*, 2010) (and often come with a significant contribution by the atmosphere to the signal), yet the detected signal can also be influenced by the aggregate state and other physical/optical characteristics of the uppermost surface layer, such as its grain size. By contrast, the radar signal is not modified by the atmosphere and reflects the character of the surface from a more physical perspective (e.g. regarding surface roughness). Radar-SAR is sensitive to the upper centimeter down to ten meters below the surface, depending on the radar wavelength and the target material (*Elachi et al.*, 2004; *Paillou et al.*, 2006). Thus, both datasets are not necessarily comparable and there is hardly any correlation

[3] http://ciclops.org/maps/maps.php
[4] http://www.esri.com

between them (*Soderblom et al.*, 2007a; *Le Mouélic et al.*, 2008). On the other hand, data provided by the two instruments are not redundant, and help investigate the surface properties in two different ways.

**Spectral analysis of VIMS data**

The analysis of VIMS data in this work is twofold: On the one hand, global views of spectral data were generated to broadly classify fluvial terrains in terms of their spectral properties. On the other hand, detailed spectral analyses were performed in selected areas. In some cases, spectral subsets were created in order to eliminate methane absorption bands and to focus on subtle spectral differences. To deal with the unfavorable signal-to-noise-ratio especially toward longer wavelengths, spectral bands within one methane window were sometimes averaged ('coadding'). A detailed description of this technique is given in Section 4.2.

A number of techniques were designed to remove or reduce the unfavorable effects of the atmosphere on VIMS spectra. Due to the unknown composition and dynamics of the atmosphere and the unknown exact surface albedo, physical approaches to remove atmospheric effects have little prospect of success. Physical correction algorithms based on simplifying assumptions about physical properties of the atmosphere might also remove surface features. Empirical approaches are to be preferred, which derive optical and atmospheric properties from the dataset itself in a fast and simple way (*Rodriguez et al.*, 2006, 2009b). Empirical approaches take the varying influence of the atmosphere into account when studying data obtained at different viewing angles (*Le Mouélic et al.*, 2010). Many of the empirical methods take advantage of the negligibly low aerosol scattering at 5 µm, using it as a reference (*Rodriguez et al.*, 2006; *Le Mouélic et al.*, 2010). Currently, one of the most straightforward techniques to remove the additive component of the measured signal in order to obtain fully homogeneous large-scale or even global maps is to remove the measured reflectance at the edge (or bottom) of the spectral transmission window from the signal at the center of the window (*Le Mouélic et al.*, 2010). A general drawback of empirical corrections is that a particular method is often only applicable to the dataset by means of which it is generated, because the algorithms are still very sensitive to the pronounced variations resulting from varying phase angles.

To enhance the surface-related spectral contrast and to account for illumination differences, simple band ratioing of atmospheric wavelength bands was preferred. Ratio-images were generated to provide a general idea of the spectral character of certain areas and to emphasize overall spectral variations. Ratioing is the application of simple band arithmetics to wavelength bands, performed for each image pixel separately (*Clark and Roush*, 1984; *Lillesand et al.*, 2003). Division and subtraction of two different wavelength bands is often applied in imaging spectroscopy of terrestrial or planetary targets (e.g. *Barnes et al.*, 2007a; *Clark et al.*, 2010). Ideally, adjacent spectral bands are selected to study the absorption of certain compounds, given that the

absorption properties of potential target materials are known. Ratios illustrate the variances in slope of reflectance curves and enable the isolation and measurement of diagnostic absorption depths of certain materials (*Lillesand et al.*, 2003). In the case of Titan, the identification of potential surface materials is only conceivable within the 5.1 µm and (possibly) the 2.7 µm atmospheric window (*Clark et al.*, 2010). The narrow size of the other atmospheric windows prevents the secure identification of any absorption band. Besides, the distance between individual atmospheric windows is too great to allow measuring of the depth of potential absorptions.

Ratioing can also be applied to wavelength bands which are at a significant distance from each other within the spectral profile, with the result of enhancing spectral variations and reducing the effects of different illumination conditions, topography, and shadows within one scene or between different observations (*Lillesand et al.*, 2003). Appropriate band ratios stretch the reflectance values with the effect of higher image contrast and better discernibility of surface types (*Lillesand et al.*, 2003). It is assumed that albedo differences due to the atmosphere, illumination geometry, and shadows have a multiplicative effect on the entire pixel spectrum. Since illumination effects and the atmospheric influence also have an additive component (both in the case of Titan and Earth) atmospheric distortions tend to be increased rather than reduced through ratioing. This applies where spectral bands are included that are influenced by atmospheric scattering and absorption to a different degree and in a non-multiplicative way.

In any case, the pixel values contained in the resultant graytone-ratio image do not represent physical characteristics of the surface anymore (i.e. its reflectance) but must be regarded as a processed mapping product. To further increase the information content of the generated image, three different ratio maps of the same investigation area can be displayed within one false-color RGB-composite (*Lillesand et al.*, 2003). For the purpose of spectral mapping of Titan's surface, an RGB-composite with the following specifications is frequently used: R: 1.58/1.28 µm, G: 2.0/1.28 µm, B: 1.28/1.08 µm. The resultant ratio image emphasizes subtle spectral contrasts (see Figure 6 in *Jaumann et al.* (2008) and Figure A.5, Appendix) thus revealing the spatial distribution of certain surface units/materials.

**Mapping of fluvial features based on radar data**

Radar-SAR provided the primary database for the identification of fluvial valleys and to create a global valley database. Titan's linear, putatively fluvial features emerge as radar-dark and radar-bright linear features or as a pair of bright and dark lineaments resulting from the topographic incision of the channel. The key criteria for visually identifying linear topographic depressions as valleys, according to *Lorenz et al.* (2008a) and *Burr et al.* (2009), are their linear shape and a substantial contrast to the surrounding terrain, a typical bright/dark pairing, and a morphological resemblance to terrestrial rivers, i.e. their arrangement in hierarchical branching networks.

The resulting map of fluvial valleys of Titan's lower and mid-latitudes is depicted in Figure 5.12 and Figure A.7 (Appendix); the high latitudes of both hemispheres are shown in Figure A.8 (Appendix). In order to gain a deeper understanding of fluvial flow on Titan, descriptive data on the particular fluvial features were studied and recorded in the database, such as their length, width, morphological characteristics, and the complexity of the network as determined by their drainage pattern. Stream order labels were used to mark the number of tributaries counted upstream from the receiving stream (*Butzer*, 1976; *Ahnert*, 2003).

Putative fluvial lineaments were captured and processed as vectors due to their predominantly linear shape (see Figure 3.2). Only a few valleys have widths of several kilometers, thus possessing a rather laminar shape according to the spatial capabilities of the radar sensor. In this case, the course of the center line of the valley was recorded. The perceptibility of linear landforms further depends on the viewing geometry. Linear features aligned orthogonal to the viewing direction of the radar sensor are favored as this geometry enables topographic shading and thus provides a pronounced contrast in radar images (*Burr et al.*, 2009).

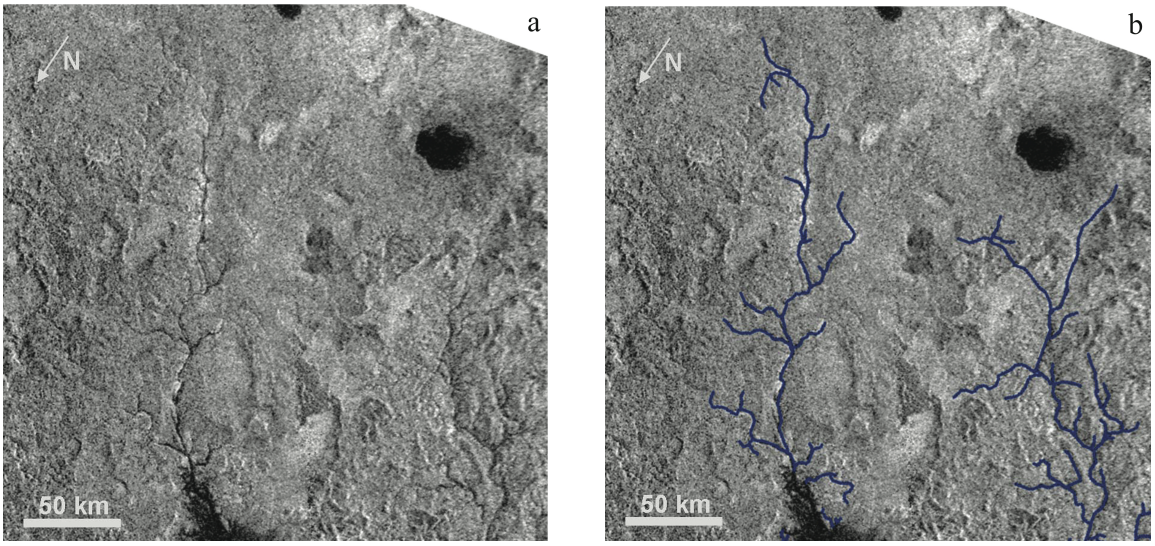


**Figure 3.2:** Mapping of fluvial channels close to Titan's north pole. a: Radar-SAR observation T28 (April, 10, 2007). b: Mapping of fluvial channels. Fluvial valleys were gathered as vectors in a GIS environment, highlighted in blue. Images are centered at 248°W, 73°N.

The GIS-based database of fluvial features on Titan offers tools to assess the geometric dimensions (such as lengths and widths) of linear features. These dimensions are relevant for comparisons with Martian and terrestrial valleys as well as to estimate the channels' discharge volumes. The length of fluvial valleys can be determined automatically. Estimating the width of a valley is made difficult by the fact that the lateral extent of most of these features is small, i.e. near the resolution limit of the radar instrument. Generally, extended linear features with a high contrast can be recognized even if their width is below the image resolution (*Schowengerdt*, 1997; *Barnes et al.*, 2007b). However, it is not possible to ascertain the minimum size of an

object detectable by radar, since its visibility depends on intrinsic physical and morphological properties of the object and its surroundings (such as composition, slope, and roughness of the surface) as well as on the viewing geometry and the ground resolution at that specific location. Generally, reasonable minimum sizes, which are necessary to securely identify an object as a discrete entity range between the size of one pixel and up to 3 $\times$ 3 pixels (*Knight and Lunetta*, 2003). If one defines valleys as extended linear features, it is plausible to expect their minimum width required for a secure identification to be below the pixel size since linear features can be recognized even through a series of mixed pixels (*Barnes et al.*, 2007b).

The bright/dark pairing of deeply incised fluvial channels caused by certain observation geometries entails unknown fractions of the valley escarpment and valley floor being hidden by radar shadow. Further uncertainties arise from the fact that the interior channel, which has experienced or still experiences fluid flow up to bankfull stage (referred to as 'channel'), and the surrounding eroded valley, which is occupied by the channel (referred to as 'valley') are often hard to distinguish (*Perron et al.*, 2006; *Komatsu*, 2007; *Jaumann et al.*, 2008). The negative relief of a valley may have been shaped by long-term incision of the interior channel in the vertical direction and frequent shifts and relocations of the riverbed horizontally. It must be assumed that the linear features visible in radar images represent the size of the entire valley, rather than that of the interior channel. Therefore, gathering morphological information is complicated, especially in relict landscapes, geometric measurements (i.e. the width of the riverbed) can be imprecise and calculations of channel discharges provide only upper limits. However, SAR data provide an overview of the geometric dimensions of Titan's valleys and permit comparing Titan's valleys to those on Mars and Earth.

Radar-SAR data were also used to gain a general geological overview of the entire terrain and in order to understand the geological context since it allows the recognition of medium and small-scale landforms, such as mountains, dunes, and craters. The high resolution provided by radar makes it possible to exhaust the full potential of the Cassini imaging instruments.

# Chapter 4

# Analysis of Surface Units and Stratigraphic Relation

## 4.1 Introduction

This Chapter presents the results of spectral mapping based on VIMS and ISS data. The optimal handling of VIMS data utilized in this research will be explained. Next, Titan's overall spectral properties will be introduced as well as the distribution and interrelations between the spectral surface types. The last Section of this Chapter outlines Titan's small and medium-scale geologic features and their spatial distribution.

## 4.2 Surface Map

Monochromatic VIMS maps and images obtained by the ISS instrument reveal the stratification of Titan's surface into bright and dark terrains (cf. Section 2.3.2). Figure A.3 (Appendix) shows a monochromatic VIMS map of Titan's lower and mid-latitudes (reflectance at 2.0 µm) with a spatial resolution of 10 km. Figure A.4 (Appendix) depicts Titan's reflectance at 938 nm wavelength within the same region at a ground resolution of 4 km, acquired by the ISS camera. Obviously, ISS and VIMS maps return the same distribution of bright and dark surfaces, confirming the correlation between Titan's reflectance at 0.94 µm and at 2.0 µm proposed by (*Lemmon et al.*, 1993). To improve the contrast delivered by the VIMS map, three different band-ratio images of wavelength bands within Titan's atmospheric windows are combined and displayed as false-color RGB-composites. At the ratio of R: 1.59/1.27 µm, G: 2.03/1.27 µm, and B: 1.27/1.08 µm, the subdivision of the dark surfaces into dark blue and dark brown terrains becomes apparent (see Figure A.5, Appendix) (*Barnes et al.*, 2007a; *Soderblom et al.*, 2007a; *Jaumann et al.*, 2008; *Le Mouélic et al.*, 2008; *Jaumann et al.*, 2009; *Stephan et al.*, 2009). The distribution and outlines of bright terrains are still fully consistent with those of ISS and monochromatic VIMS maps (cf. Figure A.3, Figure A.4, and Figure A.5, Appendix).

**Spectral Surface Units**

Figure A.5 (Appendix) depicts a global color composite of Titan's surface based on VIMS data that is rescaled to 10 km pixel size. This reference scale provides a manageable dataset at an adequate precision, regardless of the fact that many datasets used are of a finer spatial resolution. The VIMS cubes incorporated in that image are listed in table 3.1. The VIMS coverage broadly spans Titan's lower latitudes; mapping of surface units was therefore limited to regions between 30°N and 30°S. VIMS data of higher latitudes were excluded, partly because of the insufficient spatial resolution of the cubes and partly due to disadvantageous illumination geometries. The results of visual mapping of spectral surface units between 30°N and 30°S based on the color-composite of Figure A.5 (Appendix) is shown in Figure A.6 (Appendix).

The spatial pattern of spectral surface units together with their spectral fingerprint can help to shed light on the origin of the subdivision of the surface. The largest unit in terms of area is the bright surface unit (about 60% of the area under investigation). Bright units are arranged in the form of islands and larger continents, such as Xanadu, Titan's largest continuous continent. Bright surfaces are interpreted to be older and elevated in contrast to dark 'nominal' surfaces (*Griffith et al.*, 1991; *Smith et al.*, 1996; *Barnes et al.*, 2007a; *Soderblom et al.*, 2007a; *Jaumann et al.*, 2009) and seem to be connected at higher latitudes. The bright unit is characterized by its high albedo in each of the atmospheric windows at short wavelengths, especially at 2 µm as well as in the ratio composite used. Bright continents and islands are interrupted by brown surfaces that broadly correlate with Titan's equatorial dunefields (*Lorenz et al.*, 2006; *Barnes et al.*, 2007a; *Soderblom et al.*, 2007a; *Le Corre et al.*, 2008).

The brown terrain is the second largest unit by area with nearly one-third coverage at low latitudes. Reflectance of the brown unit is comparably low in all atmospheric windows (*Barnes et al.*, 2007a) producing a dark brown tone in the false-color composite.

The third spectral unit appears blue in the ratio composite of Figure A.5 (Appendix) and often occurs at the eastern and southern boundaries of bright terrains (*Barnes et al.*, 2007b,a; *Jaumann et al.*, 2008). This unit has a low reflectance at longer wavelengths ($\geq$ 1.6 µm), and an increased reflectance at shorter wavelengths ($\leq$ 1.3 µm) (*Barnes et al.*, 2007a), which results in a higher ratio value in the blue channel of the ratio composite. The blue material probably has a higher water ice content compared to the other surface units, even though the entire spectral footprint and the geological significance is not fully explained so far (*Rodriguez et al.*, 2006; *Barnes et al.*, 2007b; *Soderblom et al.*, 2007a; *Jaumann et al.*, 2008). Some authors argue that the blue surfaces represent fluvial deposits (*Barnes et al.*, 2007b; *Jaumann et al.*, 2008), whereas, *Le Mouélic et al.* (2008) suggests that a non-dune eolian deposition, forming a very flat superficial layer, may account for the blue surfaces. This hypothesis will be verified in Section 5.3 of this work.

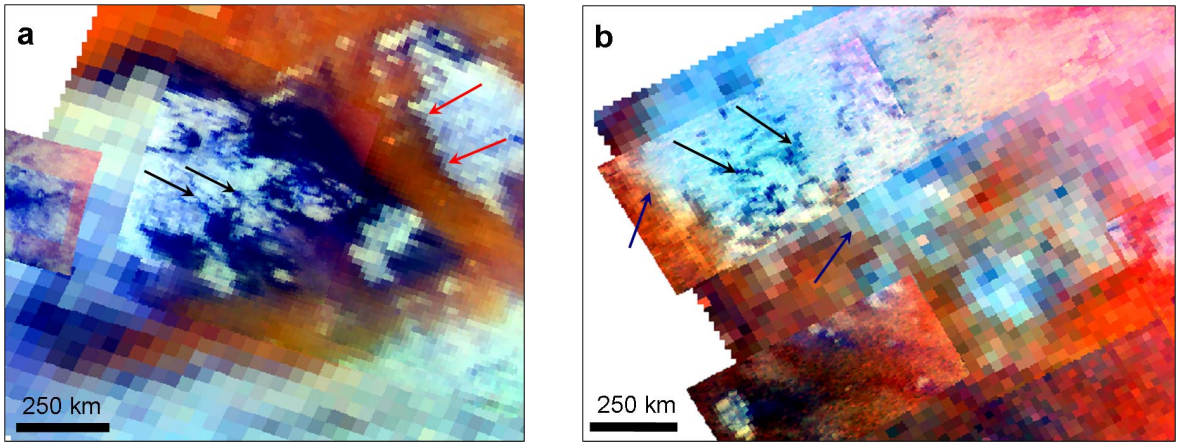


**Figure 4.1:** Boundaries of spectral units on Titan. a: VIMS observation T9 (December 26, 2005), subset. Image is centered at 50°W, 10°S. b: VIMS T13 (April 30, 2006), subset. Image is centered at 50°W, 20°N. Both images are coadded and ratioed (R: 1.59/1.27 µm, G: 2.03/1.27 µm, and B: 1.27/1.08 µm) in order to enhance the signal-to-noise ratio and the spectral contrast. The bright terrain has frayed eastern margins (blue arrows) and sharply defined western contours (red arrows). Blue streaks are integrated within the bright surfaces (black arrows).

Analyzing the boundaries of the surface units is crucial in order to understand their interplay and stratigraphy. The bright terrain has very distinct and clear-cut borders against the blue and brown units at its western margins. The eastern and sometimes the southern margins of the bright continents show rather frayed and diffuse transitions to the dark terrain (see Figure 4.1a). This morphology might be suggestive of eastward fluid transport (*Porco et al.*, 2005), which dissipates and blurs the eastern boundaries of bright units. Predominantly definite contours of the bright terrain at the western margins indicate that bright terrains might be older and raised above the dark lowlands (*Griffith et al.*, 1991; *Smith et al.*, 1996; *Barnes et al.*, 2007a; *Soderblom et al.*, 2007a; *Jaumann et al.*, 2009). Bright terrains might be remainder of a former continuous bright surface, but the reason for the subsequent division into near-infrared dark and bright regions is controversial. At some places the boundaries of the bright unit seem to be dissected by blue material, with a stubby but linear pattern (*Barnes et al.*, 2007b) (see Figure 4.1). This particular morphology led to the idea of fluvial erosion shaping the eastern boundaries of the bright continents (*Porco et al.*, 2005).

The transition between dark brown and dark blue terrains is mostly smooth. An exception to that observation can be found at the Sinlap crater, depicted in Figure 4.4 (Titan's nomenclature is shown in Figure A.1, Appendix) where distinct and clear-cut boundaries between blue and brown terrains prevail. However, the predominantly gradual transitions between blue and brown surfaces indicate a possible sedimentary origin of either or both units. Conceivably, smooth transitions might also be the result of data resolution. Whether the blue units immediately end at the brown dune unit or if they are located beneath each dunefield can not be determined. Which of these units is younger and superimposes the other is not resolved in this global frame.

**Pixel-based Analysis of the Spectral Characteristics**

Mean spectral profiles of the above-mentioned surface units are shown in Figure 4.2. For reasons of comparability, these spectra have been extracted from only one VIMS observation (T13 encounter, April 30, 2006, see Figure 4.4). This particular dataset has been chosen for the remarkably high contrast of the surface units at a favorable spatial resolution. For representativity, mean spectra were generated for each spectral unit over more than a hundred pixels. Figure 4.2 depicts the entire spectral range, where VIMS is sensitive, whereas in Figure 4.3 wavelengths bands within the atmospheric absorptions were cut out to increase perceptibility. Within the atmospheric windows, only minor differences were found between the three surface types in terms of their reflectivity. The most pronounced differences pertain at 2 µm. Less surprisingly, spectra of the bright surface unit have the highest reflectance in all the atmospheric windows considered. Blue surfaces have higher albedos than brown surfaces at shorter wavelengths ($\leq$ 1.3 µm) and a lower reflectance at longer wavelengths ($\geq$ 1.6 µm). The spectral curve of the dark brown surface unit has the flattest gradient compared to that of the other spectral units.

Another important aspect regarding the analysis of spectral properties of Titan's surface is the general decrease in brightness with increasing wavelengths due to the lower solar flux and detector sensitivity at longer wavelengths (see Figure 4.2) (*Barnes et al.*, 2007a). The low signal, particularly in Titan's widest atmospheric window around 5 µm, entails a low signal-to-noise ratio, which leads to a certain dithering of the spectrum (*Barnes et al.*, 2007a; *McCord et al.*, 2008; *Barnes et al.*, 2009a). Despite the unfavorable signal-to-noise ratio at long wavelengths, it is still possible to detect certain absorption bands of complex hydrocarbons (*McCord et al.*, 2008; *Clark et al.*, 2010). Certainly, the 2 µm window provides the best contrast of surface features and an optimal tradeoff between the influence of atmospheric haze, effective at shorter wavelengths, and the decreasing surface reflectance toward greater wavelengths (*Barnes et al.*, 2007a; *Le Mouélic et al.*, 2008).

Another particularity of the majority of Titan's spectra is a characteristic double-peak at 2.7/2.8 µm. The small drop between 2.7 and 2.8 µm is not to be mistaken for an absorption band but is due to a decrease of the methane transmittance of the atmosphere (*McCord et al.*, 2006, 2008). The spectral slope of these subwindows with a lower reflectance at 2.7 µm than at 2.8 µm argues strongly against water ice as a compound of Titan's surface (e.g. *McCord et al.*, 2006).

Figure 4.4 shows the three spectral units in a ratioed image, using the example of the Sinlap crater. Figure 4.4a depicts the result of simple ratioing of designated wavelength bands. To introduce the effect of spectral averaging (coadding) of adjacent wavelength bands within the atmospheric windows considered, the same dataset is displayed in Figure 4.4b, whereas coadding was performed before ratioing. In this dataset the pixel values of one particular spectral unit appear to be smoothed; the image shows less variation within uniform areas, e.g. within the brown surface unit.

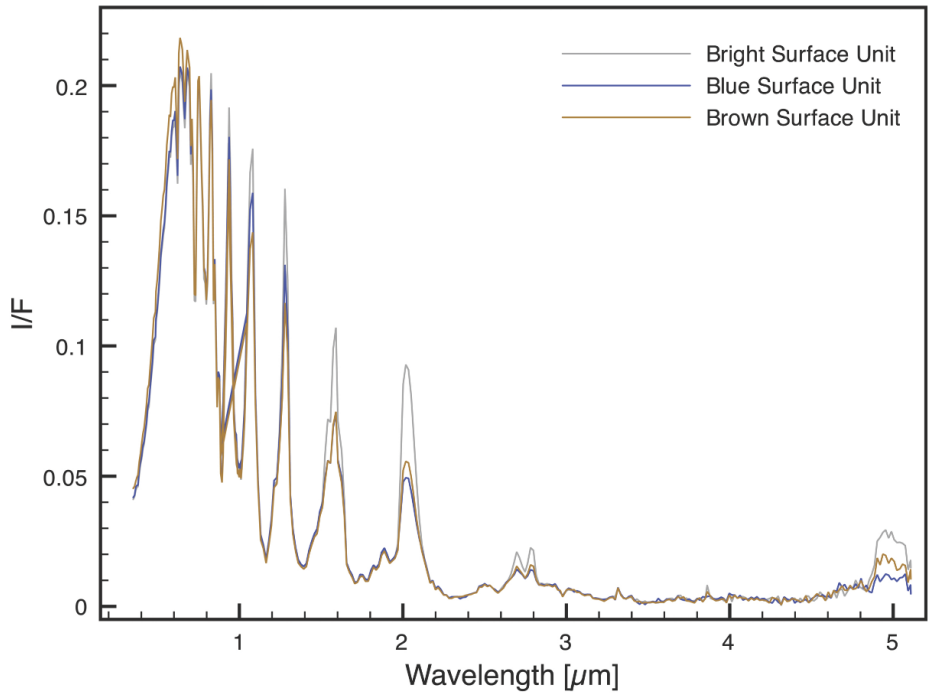


**Figure 4.2:** Mean spectra of the bright, dark blue, and dark brown spectral units. Extracted from VIMS T13 (April 30, 2006). The corresponding VIMS image is shown in Figure 4.4

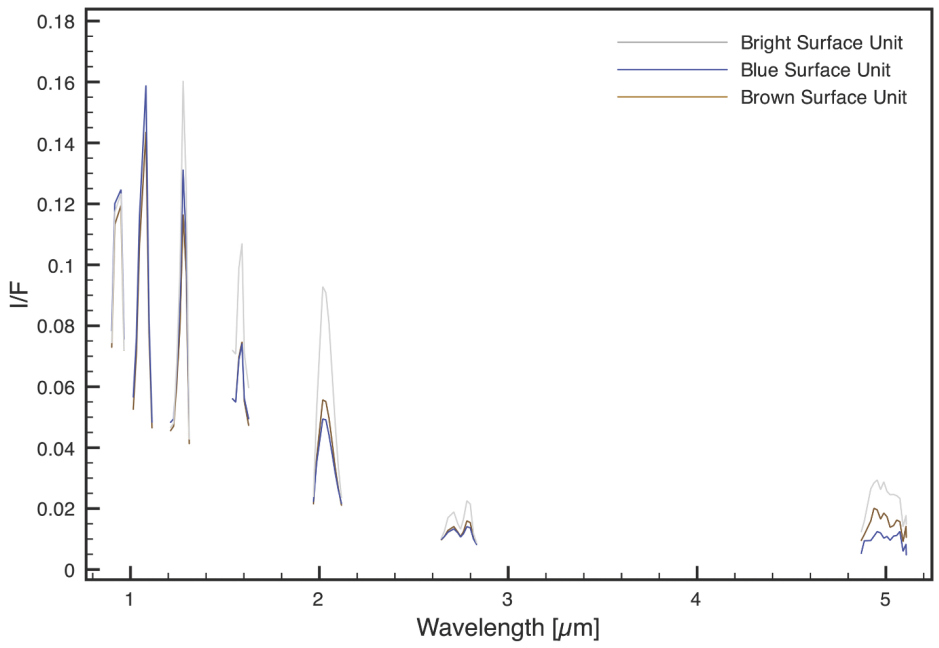


**Figure 4.3:** Same mean spectra as in Figure 4.2. Reflectance bands within the atmospheric absorption bands are omitted.

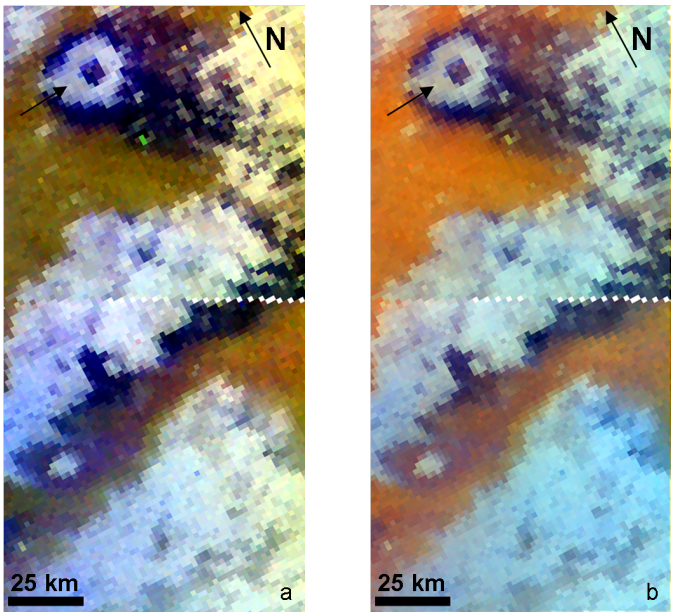


**Figure 4.4:** Spectral surface units in the Sinlap-region, VIMS observation T13 (April 30, 2006). Images are centered at 18°W, 0°N; the arrow indicates the position of the Sinlap crater. a: RGB ratio composite (R: 1.59/1.27 µm, G: 2.03/1.27 µm, B: 1.27/1.08 µm). b: RGB ratio composite, spectral averaged prior to ratioing (R: 1.59/1.27 µm, G: 2.03/1.27 µm, B: 1.27/1.08 µm).

Further, slight brightness gradients can be reduced by means of coadding, which becomes obvious at the bright surfaces distributed over several locations of the scene. Bright terrains show a distinct brightness gradient (Figure 4.4a) which seems to be considerably weaker after coadding (Figure 4.4b). Moreover, the overall brightness of the image seems to be reduced through spectral averaging. As a disadvantage of the technique, boundaries between blue and brown surface units are blurred. This effect most likely results from the incorporation of wavelength bands near the edges of the atmospheric windows, which tends to increase the overall influence of the atmosphere on the ratio.

The averaged spectra from Figure 4.2 are depicted as ratio spectra in Figure 4.5. Figure 4.5b depicts the effect of coadding on VIMS cubes prior to ratioing. Note that these spectra are averaged both spectrally and spatially. The overall shape of the ratio spectra remains the same even after coadding. However, the absolute differences between the ratio curves are reduced. This convergence is probably also due to an increased fraction of the atmospheric signal within the ratio, since wavelengths bands at the transition of surface signal and atmospheric signal, i.e. at the wings of the atmospheric windows, are included. Notably, the spectra of blue and brown units approach each other so that the distinction between these two units is more difficult to retrace (cf. Figure 4.4b).

Although the spectral properties within one individual surface unit are supposed to be similar, a certain variance of the pixel reflectance pertains. This variation, which often resembles salt and pepper noise, can result from instrument effects, from spatially varying influences of the atmosphere or from real surface (spectral) variability close to the pixel resolution, i.e. through integration of features smaller than the pixel size with distinct spectral properties. The degree of variation can be estimated by simple visual evaluation or by statistical parameters. Visual interpretation depends

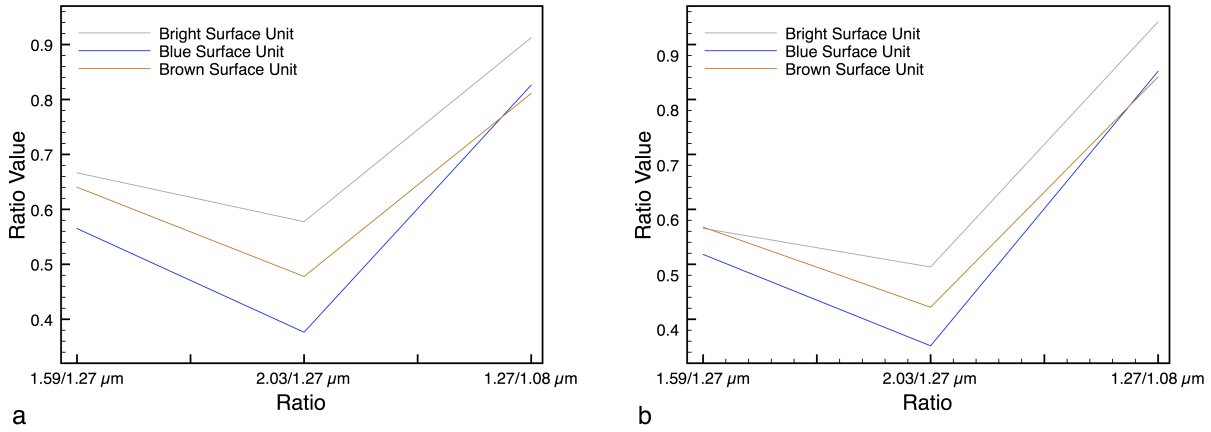


**Figure 4.5:** a: Ratio spectra of the spectral units, extracted from VIMS T13 (spatially averaged) (see Figure 4.2). b: Coadded ratio spectra of the spectral units (coadding of bands in the 1.08 µm-window: 4 wavelength bands between 1.06 and 1.11 µm; 1.29 µm-window: 3 wavelength bands between 1.27 and 1.31 µm; 1.58 µm-window: 8 wavelength bands between 1.52 and 1.64 µm; 2.03 µm-window: 9 wavelength bands between 2.00 and 2.13 µm).

on the stretch factor applied to the pixel values when displaying the image, while statistical parameters remain independent from the image processing and from subjective perception.

To determine the statistical variability of reflectance, the variance within one surface unit can be described by the standard deviation of the pixel values at one specific wavelength band (or ratio). This parameter specifies the averaged deviation of the values from the arithmetic mean. The standard deviations of the ratio spectra (from Figure 4.5) are plotted in Figure 4.6. The absolute value of this parameter is given through its distance to the x-axis and depends on the albedo of the unit. Thus, the bright surface unit has the highest standard deviation (high values are also achieved by each spectral unit at large ratio values, i.e. at 1.27/1.08 µm). The relative or comparative variance of the data can be determined based on the distance between the graphs of two spectral units. Again, the bright unit shows the maximum variance, indicative of a heterogeneous surface in spectral terms. Brown and blue units are statistically more uniform than bright surfaces. The blue unit has the smallest variance of all spectral units. The intermediate variance of the brown unit is consistent with observed spectral/compositional differences within that unit, as explained by *Barnes et al.* (2008). The observed differences between the standard deviations of the different surface types are most likely not caused by atmospheric or instrumental effects since such variations would have the same effect on all the surface types.

According to the visual survey and considering the variance, the blue unit is a comparably homogeneous surface unit. This suggests that any spectrally distinct features present within that unit are significantly smaller than the resolution of VIMS. The absence of mixed pixels confirms that the pixel size is an order of magnitude larger than any potential spectrally distinct features. *Jaumann et al.* (2008) discovered a certain structuring or succession within the blue surface unit located at Bohai Sinus,

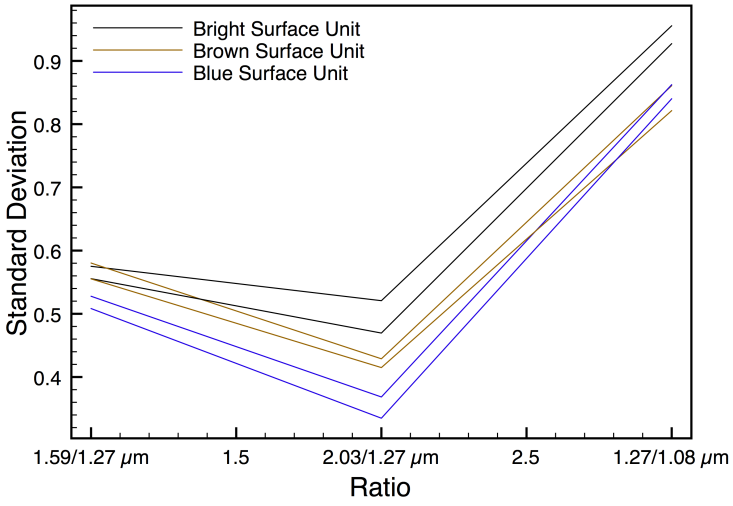


**Figure 4.6:** Standard deviations of the ratio value of the bright, blue, and brown spectral units, obtained from VIMS observation T13.

south of Quivira. The spectral diversity detected in this area could be explained by a transition in particle size or slight systematic compositional transitions. The observed stratification is most likely due to the high spatial resolution of VIMS data at this particular location, which is significantly coarser in the Sinlap-region analyzed in the present study. Brown areas exhibit a randomized salt-and-pepper effect, most likely because of their shallow spectral curve. Dark, absorbing surfaces (or spectral bands) tend to be more subject to instrument or random noise. The bright surface unit is the only one that shows structures which might reflect geologic/geomorphologic phenomena of a larger scale, such as topographic features or fluvial valleys (see bright units in Figure 4.1 and Figure 4.4). However, the size of those features is close to the resolution of the VIMS data which makes their geological interpretation difficult. Radar data of the regions mentioned reveal a rugged topography, sometimes in combination with fluvial features (cf. Section 5.1.1, Figure 5.1 and Figure 5.2). Compared to the blue and brown surface unit, albedo differences within the bright unit, such as the bluish streaks in Figure 4.1b, appear to be non-random and contiguous, with spectral properties halfway between those of the bright and blue units. Section 5.3 in the main Chapter of this work returns to this issue.

**Uncertainties**

Problems in interpreting the data mainly result from Titan's atmospheric interference. All the imaging techniques described, with the exception of radar, are influenced by Titan's dense atmosphere, to a different degree and depending on the wavelength.

Haze and limb brightening complicate image analysis, particularly at long path lengths and at shallow observation angles. As a consequence, near-infrared observations with different observation geometries are not necessarily comparable due to a combination of additive and multiplicative effects on the spectrum (*Rodriguez et al.*, 2009b). This is visible in the global view provided by VIMS in Figure A.3 (Appendix) and even in the ratio map (see Figure A.5, Appendix) in the form of many abrupt transitions between different datasets, which make the distinction of surface units

difficult. Further variations of the atmospheric opacity can result from cloud activity, the consistency of the haze, and from variations of atmospheric constituents.

Near-infrared images of Titan, including Cassini ISS and VIMS data, cover mainly equatorial regions and mid-latitudes; the near-infrared devices have only recently begun to cover the polar regions. Although Cassini radar offers insights into Titan's higher latitudes, spectral investigations were limited in these areas until the August 2009 equinox due to the northern winter darkness. Thus, the fraction of the surface covered by several instruments is small, which limits the validity of the results.

## 4.3 Titan's Geology, Topography, and Stratigraphy

This Section provides a brief introduction to landforms and geologic features on Titan and outlines their relations to spectral units and fluvial features. More detailed information is offered by the references given. Geologic features resulting from the action of liquid-related processes, namely fluvial channels and lakes, as the principal subject of this work, are discussed extensively in Section 5.

### 4.3.1 Dunes

Extensive dunefields, located around Titan's equator were first discovered by the radar mapper and described by *Lorenz et al.* (2006) and *Radebaugh et al.* (2008). With more than 5% ground coverage, sedimented dunes represent a substantial fraction of the surface. Dunes are located mainly between $\pm$ 30°; at higher latitudes the dunefields thin out into more isolated dune patches (*Radebaugh et al.*, 2008). Dunes appear linear and radar-dark on a slightly brighter interdune background. Dunes are oriented in quasi-west-to-east direction and divert and reconvert around radar-bright (elevated) features, which suggest a west-to-east relocation of the dune material by wind (*Lorenz et al.*, 2006; *Radebaugh et al.*, 2008). Titan's dunes resemble terrestrial longitudinal or linear dunes, such as the dunes of the Namib desert (*Lorenz et al.*, 2006). Titan's zonal dunes measure more than one hundred kilometers in length, at widths of 1 to 2 km, and with spacings between 1 and 4 km (*Barnes et al.*, 2008). Dune heights were estimated to range between 100 and 150 m (*Lorenz et al.*, 2006; *Radebaugh et al.*, 2008). Continuous dunefields cover regions of up to 1,500 by 200 km. The dunes are presumably composed of water ice and organic solids in unknown proportions (*Lorenz et al.*, 2006). High fractions of organic compounds are suggested through their allocation in optical- and near-infrared-dark areas (*Radebaugh et al.*, 2008).

In spectral terms, the dunefields on Titan correlate well with the dark brown spectral unit although a few percent of them also occur on bright and blue terrains (*Soderblom et al.*, 2007a; *Barnes et al.*, 2008; *Le Corre et al.*, 2008). Small discrepancies are assigned to slight spatial misalignments between radar and VIMS data.

The presence and distribution of dunes constrains some of Titan's environmental conditions and provides information about the global wind field. Titan's gravity and

its particle and atmospheric density constrain the threshold wind speed required to explain the presence of dunes which is supposed to range between 0.1 and 0.7 $ms^{-1}$ (*Lorenz et al.*, 1995, 2006). The development of linear dunes is favored at wind-regimes with persistent winds, one dominant wind direction, but periodically or seasonally changing directions. The proposed west-to-east wind is confirmed by the alignment of the dunes at topographically raised obstacles (*Radebaugh et al.*, 2008). To explain the formation of persistent dunes it has to be assumed that relatively dry conditions prevailed, or else the transported sand would have been trapped in open bodies of liquids, i.e. rivers or lakes. The fact that most dunes are concentrated in regions $\pm$ 30° provides insights into the current latitudinal near-surface humidity. Another geological constraint implied in the abundance of dunes is that there must have been a supply of particles of a specific size (100-300 µm) in substantial amounts ($10^4$ to $10^5$ $km^3$) (*Lorenz et al.*, 2006). The source of the sand is still debated. According to *Lorenz et al.* (2006) and *Jaumann et al.* (2009) several scenarios are conceivable: One plausible source might be fluvial activity and the breakdown of fluvial sediments (*Jaumann et al.*, 2009), which supplies smooth fluvial sediment that is fine-grained and sorted. It is, however, questionable whether fluvial processes can produce such an amount of sand, in particular because the substrate has to dry out before it is relocated (*Lorenz et al.*, 2006). Impact ejecta, too, can yield dune-forming sands, but it is unlikely that impactors account for such a high amount of material. A third scenario favors atmospheric photochemistry and fallout, yielding a quasi ubiquitous inventory of dune-forming sand. If this is the case, the processes that cause sorting, alteration, and relocation of the material require an explanation. Furthermore, *Fortes et al.* (2007) proposed material delivered by cryovolcanic flows to account for the dune-forming sediment. If the sand supply has its origin in fluvial processes, meridional winds are required to explain the particle transport over long distances. The same transport mechanisms are also required if the atmospheric fallout scenario is valid.

In general, short timescales are required to explain the formation of dunes, i.e. thousands to tens of thousands of years for the accumulation of sediments prior to their relocation (*Radebaugh et al.*, 2008). Although the recent activity of dunes is not definitely proven, they certainly indicate geologic processes of the recent past. Conceivably, dunes even mark the most recent landform on Titan.

Despite the uncertainty regarding their sand supply, Titan's dunes are highly relevant regarding fluvial erosion. To determine the relations between fluvial and eolian processes these features as well as their distribution are investigated in Section 5.2 and Chapter 6.

### 4.3.2 Mountains

Isolated mountains, ridges, hummocky terrain, and blocks are obvious from image data of the Cassini sensors. Radar unveiled linear mountain chains with lengths of up to 300 km mainly in the equatorial region (*Lopes et al.*, 2010). Titan's mountains

are characterized by their high radar return, indicative of rough surfaces relative to the radar wavelength. Mountains are presumably composed of water ice, which has a similar consolidation as silicate rocks on Earth (*Radebaugh et al.*, 2007; *Lopes et al.*, 2010). Xanadu, as a large, continent-sized raised and rough geologic formation, is a special case within this morphologic unit owing to its enormous spatial extent.

The formation of mountains on Titan probably happened some 20-100 million years ago (*Radebaugh et al.*, 2007). Interestingly, the mountains themselves exhibit signs of fluvial erosion, such as diffuse blankets surrounding their peaks (*Radebaugh et al.*, 2007; *Stiles et al.*, 2009). An earlier formation of the mountains cannot be ruled out, according to *Radebaugh et al.* (2007), since easily erodible material might have covered preexisting mountains, which were uncovered by fluvial incision at a later stage. *Radebaugh et al.* (2007) discussed several formation scenarios for mountains: Their prominent orientation in west-to-east direction is suggestive of preferential lateral crustal compression. An alternative origin as ejecta blocks is conceivable for at least some of the elevated topographic features. Extensional tectonism can account for horst and graben structures but this process has not been evidenced so far. Considering the small number of volcanic features, cryovolcanism is expected to be less significant for the rich abundance of mountainous features at Titan's surface (*Baines et al.*, 2006).

Mountains are generally characterized by low slopes with peak heights below a few hundred meters (e.g. *Radebaugh et al.*, 2007; *Jaumann et al.*, 2009). The estimated maximum height of Titan's mountains is 2 km with dominant altitude differences of several hundred meters (determined from radarclinometry and SARTopo, according to *Radebaugh et al.* (2007) and *Stiles et al.* (2009)). Although the outlines of mountains as seen in radar are not visible in VIMS data, near-infrared data unveil a spectral distinctness of mountainous terrain (*Barnes et al.*, 2007b). Most noticeably, rugged terrains with slopes around 30° coincide with to those regions that appear bright at near-infared wavelengths and in radar, while VIMS-dark terrains seem to be flat (*Soderblom et al.*, 2007b). Similar results are found concerning Xanadu; this continent appears bright in images of all Cassini imaging sensors and is interpreted to be elevated relative to the dark terrains. But, the relative height of Xanadu is controversial since *Stiles et al.* (2009) recently determined Xanadu to be lower standing in relation to most of Titan's terrain at similar latitudes. This finding is based on the SARTopo technique, which calculates altimetry height profiles through the overlap of the antenna footprints on the ground (*Stiles et al.*, 2009). Nevertheless, the VIMS-bright spectral footprint seems to indicate a comparatively rugged surface texture, often associated with mountains, and sometimes even channels (see Section 5.3) compared to the dark brown and dark blue surface units which seem to be linked to flat and smooth surfaces.

### 4.3.3 Impact Craters

Impacts by projectiles from space leave behind circular depressions at the surface of a larger (solid) body. Among the many features at the surface of Titan that morphologically resemble impact craters, five have been affirmed so far, namely Menrva (∅ 392 km), Sinlap (∅ 80 km), Ksa (∅ 29 km), Afekan (∅ 115 km), and Selk (∅ 80 km) (see Titan's nomenclature shown in Figure A.1, Appendix). Even if the number of unconfirmed craters is added, their total number does not correspond to the expected overall crater density for the Saturnian System of 100-200 craters per million km$^2$ (*Lorenz*, 1997; *Lorenz et al.*, 2007).

It is assumed that Titan's dense atmosphere has a certain shielding effect against smaller impactors. Atmospheric disruption is considered for bolides smaller than 20 km (*Engel et al.*, 1995). The lack of impact craters of that size supports the theory of a long persistence of the atmosphere. The maintenance of the atmosphere is thus evidenced at least for the timespan required for resurfacing through fluvial and eolian erosion. The number of medium-sized craters, which is also low, strongly suggests a high rate of erosion and burial by dunes, fluvial, or cryovolcanic flow. The density and distribution of craters provide information about fluvial and eolian erosion. The global distribution of craters was therefore included in a map, combined with the distribution of fluvial networks and the outlines of spectral units, and discussed in Section 5.4.2.

An analysis of the size-frequency distribution of craters is often performed to estimate the absolute age of surfaces. However, Titan's intense resurfacing processes are expected to blur its real age. Furthermore, this statistical approach has only limited significance in the case of Titan since the coverage obtained by radar-SAR is incomplete (20% at the time of the investigation by *Jaumann and Neukum* (2009)). Based on five confirmed and 44 possible impact features (*Wood et al.*, 2010), the surface age of Titan was determined to range between 3.9 Ga and 2 Ma, depending on the model chosen (*Jaumann and Neukum*, 2009).

Only the largest craters, namely the Sinlap and Selk craters, can be investigated by means of VIMS data. In both cases, even small details (rim, central peak) can be discerned (e.g. *Le Mouélic et al.*, 2008; *Soderblom et al.*, 2010a). Again, spectral characteristics seem to reflect the height conditions, since elevated parts, such as the rim and the central peak appear bright in VIMS, whereas the crater floor as well as the putative flow features appear dark blue.

### 4.3.4 Cryovolcanism

Complementing the complex geologic condition of Titan's surface, potential cryovolcanic features are identified at different locations of the moon by VIMS and radar images (*Neish et al.*, 2006; *Lopes et al.*, 2007a; *Le Corre et al.*, 2009), which is in accordance with predictions made before the Cassini mission by *Lorenz* (1996). The putative

volcanic flows detected so far are of a substantial size, measuring about 160 km in length (*Le Corre et al.*, 2009) and 180 km up to several hundred kilometers (*Lopes et al.*, 2007a). The positive identification of lava flows and calderas confirms the contribution of volcanism to the shaping of Titan's landscape.

The preconditions for (cryo-) volcanic activity as well as the underlying methane cycle are discussed in Section 2.3.4.3. At this point it is still controversial which constituents are involved in Titan's volcanism. Possible constituents of the cryolava are $CH_4$, $H_2O$, and $CO_2$ from the survey of VIMS data (*Le Corre et al.*, 2009), and $(NH_4)_2SO_4$ (ammonium sulfate) from modeling of Titan's chemical evolution (*Fortes et al.*, 2007). Volcanism is one of the potential sources resupplying methane to the atmosphere (see Section 2.3.4.1), which is why the identification of associated geologic features is of high relevance (e.g. *Mitri et al.*, 2008).

Cryovolcanic features are almost exclusively identified on the TA and T3 radar swaths and, thus, situated on the bright spectral terrains or in regions with unknown spectral properties (see Figure 5.23 and Figure A.6, Appendix). High-resolution VIMS data, analyzed in *Le Corre et al.* (2009), revealed a caldera and its flow, characterized by spectral properties of bright surfaces. Fluvial erosion has not been detected in the immediate surroundings of potential cryovolcanoes so far.

# Chapter 5

# Investigation of Fluvial Processes on Titan

The objective of this Chapter is to present a comprehensive analysis of the diverse morphologies associated with flowing liquids on Titan. The valleys are categorized into different morphologic types in the first Section of this Chapter. Furthermore, the morphologic properties of Titan's valleys, their spatial distribution, and spectral characteristics are described. Moreover, landforms associated with fluvial flow, such as lakes and deltas, are reviewed. The Chapter concludes with a comparison of fluvial valleys observed at various other planetary surfaces. Combining all these aspects helps to characterize Titan's methane cycle further and to gain deeper insights into Titan's global dynamics both from a climatic and from a geological/geomorphological perspective. Parts of this Chapter are based on the publication 'Titan's fluvial valleys: Morphology, distribution, and spectral properties', which is accepted for publication by *Planetary and Space Science*.

## 5.1 Valley Types on Titan

In the following, a classification of fluvial valleys is given which is mainly based on morphologic properties visible in radar-SAR but also considers Titan's particular environmental conditions. That is, valleys with morphologies pointing to similar boundary conditions (such as the climate) were combined into a singular valley class, irrespective of differences in morphology.

Until now, the action of liquid methane on Titan can only be indirectly studied by analyzing sets of remote sensing image data. The origin of a landform is inferred from its physiography and by comparison with terrestrial landforms/processes. Thus, the quality of geological interpretation depends on the knowledge deduced from terrestrial geology. Additionally, geological interpretation is complicated by the fact that different geologic processes can result in similar landforms (known as the *concept of equifinality* according to *von Bertalanffy* (1968)). This principle is highly relevant for Titan's surface since many geologic features are at or even beyond their resolution limit

of 350 m per pixel of the radar-SAR sensor. Furthermore, geologic/geomorphologic processes can significantly alternate on planetary bodies other than Earth with different environmental conditions. The origin of some valleys remains uncertain since the linear shape of a valley is not uniquely attributable to fluvial flow caused by precipitation. Linear landforms can also arise as a result of volcanic or tectonic action (geologic faulting/rifting), or be caused by erosion through subsurface liquids. In order to identify the processes responsible for the formation of a particular landform, interpreting its morphology and geometry are essential. The degree of certainty of their development from rainfall is discussed in this Section for each of the valley types separately. The morphological classification corresponds to that given in *Langhans et al.* (2011).

For a morphological analysis it is essential to consider the subdivision of valleys in terms of their longitudinal profile. The source region and the upper reaches of rivers are characterized by relatively steep slopes of the rocky river bed, high flow velocities, and high variations of the discharge (*Illies*, 1961). At the lower reaches the topographic gradient flattens and the flow velocity is decreased (*Illies*, 1961; *Leopold et al.*, 1964). Toward the mouth of a river the cross-section and the discharge increase due to the growing number of tributaries draining into the major stream (*Leopold et al.*, 1964). Terrestrial rivers tend to deposit their load and evolve meanders within this zone. The distinguishing characteristics for both of these zones, by inference, deliver information about the regional and local conditions, such as the topography, the discharge regime, and the bedrock. This longitudinal subdivision is not to be confused with the valley types presented in the following.

### 5.1.1 Dendritic Valleys

Titan's most evident valleys are arranged in integrated dendritic networks. Dendritic valley systems form networks with many contributing branches that converge into larger receiving streams. The recipient stream often drains into a lake or sea. Besides valleys modified by glacial processes, dendritic valley networks constitute the most common type of drainage systems on Earth, featuring a typical V-shaped cross-section and situated on less permeable or impermeable bedrock (*Williams and Phillips*, 2001; *Sahlin et al.*, 2009). Meanders are prevalent phenomena due to relatively steady stream flow without substantial variations and at relatively slight slopes of the terrain (*Radebaugh et al.*, 2010). These unstable landforms adjust to discharge variations through increase/decrease of meander wavelength and wave amplitude (*Butzer*, 1976). Meandering can be regarded as a morphological counterpart to braiding of channels, which becomes manifest in frequent shifts and relocations of the riverbed caused by high variations in stream flow (*Butzer*, 1976). Bifurcation, i.e the partition of the channel into two distributaries, is an unstable phenomenon from a morphologic standpoint and is not to be confused with braiding within streams or deltas. Bifurcation occurs only occasionally due to the flow mechanisms in streams, which follow the principles of minimum work and maximum possible entropy (*Leopold*, 1994).

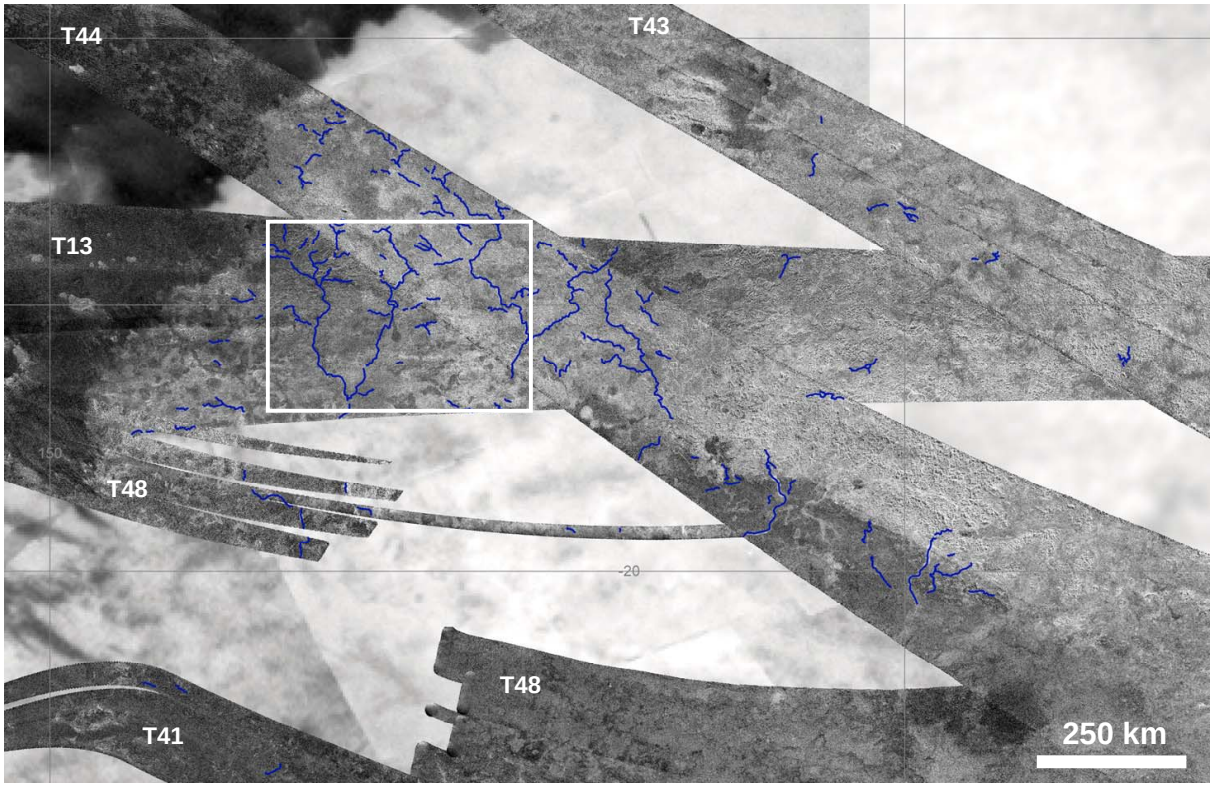


**Figure 5.1:** Fluvial valleys at western Xanadu. Radar-SAR swaths T13 (April 30, 2006), T41 (February 22, 2008), T43 (May 12, 2008), T44 (May 28, 2008), T48 (December 05, 2008). Background: ISS image. Image is centered at 120°W, 18°S. The white rectangle indicates the position of Figure 5.2.

The morphological characteristics of dendritic systems on Earth are reproduced by Titan's dendritic channels which emerge near the equator, especially at western Xanadu (*Barnes et al.*, 2007b; *Lorenz et al.*, 2008a) (see Figure 5.2 and Figure 5.1), at the Huygens Landing Site (*Tomasko et al.*, 2005; *Perron et al.*, 2006; *Soderblom et al.*, 2007b) (see Figure 5.4), and near the north pole (*Mitchell et al.*, 2007a; *Stofan et al.*, 2007) (see Figure 5.3).

The dendritic valleys at western Xanadu are covered by several radar swaths, which partly overlap each other (T13, T41, T43, T44, and T48, see Figure 5.1). Unfortunately, these swaths do not cover the entire area of the drainage network. VIMS data also reproduce large parts of this region, so that some of the largest channels can be recognized even in VIMS maps but at a lower spatial resolution (*Barnes et al.*, 2007b). The valleys' source regions and their upper reaches are apparently situated at north-western Xanadu, covered by the T13 and T44 radar swaths. Small channels are located near the source of the stream, presumably associated with steeper slopes and higher flow velocities, whereas the receiving streams meander and broaden toward the south of the considered region. The broader receiving streams are exclusively directed to the south. The course of some valleys at western Xanadu seem fragmentary and degraded, possibly due to mechanical erosion or impact cratering subsequent to fluvial erosion; although this could also be an effect of deficient resolution and

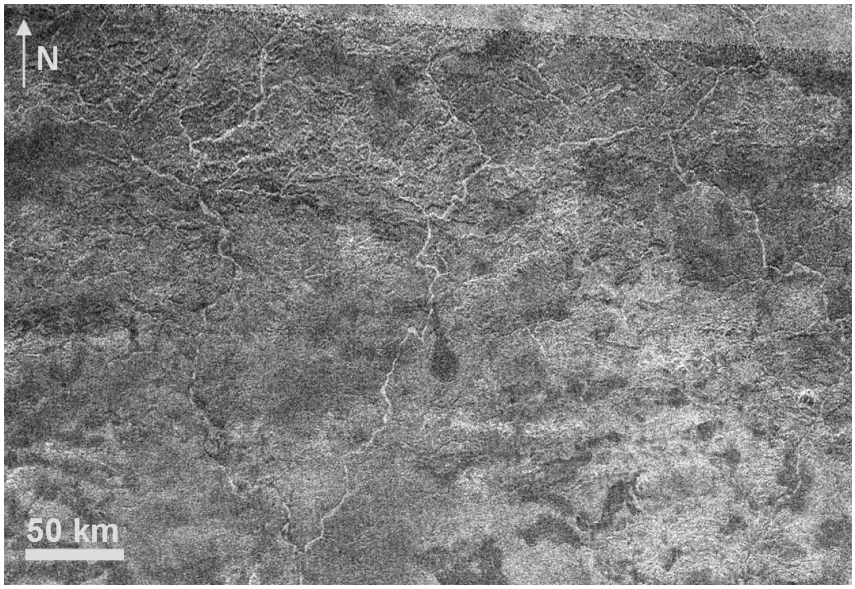


**Figure 5.2:** Dendritic valley network at western Xanadu acquired by radar-SAR observation T13, see Figure 5.1 for context (April 30, 2006). Image is centered at 138°W, 10°S.

coverage. Radar swath T44 reveals broad channels, possibly the definite receiving streams of the northern channels (*Le Gall et al.*, 2010; *Radebaugh et al.*, 2010). At least two valleys are resolved that emanate from the boundary of the bright highlands to the north (southern boundary of Xanadu), unify at the boundary of radar-bright and dark homogeneous terrain and abruptly vanish at the southern border of the T44 radar swath. Whether the channels of swaths T13 and T44 are in fact parts of one and the same network cannot be proven due to the lack of data in between.

Major portions of the entire Xanadu area do not feature any valleys at all, which might suggest the presence of smaller branches, invisible at the current image resolution. Well-defined valleys with meandering and complex courses and a high stream order are only found in Xanadu's western regions. Several thousand km$^2$ are covered with interconnected streams. Xanadu's channels have lengths of several hundred kilometers (the longest of them exceeding 450 km, cf. Table A.1, Appendix), and widths between 350 up to about 2500 m. The total length of all valleys in the system adds up to an enormous figure, given the large number of branches.

An area of remarkable size is the one that is covered by large lakes and dendritic valley networks near the north pole. In this particular area, many tributaries join into receiving streams many of which in turn lead into one of the lakes. Many valleys are entirely resolved, from their (approximate) sources to their mouths. Valleys near the north pole have widths between the resolution limit of the radar instrument of 350 m up to 5 kilometers, with lengths of up to 250 km (see Table A.1, Appendix). Some of the valleys broaden when they open out into the sea, resembling terrestrial estuaries with changing water levels (cf. Figure 5.3). Due to the extremely low radar return of fluvial and lacustrine landforms in this area, the course of the channels is well-defined with a high contrast to their surroundings. Further, the entire area between the lakes seems to be occupied by valleys. Whether the remarkable perceptibility of the valleys is an effect of the resolution, the contrast, or the channel width remains uncertain.

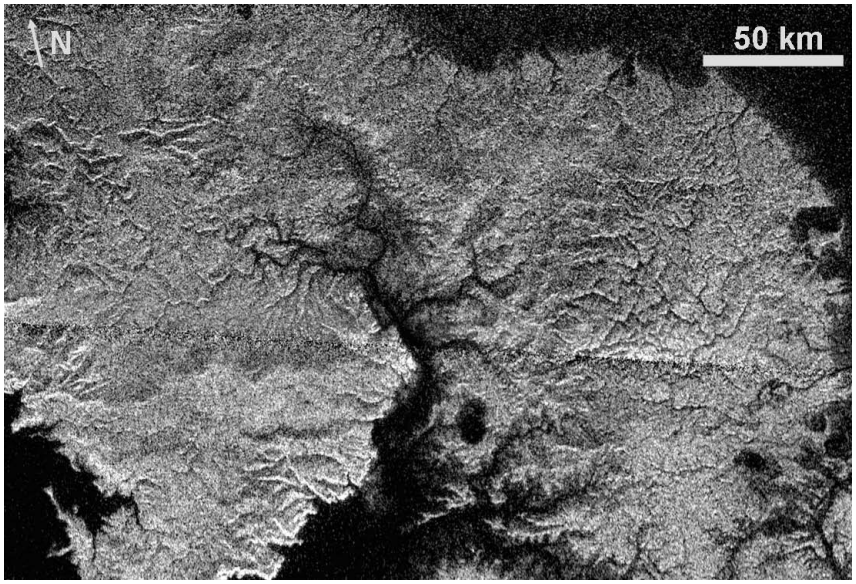


**Figure 5.3:** Dendritic valley network near the north pole, imaged by radar-SAR observation T28 (April 10, 2007). Image is centered at 280°W, 78°N.

Dendritic valleys near the HLS (see Figure 5.4) are unique regarding their spatial dimensions resolved by the DISR imager onboard the Huygens Landing Probe (*Tomasko et al.*, 2005; *Perron et al.*, 2006; *Soderblom et al.*, 2007b). Before landing the instrument took several images of the surface at exceptional spatial resolutions, unprecedented for a body of the outer Solar System. The network of channels is visible in a projected mosaic obtained at 17 to 8 km altitude with 17 m/pixel ground resolution (see Figure 5.4). Dark, narrow channels are incised into bright highlands and run in the direction of the darker lowlands, crossing an area a few kilometers to the north-west of the actual landing site. The channels end abruptly at a sharply-defined albedo boundary to the south of the image, which is interpreted to be the coastline of a former terminal sea or lake that has meanwhile run dry (*Tomasko et al.*, 2005; *Soderblom et al.*, 2007b). The widths of the channels obtained by DISR vary between 17 and 250 m, with the main receiving stream having a length of up to 15 km (*Perron et al.*, 2006; *Jaumann et al.*, 2008, 2009). The HLS channel system is also covered by the imaging devices onboard the Cassini mothership but it is not resolved due to its small size.

The dendritic drainage systems near the north pole and at western Xanadu are located on, or are at least surrounded by, mountainous terrain. Topographic models of the valley system near the HLS also revealed a rugged topography with peak-to-peak relative topography variations of about 200 m and steep slopes of up to 30° (*Tomasko et al.*, 2005; *Soderblom et al.*, 2007b; *Jaumann et al.*, 2009). The overall slope of the terrain can be deduced from the network geometry of the system. In the case of dendritic systems near the equator (see Figure 5.2) the receiving streams are mainly directed southwards. Xanadu is assumed to have a rugged topography, while the relative elevation of that 'continent' is still debated. The presence of valleys at western Xanadu is consistent with a relative elevation of that region in contrast to the eastern part of Xanadu, which is suggested to be lower lying (*Stiles et al.*, 2009) (see Section 4.3.2).

North-polar valleys have different flow directions, as almost each of them directly or indirectly ends in one of the numerous lakes, acting as local sinks. The channels at the HLS all run in a south-eastern direction.

*Implications for climate and substrate:* Valleys from the dendritic type certainly develop as a result of precipitation since they require a distributed rather than a local source of liquids (*Mangold et al.*, 2004; *Tomasko et al.*, 2005; *Perron et al.*, 2006; *Soderblom et al.*, 2007b; *Lorenz et al.*, 2008a; *Jaumann et al.*, 2009). The high branching complexity with network orders of up to sixth or seventh (cf. Figure 5.1, Table A.1, Appendix) (*Langhans et al.*, 2011)), which also makes this the most complex fluvial network detected so far, is an indication for an origin from rainfall. The enormously extensive areas covered by dendritic systems as well as the length of the valleys (often exceeding several hundred kilometers) at relatively narrow widths argue against a development from spring-fed flows or sapping of subsurface liquids. The latter would require a profound subsurface methane table to enable extensive seepage erosion, a precondition that is difficult to fulfill without precipitation and infiltration over a long period of time. Furthermore, the location of most of the dendritic networks within rugged and most likely elevated terrain argues against the presence of a subsurface methane table as it would more likely be found in lowlands or even in topographic depressions. Thus, a formation through sapping is unlikely and a formation by pluvial/fluvial processes is the most probable explanation for dendritic channels (*Tomasko et al.*, 2005; *Perron et al.*, 2006; *Soderblom et al.*, 2007b; *Lorenz et al.*, 2008a; *Jaumann et al.*, 2009).

Dendritic river systems on Earth are to be found even in the dryest deserts. By way of an example, Figure 5.5 shows a terrestrial dendritic network located in an arid environment in Yemen. This image highlights the very complex morphology of terrestrial dendritic systems. This region, totally arid today, bears witness to former humid climatic conditions. Thus, it is not possible to deduce recent climatic conditions

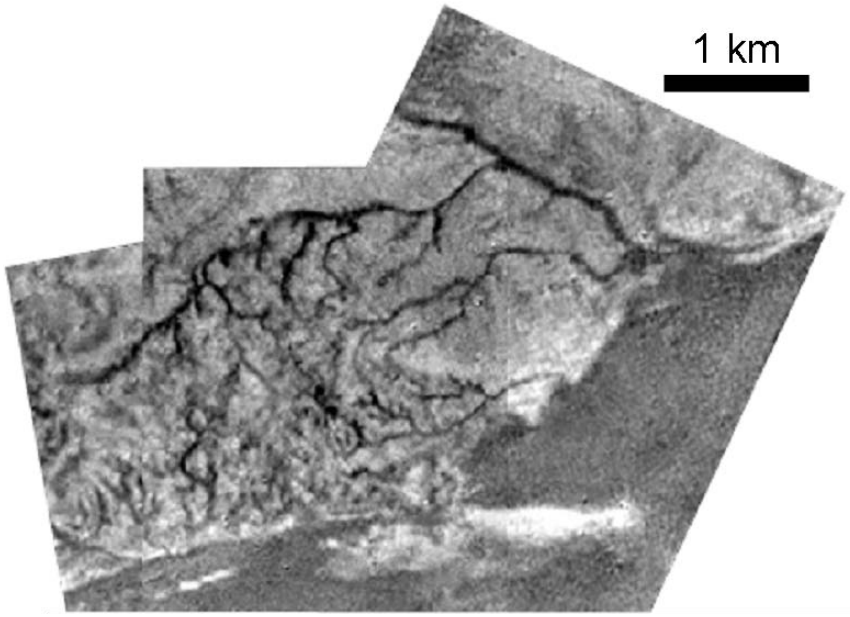


**Figure 5.4:** Dendritic valley network at the Huygens Landing Site, acquired by the DISR High and Medium Resolution Imager, panoramic mosaic (January 14, 2005). Image is centered at 192°W, 10°S (from *Tomasko et al.* (2005), modified).


**Figure 5.5:** Terrestrial dendritic network in Yemen. Image is centered at 15.0°N 48.5°E. Source: http://www.lpi.usra.edu

from the presence of dendritic systems alone since an area's physiography might also reflect ancient climatic conditions. Xanadu's valleys appear bright in radar, which is indicative of a recent inactivity of the entire network (cf. Section 5.5). Despite this, precipitation is likely to have played a significant role in the past. However, both the reason and the timescales for a possible climatic change in this region remain unknown.

The DISR image of the Huygens Landing Site shows two albedo units that are separated from each other by a sharp boundary (see Figure 5.4). The valley network is situated on the bright albedo terrain. This network ends abruptly at the candidate shoreline, which is the boundary to a possibly relict lacustrine landform (*Tomasko et al.*, 2005). This fact also indicates dryer conditions at the acquisition time compared to the time when the features developed. The high complexity of the networks argues for steady rainfall over a comparably long timespan, rather than episodic storm events, but this development scenario is not conclusive. The underlying bedrock is presumably mainly impervious, thus preventing infiltration on a large scale. Concerning their network geometry as well as their dimensions, polar and equatorial networks are very similar. Interestingly, the geologic background is quite different in these three examples, from mountainous (Xanadu) to lacustrine (north pole), to presumably relict lacustrine (HLS). The location of many dendritic valleys within or close to mountainous terrains suggests but not necessarily requires a development from or contribution by orographic rainfall (*Barth*, 2010; *Lopes et al.*, 2010).

Due to their high complexity and the relative scarcity of impact craters in their vicinity (see Figure 5.23), dendritic networks must be among the oldest fluvial systems on Titan, although their absolute age cannot be determined. On Earth, an absence of

tectonic or lithologic influences, often observed in dendritic systems, points to a relatively old age (*Ahnert*, 2003). By tendency, dendritic networks develop on fine-grained substrates (e.g. sediments) with a low permeability rather than in mountainous terrains (*Zepp*, 2008). Meanders develop on fine-grained material, at relatively slight slopes of the terrain and with a steady flow over a considerable time, which is typical of the lower reaches of a river (*Butzer*, 1976). On the other hand, *Burr et al.* (2009) make a case for tectonics having influenced the geometric alignment of Xanadu's valleys. Tectonic control is also evident at the HLS due to the proposed steep slopes of the terrain and substantial incision of the channels (*Tomasko et al.*, 2005; *Soderblom et al.*, 2007b; *Jaumann et al.*, 2008, 2009). At Titan's north pole, tectonics appear to have had a significant impact on the network geometry as the general shape of the valleys is rectilinear with sharp angular junctions, rather than sinuous (see Figure 5.3). Thus, dendritic systems leave us with conflicting impressions since their high stream order and complex geometry point to long development times while the high tectonic control rather indicates a relatively short persistence of fluvial erosion and/or a high resistance of the underlying bedrock.

Compared to Earth, well developed dendritic networks are relatively rare on Titan's surface. The 40% radar coverage reveals only three regions shaped by dendritic valleys, although it must be assumed that only the largest of the valley networks are resolved. Nevertheless, those areas provide compelling evidence for atmospheric precipitation, besides showing that this precipitation probably took place in the past, which is particularly likely in case of the equatorial networks. The north polar dendritic networks have probably been experiencing precipitation even recently.

### 5.1.2 Dry Channels

Several putative drainage networks can be found at Titan's surface with a morphology reminiscent of terrestrial wadis (*Lorenz et al.*, 2008a), or Martian outflow channels. Despite the morphological diversity within this valley type, all putative dry valleys are summarized in this Section on the basis of the (assumed) similarity of the climatic conditions that have brought about these physiographies (*Langhans et al.*, 2011).

Figure 5.6 shows examples of two putative dry channels on Titan. Figure 5.6a depicts the Elivagar Flumina channel system (see also Figure 3 in *Lorenz et al.* (2008a)) east of Menrva crater. Although this landform has certainly been caused by fluvial flow, its morphology is characterized by a low branching level with only few tributaries. The valleys are bright in radar relative to their surroundings. Figure 5.6b shows a system of putative dry valleys at southern mid-latitudes which appear like broad and straight streams. Their course resembles laminar surface runoff or denudation, unlike the linear, channelized flow in valleys. The suspected flows are oriented nearly in parallel and appear darker on radar than their surroundings. Conceivably, the channels left behind a thin layer of fine deposits that is causing the darker tone in the radar image. However, it is not clear whether the geologic feature illustrated

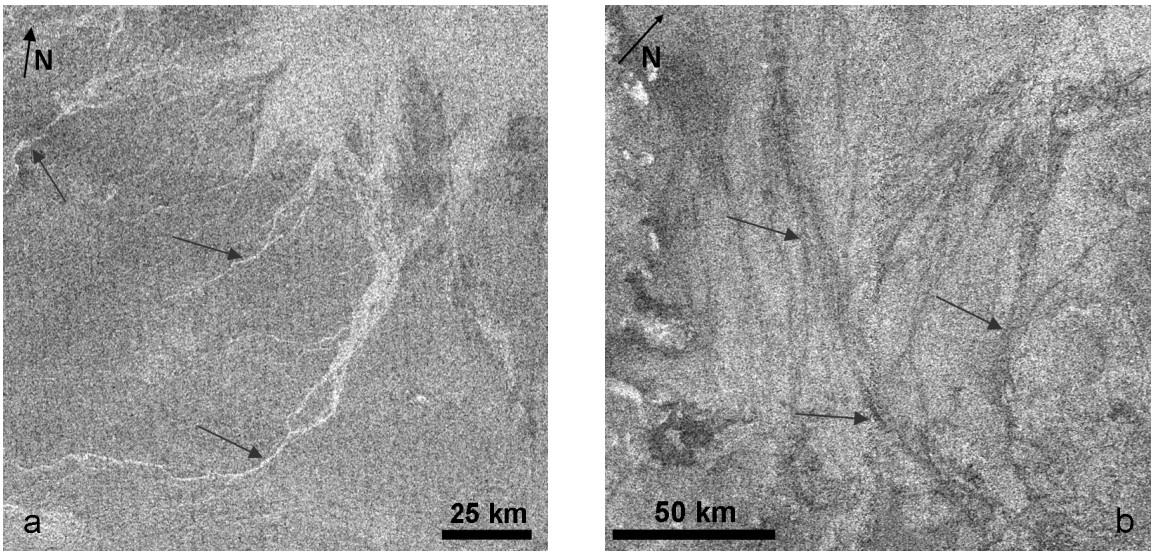


**Figure 5.6:** Dry channels from radar observations (indicated by arrows). a: Elivagar Flumina channel system (see also Figure 3 in *Lorenz et al.* (2008a)), radar-SAR observation T3 (February 15, 2005). Image is centered at 80°W, 20°N. b: Candidate channel system at southern mid-latitudes, radar-SAR observation T7 (September 07, 2005). Image is centered at 7°W, 60°S.

in Figure 5.6b is actually caused by fluvial erosion. Further, the prevalent flow direction is not apparent from the radar image. Nevertheless, their overall morphology is largely similar to that of wadis in terrestrial deserts, as the one in Figure 5.30c.

In the case of the dry valleys, particularly those of Figure 5.6b, the boundaries between the interior channel and the entire negative relief are sometimes hard to distinguish. Even the valley escarpments are often not perceptible in radar images due to the low contrast between the interior channel and its surroundings. Neither of the channel systems in Figure 5.6 has a clear a subdivision into an interior channel and a valley. Thus, flat cross-sections of the channels must be assumed (*Lorenz et al.*, 2008a) as opposed to the deeply incised, V-shaped valleys of the dendritic type (*Williams and Phillips*, 2001; *Tomasko et al.*, 2005; *Sahlin et al.*, 2009) (cf. Section 5.1.1). Dry valleys seldom exhibit meanders and are generally straighter, sometimes braided (see Figure 5.6a).

Compared to valleys within integrated dendritic networks, Titan's dry valleys are generally shorter and broader than valleys integrated within dendritic networks, with lengths of up to 300 km and widths up to 8 km (see Figure 5.6 and Table A.1, Appendix).

Dry valleys are found in plain and homogeneous environments (see Figure 5.6a). Their occurrence is confined to the mid-latitudes of both hemispheres away from the mountain ranges. In contrast to dendritic fluvial systems, terrains covered by dry valleys are less extensive and distributed only over a small proportion of the total surface of Titan (*Langhans et al.*, 2011).

Some channels of this type border on homogeneous and smooth terrain, which in shape and texture resembles that of floodplains (see outlines in Figure 5.7, bottom). In

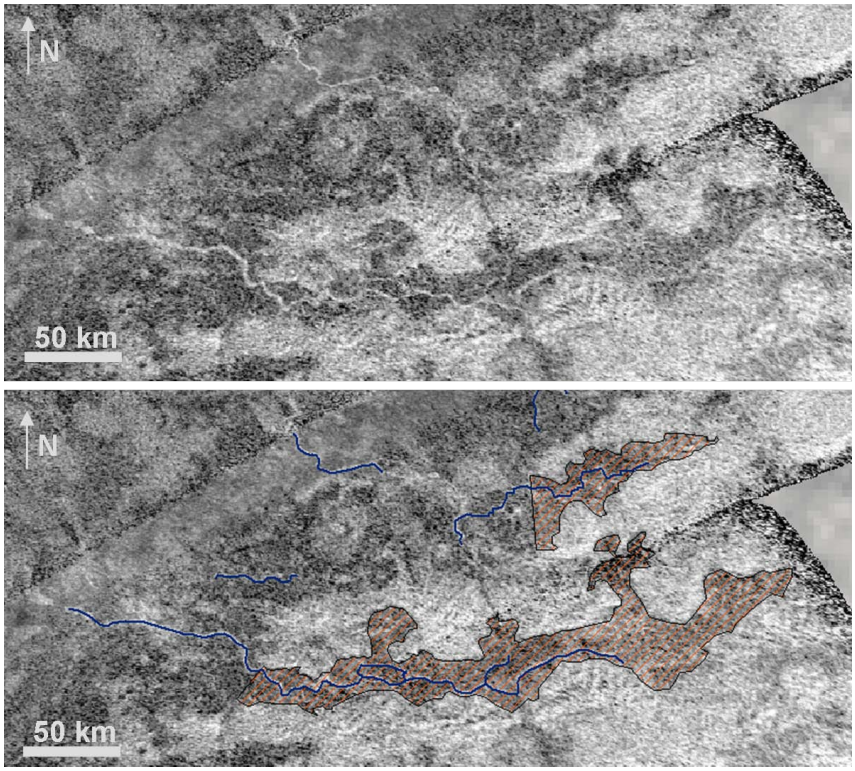


**Figure 5.7:** Interior channel surrounded by putative floodplains, derived from their radar-reflectivity and morphology. Top: Radar-SAR observation T41 (February 22, 2008). Image is centered at 67°W, 27°S. Bottom: Radar image with riverbed marked in blue, putative floodplains highlighted in red (striped). Flow direction is from the right to the left.

this case, a comparably narrow radar-bright channel south of Xanadu is surrounded by broad, relatively homogeneous radar-dark areas. These putative floodplains are possibly covered by smooth sediments, as the strength of the radar return depends, among other factors, on the roughness of the reflecting surface (*Elachi et al.*, 2006) (cf. Section 5.5). The observed difference in brightness may alternatively be the result of the topographic situation, e.g. the different inclination of the surface units against the sensor. This explanation is in general consistent with a fluvial origin of the landform in Figure 5.7, e.g. through different slopes and inclinations of fluvial terraces. Terracing is suggestive of climatic and discharge variations (*Ahnert*, 2003). Further, the floodplains have relatively clear-cut boundaries with their surroundings, which in turn appear bright in radar. Interestingly, the valleys seem to vanish and the channel course is no longer discernible at the left (western) image margin. Typical landforms of fluvial mouths, such as estuaries or deltas, are not apparent at the ends of dry channels. All these characteristics argue for high variations in stream flow over a relatively short period, resulting in extended floodplains, and high evaporation or infiltration due to the lack of receiving landforms. However, a lesser but steady discharge is required to explain the formation of the sharply-defined interior channel.

This particular morphology permits an alternative theory concerning its geological background. Due to its morphology, with a broad radar-dark valley floor

surrounding a narrow, bright interior channel, it resembles U-shaped valleys on Earth eroded by glaciers. The bright river bed of the interior channel makes up just a small portion of the entire valley. The radar-dark valley floor probably emerged as a result of long-lasting lateral erosion, in which the channel oscillated and often changed its course, having eroded and deposited its debris over a long span of time. Whether this morphology is due to flooding, as stated before, or due to lateral erosion coupled with an old age of the system, cannot be verified yet. Possibly it relates to smooth sediments deposited due to decreased flow velocity. Morphologically, this portion of the channel must be assigned to a section of the longitudinal profile of streams in the middle or near the mouth of the entire channel (lower reaches), since a shallow slope in the terrain is required to explain the deposition of fine sediments and the presence of meanders.

Compared with the dendritic channel system in the HLS area (Figure 5.4), this network has a larger areal extent. The length of the main channel is about 350 km, compared to only 15 km length at the HLS. Both valley systems have a branching pattern with orders of tributaries of up to four (HLS, Figure 5.4) and two (Figure 5.7), indicative of a fluvial/pluvial origin. Nevertheless, the channels near the HLS do not possess any extended floodplains (see Figure 5.4), which makes this valley system more consistent with an unchanging stream flow over time.

*Implications for climate and substrate:* Morphological considerations suggest a similar origin of the dry channels on Titan and desert wadis on Earth. Although the overall situation is predominantly arid, sudden, infrequent, but strong rainfall events account for large-scale surface runoff, sheet-floods, and sporadically filled streams. In some Earth regions, these climatic conditions have caused the paradox of a low mean rainfall rate despite of the presence of very obvious valleys. It can be assumed that an ephemeral discharge regime induces the relocation of large volumes of liquids in a very short time at long recurrence intervals on Titan (*Lorenz et al.*, 2008a). The episodic discharge of several terrestrial and Martian valleys entails braided and anastomosing patterns and fractions of residual uplands left within the riverbed (*Baker*, 2001). This idea is also consistent with observations of ephemeral clouds and with the results of atmospheric models (*Lorenz*, 2000; *Griffith et al.*, 2005; *Hueso and Sánchez-Lavega*, 2006; *Rannou et al.*, 2006; *Jaumann et al.*, 2008, 2009; *Rodriguez et al.*, 2009a).

The radar-bright tone of the valleys in Figure 5.6a points to a riverbed covered by coarse material (cf. Section 5.5). Coarse-grained material can only be transported if the initial flow velocity was high (e.g. *Baker and Milton*, 1974), although the exact flow rates cannot be determined (*Burr et al.*, 2006; *Jaumann et al.*, 2008). Deposition occurs when the stream velocity decreases. Hence, the radar-bright tone of the valleys is another indication of previous high discharge rates. It is also a sign of the current inactivity of the valley, at least at the time of the acquisition of the image.

Outflow events due to sudden melting of large volumes of ice account for broad, anastomosing and braiding flows on Mars (cf. *Komar*, 1979) but can be ruled out

for Titan due to its environmental conditions which preclude glaciation (*Lorenz and Lunine*, 1996) and owing to the widths and lengths of Titan's channels, which are significantly inferior to the dimensions of Martian outflow channels (cf. *Baker* (2001).

It is conceivable, however, for at least some of the valleys assigned to this type to have been produced by geologic processes other than rainfall. Some features discussed here may also have been formed by geologic processes, such as volcanic flow (see Figure 5.6b). Effusive lava flows with a low viscosity can result in laminar morphologies, too (cf. *Heslop et al.*, 1989). Due to the absence of diagnostic geologic features pointing to either of these processes, such as receiving lakes, seas or coastlines suggesting a fluvial origin, or calderas suggesting an alternative volcanic origin, it is difficult to assess which process is responsible for the formation of a particular morphology (*Langhans et al.*, 2011).

### 5.1.3 Sapping Channels

It has been suggested that another process that may have sculptured Titan's surface is erosion by liquids emerging from the subsurface (*Tomasko et al.*, 2005; *Perron et al.*, 2006; *Jaumann et al.*, 2009). The equivalent process on Earth and Mars is known as 'groundwater sapping' (*Howard and McLane III*, 1988; *Baker et al.*, 1990; *Lamb et al.*, 2006, 2008). Valleys created by sapping or seepage erosion tend to produce different morphologies compared to those formed by precipitation (*Baker et al.*, 1990; *Lamb et al.*, 2006), although there is no case in which a definite and exclusive origin from subsurface liquids has been confirmed, even on Earth or Mars (*Lamb et al.*, 2006, 2008). Candidate sapping channels on Earth and Mars are deeply incised, develop amphitheater-shaped heads and are generally shorter and broader compared to valleys formed by rainfall (cf. *Howard and McLane III*, 1988).

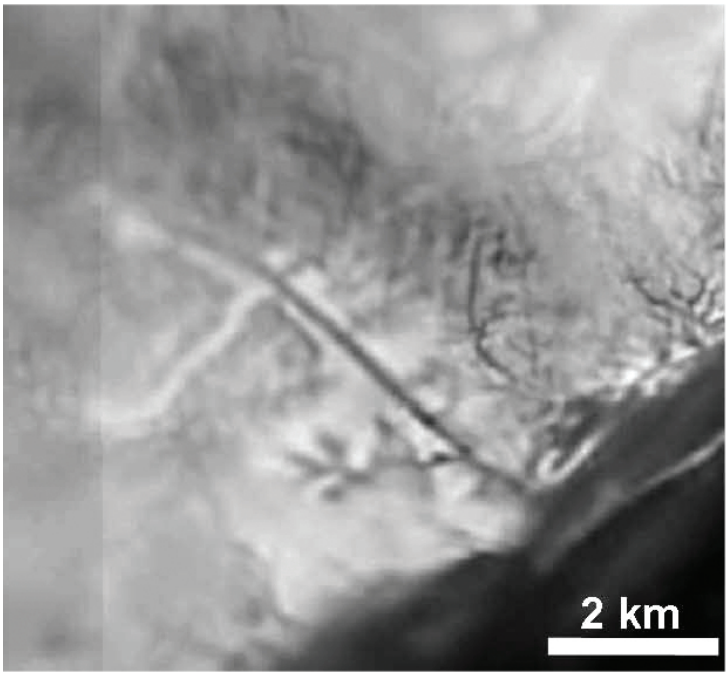


**Figure 5.8:** Sapping channels from the DISR High and Medium Resolution Imager, panoramic mosaic (January 14, 2005). Image is centered at 10°S, 192°W (from *Tomasko et al.* (2005), modified).

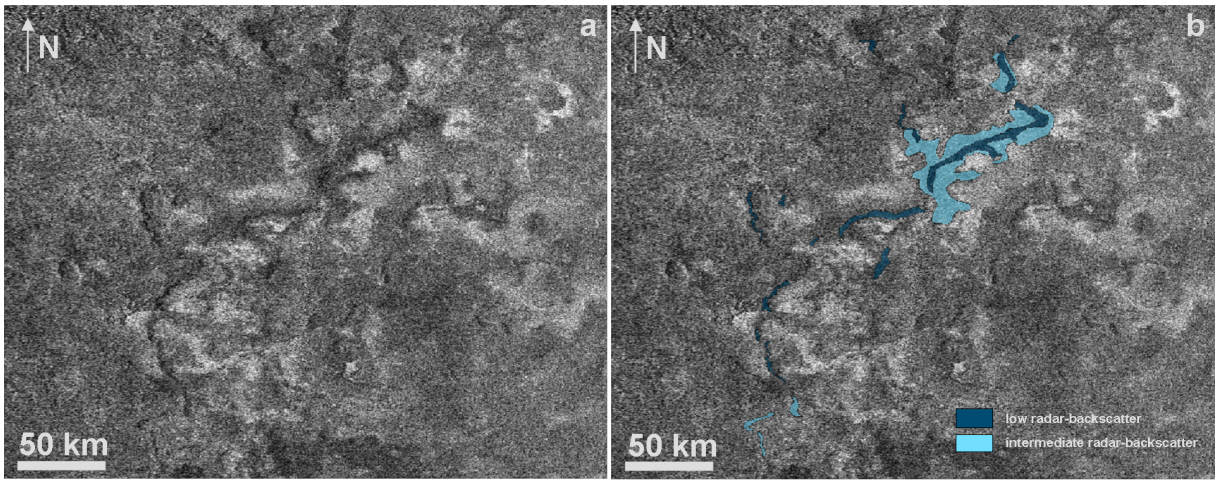


**Figure 5.9:** a and b: Relict canyon system from radar-SAR observation T16 (July 22, 2006). Images are centered at 143°W, 50°N. b: The presumed course of the canyons is highlighted in blue.

Morphological indications of sapping of subsurface liquids can be found only at two locations on Titan so far. Data of the Descent Imager reveal a putative sapping network near the Huygens Landing Site (see Figure 5.8), situated close to the dendritic valley system mentioned before (Figure 5.4). This candidate sapping system possesses a dendritic arrangement of broad and stubby branches that converge at large angles with the receiving stream. The channel network drains southward, toward the same abrupt albedo boundary described in the context of dendritic valleys (see Section 5.1.1), which is interpreted to be a putative relict coastline (*Tomasko et al.*, 2005; *Soderblom et al.*, 2007b; *Jaumann et al.*, 2009). The area covered by the valley system is very small, with lengths of the main channel below 15 km and widths up to 100 m (*Jaumann et al.*, 2009).

Another landscape likely to have been formed by sapping is revealed by radar-SAR around 143°W, 50°N (see Figure 5.9) (*Langhans et al.*, 2011). The curvilinear features at this location resemble deeply incised canyons on Earth (cf. *Schumm et al.* (1995)) with considerable lengthwise and lateral dimensions (width of up to 5 km; the length of the system adds up to about 200 km, see Table A.1, Appendix). However, the channel course seems unconnected. The broad interior channels have a substantially lower radar return than the adjacent areas. The pronounced contrast in SAR can result from differences in surface roughness between the interior valley, the valley escarpment, and its surroundings. It is certainly not the result of radar shadow because the valley escarpments have rather shallow slopes. This landscape, possibly a relict of earlier sapping, is geometrically very simple as only some valleys drain into the larger putative terminal valley. In both cases, the branches are of short and stubby shape, with large confluence angles between the tributaries.

These candidate sapping channels are located at mid-latitudes as well as near the equator and are the only instances of this channel type found so far.

*Implications for climate and substrate:* Although a fluvial origin is very likely, a definite contribution by subsurface liquids cannot be verified, especially in the case of Figure 5.9. The observed features can also result from tectonic processes. Strong tectonic control and preferential erosion in pre-existing fissures combined with less resistant bedrock and steady rainfall might also explain morphologies with high angles of the tributary junctions (e.g. *Burr et al.*, 2009), although the sinuous shape of the branches is more consistent with fluvial flow. High tectonic control is also suggested by *Jaumann et al.* (2009) in the case of the putative sapping landscape at the HLS (see Figure 5.8). An origin only from rainfall, without the influence of sapping of subsurface liquids, is unlikely, since this process would result in dendritic and branching morphologies with high stream orders, which is not borne out by the present image database. On the other hand, even on Earth and Mars it is currently still controversial whether sapping alone without a contribution from rainfall and flood events is able to cause these comparatively deep negative reliefs especially in resistant rock (*Lamb et al.*, 2006, 2008). In the case of the putative sapping system at the HLS, an influence through erosion by rainfall is likely due to the close proximity to the dendritic network located only some km away (see Figure 2 and Figure 5 in *Tomasko et al.* (2005)). Although the origin of these features cannot be specified further, a development from fluvial processes is likely due to their sinuous shape. However, the fragmentary, incoherent course of the features in Figure 5.9 argues against recent fluvial activity.

If the origin of these channels from sapping is, in fact, a valid conjecture, their presence indicates long-lasting processes of groundwater action in combination with a relatively low resistance of the bedrock material. In this respect they resemble terrestrial landforms with a background from seepage which, too, are known to develop only on less resistant sedimentary bedrock (*Lamb et al.*, 2006).

As proposed by *Stevenson* (1992) the suggested sapping processes will have required high amounts of liquids stored in a subsurface aquifer. Further, the valleys must have substantial depths to intersect this aquifer, a condition that seems to be fulfilled at least at some localities. However, the idea of a subsurface methane reservoir, located relatively closely underneath the surface, was adopted by *Stofan et al.* (2007) in the context of possible interactions between the lakes close to the north pole and that 'methanifer'. Thus, sapping through subsurface liquids is generally considered conceivable.

### 5.1.4 Valleys in Mountains

Mountain chains on Titan are suggested to have been subject to intense resurfacing, at least partly due to fluvial erosion (*Radebaugh et al.*, 2007; *Lunine et al.*, 2008a; *Jaumann et al.*, 2009). In fact, many of Titan's mountain chains exhibit putative channels, the majority of them appear inactive, incipient and short, with lengths of several tens of kilometers and widths below 3 km (see Figure 5.10a and Table A.1, Appendix) (*Langhans et al.*, 2011). An exception to this is western Xanadu, which is traced by

extended dendritic valley networks, as discussed in Section 5.1.1. Valleys within individual mountain ridges often display a bright/dark pairing in radar images and possess a rather simple geometry. This type of mountain valley is often at or even below the radar instrument's resolution limit. Most of these channels must therefore be regarded as uncertain fluvial features owing to their small size. Furthermore, most of them are too short to identify certain morphologic characteristics or even network geometries that would to some extent confirm their fluvial origin. The course of those channels is difficult to trace because of the low contrast to their surroundings. Supporting a possible fluvial origin, some of these putative valleys are sinuous in shape, sometimes with several interconnections. If the observed features are, in fact, fluvial channels, their location in mountainous terrain suggests a high degree of vertical erosion due to steep slopes and high flow velocities. The distribution of this kind of channels is restricted to Titan's mountain chains, which in turn are situated at low and mid-latitudes. Regarding the longitudinal profile of rivers, these channels most likely represent the upper reaches of valleys. The distinction between interior channel and valley is not relevant for valleys within mountains, since erosion in a vertical direction overbalances lateral erosion, which is rather typical for the upper reaches of a valley with steeper gradients (*Louis and Fischer*, 1979).

An example of such possible mountain valleys is visible at 347°W, 54°N (see Figure 5.10a). Here, a surface feature with a west-eastern orientation can be identified that is clearly detached and totally distinct from the adjacent terrain, especially regarding its surface structure (*Langhans et al.*, 2011). It appears to be an elevated ridge, dissected by numerous channels. Although several sinuous valley-like features can be traced, the course of every channel and the underlying network geometry and their flow direction are beyond the resolution of the image data. The putative channels show a dominant orientation from NNE to SSW. Given the deep incision they seem to have made into the terrain these potential fluvial features show a remarkable bright/dark pairing in radar (cf. *Burr et al.* (2009) and Section 3.5). The observed features are most likely currently inactive since channels filled with fluids would appear dark in radar images (cf. Section 5.5). The longest valley at the eastern margin of the ridge has a length of 50 km and a width of up to 3 km (see Figure 5.10a). As in the Himalaya Range in Figure 5.10b, which is a comparably young formation, a relatively resistant basement seem to suppress the effect of resurfacing through fluvial erosion. The putative mountain ridge on Titan is surrounded by smooth homogeneous plains, as can be inferred from the undifferentiated and radar-dark characteristics of that terrain (cf. Section 5.5). Most valleys end abruptly at the edges of that mountain chain; their lower reaches or recipients are not visible, which might be a resolution effect. Alternatively, this vanishing is either due to high evaporation rates or the recipients have been subsequently eroded or covered by another (sedimentary) layer. Taking into account the probable smoothness of adjacent areas it can be assumed that the surrounding terrain is younger and possibly sedimentary in origin (*Langhans et al.*, 2011).

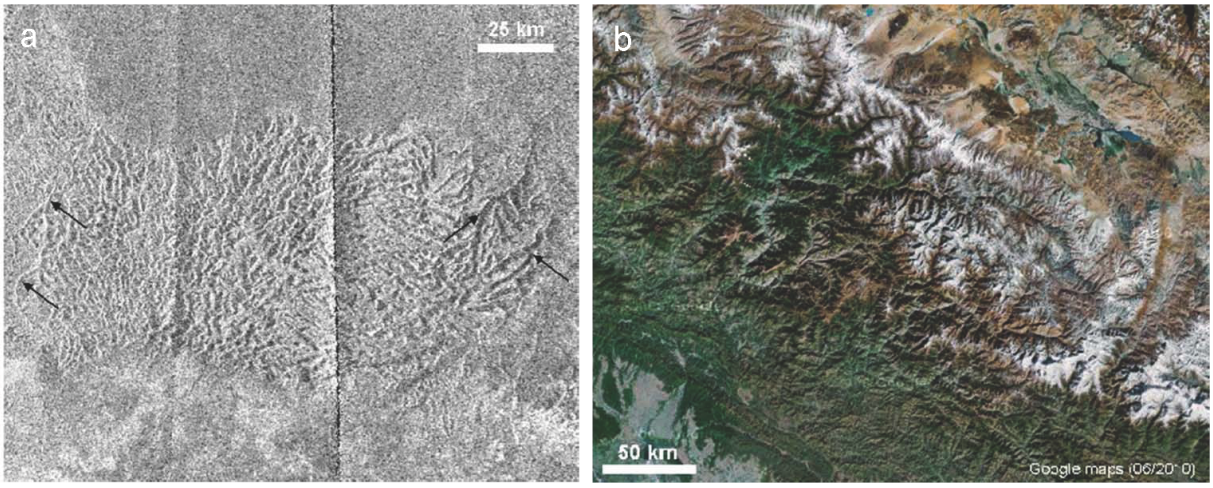


**Figure 5.10:** a: Mountain ridge with numerous potential channels. Radar-SAR observation T16 (July 22, 2006). Image is centered at 347°W, 54°N. Putative fluvial features are marked by arrows. b: Mountain chain on Earth (Himalaya, northern Nepal). Image is centered at 29.4°N, 82.5°E, true color (2010 ©Google-Map data).

Supporting this, *Radebaugh et al.* (2007) proposed blankets of fluvial deposits that constitute the diffuse plains surrounding many mountain chains.

Their stratigraphic relation to the mountains as well as to the adjacent terrain suggest an age similar to (or younger than) that of the mountains. The surrounding plains are most likely younger than the mountains and channels, as they probably overlay their lower reaches and recipients. If these layers consist of fluvial sediments, that is restored after deposition, their time of origin was slightly later than that of the channels. While the origin of mountain chains on Titan is still debated (cf. *Radebaugh et al.*, 2007), it is very likely that mountains on Titan are composed of bedrock material whose resistance against erosion differs from that of the lowlands, and whose geologic age is most likely older (*Stofan et al.*, 2006; *Jaumann et al.*, 2009; *Lopes et al.*, 2010).

*Implications for climate and substrate:* Possibly, dissected mountains on Titan represent remnants of former mountainous terrains traced by numerous fluvial networks, which covered the surface of Titan continuously. In this case, the bright or mountainous areas bear witness to a former wetter climate, strong tectonic processes and/or sedimentation. This assumption is supported by the fact that fluvial features in mountains terminate at the boundaries of mountain chains. If these features would be younger than the terrain surrounding the mountains, their course would most likely be traceable there. In fact, only the upper reaches of the valleys are visible, and possible recipients are covered by sedimentary layers. On the other hand, the orientation and shape of mountain ridges is suggestive of a tectonic origin (*Radebaugh et al.*, 2007), which argues against the idea of a divergence of a candidate primordial surface unit. The processes that lead to the divergence into mountainous areas and lowlands and to sedimentation remain controversial.

Alternatively, fluvial features within mountain chains could be interpreted as evidence of orographic rainfall (*Lopes et al.*, 2010; *Barth*, 2010), with topographic obstacles

forcing airmasses to rise and cool, followed by condensation and formation of clouds, a common process on Earth. However, this interpretation does not explain why the majority of the channels end abruptly at the edges of mountains. The fact that the vertical extension of Titan's mountains is rather flat (*Radebaugh et al.*, 2007) (see Section 4.3.2) argues against any large-scale rising motion. Furthermore, there is no definite evidence that the valleys in mountains originate from precipitation, although this is suggested by their linear and often sinuous shape (*Langhans et al.*, 2011). A glacial origin of the features can be ruled out due to Titan's environmental conditions (*Lorenz and Lunine*, 1996; *Perron et al.*, 2006).

### 5.1.5 Individual (elongated) Valleys

Another type of valleys is to be found in regions that appear diffuse and homogeneous in radar images, labeled as undifferentiated plains by *Stofan et al.* (2006) and *Lopes et al.* (2010). Valleys within plains appear bright, with a strong contrast to their radar-dark, featureless surroundings (see Figure 5.11). This type of valleys differs from others by its straight course and few branches. Sinuous reaches, meanders and braiding features rarely occur and the channel bends are of an angular rather than sinuous shape. Due to the incomplete coverage of the radar data, the sources and mouths of the channels are not imaged, and their course is often fragmentary. Deltas or terminal deposits are also not recognizable in valleys of this type. Owing to the low number of branches, the fundamental network geometry and the flow direction cannot be determined in most of the cases (*Langhans et al.*, 2011).

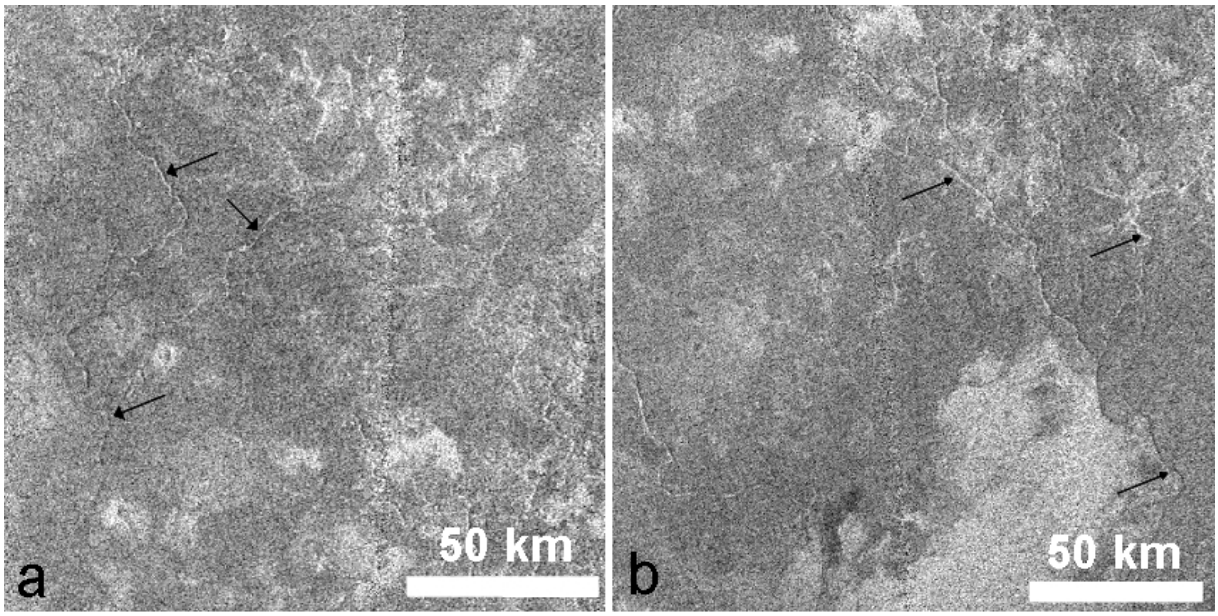


**Figure 5.11:** Elongated Valleys. a: Radar-SAR observation T7 (September 07, 2005). Image is centered at 12°W, 56°S. Arrows indicate putative fluvial valleys. b: Radar-SAR observation T7 (September 07, 2005). Image is centered at 6°W, 58°S.

Valleys of this type emerge at all latitudes of Titan, except for the poles. Their global distribution is scattered but confined to the radar-dark featureless plains which, in turn, are quasi uniformly distributed over all latitudes (*Lopes et al.*, 2010). Valleys of this type are not wider than 3000 m with lengths well below 100 km (see Table A.1, Appendix), although their lengths may in some cases be underestimated due to a fragmentary course in radar.

*Implications for climate and substrate:* The morphological characteristics of these putative valleys are in general indicative of a steady transport of liquids downstream, due to the valleys being of nearly constant width. If these features do, in fact, represent valleys created by fluvial flow, the delivery of liquids and the ambient conditions within undifferentiated terrains have conceivably been constant at the time of their formation (*Langhans et al.*, 2011). However, the radar-bright tone of the channels is an indication of their current inactivity and of dry climatic conditions (cf. Section 5.5). The simple shape and the absence of typical fluvial characteristics such as meanders suggest that these valleys were active for a shorter period than other types of fluvial valleys on Titan because complex hierarchical geometries of channels with meanders and curvilinear shapes require a substantially longer time to develop (*Ahnert*, 2003).

A volcanic origin is also conceivable from a morphological point of view, given the predominantly constant width of the channels and the lack of integrated tributaries; attributes that are also typical seen in sinuous rilles on Venus and (Earth's) Moon (cf. *Komatsu and Baker* (1996), *Komatsu* (2007) and references herein). If this applies, the high radar backscatter of the channels would signify a rough surface consisting of solidified cryolava (*Langhans et al.*, 2011). Several putative cryovolcanic domes and associated landforms are still under debate, such as lava flows, calderas, etc. (e.g. *Le Corre et al.*, 2009; *Jaumann et al.*, 2009; *Lopes et al.*, 2010), which underlines the significance of volcanic processes. On the other hand, lava flows on Titan show a laminar rather than linear flow as shown in Figure 5.11, which argues against the assumption that the linear channels shown here originate from volcanic action. An alternative development from rainfall is conceivable but cannot be verified because the source regions of these channels are not resolved. Seepage erosion is certainly not involved in the formation of these features, given the narrow widths of the features and the lack of morphological indications of any such process.

Two channels (or channel systems) obtained from *Paganelli et al.* (2005) and *Wall et al.* (2010) could not be assigned to any specific channel class. These are the 'fan-like' and the 'flooded' channel, see Table A.1 (Appendix). The two denotations are adapted from the literature.

## 5.2 Geographical Distribution of Fluvial Valleys

The global distribution of drainage valleys sheds light on to Titan's stratigraphy and its recent geologic history because channels are expected to be among the youngest features found on the surface of Titan (*Lopes et al.*, 2010). The arrangement of channels and their geometry mirror the topographic context and even permits a broad assessment of the climatic conditions prevailing at the time of their formation. Furthermore, this Section outlines the spatial distribution, stratigraphic and functional relationship between the channels and other geologic units. In the absence of global, well-resolved digital elevation models, as well as weather and rainfall scenarios, this information is of great benefit. The following Section discusses the implications of the distribution of valleys for Titan's climate, seasonal dynamics, and the correlation of these data with the distribution of clouds.

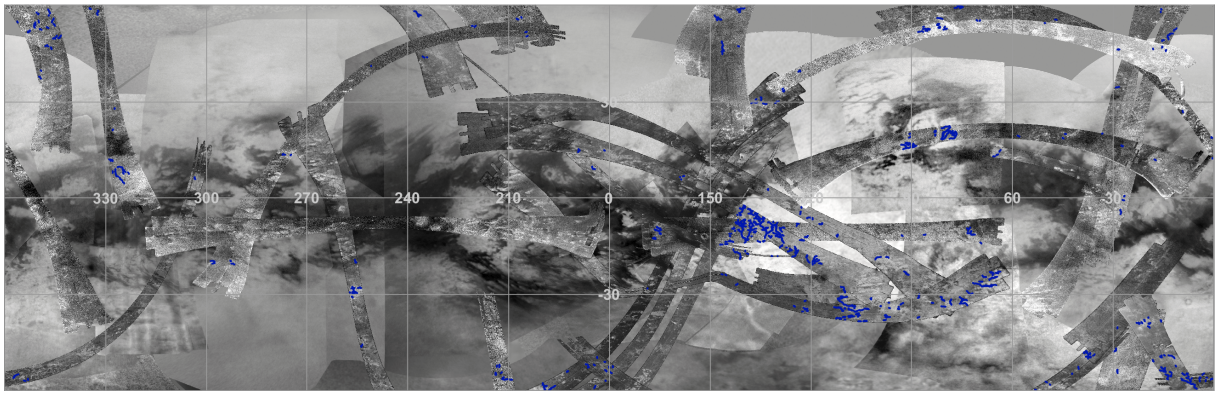


**Figure 5.12:** Fluvial valleys (marked in blue) are overlaid on global radar observations and near-infrared ISS map. Simple cylindrical projection of lower and mid-latitudes. Image is centered at 180°W, 0°N. See Figure A.7 (Appendix) for an enlarged view.

Fluvial valleys are, by tendency, distributed over all latitudes (see Figure 5.12, Figure 5.13, Figure A.7, Figure A.8, and Table A.1, Appendix), which confirms the idea of a predominantly solid surface that is not covered by large standing bodies of liquids, as assumed after the Voyager encounters (*Flasar*, 1983; *Lunine et al.*, 1983). Despite their widespread presence, valleys are not homogeneously distributed. A detailed view discloses centers of fluvial activity with a high drainage density at some locations, while other areas are devoid of channels (see Figure 5.13, 5.12), although the absolute number of channels detected obviously depends on the fraction of the surface effectively covered by radar-SAR (see Figure 5.14, gray line) (*Langhans et al.*, 2011). The majority of channels are shorter than 50 km, irrespective of their location. The largest channels are situated between 10°S and 40°S (associated with western Xanadu) and at about 20°N (around the Elivagar Flumina channel system, located east of Menrva). Less surprisingly, areas with a relatively high channel density host the largest channels (*Langhans et al.*, 2011). These dense networks are located at western Xanadu (*Barnes et al.*, 2007b; *Lorenz et al.*, 2008a), near the HLS (*Tomasko et al.*, 2005),

as well as close to the north pole (*Mitchell et al.*, 2007a; *Stofan et al.*, 2007), all of them assigned to the dendritic channel type.

If one divides the imaged areas into 225 km wide boxes (5° at the equator), only 20.5% of boxes of the total imaged area contain channels. Landscapes not influenced by fluvial erosion clearly prevail and valleys (or valley systems) are concentrated in comparatively small regions (*Langhans et al.*, 2011).

In general, fluvial landforms seem to be associated with mountainous terrain as many of Titan's valleys emerge in radar-bright areas (*Radebaugh et al.*, 2007; *Lopes et al.*, 2010; *Radebaugh et al.*, 2010; *Langhans et al.*, 2011). Indeed, the most evident geologic process within Titan's mountains appears to be fluvial erosion and degradation, particularly at Xanadu. Similarly, channels have been found in association with impact craters (*Elachi et al.*, 2006; *Lorenz et al.*, 2008a; *Soderblom et al.*, 2010a). Thus, channels appear to be linked to regions with comparatively high slopes and substantial elevation differences. Long and sinuous valleys occur in the vicinity of the large north polar lakes (>70°N, 210-360°W) (*Mitchell et al.*, 2007a; *Stofan et al.*, 2007). However, the north polar region is dichotomic regarding the distribution of fluvial features. In spite of the large number of small lakes between 0 and 150°W at high northern latitudes, which are partly drained and liquid-filled (*Stofan et al.*, 2007), valleys are sparse, short, and stubby in that region (see Figure A.8, Appendix), more consistent with processes due to interaction with a subsurface methane table (*Stofan et al.*, 2007).

Only a small number of valleys with simple network geometries appear near the south pole (see Figure A.8, Appendix) and on undifferentiated plains, at mid-latitudes (*Langhans et al.*, 2011). Nevertheless, some valleys can be found on the featureless dark plains, which in turn are interpreted to be sedimentary in origin by *Lopes et al.* (2010) (see Figure 5.15b). Nearly no valleys occur within the flat dune

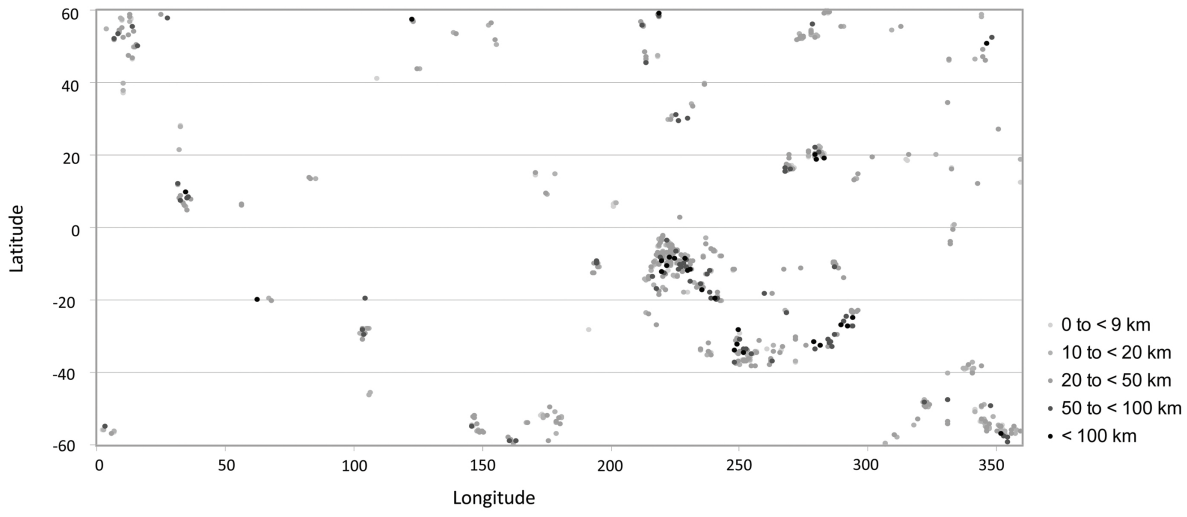


**Figure 5.13:** Scatterplot of the geographic position of fluvial valleys on Titan. Valley-length is indicated in levels of gray.

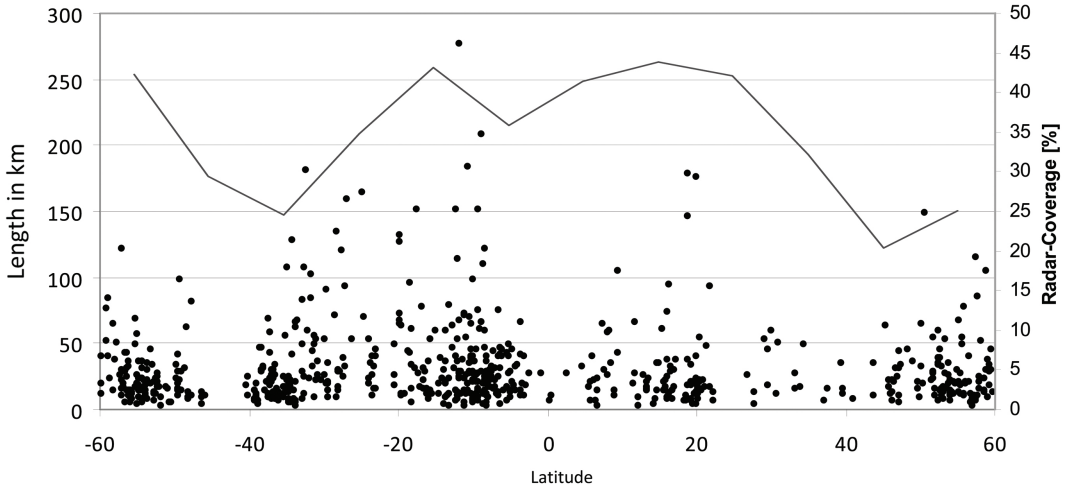


**Figure 5.14:** Scatterplot of channel-length vs. latitude. Radar coverage in percent (gray line).

fields (see Figure 5.15a) that cover almost one-third of the surface at low latitudes. Only one possible channel has been found so far that is actually located in a dunefield (*Barnes et al.*, 2008). Fluvial and eolian erosion are competing in the sense that each of these processes - if dominating over a substantial time - tend to substitute or even out the landforms created by the other process. Several scenarios explain the deficit of fluvial features in Titan's dunefields: Fluvial and eolian erosion are certainly the youngest processes taking place on Titan (*Barnes et al.*, 2008; *Lopes et al.*, 2010). Possibly, the accumulation of dunes took place subsequent to the incision of channels and maybe even proceeds today so that dune layers might be covering subjacent

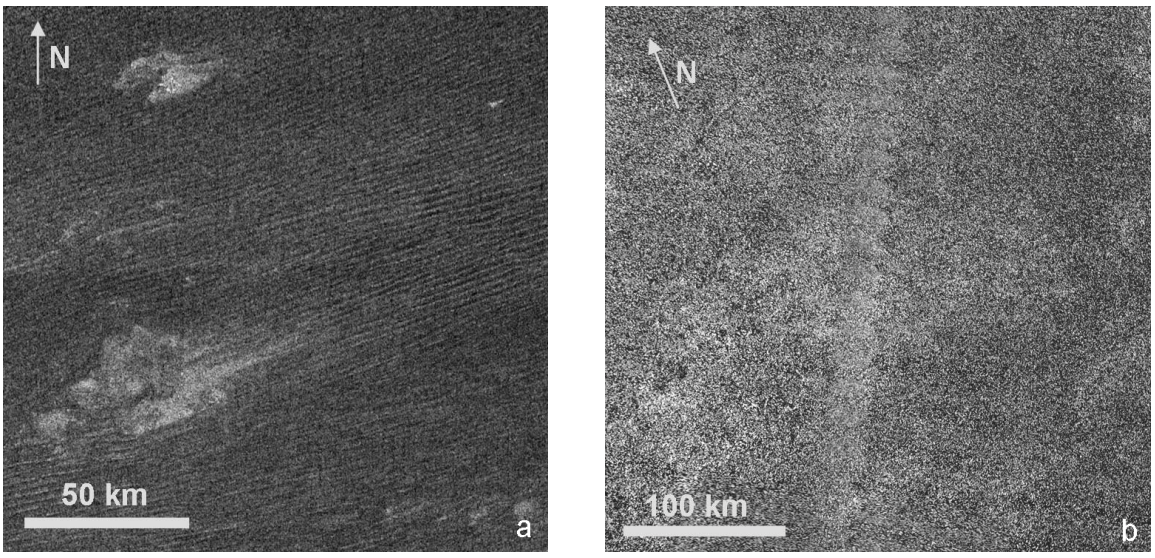


**Figure 5.15:** Geomorphological units from radar observations. a: Longitudinal dunes close to Titan's equator, imaged by radar-SAR observation T8 (October 28, 2005). Image is centered at 255°W, 7°S. b: Featureless plains, imaged by radar-SAR observation T36 (October 2, 2007). Image is centered at 30°W, 32°S

.

valleys (*Barnes et al.*, 2008; *Lopes et al.*, 2010). An alternative assumption would be that fluvial erosion is not equally distributed, with rainfall being restricted to certain areas, analogous to the situation on Earth. Supporting this, the formation of dunes requires dry and desert-like conditions, which generally argues against a simultaneous development of channels. On the other hand, the distribution of valleys is highly correlated to the presence of mountains, which can be an indication for orographic rainfall (*Barth*, 2010; *Lopes et al.*, 2010) and a deficit of precipitation in the plains. Another explanation for the apparent absence of fluvial valleys within the dunefields, apart from climatic reasons, is that valleys are present but too small and narrow to be resolved by radar, yet. This explanation is rather unlikely since larger channels are resolved at all latitudes on Titan and the complex distribution of channels is certainly due to the climatic and/or geological reasons described above (*Langhans et al.*, 2011).

**Channel distribution and clouds**

Generally, the global ubiquity of valleys is not consistent with the recent scarcity of tropospheric clouds and their confinement to certain latitudes within the last six years of Cassini-observation (see Figure 5.16, *Lorenz et al.* (2005b), *Brown et al.* (2010) and references herein).

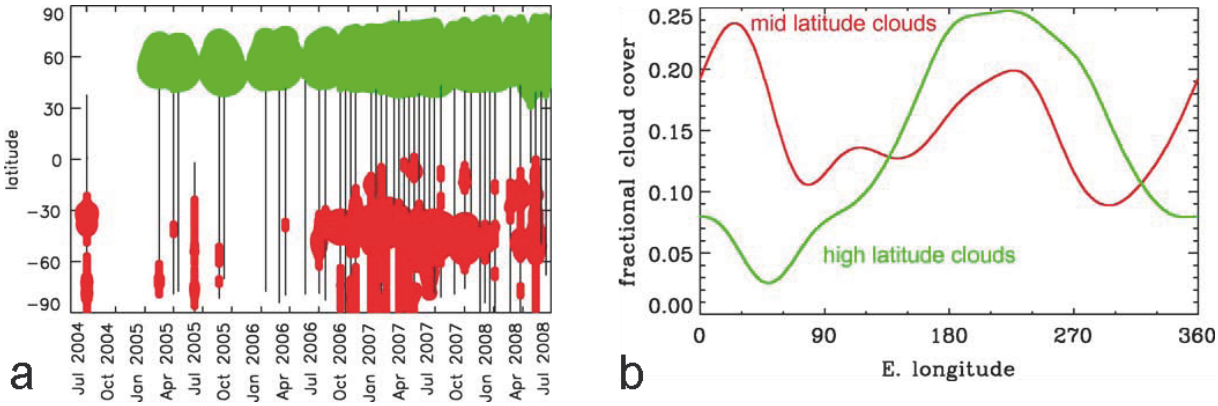


**Figure 5.16:** Distribution of clouds during the Cassini prime mission (from *Brown et al.* (2010)). Red circles show tropospheric clouds while the green circles show the near-tropopause ethane cloud. a: Cloud distribution vs. latitude. Solid line indicates the time of the flyby and the range of latitudes covered. b: Fractional cloud coverage vs. longitude.

Clouds are frequent around 60° northern latitude as well as at southern mid-latitudes (see Figure 5.16a). Figure 5.16b illustrates the longitudinal distribution of clouds. The location of the northern-hemispheric high-latitude clouds (green) correlates well with the location of the large lakes and channels in this region. Tropospheric clouds of the southern hemisphere give reason to expect dense and active channel networks at these latitudes, which is not observed (cf. Figure A.8, Appendix). If the fractional cloud coverage of Titan's atmosphere is compared to the terrestrial situation (see Figure 5.17) the ubiquity of clouds on our home planet is apparent. Less surprisingly, the cloud coverage is highest over the oceans. Titan's substantially lower fractional cloud coverage can be explained by the deficit of open bodies of liquids,

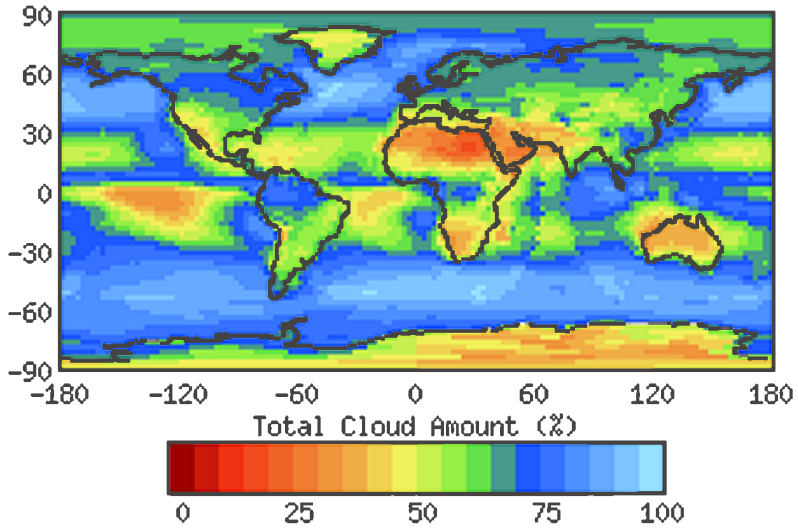


**Figure 5.17:** Mean global annual cloud coverage on Earth from 1983 to 2008 (Source: http://isccp.giss.nasa.gov).

which is both responsible for and also an expression of the dryer climatic conditions on Titan.

However, it is difficult to explain the distribution of channels from recent cloud observations. Dendritic valleys are located both at high and low latitudes, while the mid-latitudes are dominated by dry channels. Candidate sapping channels emerge only at two locations (at the HLS and at mid-latitudes), whereas the lakes are confined to high northern latitudes (*Hayes et al.*, 2008). The distribution of mountain valleys is restricted to rugged, radar-bright terrains, which, in turn are scattered around Titan's lower latitudes (mainly between $\pm$ 30°, (*Radebaugh et al.*, 2007; *Lopes et al.*, 2010)) and seem to be more affected by orographic processes than by the global circulation. Individual elongated valleys are scattered over all latitudes of Titan with the exception of the polar areas. As in most of the other types of valleys, these features are indicative of previous rainfall, possibly a wetter climate in the past and a predominantly dry climate today (*Griffith et al.*, 2008; *Lunine and Lorenz*, 2009).

Except for the region close to Titan's north pole, the majority of channels is certainly empty today (see Section 5.5). The distribution of clouds and channels leads to two different interpretations: Either, the climatic conditions in the past have been more humid than the dry situation today, or rainfall and fluvial incision are ephemeral phenomena in space and time, responding to the likewise ephemeral clouds (*Griffith et al.*, 2005) coupled with occasional rainfall events. Supporting this, many valleys show a morphologic resemblance to dry valleys and wadis on Earth (see Section 5.1.2), consistent with the second interpretation attempt.

**Seasonal dynamics**

High latitudes, both the north polar as well as the south polar region, exhibit fluvial valleys (see Figure A.8, Appendix). However, the valley (and lake) density is higher around the north pole and, most importantly, north polar valleys are currently active

(*Stofan et al.*, 2007; *Wye et al.*, 2009; *Stephan et al.*, 2010), which is further supported by cloud observations at these latitudes by *Brown et al.* (2010). On the other hand, clouds have also been observed near the south pole, which weakens the argument of a pronounced seasonality (*Rodriguez et al.*, 2009a; *Brown et al.*, 2010). So far, only few, smaller and eroded lakes have been found close to the south pole (*Lunine et al.*, 2008b). Spectral observations suggest a shrinking of the southern Ontario Lacus, the largest and most prominent lake of the southern hemisphere (*Barnes et al.*, 2009b; *Hayes et al.*, 2010a; *Turtle et al.*, 2010). Supporting that observation, only few channels emerge in this region (see Figure A.8, Appendix), and most of them are empty, although several, probably active channels drain into Ontario Lacus (*Wall et al.*, 2010). The distribution of dry versus filled channels within the polar regions mirrors the state of the lakes. These observations support findings by *Stofan et al.* (2007) and *Lunine et al.* (2008b), who suggested that a transport of moisture in the atmosphere is taking place between the two hemispheres. This turnover is possibly a seasonal effect, since evaporation is attributed to the summer hemisphere while rainfall is suggested to take place in the winter hemisphere (*Rannou et al.*, 2006; *Stofan et al.*, 2007). Currently, the southern hemisphere switches from summer to autumn (*Lorenz et al.*, 2009) and a reversing of climatic conditions is expected (*Stevenson and Potter*, 1986; *Stofan et al.*, 2007; *Lunine et al.*, 2008b; *Rodriguez et al.*, 2009a). Alternatively, the observed unequal distribution of filled and abandoned lakes and channels and the obvious differences in precipitation and evaporation between Titan's hemispheres might be the result of Saturn's eccentricity (*Aharonson et al.*, 2009). In addition, recent studies report on increased summer precipitation at high latitudes based on models of Titan's atmosphere and circulation (*Mitchell et al.*, 2009; *Tokano*, 2009). These models are contradictory to the observations of active fluvial features in the present study. To prove any seasonal variations in rainfall, the rate and variation of precipitation and evaporation have to be significant. Otherwise the distinctly unequal distribution of active and abandoned lakes and channels is more likely to be a regional or orographic phenomenon (*Langhans et al.*, 2011).

Another clue concerning the global distribution of valleys is given by their close association with mountains (*Radebaugh et al.*, 2007) and their conceivable orographic origin (*Barth*, 2010; *Lopes et al.*, 2010). Despite a rather flat topography in the order of several hundred meters difference in elevation (see Section 4.3.2), a correlation between these landforms is apparent. Alternative explanations for the correlation between rugged terrains and channels are that mountainous terrain is less resistant to fluvial incision, or that mountains, as opposed to plains and dunefields, are not subject to sedimentation. Within the plains, fluvial landforms are possibly superposed by younger sedimentary layers. Unfortunately, these hypotheses cannot be verified at the current image resolution and coverage.

**Uncertainties**

The evidential value of this analysis is limited for different reasons. Some linear features visible in radar have a yet uncertain origin and their development from rainfall cannot be proven. Besides, the only lineaments identified so far are those that are marked by a distinct contrast to the surrounding terrain and with a sufficient size. Remarkably, fluvial valleys have been imaged by the DISR sensor at excellent image resolutions of some tens of meters (*Tomasko et al.*, 2005). It must however be assumed that there is yet an unpredictable number of additional fluvial features, beyond the resolution limit of the radar sensor, and that the current inventory represents only a snapshot based on recently accessible information. Hence, the distribution of fluvial features and their association to other geologic features observed here might be distorted with respect to the real situation. Further, none of the Cassini instruments provide 100% surface coverage at a reasonable resolution. The 40% ground coverage achieved by the radar instrument up to now is far from complete. Thus, without question our current impression of the distribution of valleys is incomplete and any assessment of the global fluvial inventory, regardless of the instrument used, is caught in a conflict between image resolution and coverage.

Moreover, differentiating between active and abandoned valleys and thus evaluating possible seasonal dynamics on Titan is - strictly speaking - not possible from current image data. The radar sensor provides only indirect indications on the state of valleys as it does not determine the composition and the aggregate state of the reflecting surface. Finally, the mixed-pixel effect which often blurs the outlines or morphologic characteristics of valleys narrows the explanatory power of radar-SAR.

## 5.3 Spectral Properties of Fluvial Terrain

### 5.3.1 Global View

VIMS data unveil the subdivision of Titan's surface into at least three different surface units (*Porco et al.*, 2005; *Barnes et al.*, 2007a; *Soderblom et al.*, 2007a; *Jaumann et al.*, 2008; *Le Mouélic et al.*, 2008; *Jaumann et al.*, 2009; *Stephan et al.*, 2009), visibly obvious in false-color composites of spectral bands within Titan's atmospheric windows with the following specifications: R: 1.58/1.28 µm, G: 2.0/1.28 µm, and B: 1.28/1.08 µm. The subdivision of Titan's surface into bright continents and islands, blue surfaces, and brown dune plains is specified in Section 4.2.

Figure 5.18 shows the distribution of spectral surface units at Titan's lower latitudes as seen by the VIMS instrument, overlayed with the database of fluvial valleys. Since the overlap between these data layers comprises only areas between 30°N and 30°S (and only those which are effectively covered by SAR, i.e. about 20% of the total surface of Titan), the results are not necessarily representative of the entire surface. However, the percentages indicate a strong tendency of the fluvial channels to be situated on the bright surfaces, as is visible in near-infrared images (see also Table 5.1).

Bright continents and islands host 84.4% of the valleys (percentage of the total channel length normalized by the surface area of bright surfaces) (*Langhans et al.*, 2011). Since bright surface units are expected to be elevated (and possibly older) terrain, fluvial erosion might also be a relict process. Nevertheless, the presence of the bright surface unit is not necessarily an indication of fluvial incision since this terrain is not entirely covered by channels. Alternatively, the dearth or absence of channels in some VIMS-bright areas might be a resolution effect since possible smaller channels of a sub-pixel size are not within the range of our imaging sensors. Only 3.5% of valleys emerge on the dark brown unit, and 12.1% of the normalized valley-km at low latitudes relate to the dark blue surface unit. The majority of them is situated near the boundary of bright and blue/brown terrain, many of them run through more than one spectral unit. The small fraction of valleys outside bright terrains can result from a spatial offset between VIMS and SAR data due to the spatial resolution of VIMS being significantly coarser than the radar resolution. In VIMS images with a resolution of 10 km/pixel, boundaries between spectral units can be blurred (mixed-pixel effect) and channels situated near that boundary are assigned to that spectral unit which dominates regarding its areal extent within the pixel. Nevertheless, the majority of valleys are located too far from these transitions, i.e. at least several VIMS pixels away from the boundary between spectral units, which makes the influence of mixed pixels less significant. Despite this, at least one possible channel cutting through dunes has been published in *Barnes et al.* (2008). But, although dark blue and brown surfaces together account for almost 40% of the surface near the equator, only about 15% of the valleys are situated here (*Langhans et al.*, 2011).

Spectral investigations of high-resolution VIMS data combined with SAR images suggest a spectral analogy between the material covering fluvial channels situated at Titan's low latitudes and the dark blue surface unit (*Barnes et al.*, 2007b). Due to the high relevance of fluvial incision on Titan evidenced by the high number and the widespread ramifications of valleys, it seems reasonable that fluvial sediments cover correspondingly large areal fractions of the surface, possibly those 7% of the surface covered by the dark blue material at lower latitudes (*Langhans et al.*, 2011). However, a direct correlation between the dark blue unit and Titan's valleys is not detectable on this large scale, although there seems to be a correlation on a local scale (e.g. *Jaumann et al.*, 2008). Extended VIMS-blue terrains occur around Titan's equator, but there appear to be only few channels here (see Table 5.1). However, many more minor valleys

**Table 5.1:** Allocation of channels to spectral units.

| Spectral Unit (Percentage of the total area between $\pm$ 30°) | Number of channels (percent of the total number) | Lengths of the channel (percent of the total channel length) | Percentage of the total channel length normalized by the surface area |
|---|---|---|---|
| Bright spectral unit (59.5%) | 341 (93.94%) | 12,071.32 km (96.2%) | 84.4% |
| Blue spectral unit (7%) | 7 (1.93%) | 201.48 km (1.6%) | 12.1% |
| Brown spectral unit (32%) | 14 (3.86%) | 269.67 km (2.2%) | 3.5% |

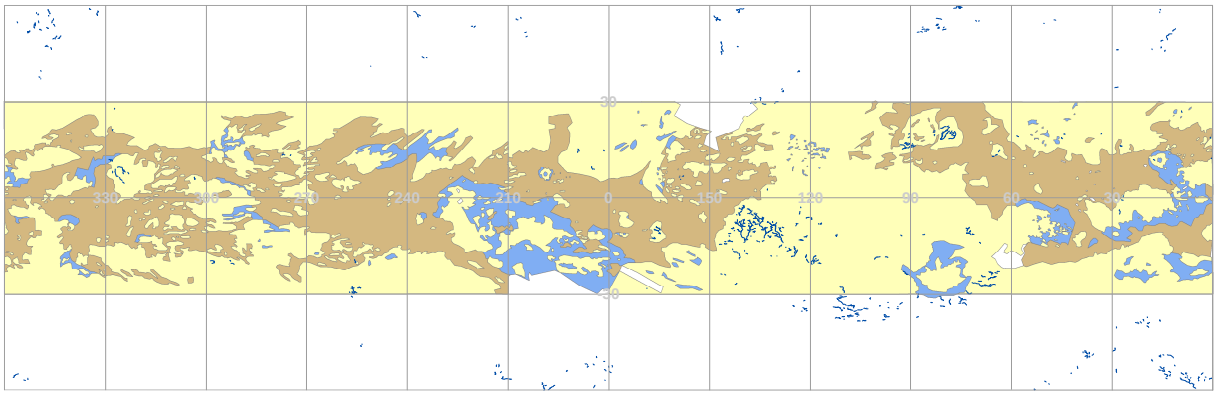

**Figure 5.18:** Map of spectral units on Titan with the same coloring as introduced in the text. Fluvial valleys are highlighted in blue. Simple cylindrical projection of Titan's lower and mid-latitudes, centered at 180°W, 0°N. See Figure A.9 (Appendix) for an enlarged view.

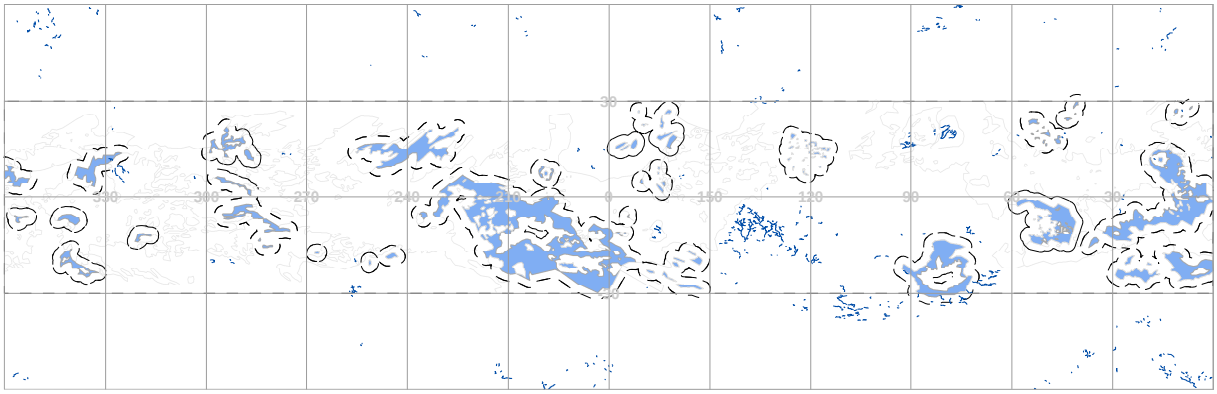

**Figure 5.19:** Map of Titan's low and mid-latitudes, simple cylindrical projection, centered at 180°W, 0°N. Buffer (100 km, dashed lines) around the blue unit (light blue). Fluvial valleys are highlighted in blue. See Figure A.10 (Appendix) for an enlarged view.

are expected to exist that are too narrow and too short to be resolved by VIMS and radar (e.g. *Jaumann et al.*, 2008). At the maximum spatial resolution achieved by the Cassini-Huygens instruments, a number of very distinct channels appear at the HLS and at Chusuk Planitia, originating from the bright areas and draining into the blue terrains, supporting the correlation of blue surface units and fluvial erosion. The coverage by image data from the various sensors is still far from complete, which reduces the reliability of this statistical approach. Although the observed deficit of channels around the blue surface unit might be due to insufficient resolution or coverage, the fact that channels are closely associated with bright surfaces seems to preclude the assumption of fluvial deposition causing the accumulation of dark blue sediments. Further, only 7% of the valleys at low latitudes (between $\pm$ 30°) are located less than 100 km away from the blue surface unit as shown in Figure 5.19 (or just under 10% calculated by valley length) (*Langhans et al.*, 2011).

The observed unrelatedness of blue surfaces and channels points to another conceivable origin of the blue surfaces, proposed by *Le Mouélic et al.* (2008), in which blue surfaces are interpreted to be a fine-grained non-dune eolian deposition of material lighter than the dune sand. This idea is supported by the location of the blue material

at the eastern boundaries of the bright terrains, i.e. behind topographic obstacles. However, the arguments and indications supporting the correlation of blue materials with either fluvial or eolian processes are relatively weak, which makes it difficult to recognize the real origin of the blue material.

### 5.3.2 Local View

Several localities at Titan's surface are suitable for studying the spectral properties of fluvial terrains and possibly even the spectral characteristics of their interior valleys. Detailed spectral analyses are possible either due to well-resolved VIMS data, or - indirectly - through an overlap of VIMS and radar-SAR, which permit the spectral analysis of fluvial channels invisible in VIMS data alone. *Barnes et al.* (2007b) analyzed fluvial channels with lengths of several hundred kilometers and widths up to 2 km, as imaged by VIMS and radar-SAR. Figure 5 in *Barnes et al.* (2007b) depicts a valley that is visible as a series of mixed VIMS pixels with a bluish spectral footprint. Remarkably, the estimated width of the valley (based on radar observation) is significantly smaller than the VIMS resolution at that location (between 4.5 and 6.6 km per pixel). *Jaumann et al.* (2008) confirmed the correlation between fluvial features and the bluish surface unit through spectral investigations of fluvial features in other regions, e.g. at Chusuk Planitia. In this case, channels drain into a putative former receiving sea or bay that is covered by dark blue sediments. An important implication of that observation is that the blue material is probably deposited both in the river bed and at its mouth. When the recipient is reached, fluvial debris is systematically sedimented due to the lower flow velocity (*Jaumann et al.*, 2008). Sedimentation at the channel mouth is also verified at the HLS, where channels drain into a putative lake that is characterized by spectral properties of the bluish material (*Rodriguez et al.*, 2006). It is noticeable that bright continents are in many places dissected by streaks or basins of bright-bluish color. In fact, the bright surface unit is spectrally the least homogeneous unit, and exhibits substantial albedo differences (cf. Section 4.2 and *Langhans et al.* (2011)). Moreover, high-resolution VIMS data reveal that a mixture between the dark blue and bright spectral signatures yields a distinct reflectance of individual channels (*Barnes et al.*, 2007b; *Langhans et al.*, 2010). Figure 5.20 shows ratio spectra of fluvial terrains, extracted from western Xanadu. Spectra of the bright and the blue surface units are added for comparison. Pixels in the vicinity of fluvial features appear as a mixture of bright and blue surfaces in spectral terms.

This observation suggests that dark blue areas or streaks, integrated within the bright continents, are the result of fluvial erosion in those regions. Candidate channels are too small to be detected but cause mixed pixels within the bright unit. Bright materials have a higher spatial fraction of the pixel, resulting in their assignment to the bright surface unit. High-resolution spectral data of the HLS overlayed with DISR-images as well as VIMS data of Chusuk Planitia support the assumption of channels draining from bright highlands into dark blue lowlands, where sedimentation

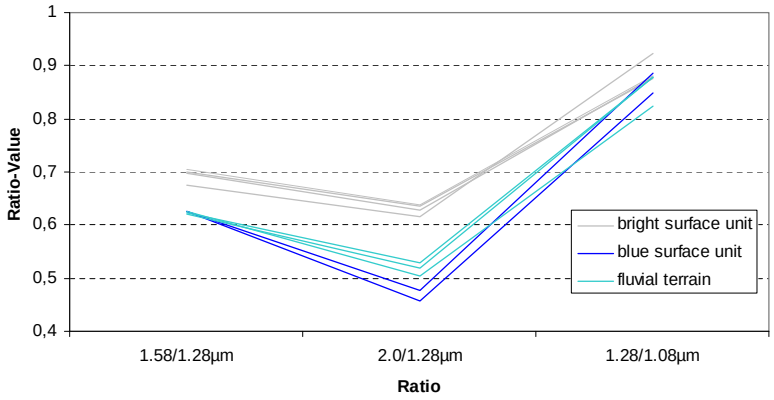


**Figure 5.20:** Ratio spectra of fluvial terrain, bright, and blue surface units (R: 1.58/1.28 µm, G: 2.0/1.28 µm, and B: 1.28/1.08 µm), western Xanadu. Valleys are identified and traced by means of radar data observation T13 (April 30, 2006). VIMS data (observation T12, March 18, 2006, max. resolution of 7 km/pixel) were overlayed and spectra were extracted at locations dissected by fluvial features. Spectra of pure blue and bright pixels are added for comparison. VIMS-pixels are considerably larger than the estimated width of the valleys. Nevertheless, the fluvial terrain exhibits spectral properties intermediate between bright and blue surfaces.

conceivably causes the blue spectral characteristics of the uppermost surface layer (*Jaumann et al.*, 2008).

It should be noted, however, that the spatial resolution of VIMS data as well as the shielding effect of the atmosphere are factors that limit a precise determination of spectral properties of the surface. The explanatory power of VIMS at moderate spatial resolutions is diminished due to mixed pixels that obviously do not reflect the pure spectral fingerprint of valleys and other features of a small spatial extent.

## 5.4 Morphological Properties of Valleys

### 5.4.1 Geometric Dimensions of Valleys

Titan's valleys have considerable physical dimensions, with lengths up to several hundred kilometers (see Table A.1, Appendix). Dendritic valleys have the highest lateral dimensions. The average length of all valleys imaged until T57 (June 2009) is 30 km, but this value is certainly underestimated as a result of incomplete coverage and the segmented storage of valleys in the database. In most of the cases, the width of the valleys does not exceed a few pixels, sometimes with unknown fractions hidden by radar shadow (see Figure 5.26a). Most of the broader, north polar valleys, which are assumed to be active recently, have widths of 1-2 km (see Figure 5.26b). Some of the valleys (labeled as 'dry valleys' here) reach widths of several kilometers (10 km in T3, Figure 5.26c; up to 8 km in T44, Figure 5.26d, see Table A.1, Appendix). Thus, valleys on Titan, in terms of their geometric dimensions, are comparable to major terrestrial and Martian channels formed by rainfall (*Jaumann et al.*, 2010). Only some Martian outflow channels formed by the melting of large volumes of ice, such as Kasei Vallis (*Baker*, 2001), have substantially larger dimensions than Titan's channels.

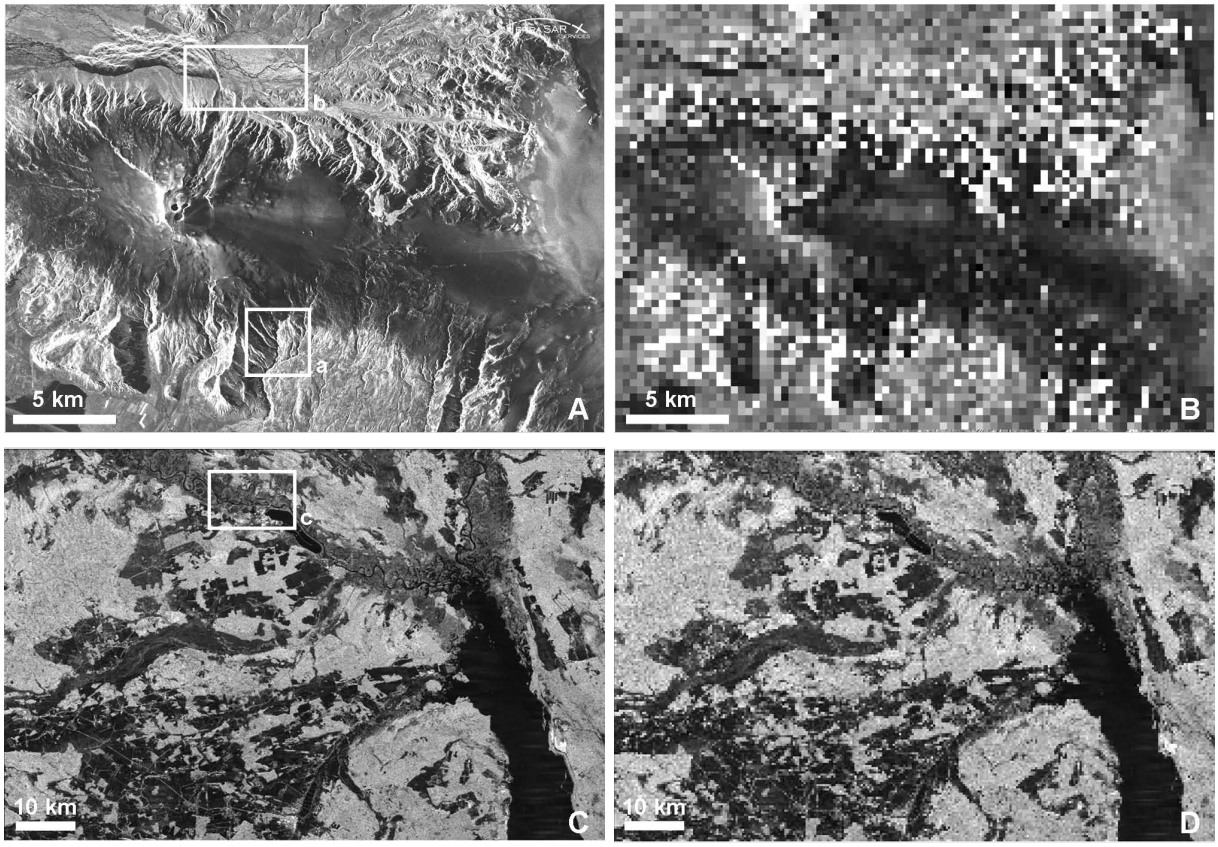


**Figure 5.21:** Radar-SAR imagery of terrestrial targets. Rectangles indicate the positions of Figures 5.22a, b, and c. a: TerraSAR-X image of the Eyjafjallajoekull Volcano, Iceland (63.38°N, 19.36°W, April 15, 2010). Many fluvial channels are apparent at the northern and southern slopes of the volcano (image source: http://infoterra-alt.mywebsedit.info/image-gallery/images.html). b: Same region as in a, rescaled to 350 m/pix. c: Spaceborne Imaging Radar-C and X-band SAR-image of the Chernobyl nuclear power plant and its surroundings (51.17°N, 30.15°W, October 1, 1994). Fluvial channels and lakes are obviously visible (Source: http://www.nasaimages.org/luna/servlet/detail/NVA2~14~14~24639~124293: Chernobyl,-Ukraine-B&W,-L-band). d: Same region as in c, rescaled to 350 m/pix.

Figures 5.21 and 5.22 elucidate the effect of spatial resolution on the visibility of valleys of various geometric dimensions, using radar-SAR images of some Earth regions as examples. Figures 5.21a and c show SAR imagery in original resolution, whereas Figure 5.21b and d are rescaled to the Cassini radar resolution of targets on Titan of 350 m/pix. To analyze the effect of resolution on the visibility of channels, the streams in both areas are magnified and displayed in true-color images (Figure 5.22 a-c). The deeply-incised channels close to Eyjafjallajoekull Volcano (Iceland) in the upper part of Figure 5.21a are invisible at the resolution of 350 m/pix. The interior channels have only widths below some tens of meters (see Figures 5.22a and b), whereas the valley occupied by the channel appears to be substantially broader. Further, the valleys seem to be inactive due to their bright tone in radar and also in optical images (see Figures 5.22a and b). By contrast, the river near Chernobyl (see Figure 5.21c) can be recognized even at the resolution of Cassini radar-SAR (see Figure 5.21d). The close-up in Figure 5.22c reveals that this meandering river is surrounded by several oxbow lakes, and, most importantly, it is currently active, as is shown by its

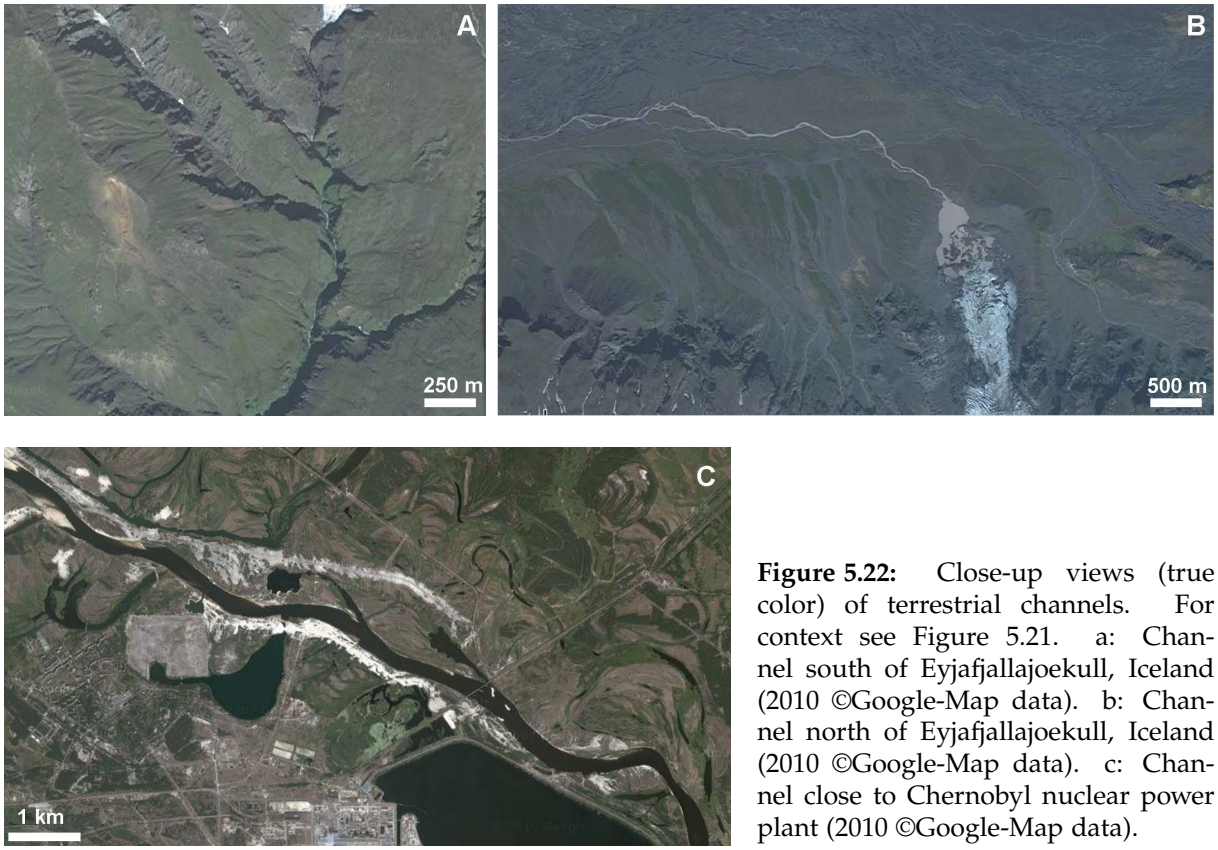


**Figure 5.22:** Close-up views (true color) of terrestrial channels. For context see Figure 5.21. a: Channel south of Eyjafjallajoekull, Iceland (2010 ©Google-Map data). b: Channel north of Eyjafjallajoekull, Iceland (2010 ©Google-Map data). c: Channel close to Chernobyl nuclear power plant (2010 ©Google-Map data).

very low radar backscatter. The pronounced contrast of the filled channel compared to its surroundings in SAR most likely causes its visibility even at lower resolutions. Further, the width of the river of up to 500 m at some places is significantly greater than that of the rivers observed in Iceland. Thus, the visibility of a linear channel in radar-SAR appears to be a function of its width and its tone in radar which is the result of the activity/inactivity of the channel at the time of the image acquisition.

### 5.4.2 Relative Ages of the Valleys and Stratigraphy

The dating of planetary surfaces is indirectly possible by investigating the crater size-frequency distribution (*Neukum and Hiller*, 1981; *Neukum*, 1983; *Neukum et al.*, 2010). Titan's noticeable deficit of craters results from intensive erosional and resurfacing processes and from Titan's atmosphere, which has protected it from being hit by smaller projectiles (*Engel et al.*, 1995; *Wood et al.*, 2010). Assessing Titan's crater size distribution with the purpose to obtain surface ages is additionally complicated by the deficit of data with resolutions better than a few hundred meters (*Jaumann and Neukum*, 2009). The age of Titan's surface was determined by *Jaumann and Neukum* (2009) on the basis of crater inventories published by *Malaska* (2007) and *Wood et al.* (2010). Model ages for the surface of Titan range between a few million years up to 3.9 GA, depending on the model chosen and its assumptions. Relative or comparative statements about the surface age of different surface units can only be made through the interpretation of stratigraphic relations.

The stratigraphy between different surface units can be deduced from the distribution of valleys versus that of craters and dunes on Titan, as displayed in Figure 5.23. Dunes are considered among the youngest geologic landforms on Titan (e.g. *Lopes et al.*, 2010). The observation that a certain number of craters are found within the dune fields (see Figure 5.23) weakens the interpretation of dunes as the youngest surface features. There are several craters, which are not entirely covered by dunes, and thus still visible, although they are certainly older than the dunes. This stratigraphy is confirmed at the Sinlap crater based on the observation that the alignment of the dunes is influenced by the crater, i.e. dunes divert and reconvert around this topographic obstacle (*Le Mouélic et al.*, 2008). Although Sinlap is expected to be a relatively recent crater due to its comparably undegraded morphology, fluvial and eolian processes are suspected to have taken place subsequent to the impact (*Le Mouélic et al.*, 2008). This chronology is also proposed in the environment of the Selk crater, although the dune alignment is not entirely resolved in radar-SAR data (*Soderblom et al.*, 2010a). Both Sinlap and Selk appear to have sufficient relief to obstruct the encroachment by dunes (*Le Mouélic et al.*, 2008; *Soderblom et al.*, 2010a).

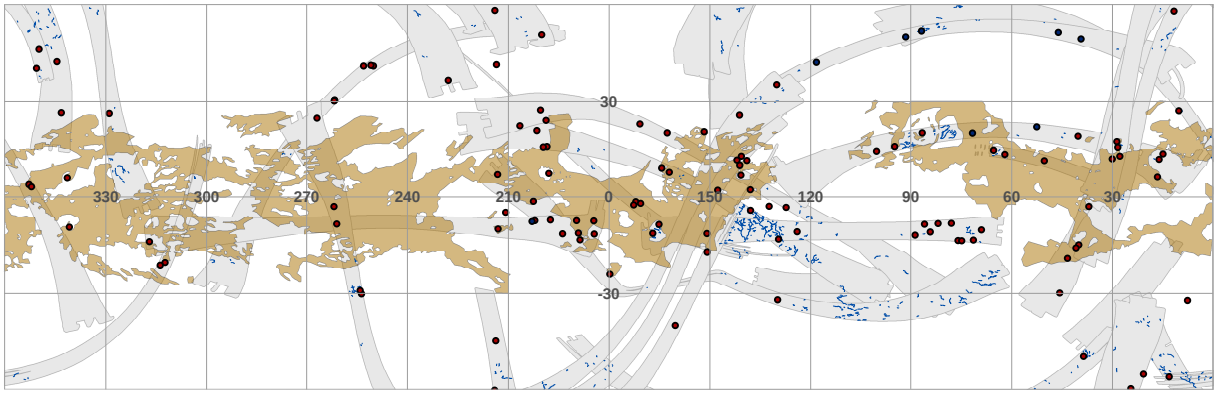


**Figure 5.23:** Map of Titan's lower and mid-latitudes, craters (red circles) and channels (blue lines) are indicated. Radar coverage is highlighted in gray. The crater inventory is marked by red circles and is based on crater catalogs in *Malaska* (2007), *Jaumann and Neukum* (2009), and *Wood et al.* (2010). This inventory is complemented by visual mapping of craters of the radar swaths T41 through T57. Blue circles indicate the location of cryovolcanic features based on *Lopes et al.* (2007a) and *Le Corre et al.* (2009). See Figure A.11 (Appendix) for an enlarged view.

The incision of fluvial valleys, along with the accumulation of dunes, is certainly among the most recent processes on Titan's geologic timescale (e.g. *Jaumann et al.*, 2009; *Lopes et al.*, 2010). Fluvial terrains should be more or less free of craters and dunes since channels tend to even out these landforms given that fluvial erosion has been active for a substantial amount of time. In fact, western Xanadu is shaped by close-knit channel networks rather than by craters or dunes. Eastern Xanadu hosts a significantly lower number of channels, a higher density of craters, and is interpreted to be old terrain (e.g. *Radebaugh et al.*, 2010). Note also that there are many localities with neither channels, nor craters, nor dunes. The characteristics and the origin of these undifferentiated terrains remain largely unknown (*Lopes et al.*, 2010).

When comparing different types of fluvial valleys regarding the relative age, their morphology provide useful clues. V-shaped valleys as well as steep and rough courses point to a more recent development. Younger stream networks in regions with a high structural control tend to have rectangular drainage geometries with fewer tributary junctions. With increasing age of a system the lithologic control decreases and its sinuosity, meanders, network density and complexity increases. The more integrated the drainage system and the more distinct the hierarchy of minor and major streams, the older is the underlying sheet (*Leopold et al.*, 1964; *Zepp*, 2008). Branches oriented in a single dominant flow direction indicate an older age of the system compared to a channel network with a more chaotic, unconsolidated, and directionless arrangement in which the branches follow local slopes (*Ahnert*, 2003; *Zepp*, 2008).

Dendritic valleys seem to be the oldest systems (or the ones that have been active for the longest period of time) because their physiography can only be explained by a steady flow over a certain period of time; taking into account their network complexity (*Ahnert*, 2003).

The other end of the scale - the youngest fluvial features - is difficult to assess since the absolute date of origin of fluvial features cannot be determined. On Earth and most likely also on Titan, sinuous, linear landforms due to fluvial flow can develop in a comparably short time (minutes to hours), possibly as a result of rapid cloud evolution and severe rain accompanying the storms (*Hueso and Sánchez-Lavega*, 2006). Relict valleys can, in the absence of other resurfacing processes, remain at the surface for a substantial time. However, Titan's valleys seem young due to their pristine and undegraded morphology (*Soderblom et al.*, 2007b; *Lunine and Atreya*, 2008). Further, fluvial features shape preexisting landforms, e.g. craters and mountains at many locations on Titan (e.g. valleys associated to Menrva crater, *Lorenz et al.* (2008a) and Xanadu's valleys, *Radebaugh et al.* (2010)), supporting the idea of the relative recency of fluvial erosion.

Valleys with a pristine and young morphology emerge in mountains (e.g. channels in Figure 5.10). The valleys' courses appear straight, following the slope of the terrain, and the valleys seem to be unaltered by other resurfacing processes. The often fragmentary course of these valleys possibly indicates degradation, either by mechanical erosion or by impact cratering, yet it could also be a resolution effect. Alternatively, the undegraded morphology of those channels might result from very resistant rock in steep, mountainous terrain.

Valleys and lakes near Titan's north pole are certainly the result of liquid-related processes in recent times and constitute a strong evidence that rainfall and erosion currently take place on the basis of their very low radar reflectivity (*Stofan et al.*, 2007). On the other hand, it would be a misconception to think of the active northern valleys as the youngest geologic features. It is equally possible for the entire north polar fluvial system to be relatively old and active on seasonal timescales. This idea is supported by the high complexity of dendritic channels near the north polar lakes.

As can be seen from the numerous different valley types (see Section 5.1) the morphology of valleys on Titan varies considerably. One possible explanation for the difference in morphologies described here might be the different formation ages of the respective channels or even of the bedrock on which they are situated, so that a general statement about the age of Titan's channels and the overall duration of fluvial erosion seems implausible.

Although stratigraphic relations between different surface units and geologic landforms can be assessed, the limited resolution and coverage of recent image data makes their interpretation difficult. Further, due to incomplete radar coverage and resolution the possibility of estimating the crater inventory is limited so that definite assertions cannot be made.

### 5.4.3 Branching Complexity and Network Geometry

Another approach to characterizing the morphology of stream systems is provided by the Strahler (or flow) order, which quantifies the branching complexity, density, and hierarchy of fluvial networks. It labels the number of tributaries counted upstream from the receiving stream and thus describes the physiography of river systems (*Butzer*, 1976; *Ahnert*, 2003). The concept of stream order is based upon the fact that terrestrial river networks usually form a typical dendritic, i.e. tree-shaped structure, with many distributed sources and branches that join together to form larger and larger receiving streams (see Section 5.1.1). The flow order helps to deduce the origin and development of the valley network. Generally, with increasing branching complexity the size of the catchment increases. Large flow orders thus are a certain indication that a valley system originates from precipitation that occurred in an extensive area.

Although the absolute age of geologic features cannot be determined, a qualitative assessment of the network geometry can be used to estimate and compare the relative ages of different channel networks. Subsurface tectonic control manifests itself in the general shape or structure of the channel network (*Ahnert*, 2003; *Zepp*, 2008). Inversely, the higher the complexity, density, and stream order of the network, the lower the total slope and flow velocity (*Leopold et al.*, 1964). But, due to the varying influence and resistance of the bedrock in different regions, no definite statements can be made, and even comparative studies have only limited validity.

Currently, three localities are apparent where complex dendritic networks are resolved (see Section 5.1.1). One of these networks is located at Xanadu, covered by radar swaths T13 and T44. The major receiving streams of that network are oriented into a southern direction. The network system is located on raised terrain. This network has a fragmentary course at some locations, either as an effect of resolution or due to subsequent (non-fluvial) erosion. The region has a high radar backscatter, indicative of a rough surface. The channels are even brighter in radar, pointing to a riverbed that has been dry and inactive in recent times. However, these networks


**Figure 5.24:** Mapping result, dendritic channel networks close to Titan's north pole, channels and lakes are mapped based on radar observation T28 (April 10, 2007).

evolve flow orders of up to seventh (see Table A.1, Appendix). It has to be remarked that the course of Titan's channels is disconnected and fragmentary at many places, thus the assessment of the stream order relies on the image resolution, it is not objective and cannot serve as an absolute measure. Several other examples of dendritic networks are located in extended areas around the north pole (see Figure 5.24). These networks with flow orders up to sixth cover almost the entire area between the large lakes and most of them finally drain into the lakes. These channels, as well as the lakes, have a low radar return, thus, channels and lakes are interpreted to be filled with liquid hydrocarbons at the time of image acquisition (*Stofan et al.*, 2007; *Wye et al.*, 2009; *Stephan et al.*, 2010) (see Section 5.5). Channel systems at the Huygens Landing Site feature flow orders up to fourth. The fact that dendritic valley systems with a substantial complexity are found at several locations on Titan underlines the significance of rainfall, which seems to be anything but a local phenomenon.

Besides this, a great number of valleys appear with a simple course, and a low number of tributaries. A lot of those valleys appear in Titan's mountains at mid-latitudes. These valleys tend to vanish and their mouth or recipient often cannot be recognized. These morphologic characteristics point to dry conditions with irregular runoff, possibly indicating precipitation by thunderstorm events (*Hueso and Sánchez-Lavega*, 2006; *Jaumann et al.*, 2008) and/or the presence of relatively permeable bedrock.

The fact that Titan's channels evolve a range of network orders, from very simple to relatively complex ones, suggests that a likewise high variability of bedrock resistances, rainfall and runoff regimes prevails. High-order networks can be found at only a few places whereas no latitudinal dependence is apparent from current image data, as complex networks occur both at high and low latitudes. A high variability concerning the formation ages of the valleys is obvious and also regarding the duration of the process of fluvial erosion, since the high-order networks have likely been active for the longest period of time compared to channels (or channel systems) with a more simple geometry (see Section 5.4.2).

However, because of the limited spatial resolution of the radar sensor, it must be assumed that smaller tributaries are present but currently invisible. Therefore, the true branching complexity is most likely to be significantly higher than that determined based on Cassini imaging data.

## 5.5 Brightness/Appearance in Radar Images

Fluvial valleys are either radar-bright (e.g. around Xanadu, see Figure 5.26c and d), radar-dark (e.g. near the north pole, see Figure 5.26b), or they appear as a pair of parallel bright-dark linear features (see Figure 5.26a) (*Lorenz et al.*, 2008a; *Burr et al.*, 2009; *Langhans et al.*, 2011). The strength of the radar return depends, among other physical properties, on the roughness of the reflecting surface (*Elachi et al.*, 2006) (see Section 3.3), thus, it is to some extent possible to infer whether a particular channel has a smooth surface or not. Low radar backscatter is caused by materials that are smooth at the radar wavelength of 2.17 cm. A smooth surface can result from a layering of fine-grained sediments, indicative of slower-moving flows or even owing to an open body of standing liquids (*Lorenz et al.*, 2008a). Radar-bright channels (see Figure 5.26c and d)) are interpreted to be covered by coarser sediments, e.g. rounded icy blocks (*Le Gall et al.*, 2010). However, the intensity of the radar return depends upon several factors other than the roughness and surface structure, such as the layering, surface slope, inclination, composition, volume scattering, and the dielectric constant of the material (*Thompson and Squyres*, 1990; *Elachi et al.*, 2006; *Kirk et al.*, 2007). Clear correlations between the signal strength and the roughness/smoothness or even the recent activity of the channel are therefore not necessarily implied. Nevertheless, at least relative or comparative statements about the channel floor relative to its surroundings or between different channels are possible (*Langhans et al.*, 2011).

Where the observation geometry of the radar instrument is such that its viewing direction is perpendicular to the alignment of the valley, and where the incision made by the valley into the bedrock is substantial, some valleys are visible as a series of bright/dark pixels (see Figure 5.26a and Figure 5.25) (*Burr et al.*, 2009). This bright/dark pairing occurs because the escarpment facing the sensor appears bright while the escarpment facing away from illumination is in radar shadow, and no signal is detected (*Burr et al.*, 2009). This phenomenon provides no evidence as to whether or not a valley is active.

Valleys with a very low radar return of their interior channels are presumably filled with liquids (see valleys close to the north pole, Figure 5.26b). The receiving lakes are likewise interpreted to be filled with liquids due to their characteristic shape, spectral properties, and low radar return (*Stofan et al.*, 2007; *Brown et al.*, 2008; *Jaumann et al.*, 2009; *Wye et al.*, 2009; *Stephan et al.*, 2010). Since the lake-surrounding valleys have a similarly low radar backscatter, their recent activity is also very likely (*Langhans et al.*, 2011). These valleys have numerous interconnections and a well-defined

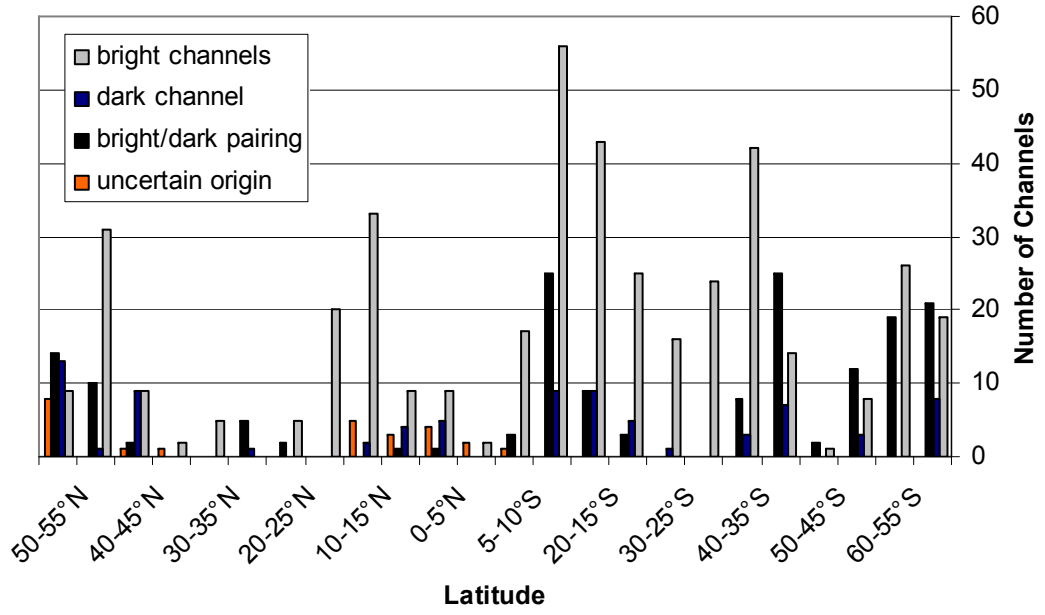


**Figure 5.25:** Geographic position of fluvial valleys on Titan. Appearance in radar is indicated by the color of the bars.

course (see also Figure 5.3), arguing for a substantial topographic depression caused by fluvial incision.

In contrast, the valleys of western Xanadu have a high radar return. Those valleys are certainly not liquid-filled and presumably covered by material of sizes larger than the radar wavelength of 2.17 cm, e.g. rounded rocks or pebbles (*Le Gall et al.*, 2010). Many of the other valleys on Titan, either integrated within networks or as individual valleys, exhibit a high radar return (see Figure 5.25). The majority of them emerge at southern latitudes where also a significant number of radar-dark channels are apparent. Channels with bright/dark pairing are the second most common group of valleys. Their distribution is coupled with the overall channel density, and their abundance depends on the viewing geometry. Radar-dark channels are relatively rare compared to bright ones, although the observed proportion can shift when the availability of data increases. It has to be remarked that the radar-dark channels considered in Figure 5.25 at lower and mid-latitudes are still brighter than valleys near the north pole as the radar-brightness/darkness of the channels is assessed with respect to the surroundings of the channels. This observation is more consistent with a layer of smooth sediments that cover the channel floor rather than with the interpretation that the channel is currently filled with liquids.

## 5.6 Sedimentation

Fluvial channels deposit their load at decreasing flow velocities as they approach their recipient. However, current Cassini data only detected few landforms that can positively be ascribed to sedimentation of fluvial material, such as alluvial fans and deltas.

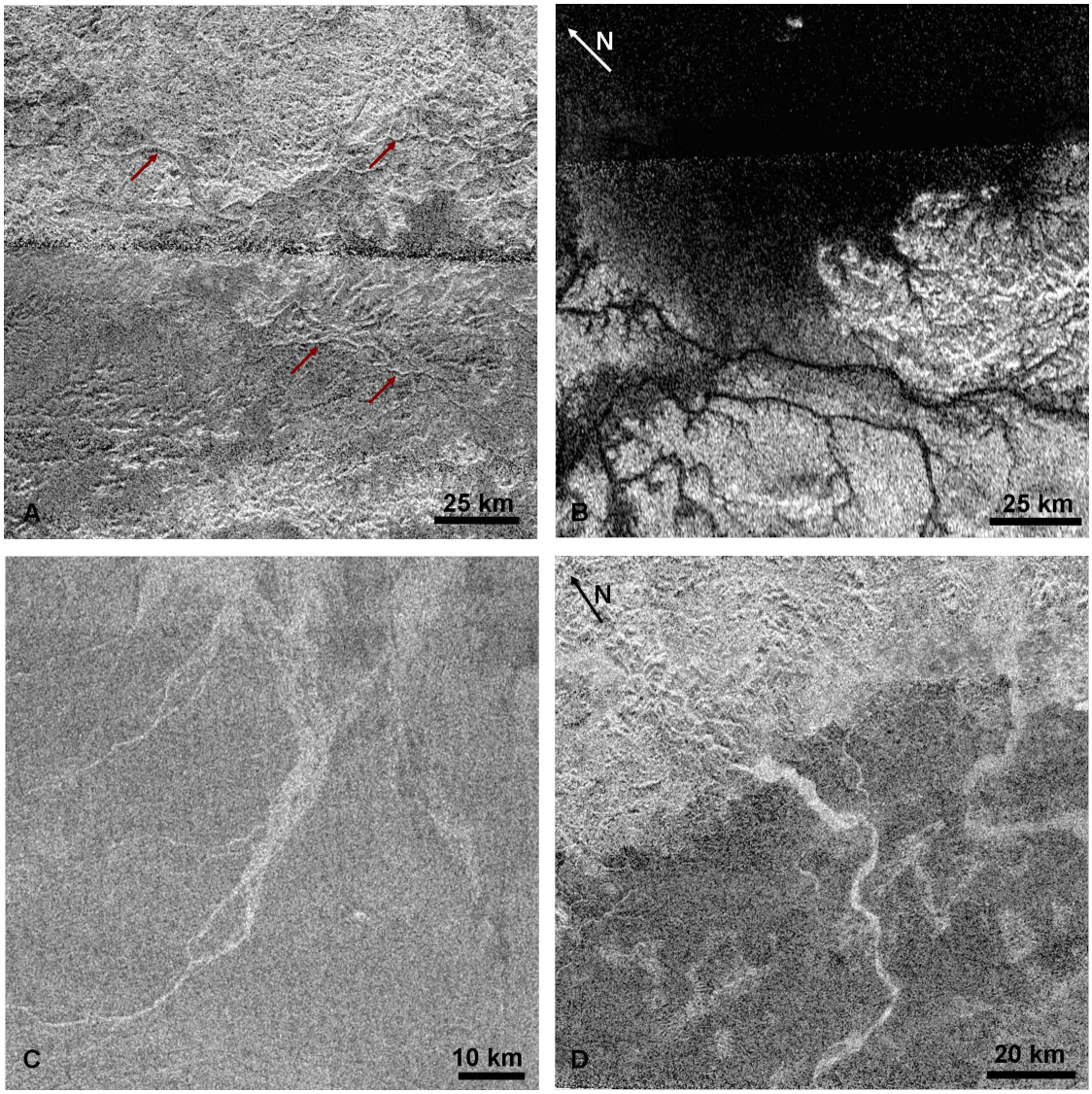


**Figure 5.26:** Geometric dimensions of fluvial valleys on Titan. a: Putative fluvial valleys south of Xanadu, imaged by radar-SAR observation T41 (February 22, 2008). Image is centered at 36°S, 107°W. Radar shadows highlighted by red arrows (illumination from south). b: Fluvial valleys near the north pole, as imaged by radar-SAR observation T28 (April 10, 2007). Image is centered at 76°N, 263°W. c: Dry fluvial valleys east of Menrva crater, imaged by radar-SAR observation T3 (February 15, 2005). Image is centered at 19°N, 77°W. d: Fluvial valleys south of Xanadu, imaged by radar-SAR observation T44 (May 28, 2008). Image is centered at 17°S, 125°W.

According to *Burr et al.* (2006), potential sediment material can be water ice from the crust and organic material coming from the atmosphere. Distributary patterns were identified by radar-SAR swath TA by *Paganelli et al.* (2005); *Stofan et al.* (2006); *Lopes et al.* (2007a); *Lorenz et al.* (2008a) associated with Ganesa Macula, where channels as well as delta-shaped landforms appear in a radar-bright tone. Chusuk Planitia is another region where well-resolved VIMS data reveal a potential sediment accumulation zone (*Jaumann et al.*, 2008). Another likely region of fluvial deposition resolved by radar-SAR is Elivagar Flumina, east of the Menvra impact structure (*Stofan et al.*, 2006; *Lopes et al.*, 2010). Extensive bright, diffuse plains surrounding mountains are

interpreted to have their origin in fluvial sedimentation (*Radebaugh et al.*, 2007). Moreover, *Wall et al.* (2010) identified a candidate delta at the shoreline of Ontario Lacus at the end of a channel that drains into the lake. This putative delta is visible on radar imagery. In the context of the present study, some further candidate fluvial sediments are marked in Figure 5.7. Note the deficit of receiving landforms of fluvial flow, with many localities where fluvial features seem to vanish (e.g. in Figure 5.7, Figure 5.31). This deficit is in stark contrast to the vast number of channels, and is possibly to be explained by high infiltration or aridity.

## 5.7 Estimation of Discharge

Calculations on the basis of terrestrial and Martian channels suggest the correlation of the channels' geometric dimension and their rates of discharge and sediment transport (e.g. *Jaumann et al.*, 2005; *Kleinhans*, 2005). Thus, the enormous extents and large number of channels on Titan point to high transport rates (of liquids and solid sediments) resulting in a high relevance of fluvial processes, despite the fact that the smaller branches are most likely not even resolved. In fact, erosion rates on Earth and Titan are comparable but some uncertainty factors remain (*Collins*, 2005).

Given the morphological resemblance of terrestrial rivers and valleys on Titan, and the similar rate of bedrock incision through fluvial erosion (*Collins*, 2005), relations between stream flow and channel incision should be comparable on Titan and Earth, too. Average flow rates of liquids flowing through individual channels have been determined by means of empirical data gathered on Earth transferred to the conditions on Mars and Titan (*Kleinhans*, 2005; *Perron et al.*, 2006; *Jaumann et al.*, 2008, 2010). Required parameters for such estimates are the geometric dimensions of the specific channel cross-section, at least a minimum of topographic information, and the gravity of the body since stream flow is a function of channel depth, width, and flow velocity (e.g. *Komar*, 1979; *Baker*, 2001). Generally, the steeper the slope (and the higher the gravity of the body), and the larger the cross-sectional area, the higher the discharge rate. It is further known that higher flow velocities are required to transport coarse sediment particles than for entraining small particles, while the transport of coarse-grained material is in theory facilitated by an increase in the concentration of the flow, i.e. through an enrichment with fine-grained particles (*Burr et al.*, 2006). Based on the determination of streamflow volumes for Titan's channels the methane cycle can be characterized further, since discharge and sediment transport rates provide a retrospect constraint of the rainfall rates necessary to shape the channels (*Jaumann et al.*, 2008).

Up to now, determining the height of surface elevations that would have been required on Titan to obtain the flow velocity is challenging. The radar-altimeter does deliver elevation profiles, but that mode is not activated when SAR imagery is recorded due to incompatible observation geometries of the two techniques (*Stiles et al.*, 2009).

Thus, altimeter data cover only a limited area of Titan (*Radebaugh et al.*, 2007). SAR-stereo and SAR-Topo are other techniques to obtain topographic data which, however, require an overlap between different radar swaths. If this condition is fulfilled at several locations, SAR-Topo can assess the elevation conditions even in regions covered only once (*Stiles et al.*, 2009). Shape from shading (or radarclinometry) benefits from topographic shading due to the radar illumination. Relative height information can also be indirectly derived from the network geometry of channels and from the interpretation of stratigraphic relations.

Due to the limited resolution of the Cassini sensors, which often does not permit any distinction between an interior channel and the entire valley (*Perron et al.*, 2006; *Komatsu*, 2007; *Jaumann et al.*, 2008), the estimation of discharge has only limited validity. The spatial resolution provided by Cassini imagery results in significant uncertainties in determining the widths of the channels since their lateral extent rarely exceeds one or two pixels. As a result, discharge estimates can, at most, provide the upper limits of fluvial flow. Another simplifying assumption is the expected stream flow at bankfull stage, which relates to the amount of liquids when the entire inner channel is filled. It is yet impossible to assess up to which level a channel on a remote target is or has in the past been filled. Moreover, the precise mapping of the channel catchment is not possible yet due to the current lack of digital elevation models in an adequate resolution and coverage. Topographic parameters such as slopes cannot be measured directly but are estimated. Deviations or errors in the estimation of the drainage area have an immediate effect on the calculated discharge rate and on the calculated rate of rainfall per unit area. However, the geometric dimensions of valleys yield at least relative values when different valleys, or systems of valleys, are compared. To evaluate rainfall rates, it is important to take the size of the catchment into account. Extended catchments with only very narrow channels point to lower rainfall rates than stubby channels in a small drainage area at otherwise identical conditions. Valleys with a significant rate of stream flow that has been constant over time can in general be distinguished from valleys with a more episodic stream flow as the latter are characterized by an irregular channel geometry and abrupt changes in width. Thus, correlations between the channel geometry and the rates of rainfall, discharge, and sediment transport are essential in quantifying Titan's methane cycle and in comparing different channels (or channel systems).

Based on the boundary conditions provided by the particle size of fluvial sediments observed at the Huygens Landing Site, the geometric dimensions of fluvial channels observed at different localities with different imaging instruments, and factoring in the effect of putative infrequent methane thunderstorms (*Hueso and Sánchez-Lavega*, 2006), the estimated discharge rate is 1,600 $m^3/s$ with a rainfall rate of 0.6-60 mm/h, at short recurrence intervals (*Jaumann et al.*, 2008). Depending on the recurrence interval assumed, the range of conceivable discharge rates is quite wide, with values from <1$m^3$/s for the channel system at the Huygens Landing Site at short

repetition rates, up to several thousand $m^3/s$ for larger channel systems at longer recurrence intervals (*Jaumann et al.*, 2008). The rainfall events are expected to be separated by long droughts of up to 1,000 years, which explains the relative intensity of rainfall events (*Jaumann et al.*, 2008). The largest storms on Earth yield rainfall rates of 0.2 to 0.4 $m^3/h$ (*World Meteorological Organization*, 1994; *Perron et al.*, 2006). Martian valleys in the Western Libya Montes drainage system have had an average discharge between 15 and 430 $m^3/s$ (*Jaumann et al.*, 2010). Unfortunately, it is not possible to assess the duration of the process of fluvial erosion as a whole, and to determine whether it has still been an active phenomenon in recent times, considering the long recurrence intervals.

## 5.8 Lakes on Titan

Besides fluvial valleys, Titan's surface exhibits extensive lakes, which act as reservoirs and sinks of open liquids. The presence of lakes at Titan's surface was considered possible even before their existence was evidenced by Cassini data (*Muhleman et al.*, 1990). Several hundred lakes of various sizes exist near the north pole, visible as radar-dark patches (*Lopes et al.*, 2007b; *Stofan et al.*, 2007; *Hayes et al.*, 2010a). Ontario Lacus close to the south pole was discovered in 2005 by ISS and VIMS observations (*Brown et al.*, 2008; *Turtle et al.*, 2009). Subsequently, this lake was imaged by radar-SAR, too, allowing precise morphological analyses (*Hayes et al.*, 2010b; *Wall et al.*, 2010).

A parameter supporting the interpretation of a feature as standing body of liquids is its low radar signal in radar-SAR, which is indicative of flat and smooth surfaces relative to the radar wavelength of 2.17 cm. This observation also points to a low dielectric constant of the detected surface, which is consistent with the presence of liquid methane (*Lopes et al.*, 2007b; *Stofan et al.*, 2007). The assumption that the lakes are recently filled with liquids is supported by their low near-infrared reflectivity as detected by VIMS data, which indicates that almost all photons incident on the lake are absorbed, particularly in the 5 µm atmospheric window (*Brown et al.*, 2008). The observation of a specular reflection by VIMS data in Titan's north polar region, associated with Kraken Mare, provided a further confirmation that open bodies of liquid are present (*Stephan et al.*, 2010). Another confirmation for seas of open liquids comes from the analysis of the radar echo that revealed their surface to be smooth, with height differences below 3 mm (*Wye et al.*, 2009). Bodies of standing water on Earth tend to absorb most incoming near-infrared radiation with wavelengths longer than the visible light within 2 m of the surface, entailing a very dark tone in near-infrared images, too (*Lillesand et al.*, 2003). Further, their characteristic shape with quasi-circular or irregular outlines, their location in steep-sided topographic depressions as well as the fact that numerous valleys open out into them (*Stofan et al.*, 2007) are consistent with a lacustrine background of the features. The surrounding fluvial valleys possibly replenish the liquid storage of the lakes (*Wall et al.*, 2010).

The exact chemical composition of the lakes is not fully constrained, but compounds likely to be involved include methane, ethane, propane, butane, dissolved nitrogen, and higher-order hydrocarbons/nitriles (*Mitri et al.*, 2007; *Stofan et al.*, 2007; *Brown et al.*, 2008; *Hayes et al.*, 2010b). *Brown et al.* (2008) compared the lake spectrum of Ontario Lacus as detected by VIMS with a model spectrum in order to investigate possible compounds and to simulate the effects of scattering in the atmosphere. As a result, alkanes, particularly ethane, have been found to be consistent with the observations of this study (*Brown et al.*, 2008). For the northern lakes a composition from ethane and/or methane is assumed, which is in accordance with the observed specular reflection properties (*Stephan et al.*, 2010; *Soderblom et al.*, 2010b). Tholins are certainly not a component of the lakes (*Hayes et al.*, 2010b). Through evaporation, the hydrocarbon inventory of the lakes could conceivably resupply the atmospheric methane which is irreversibly decomposed by photolysis (*Stofan et al.*, 2007). Ethane is another likely compound because of its involatility at Titan's temperature and pressure regime (*Stofan et al.*, 2007). It is not known to this date whether the depressions harboring the lakes developed from karst, e.g. due to the presence of dolines or sinkholes, or if they originate from volcanic, or even glacial activity (*Lopes et al.*, 2007b; *Stofan et al.*, 2007).

The lakes near the north pole cover large areas, the largest one of which, Kraken Mare, centered at 68°N and 310°W, covers about 400,000 km$^2$, which makes it comparable in size to the Black Sea on Earth which has an area of 424,000 km$^2$ (*Turtle et al.*, 2009). Several other large lakes are situated around Kraken Mare (see Figure A.8), most of which are fed by a very dense network of local channels. Another extensive region with smaller lakes and only few valleys, which is located between 0 and 150°W at high northern latitudes, stands in contrast to the region with large lakes and indicates significant regional climatic differences. Here, precipitation, if any, took place in the past whereas evaporation or infiltration certainly dominate today (*Hayes et al.*, 2010a). It is debated, whether processes such as chemical weathering, karst formation, or the interaction with a subsurface liquid reservoir are involved in shaping the landscape at high latitudes (*Mitchell et al.*, 2007b; *Stofan et al.*, 2007; *Hayes et al.*, 2008, 2010a). Further, some lakes seem to be only partially filled with liquids or even empty, as can be seen from their frayed shorelines and their high radar backscatter, which is possibly a sign of recent climatic dynamics. At some localities the SAR images possibly reflect the properties of the lake bottom due to the large penetration depth of several tens of meters by radar in pure liquids (*Hayes et al.*, 2008; *Barnes et al.*, 2010). The entire northern lake region is interspersed by mountains.

Radar data of both polar regions allow multitemporal analyses of some lake-areas by taking repeated looks at the same ground area. Figure 5.27 shows the coastline of Jingpo Lacus as imaged in October 2006 and in April 2007, whose shoreline was traced in the earlier observation. No substantial differences in the extent and boundaries of the lake are recorded. The small deviations observed are probably due

to a slight geometric misalignment and due to different viewing geometries of the SAR data. What could be more important is the fact that the time slot covered by the Cassini mission is too short - considering Titan's seasons - to provide evidence on any substantial extensional differences, the seasonal change of evaporation and precipitation, or other climatic dynamics. These processes would be visible as the shrinking or growing of the lakes and as changes in the network geometry of fluvial valley systems in their vicinity. It is important to monitor the state of the lakes in future since their development indicates seasonal changes.

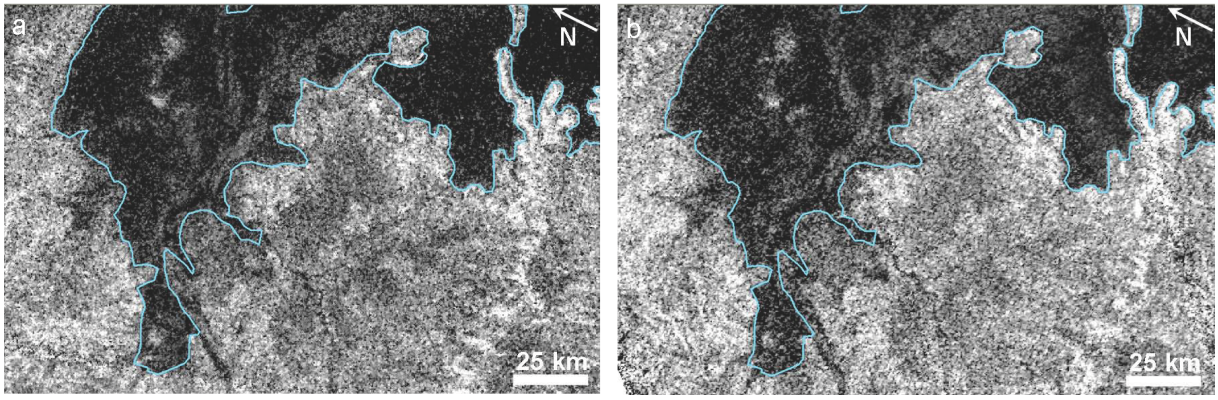


**Figure 5.27:** Jingpo Lacus, observed at two different points in time. Shoreline is traced (in light blue) based on the SAR-map on the left (a). Images are centered at 340°W, 74°N. a: Radar-SAR observation T19 (October 09, 2006). b: Radar-SAR observation T28 (April 10, 2007).

In December 2007, the VIMS instrument recorded data covering the eastern part and the shoreline of Ontario Lacus, which is centered at 180°W, 74°S, near Titan's south pole and has an area of 15,600 $km^2$. Spectral investigations provided the evidence of liquid ethane as one of the constituents (*Brown et al.*, 2008). Other candidate constituents are propane and butane. The detection of liquid methane by spectral analysis is not yet possible due to the strong spectral similarity of liquid $CH_4$ and $CH_4$ gas in the atmosphere. Atmospheric $CH_4$ outweighs the spectral footprint of potential liquid methane within the lake (*Brown et al.*, 2008). The morphological and spectral properties of the shoreline - with different spectral units arranged concentrically - possibly suggest the exposure of lake-bottom sediments and organic condensates from the lake, visible near the shore (*Barnes et al.*, 2009b). This observation seems to be an indication of a falling lake level through evaporation or infiltration, although the timescale of this climatic or seasonal change is not yet known. The subsequent imaging of the lake by radar-SAR supported the idea of a shrinking Ontario Lacus (*Wall et al.*, 2010).

The distribution of the northern lakes is confined to areas north of 70°N, consistent with the predicted climatic situation with a high ethane and methane precipitation rate close to the north pole, arid conditions, and the dominance of evaporation in Titan's tropics (*Rannou et al.*, 2006). Few and mainly empty lakes at high southern latitudes are in contradiction to cloud observations in these latitudes

(*Rodriguez et al.*, 2009a; *Brown et al.*, 2010). Owing to the undersaturation of methane in the lower atmosphere (*Flasar*, 1983; *Lunine*, 1990; *Lorenz and Lunine*, 2005) the lakes as well as the channels are most likely ephemeral and transient features that quickly respond to changing climatic conditions. In the context of Titan's methane cycle, these lakes are particularly important because they indicate - on a local or regional scale - that precipitation exceeds evaporation, at least at some time in the recent past. Irrespective the short observation time, the northern lakes seem to be comparably stable features. Another interesting aspect is that environments with standing liquids are considered to be preferential locations for a chemical and biological evolution and the development of life.

The distribution of lakes supports the assumption of a humidity gradient from the poles to the equator, whereby the lower atmosphere near the north pole seems to be more humid than the same latitudes of the southern hemisphere (*Stevenson and Potter*, 1986; *Lorenz*, 1993; *Lorenz and Lunine*, 1997). Different liquid levels of the lakes in general point to variable climatic conditions in different regions, e.g. active evaporation, which, in turn, proves the recent activity of a volatile cycle.

Ethane cannot evaporate from the lake owing to its low saturation pressure, thus only methane is subject to evaporation (*Mitri et al.*, 2007). Therefore, evaporation from the lakes necessarily causes an enrichment in ethane and a concomitant depletion of methane. By contrast, infiltration of liquids would probably not change their fractions in the solution. Determining the fraction of ethane in Ontario Lacus would with great certainty answer the question whether evaporation or infiltration is responsible for the declining lake level.

The geological relevance of the lakes is that they probably serve as suppliers of atmospheric methane (*Mitri et al.*, 2007) since evaporation even from the lakes known so far might be sufficient to replenish the atmospheric methane content. An estimated amount of 30 to 300,000 $km^3$ of methane/ethane is suggested to be stored in the lakes (*Lorenz et al.*, 2008b). Nevertheless, a lacustrine resupply of methane is limited and provides only a short-term source compared to a regolith as a candidate global methane supply.

Cassini imagery revealed an apparent dichotomy between lakes in the high northern and southern latitudes in terms of their frequency and coverage. Whether the almost complete absence of lakes near the south pole is due to seasonal effects or due to the availability of condensation nuclei near the north pole is not yet known (*Samuelson and Mayo*, 1997; *Tokano et al.*, 2001). An alternative explanation could be Saturn's obliquity, which leads to differences of evaporation and precipitation between the two hemispheres (*Aharonson et al.*, 2009). Owing to the ascending motion at the summer pole, high evaporation rates are expected to cause the shrinking of lakes at the current summer pole (*Stofan et al.*, 2007). Similar to many regions with abandoned channels over almost all latitudes of Titan, the south polar area shows signs of humid conditions in the past followed by dry conditions in recent times.

Since the north polar lakes show different fluid levels and the size of the lakes varies regionally, it must be assumed that there are regional differences in precipitation and that the climatic conditions also vary in time. Although only slight differences in the lake level of Ontario Lacus are detected by different instruments of the Cassini mission and between different points in time (*Barnes et al.*, 2009b; *Hayes et al.*, 2010a; *Turtle et al.*, 2010), it is likely that the shoreline of the lake has receded and that conditions have been more humid in the past, at least at the location studied.

## 5.9 Fluvial Valleys in the Solar System - Examples from Earth, Mars, and Titan

Drainage channels, shaped by the transport of liquids, are common geologic features on planetary surfaces, namely at the surface of Earth, Mars, and Venus. The only bodies in the Solar System currently known to host active volatile cycles are Titan and Earth, whereas Mars has all the indications of a former water cycle. Remote sensing imagery provides an optimal means to investigate landforms shaped by flowing liquids.

On the other hand, comparing different planetary surfaces is complicated as measurements or observations by remote sensing are merely indirect methods. Besides, the different datasets and images obtained are often not of uniform image quality and resolution in terms of their spatial, spectral, and temporal characteristics. Regarding spatial resolution alone, recent image data of Earth and Mars are better resolved by a factor of at least ten compared to image data of Titan's surface. On Earth, even a direct inspection of fluvial valleys is possible, revealing a wealth of details about fluvial features.

**Types of Fluid Flow**

Some of the channels on remote targets are obviously the result of *lava flow* subsequent to volcanic events, which is a common process on terrestrial bodies such as Venus, Earth, Mars, and the Earth's Moon. Besides shaping a linear channel, the basic processes leading to lava drainage are significantly different from fluvial erosion caused by rainfall, particularly as they provide no indication of an ongoing volatile cycle. Lava channels have a localized source, resulting in a nearly constant width of the channels over their entire length and a deficit or even absence of tributaries (*Komatsu and Baker*, 1996). Further, the forces at work are thermal and mechanical erosion, with constructional characteristics overweighting those of erosion (*Komatsu and Baker*, 1996). Because of their irrelevance to the analysis of Titan's methane cycle lava channels were not investigated further in the context of this work.

*Sapping by subsurface liquids* is a process that is suggested but not conclusively proven to exist at the surface of each of the targets considered here. Sapping is proposed to be the origin of several valley systems at the Martian surface on less resistant

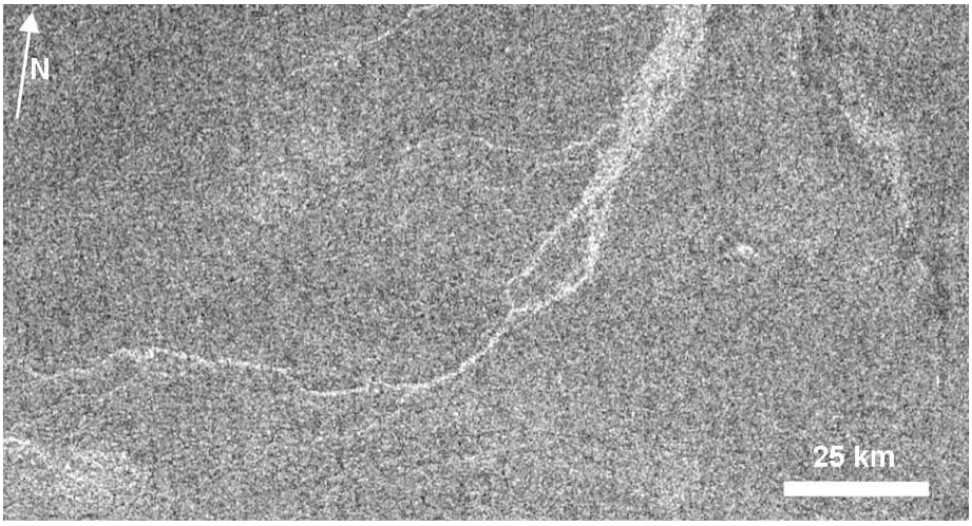


**Figure 5.28:** Valleys on Titan and Earth in (potentially) arid environments. Top: The Elivagar Flumina channel system, Titan (see also Figure 3 in *Lorenz et al.* (2008a)), radar-SAR observation T3 (February 15, 2005). Image is centered at 80°W, 20°N. Bottom: Terrestrial wadis, Egypt. Image is centered at 27°23'N, 32°3'58E (2010 ©Google-Map data).

or sedimentary substrate (*Lamb et al.*, 2006). While a contributory action of seepage appears to be reasonable, considering it to be the sole origin of the features observed is controversial, even for terrestrial landforms (*Lamb et al.*, 2008). Fluvial features on Titan with a possible origin from sapping are discussed in Section 5.1.3 and depicted in Figures 5.8 and 5.9. Further, the idea of a subsurface methane storage system on Titan - although suggested by various authors (see Section 2.3.4.1) - is not clearly proven yet.

*Gullies* are another fluvial landform that is common to Earth and Mars. These very small features with cross-sections of some tens of meters up to a few kilometers might be a very recent phenomenon which possibly developed during the past decade. These landforms putatively originate from the melting of ground ice or snow or from seepage erosion and surface runoff (*Malin and Edgett*, 2000). Small-scale features such as gullies are certainly below the resolution limit of the Cassini sensors and therefore presumably - if present - not traceable yet at the surface of Titan.

Numerous *outflow channels* are found on Mars and Earth, attributed to short-term, catastrophic water flooding leading to very drastic discharge events (*Komatsu and Baker*, 1996; *Burr*, 2009) (see Figure 5.30A). Outflow from deeply buried aquifers is presumably triggered by volcanic or impact events (*Carr*, 1979). Another suggested scenario is the catastrophic release of water through collapsed zones named the chaotic terrain (*Baker*, 2001). Outflow channels on Mars are large-scale linear features with lengths of several thousand kilometers and widths of up to 200 km (e.g. Kasei Vallis) (*Komatsu and Baker*, 1996; *Baker*, 2001) and are thus highly relevant when interpreting previous Martian climatic conditions. For Titan's channels an origin from outflow is rather unlikely, since glaciation and the sudden melting of large volumes of

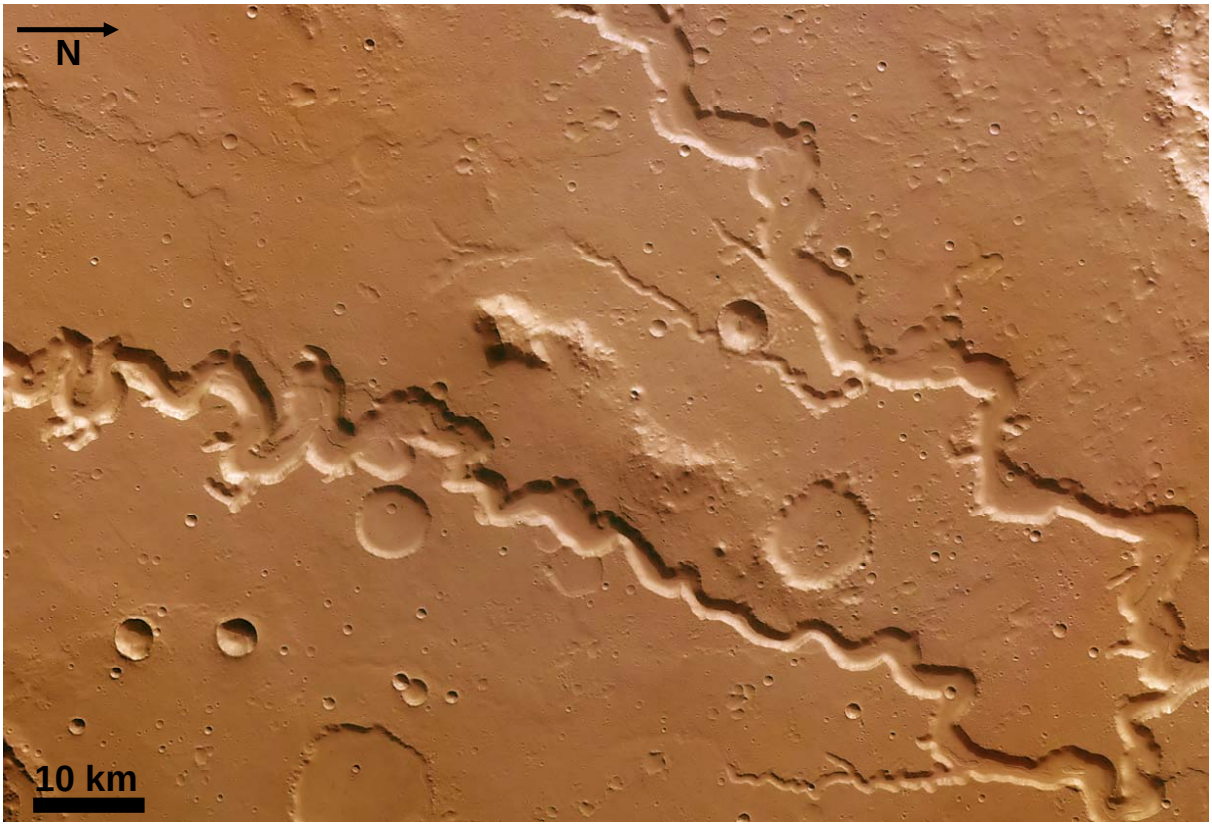


**Figure 5.29:** Nanedi Valles on Mars, obtained by the High-Resolution Stereo Camera (HRSC), October 3, 2004, ground resolution of approximately 18 m/pix, 6.0°N, 312°E (Source: ESA/DLR/FU Berlin, G. Neukum).

ice are not possible under Titan's ambient conditions (*Lorenz and Lunine*, 1996). Thus, the formation of glacial landforms including enormous outflow channels can be ruled out for Titan.

**Dimensions and Morphology of Valleys**

The dimensions of Titan's valleys with several hundreds up to more than a thousand kilometers and widths up to several kilometers (see Table A.1, Appendix) are comparable to large streams on Earth, such as the Rhine, the Danube, or even the Mississippi. Valleys on Titan are also comparable in size to drainage features on Mars, e.g. Nanedi Valles (see Figure 5.29), which has a width of up to 5 km and a length of about 800 km and even to Martian outflow channels with widths of some tens of kilometers and length of several thousand kilometers (see Figure 5.1 and Figure 5.2), although even larger systems are known on Mars (*Komatsu and Baker*, 1996; *Baker*, 2001). Many similarities in morphology between Titan's channels and rivers on Earth and Mars suggest that the valleys have developed in a similar way (see Section 5.1 and Figure 5.30), which is remarkable considering the different liquids that shape the surface of both bodies.

Rivers on Earth are very diverse in their geomorphology since water - even in

its solid phase - can shape the crust of the Earth in various ways. Terrestrial fluvial valleys are often predefined or widened by glacial erosion (*Komatsu*, 2007), for which no indication is observed on Titan. Further processes that are common on Earth include gravity flows and lava flows. Groundwater sapping also contributes to its high morphological diversity. Combined with the numerous different substrate types on which valley systems can develop and with different rainfall regimes, all this adds up to a great variety of morphologies on Earth. Generally, the diversity of relief, forms, and processes appears to be comparable on Titan, Mars, and Earth, although some processes can be ruled out under Titan's conditions. The most obvious similarity in terms of fluvial landforms is the presence of dendritic channel networks at the surface of the three bodies, indicative of a distributed source of liquids (see e.g. Figure 5.24).

**Origin of Valleys and Climate**

Valley morphologies similar to those of Martian outflow channels, such as flat cross-sections and a braiding course, also occur at the surface of Titan. These valleys most likely originate from sudden thunderstorm events with subsequent surface runoff (see Figure 5.30b) (*Hueso and Sánchez-Lavega*, 2006; *Jaumann et al.*, 2008). This morphology is a possible analog to the terrestrial desert wadis, depicted in Figure 5.28 (bottom) and Figure 5.30c, which evolve due to sudden discharge events with high volumes of liquids. The example shows that although this morphology is common at the surfaces of Earth, Mars, and Titan, different processes seem to be responsible for the formation of these features. Martian channels with flat cross-sections and a low sinuosity evolve due to outflow events, whereas some of Titan's channels and terrestrial wadis likely evolve from episodic intense rainstorms (*Hueso and Sánchez-Lavega*, 2006; *Jaumann et al.*, 2008). However, traces of fluvial erosion can remain visible at the surface for a long time at each of the targets considered here. Even in terrestrial deserts which are extremely arid, the traces of rare past events of fluvial erosion often remain evident since there is little or no vegetation and a surplus of fine grained material (see Figure 5.28, bottom).

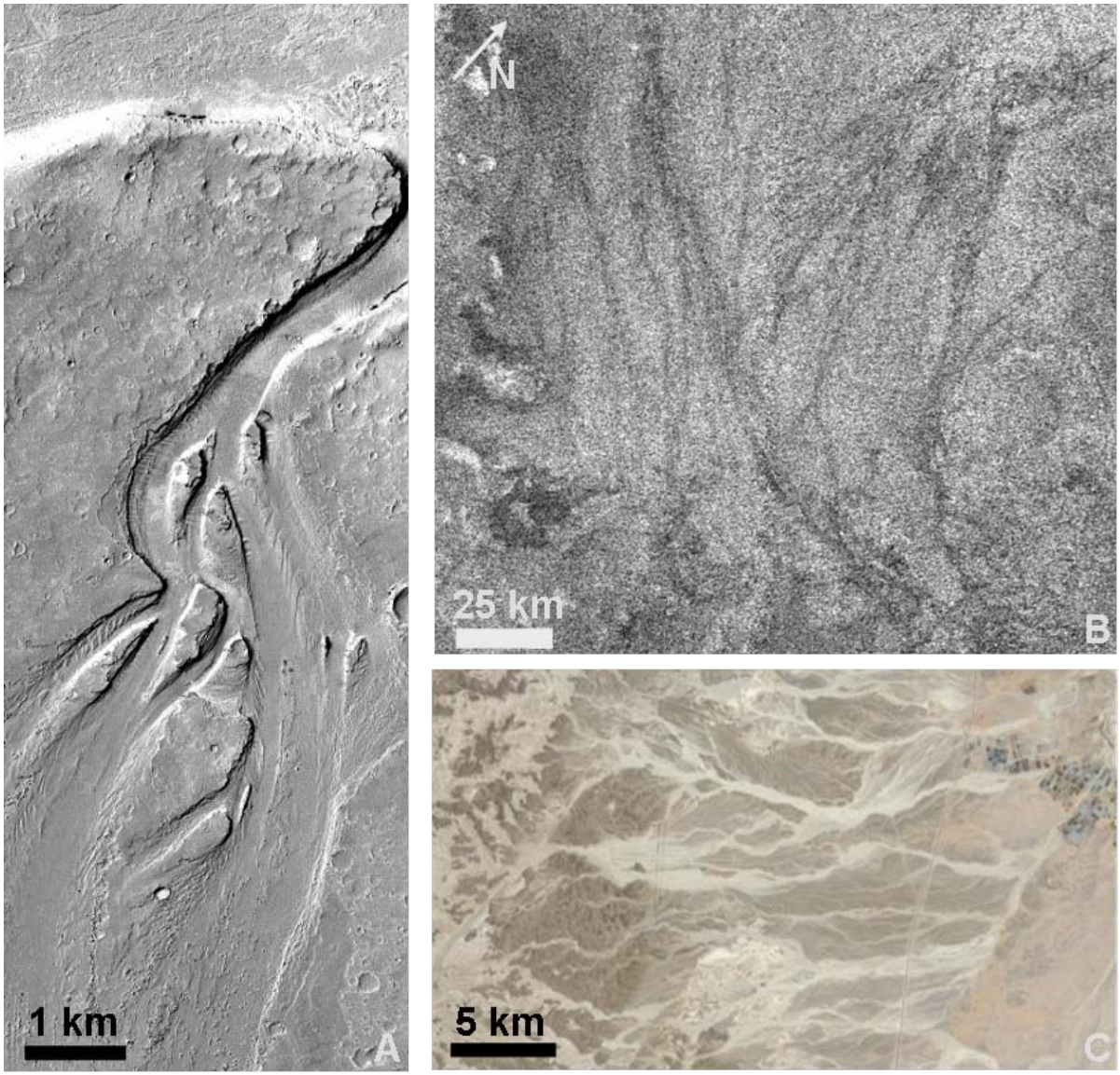


**Figure 5.30:** Comparison of valleys on Mars, Titan, and Earth. a: Martian outflow channels. High resolution Mars Orbiter Camera (MOC) image, 7.9°N, 205.8°W (from *Baker* (2001), modified). The channels have formed streamlined uplands with an anastomosing course. b: Candidate channel system on Titan at southern mid-latitudes, radar-SAR observation T7 (September 7, 2005). Image is centered at 7°W, 60°S. Frequent shifts and relocations of the potential riverbed cause this irregular morphology. Alternatively, this morphology can be explained by denudation or laminar fluvial flow due to sudden and violent rainstorms. c: Terrestrial wadis, Israel, Negev Desert (2010 ©Google-Map data). Image is centered at 30°45N, 35°13E. The braiding features are not subdivided into an interior channel and valley.

*Orographic rainfall* appears to be an analog process on Titan and Earth. Surface runoff and the incision of channels on Earth occur preferentially in mountainous areas. Although some indications exist (see Figure 5.10), this process cannot be uniquely verified on Titan, considering the comparatively low estimated mountain heights of several hundred meters (*Radebaugh et al.*, 2007). Alternatively, the elevated (and most likely older) terrain could be a relict of former - more humid - times, when intense precipitation occurred on a global scale. What weakens this idea is the presence of likely active channels near the north pole, making fluvial activity seem more like a function of space rather than time. Further, a significant number of channels have been found outside mountainous terrains, which rules out orographic rainfall as the sole origin of Titan's channels.

Many morphologic characteristics of Titan's channels point to prevailing aridity: Fluvial transport in some candidate channels takes place over hundreds of kilometers, sometimes without any convergence with other tributaries and without any morphologic changes in flow. However, a volcanic origin of these flows is equally conceivable (see Section 5.1.5, Figure 5.11). Many putative fluvial channels on Titan seem to vanish without a previous thinning out of the interior channel (see Figure 5.31), pointing to an abrupt change in boundary conditions toward dryer conditions, either in the catchment or at the vanishing point. Moreover, channels are scattered on Titan with only few and selected areas significantly influenced by fluvial erosion (see Figure 5.28, top). Lakes, the indicators of a climate in which precipitation overbalances the sum of evaporation and infiltration, cover a relatively small area compared to the area covered by oceans and seas on Earth. Furthermore, although a number of terminal lakes are observed close to the north pole (*Stofan et al.*, 2007) (see Figure 5.26b and Figure A.8, Appendix), and near the south pole (Ontario Lacus) (*Wall et al.*, 2010) it can be noted that Titan has only few large-scale recipients of fluvial flow, such as deltas, estuaries, and alluvial fans, particularly if compared to the Earth. These landforms emerge almost exclusively in high-resolution images, e.g. at the HLS (*Tomasko et al.*, 2005; *Soderblom et al.*, 2007b) and in the Chusuk Planitia region (*Jaumann et al.*, 2008). Possibly, an extensive lake situated south of Xanadu once served as a receiving lake for the northern channel network (*Barnes et al.*, 2010). Nevertheless, the relative scarcity of recipients of fluvial flow points to pronounced aridity, evaporation, or infiltration. Although the apparent lack of recipients might be a resolution effect, the numerousness of channels does not tally with the small number of recipient landforms observed so far. Except for the situation close to its north pole, Titan's climatic conditions resemble those of Mars, whose surface is crisscrossed with many relict channels and gullies formed by the action of water in the past. In contrast, the majority of fluvial systems on Earth are active today, either perennially or at least episodically/seasonally.

The fact that fluvial erosion on Titan is not restricted to certain latitudes and that at least the abandoned fluvial valleys occur at virtually all latitudes (see Figure 5.12, Figure 5.13, Figure 5.14, Figure A.7, and Figure A.8, Appendix) supports the theory

that Titan's surface has previously experienced global rainfall. The observation of the shrinking Ontario Lacus (*Barnes et al.*, 2009b; *Hayes et al.*, 2010a; *Turtle et al.*, 2010) underscores the dominance of evaporation and infiltration which, at least locally, is also an expression of an active methane cycle.

Although at Titan's low latitudes large parts of the surface are free of dunes, channels observed in this region are few and far between. Titan's valleys are distributed over most of the surface units that can be distinguished by ISS, VIMS, and radar with the exception of the equatorial dune fields. It is conceivable that Titan's dunes cover paleochannels beneath them, as does the Sahara desert (*Komatsu and Baker*, 1996; *Ghoneim and El-Baz*, 2007). This would be an indication that the formation of dunes is the youngest geologic process to have shaped Titan's surface, and fluvial erosion would have been a global phenomenon, rather than a localized or regional phenomenon that has recently subsided. In contrast to Titan, dunes in terrestrial deserts are sometimes associated with fluvial or alluvial forms since a sand supply is required for the accumulation of dunes. Yet, the dune-forming sand may equally have been transported over thousands of kilometers, making the presence of dunes independent from a local sand source in the direct vicinity (*Prospero and Carlson*, 1972; *Roda et al.*, 1993).

**Characteristics of Volatile Cycles on Earth, Mars, and Titan**

Erosion through fluid flow can only occur on those planets or bodies where temperature and pressure conditions allow liquids to circulate. At least on Earth and Titan, all the requirements for the activity of volatile cycles, such as the presence of a liquid, the solar energy supply, and the presence of an atmosphere (see Section 2.3.4.2), are met. The example of Venus demonstrates that the presence of an atmosphere and clouds alone is not enough to enable a volatile cycle and fluvial erosion, and that the environmental conditions near the surface are also highly relevant. Given that our own Solar System has only a limited number of bodies to be analyzed, the persistence of volatile cycles such as on Earth and Titan appears to be unique.

Water on Earth controls and stabilizes its temperature and climate through what is known as the greenhouse effect (e.g. *Jacob*, 1999). Water (or water vapor), transfers thermal energy between the surface and the atmosphere by evaporation and condensation, it compensates latitudinal insolation gradients and also contributes to a number of chemical reactions. The most important fact regarding the habitability of Earth is that its water cycle is a closed system, i.e. the full amount of water that evaporated reaches the ground again as rainfall, after remaining in the atmosphere for a certain residence time. The results of the present study, e.g. the observation of numerous dry, abandoned channels, morphologic indications for vanishing of channels, and the large areas covered by dunes, suggest that Titan either does not have a closed methane cycle and currently experiences 'dehydration', i.e. the depletion of liquid methane, or that the resupply of methane happens on a timescale substantially larger than the

timespan covered by Cassini-observations. The observed aridity is in contrast to the high number of abandoned channels, which point to more humid conditions at the time of their formation. Whether the continuous destruction and escape of methane leads to a cooling of the atmosphere and finally to a collapse of the gaseous envelope as suggested in *Lorenz et al.* (1997) remains unknown.

The hydrological cycle on Earth is based on the evaporation of large volumes of water over the oceans (e.g. *Marcinek and Rosenkranz*, 1996). The high abundance of water on Earth leads to a relative dominance of hydrological processes, obvious in the intensity with which the resurfacing of landscapes takes place (*Zepp*, 2008). In contrast, it is not clear what kind of source accounts for the methane content in Titan's atmosphere. Titan's surface exhibits large bodies of open liquids in the form of lakes at both poles. There are also some indications of dried lakebeds and relict shorelines at mid-latitudes (e.g. *Tomasko et al.*, 2005) (see Figure 5.4 and Figure 5.8). These landforms point to larger quantities of liquid hydrocarbons in the past and seem to be contradictory to the more or less dry environment returned by Cassini data. Considering the absence of oceans and large bodies of open liquids evaporating as they do on Earth, the wealth of fluvial features is still surprising.

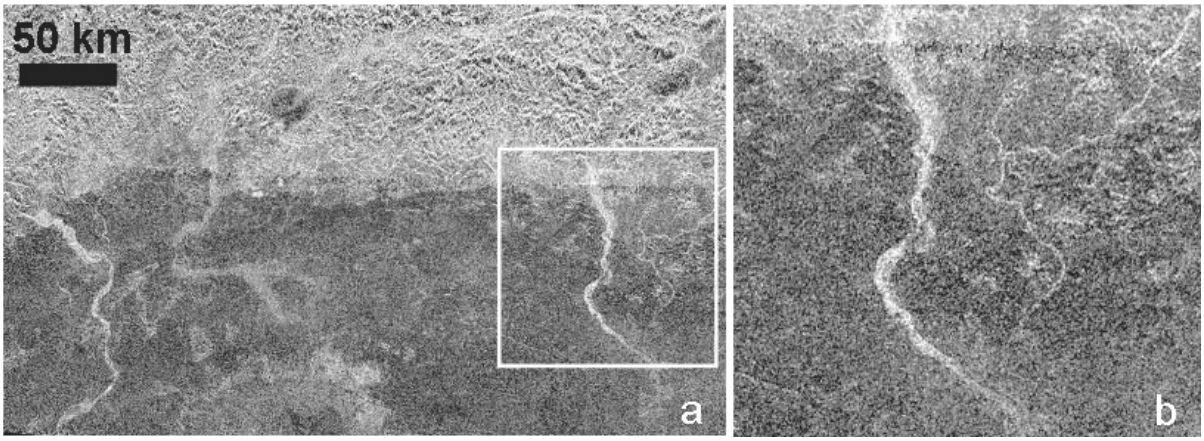


**Figure 5.31:** Valleys on Titan. a: Drainage channels south of Xanadu. Radar-SAR observation T44 (May 28, 2008). Image is centered at 20°S, 122°W. Interestingly, the channels vanish near the southern image-margin despite the substantial widths of their upper reaches. b: Subset of the context image (a).

The absence of a global ocean on Titan is also relevant regarding latitudinal energy balances. An ocean would compensate latitudinal temperature differences and large bodies of standing liquids have a significant climatic effect due to thermal inertia. Based on current knowledge, temperature gradients on Titan are only compensated by wind and by global atmospheric circulation. On the other hand, due to the reduced solar energy supply, the temperature gradient which initiates the atmospheric circulation is less pronounced than, e.g., the terrestrial temperature gradient between the tropics and the polar regions.

The water cycle on Earth as well as its geomorphological outcome - fluvial valleys at the surface - became climatologically possible when the ambient temperature in the terrestrial atmosphere dropped beneath 100°C and liquid water and even solid (water-) ice could be kept stable (*Marcinek and Rosenkranz*, 1996). Thus, fluvial erosion on Earth might have been active for about 4 billion years (*Marcinek and Rosenkranz*, 1996) and can therefore be referred to as one of the longest-running processes on Earth. However, due to intense resurfacing on Earth owing to plate tectonics, volcanism, and glaciation, mainly those fluvial streams are preserved that developed during the Quaternary (*Zepp*, 2008). By contrast, the action of water on Mars was responsible for a variety of fluvial landforms shaped in the past, many of them being strikingly similar to those on Earth. Although recent atmospheric conditions, with an atmospheric pressure at surface level of $< 6$ mbar, no longer permit any evaporation, condensation, or precipitation of water, the surface of Mars shows the signs of ancient precipitation and glaciation dating back to the early history of the planet (*Pieri*, 1976). Several periodic events occurred in Martian history in which water was active at the surface throughout each of the three stratigraphic epochs on Mars (Noachian, Hesperian, and Amazonian) for a period of altogether more than 3.5 billion years (*Baker*, 2001). The Noachian epoch was characterized by precipitation-based erosion and weathering. In the Hesperian and Amazonian epoch outflow events dominated (*Howard et al.*, 2005). Surface runoff of water from precipitation or from melting of accumulated snow has formed valleys of sinuous shapes and low structural control (e.g. *Howard et al.*, 2005; *Komatsu*, 2007). Distributed valley networks exist that developed from rainfall in warm and humid periods. Some of the flows have even been active over several periods (e.g. *Jaumann et al.*, 2010). In recent times, water is retained in the form of ice in the polar caps and in the subsurface as ground ice. The climate history of Mars shows that small changes in the environmental conditions can entail major global climatic changes, which in turn can have a significant effect on the geology.

It remains unknown for how long Titan's methane cycle has been active. The substantial influence of fluvial erosion and the high complexity and frequency of meanders in fluvial systems suggest a long-standing activity of fluvial processes. Like on Earth, eolian erosion, impact cratering, and cryovolcanism might have eroded older fluvial systems on Titan. The fact that the valleys found are either active or inactive as well as being in different states of degradation indicates that different systems are indeed of different ages, with the oldest valley systems being concentrated near the equator (see Figure 5.1 and Figure 5.2). Conceivably, several methane outgassing periods occurred in the past, as proposed in *Tobie et al.* (2006), followed by precipitation and the incision of valleys. Possibly, the methane content decreases subsequent to an outgassing event, slowing down precipitation and erosion. If this is the case, humid conditions would be a rather episodic phenomenon, similar to the climatic history of Mars which involved several distinct fluvial periods.

Both of the best-observed examples for water cycles, those of Mars and Earth, highlight a strong temporal and spatial dependence. In the case of Mars, a substantial amount of atmospheric liquids/gases is required for the action of liquid cycles. These have to be mobile, which is possible only under certain atmospheric conditions in terms of temperature and pressure. The persistence of volatile cycles seems to be very sensitive to the boundary conditions determined by the orbital parameters of the body.

Despite the fact that different compounds are involved in their volatile cycles, valleys on Mars, Earth, and Titan show a number of similarities. Striking morphological analogs have evolved in spite of differences in gravity and environmental conditions, and irrespective of the different physical and chemical characteristics of the agents involved, such as the difference in viscosity between liquid water and methane. Nevertheless, the landscape is likely to have been shaped by different geologic processes on Earth, Mars, and Titan, respectively. The surface of Mars and Earth, for instance, was partly shaped by the action of ice, which would not have been possible on Titan given its environmental conditions (*Lorenz and Lunine*, 1996; *Perron et al.*, 2006). Furthermore, these processes happen on a different scale; the enormous size of Martian outflow channels are in stark contrast to many terrestrial streams, which are orders of magnitude smaller (*Baker and Milton*, 1974; *Baker*, 2001). Martian cataclysmic flood channels have immense dimensions of 150 km width and 2000 km in length (*Baker*, 2001). The most striking contradiction observed regarding Titan's fluvial features is their vast number and their substantial dimensions despite the conceivably small amounts of liquids present, the lacking ocean, and despite the small gradients that drive the action of volatile cycles, both in terms of the topography and regarding latitudinal temperature differences.

A more detailed comparison of valleys on Titan, Mars, and Earth evaluating their areal extent, channel densities, and morphological properties is limited due to the problems regarding the comparability of image datasets of the different targets. The real density of Titan's channel networks and the number of its smaller branches are no doubt underestimated based on the current imagery.

# Chapter 6

# Conclusions

In this Section the results of the spectral investigation and stratigraphic relations of Chapter 4 and the findings of Chapter 5 about the properties of fluvial flow on Titan are summarized and set into a broader context. The main focus will be on discussing the origin of Titan's valleys, on its climatic background, and on the characterization of its methane cycle.

The global distribution of fluvial valleys is a complex issue, as shown in Section 5.2. Individual fluvial valleys are scattered over all latitudes of Titan, whereas complex dendritic systems with many tributaries are confined to high and low latitudes and have not been observed so far at mid-latitudes. Regarding their spectral properties, valleys seem to be associated to the bright surface unit, although this is not universally valid since some channels are situated on the blue and brown spectral units, too. Significant areas are completely free of channels, such as the tropic dunefields and the undifferentiated plains at low and mid-latitudes. Probably, channels are commonly associated with elevated terrain, since they often occur on rugged and mountainous terrain and are rarely found in the plains. Only the channels near the north pole appear to be currently active. They drain into large lakes, which have obviously been supplied by the channels for a certain time. By contrast, inactive channels are located near the equator and at mid-latitudes, some of them even bear resemblance to terrestrial wadis. Their morphology is more consistent with sporadic or episodic flows.

Regarding their geometric dimensions, many valleys on Titan are comparable to large drainage channels on Mars and Earth which developed from precipitation. Titan's valleys reach widths of up to ten kilometers and lengths of up to several thousand kilometers, although obviously only the major streams have been detected. Smaller valleys with widths significantly below the resolution limit of radar-SAR could not be resolved. The great range of measured stream widths, lengths, and the uncertainty of some parameters, such as the size of the catchment area, the slope, and the interconnectivity of the network, have resulted in a broad range of estimated discharge rates. The discharge volumes determined are similar to those of terrestrial streams, ranging between <1 and several thousand $m^3/s$ (*Jaumann et al.*, 2008)

depending on the particular channel studied, its geometric properties, and the recurrence interval of rainfall events. Most importantly, the estimated range of discharges bears out the idea of occasional severe thunderstorm events suggested by *Hueso and Sánchez-Lavega* (2006) and *Jaumann et al.* (2008) since it accounts for occasional runoff of large volumes of liquids. Extreme outflow events due to the melting of large volumes of ice as in the Martian history are improbable on Titan given the comparatively small size of Titan's channels and at the environmental conditions near its surface (*Lorenz and Lunine*, 1996).

A possible orographic origin of fluvial features is discussed in *Barth* (2010). This theory seems plausible since many fluvial valleys are, indeed, situated within mountainous or rugged terrain. Undeniably, fluvial valleys in Titan's mountain chains are mainly remnants of past fluvial activity. However, the idea of orographic rainfall does not seem to be the only possible explanation, given that Titan's mountains are only slightly sloped, and feature low peak heights. Moreover, an exclusively orographic origin seems unlikely if one considers the existence of the north polar valleys and the fact that many other valleys are located well away from any mountainous areas.

The clouds observed during the Cassini mission are strictly confined to certain latitudes (e.g. *Brown et al.*, 2010) with clusters of clouds around 60°N and at southern mid-latitudes, which seems to be independent of or even contradictory to the global distribution of channel systems. Compared to the meteorological conditions on Earth, Titan's mean cloud cover is poor, with clouds being rather ephemeral. Particularly, the presence of many channels in Titan's tropics is not consistent with the observed distribution of clouds, even if these valleys have without doubt been inactive recently (e.g. *Griffith et al.*, 2008). Nevertheless, the contradiction can be explained by seasonal changes as the current available database provides only a snapshot on the real cloud coverage. The observed cloud distribution is presumably not representative of the entire time of channel formation since until now the observation through instruments of the Cassini spacecraft does not even cover a single revolution period of Titan.

The presence of valleys in Titan's north polar region conforms with cloud observations in that region (e.g. *Rodriguez et al.*, 2009a). The apparent activity of liquid-related processes in the northern hemisphere, particularly in the polar area, is also consistent with atmospheric modeling (*Rannou et al.*, 2006; *Stofan et al.*, 2007). However, according to atmospheric circulation models, confirmed by the observation of persistent clouds in those regions, (*Mitchell et al.*, 2009; *Rodriguez et al.*, 2009a; *Tokano*, 2009), the latitudes around 60°N, the southern mid-latitudes as well as the south polar area should show signs of recent, intense resurfacing, too. This is not the case.

The discrepancy between the distribution of clouds and channels (particularly channels at low latitudes) could be explained by other processes. One possible explanation for the abundance of channels near the equator despite of the lack of clouds might be a formation through seepage, but the sheer size of the equatorial channel networks argues against this idea. The occasional formation of clouds due to

cryovolcanic activity seems to be a more probable explanation, but again, this idea is not entirely convincing due to the large areal extent of the fluvial network at western Xanadu. Another likely interpretation is that a more humid climate in the past, in stark contrast to the current arid climate, is responsible for the recently observed presence of (abandoned) channels near the equator. This interpretation is to be favored as it is consonant with the presence of vast dunefields and with the morphological particularities of streams at mid- and low latitudes. In view of the numerous individual fluvial features scattered over all latitudes of Titan, precipitation seems to be a strictly local phenomenon, which would be consistent with an origin from cryovolcanic activity on a small scale. This assumption, however, is difficult to verify given the low number of approved features with an assured cryovolcanic background, the lack of high-resolution imagery, and the incomplete coverage of Cassini data.

The idea of a distinct seasonality that is most pronounced at the poles seems plausible due to Titan's obliquity and due to the temperature gradient between Titan's equator and the poles with a slight difference between the summer- and winter-hemispheres (*Jennings et al.*, 2009). Further, the observation of an active methane cycle in large regions around the north pole - as opposed to predominantly dry high southern latitudes - supports this idea. The agglomeration of active channels and lakes at Titan's north pole is possibly the result of seasonal effects in combination with a temperature gradient between the polar areas and the equatorial regions. Methane, under Titan's conditions, is at its triple point, which means that a difference in temperature of only a few degrees might have a strong impact on the proportions to which the compound will be in its liquid or gaseous aggregate state. Similarly, *Lorenz* (1993) proposed a higher likelihood for raindrops to reach the surface at high latitudes - an assumption that can be partly confirmed by the observations of the present study.

The high abundance of clouds observed in the south polar area argues against a meteorological origin of the geomorphological differences between the two polar regions. The south polar region exhibits only a small number of likely active and many abandoned channels and also hosts Ontario Lacus, which is the largest open body of liquids in the southern hemisphere observed so far. Judging from the observation of clouds, liquid-related processes must be expected to be of great significance here. Despite this, high southern latitudes show substantially fewer traces of fluvial and liquid-related processes than there are in the north, possibly with a declining tendency. The recent climatic dynamics are, in fact, the opposite of what the rich presence of clouds originally suggested, considering that Ontario Lacus has been found to shrink. The argument that no significant number of fluvial and lacustrine features are apparent due to thermal inertia is unlikely to be valid, given the thermal properties of Titan's predominantly solid surface (*Mitchell et al.*, 2009) and because cloud formation, rain, and the subsequent incision of channels are processes that take effect promptly and should be highly responsive to seasonal changes. Thus, at least the southern polar area is subject to climatic changes, that might be due to seasonal

effects. Besides seasonality, other factors might be helpful in elucidating the unevenly distributed liquid-related processes, one of them being Saturn's eccentricity (*Aharonson et al.*, 2009). The question about possible seasonal effects can be addressed by an ongoing lake-level monitoring of Titan's lakes. If the northern lakes shrink over time and Ontario Lacus in the southern hemisphere does likewise, this development is consistent with a global trend to 'dehydration' or, more precisely, a depletion of liquid methane and the diminishing of liquid-related processes over time. A rising level of the northern lakes in combination with the shrinking of Ontario Lacus would rather indicate seasonal effects.

Except for the northern polar area, the results of this thesis are consistent with the notion of recent dry conditions, given the inactive state of the majority of valleys, in contrast to presumably humid climatic conditions in the past. The abundance of extended dunefields at low latitudes, the lack of active channels, and the lack of recipients of fluvial flow support the interpretation of a negative balance of liquids at surface level, owing to high rates of evaporation or infiltration. It is conceivable that several episodic 'fluvial periods' occurred on Titan with the latest one decaying now or during the recent past. Potential fluvial eras might have been initiated by outgassing events from the subsurface on a large scale, or, alternatively from outgassing of a near-surface regolith, as discussed in *Atreya et al.* (2006); *Tobie et al.* (2006) and *Mitri et al.* (2008). Subsequent to outgassing, a temporary humid period begins, followed by the weakening and slowdown of the volatile cycle. Assuming that this occasional release of large amounts of methane does, in fact, happen on Titan, the last period of fluvial activity must have occurred a relatively long time ago, since the vast areas covered by dunes can only be explained by a substantial period under dry conditions. The idea of more humid periods in the past due to outgassing from the interior or from a subsurface regolith argues against seasonal effects, or at least implies that seasonal differences have a negligible impact on the methane cycle. Although the correlation between outgassing, cryovolcanic processes, and the formation of clouds and channels is accepted (*Roe et al.*, 2005), no definite evidence has been presented until now to support this line of reasoning.

Titan's hydrocarbon cycle with evaporation, convection, cloud formation, and precipitation shows many striking similarities to the water cycle on Earth (*Atreya et al.*, 2006; *Lunine and Atreya*, 2008). However, Titan's methane cycle is suspected to have a cycle time of centuries (*Mitri et al.*, 2007), which would make it significantly slower than the terrestrial water cycle (*Lunine and Atreya*, 2008). The estimated atmospheric residence time of methane on Titan of 200 years is indeed orders of magnitude longer than the turnover time of water on Earth (*Mitri et al.*, 2007) and stands in contrast to the abundance of valleys, but is however consistent with the steady climatic conditions and the non-detection of the methane cycle during the observation period of Cassini. Water on Earth has a short residence time in the atmosphere in conjunction with a long residence time in the oceans, lakes, and streams. On Titan, the situation

seems to be the exact opposite, with a low annual rainfall rate of methane *Atreya et al.* (2009), a long residence time of methane in the atmosphere and short time at the surface, which is supported by the fact that liquid methane is not stable because environmental temperatures are near its boiling point (*Fortes and Stofan*, 2005). As a geomorphological consequence Titan's convective activity is small (*Atreya et al.*, 2006); and the formation of clouds, the shaping of channels and lakes seem to be ephemeral and short-lived processes, although landforms once shaped by liquid-related processes - like any other landform - can persist for a long time in the absence of other geologic processes. The long turnover time of atmospheric methane combined with the presence of many obvious traces of fluvial erosion points to high rates of episodic rainfall with subsequent bedrock incision. The rate of the latter is indeed determined to be comparable to the terrestrial value as postulated by *Collins* (2005).

Several morphologic attributes indicate the long-term action of fluvial processes and the absence, or merely marginal influence, of other erosional processes, although this observation cannot be definitely confirmed. A dark coating of the surface with a depth of a few hundred microns has been produced by photolysis and deposited over a period of about $10^5$ Earth-years (*Lara et al.*, 1994; *Smith et al.*, 1996). It is expected that the observed uneven bright and dark pattern in the distribution of this layer of photolytic end products is not a result of a spatially uneven fallout process but of subsequent resurfacing processes that have removed the dark layer in some (raised) regions. The presence of distinct surface features, in spite of the fact that atmospheric fallout has a tendency to homogenize the surface, implies that surface processes - particularly fluvial erosion - have been active over the last $10^5$ years.

One of the most urgent debates addresses the question whether the methane cycle is a closed cycle or not, coupled with the resupply of atmospheric methane (e.g. *Atreya et al.*, 2006; *Lunine and Atreya*, 2008; *Atreya et al.*, 2009). If the lakes both collect precipitated hydrocarbons and release methane in same amounts as it is destroyed in the atmosphere, the methane cycle would be closed. In this case, a resupply mechanism is required to maintain the total amount of methane over time, within the lakes themselves, for example in the form of a subsurface connection to a liquid methane table (*Hayes et al.*, 2008). If this is not the case, the cycle would be an open one as the initial substance is not regenerated in equal amounts over time. Although the analysis of channels as the outcome of Titan's methane cycle provides useful clues, a final statement about this issue cannot be given at this point.

Another general problem when addressing Titan is the non-detection of the methane cycle in action. Moreover, although many of the major channels are resolved, many (expected) networks of narrower channels are still concealed from view and must await future explorations. As with many other environmental processes on remote planets or bodies, remote sensing imagery will provide only circumstantial evidence of certain processes and phenomena. Thus, no definite or absolute knowledge on fluvial erosion and its outcome at the surface are provided by Cassini data.

Titan's volatile cycle, responsible for the formation of linear valleys and open reservoirs of liquids, diversifies Titan's geology and is also one of the most intriguing analogies between Titan and Earth. The significance of Titan as a target for planetary exploration is heightened by the presence of its methane cycle, although it is not the only geologic process where matter is mobilized and relocated over certain distances. The transport and mobilization of matter permits the mixing of different molecules, thus, increasing the probability of a chemical and even a biological evolution. Despite the fact that significantly different environmental conditions prevail, such as the fact that not water, but liquid methane is shaping Titan's surface, and irrespective of its generally different geologic and compositional background, the overall shape and morphology of valleys on both bodies is strikingly similar, and even the spatial dimensions of liquid-related landforms are comparable. The requirements for an active volatile cycle to function seem to be limited to a few basic circumstances, namely the presence of an atmosphere, solar energy, and boundary conditions near the triple point of at least one compound. Obviously, even a small supply of solar energy seems to be sufficient to initiate the fluvial processes described (*Atreya et al.*, 2006; *Lorenz et al.*, 2008a). By contrast, the current amount of mobile liquids, which seems to have been small on Titan at least in recent times, appears to be of minor significance to the presence of valleys. Martian history shows that the activity of a volatile cycle is apparently also a function of time. All things considered, the numerous dissimilarities between Titan's methane cycle and the water cycle on Earth as well as the large number of open questions should motivate further studies in this area.

# Chapter 7

# Outlook

Beyond the observations and results presented in this thesis, several open questions remain. These issues might be addressed by image data from the ongoing Cassini mission, which has been extended to last until the autumn of 2017. Further complementary investigations could follow, based on upcoming space missions to the Saturnian System. In order to generate a complete inventory of fluvial features, it is more than desirable to obtain a comprehensive global coverage of image data at an adequate resolution, possibly provided by a new generation of imaging devices. To understand the characteristics of fluvial processes based on another molecule than water, the analysis of better resolved imagery of known fluvial networks on Titan is essential. Digital elevation models of fluvial landscapes would boost the explanatory power of geodata. Optimally, indirect observations by remote sensing instruments should be supplemented by in-situ investigations, which offer the opportunity of validation and ground-truthing. One of the most challenging proposed missions by NASA/JPL is the in-situ examination of one of Titan's lakes (e.g. Kraken Mare) by a swimming platform. The successful realization of the *Titan Lake Probe* would enable studying the atmosphere, investigating the prebiotic chemistry of the lake, and testing for the presence of a subsurface ocean (*Waite and Niebur*, 2010).

Fluvial features on Titan with their various physiographies are distributed in a pattern that is only poorly correlated with observed and predicted clouds and the distribution of surface units. These findings raise further issues:

- Does the observed distribution of fluvial features relate to the distribution of clouds in the past? Is the current climate more arid than the past climate?
- When and how did the channels develop and how does their development relate to the genesis of other geologic features? What interplay and stratigraphy is there between different geologic landforms?
- What are the interactions between lakes, channels and a possible methane aquifer?

- Is there a correlation between the blue spectral unit and fluvial sediments? How does fluvial erosion alter the composition and, thus, the spectral properties of the terrain?
- How can the deficit of depositional constructs of fluvial processes (e.g. deltas) be explained?
- How do the methane cycle and fluvial erosion work? In what way do they interact with the atmosphere and surface? What controls Titan's weather and are there any seasonal dynamics?

Answering the above-mentioned questions will help to solve a number of more general concerns regarding Titan's surface, atmosphere, and interior. Many of them are still poorly understood:

- What is the origin of Titan in the Solar System?
- What is Titan's interior structure?
- What caused the stratification of the surface into different spectral units, their composition and physical state?
- What is the origin of mountain systems and how do tectonic processes work on Titan?
- What is the origin of methane in Titan's atmosphere and near the surface and how is it resupplied? Where/what is the sink for ethane?
- Is there a surface or subsurface methane reservoir?
- Is there any reasonable potential for habitability and an evolution of life on Titan?

# Bibliography


Aharonson, O., A. G. Hayes, J. I. Lunine, R. D. Lorenz, M. D. Allison, and C. Elachi (2009), An asymmetric distribution of lakes on Titan as a possible consequence of orbital forcing, *Nature Geoscience*, *2*, 851–854, doi:10.1038/ngeo698.

Ahnert, F. (2003), *Einfuehrung in die Geomorphologie*, Verlag Eugen Ulmer Stuttgart.

Atreya, S. (2007), Titan's organic factory, *Science*, *316*, 843–845, doi:10.1126/science.1141869.

Atreya, S. K., E. Y. Adams, H. B. Niemann, J. E. Demick-Montelara, T. C. Owen, M. Fulchignoni, F. Ferri, and E. H. Wilson (2006), Titan's methane cycle, *Planetary and Space Science*, *54*, 1177–1187, doi:10.1016/j.pss.2006.05.028.

Atreya, S. K., R. D. Lorenz, and J. H. Waite (2009), Volatile Origin and Cycles: Nitrogen and Methane, in *Titan from Cassini-Huygens*, edited by R. H. Brown, J.-P. Lebreton, and J. H. Waite, Springer.

Baines, K. H., et al. (2006), On the discovery of CO nighttime emissions on Titan by Cassini/VIMS: Derived stratospheric abundances and geological implications, *Planetary and Space Science*, *54*, 1552–1562, doi:10.1016/j.pss.2006.06.020.

Baker, V. R. (2001), Water and the martian landscape, *Nature*, *412*, 228–236, doi:10.1038/35084172.

Baker, V. R., and D. J. Milton (1974), Erosion by catastrophic floods on Mars and Earth, *Icarus*, *23*, 27–41.

Baker, V. R., R. C. Kochel, J. E. Laity, and A. D. Howard (1990), Spring sapping and valley network development, in *Groundwater Geomorphology: The role of subsurface water in earth-surface processes and landforms*, edited by C. G. Higgins and D. R. Coates, pp. 235–265, Geological Society of America Special Paper, Boulder, Colorado.

Bar-Nun, A., and M. Podolak (1979), The photochemistry of hydrocarbons in Titan's atmosphere, *Icarus*, *38*, 115–122, doi:10.1016/0019-1035(79)90091-5.

Barnes, J. W., et al. (2006), Cassini observations of flow-like features in western Tui Regio, Titan, *Geophysical Research Letters*, *33*, 16,204, doi:10.1029/2006GL026843.

Barnes, J. W., et al. (2007a), Global-scale surface spectral variations on Titan seen from Cassini/VIMS, *Icarus*, *186*, 242–258, doi:10.1016/j.icarus.2006.08.021.

Barnes, J. W., et al. (2007b), Near-infrared spectral mapping of Titan's mountains and channels, *Journal of Geophysical Research (Planets)*, *112*, 11,006, doi:10.1029/2007JE002932.

Barnes, J. W., et al. (2008), Spectroscopy, morphometry, and photoclinometry of Titan's dunefields from Cassini/VIMS, *Icarus*, *195*, 400–414, doi:10.1016/j.icarus.2007.12.006.

Barnes, J. W., et al. (2009a), VIMS spectral mapping observations of Titan during the Cassini prime mission, *Planetary and Space Science*, *57*, 1950–1962, doi:10.1016/j.pss.2009.04.013.

Barnes, J. W., et al. (2009b), Shoreline features of Titan's Ontario Lacus from Cassini/VIMS observations, *Icarus*, *201*, 217–225, doi:10.1016/j.icarus.2008.12.028.

Barnes, J. W., et al. (2010), Widespread organic evaporite deposits on Saturn's moon Titan, *submitted for publication*.

Barth, E. L. (2010), Cloud formation along mountain ridges on Titan, *Planetary and Space Science*, *58*, 1740–1747, doi:10.1016/j.pss.2010.07.013.

Barth, E. L., and O. B. Toon (2003), Microphysical modeling of ethane ice clouds in Titan's atmosphere, *Icarus*, *162*, 94–113, doi:10.1016/S0019-1035(02)00067-2.

Bell, P. M., H. K. Mao, and G. R. Rossman (1975), Absorption spectroscopy of ionic and molecular units in crystals and glasses, in *Infrared and Raman spectroscopy of lunar and terrestrial minerals*, edited by J. Karr, C., pp. 1–38, Academic Press Inc.

Brown, M. E., A. H. Bouchez, and C. A. Griffith (2002), Direct detection of variable tropospheric clouds near Titan's south pole, *Nature*, *420*, 795–797, doi:10.1038/nature01302.

Brown, M. E., J. E. Roberts, and E. L. Schaller (2010), Clouds on Titan during the Cassini prime mission: A complete analysis of the VIMS data, *Icarus*, *205*, 571–580, doi:10.1016/j.icarus.2009.08.024.

Brown, R. H., and D. P. Cruikshank (1997), Determination of the composition and state of icy surfaces in the outer Solar System, *Annual Review of Earth and Planetary Sciences*, *25*, 243–277, doi:10.1146/annurev.earth.25.1.243.

Brown, R. H., et al. (2004), The Cassini Visual and Infrared Mapping Spectrometer (VIMS) Investigation, *Space Science Reviews*, *115*, 111–168, doi:10.1007/s11214-004-1453-x.

Brown, R. H., et al. (2006), Observations in the Saturn system during approach and orbital insertion, with Cassini's Visual and Infrared Mapping Spectrometer (VIMS), *Astronomy & Astrophysics*, *446*, 707–716, doi:10.1051/0004-6361:20053054.

Brown, R. H., et al. (2008), The identification of liquid ethane in Titan's Ontario Lacus, *Nature*, *454*, 607–610, doi:10.1038/nature07100.

Burr, D. M. (2009), Palaeoflood-generating mechanisms on Earth, Mars, and Titan, *Global and Planetary Change*, *70*, 5–13, doi:10.1016/j.gloplacha.2009.11.003.

Burr, D. M., J. P. Emery, R. D. Lorenz, G. C. Collins, and P. A. Carling (2006), Sediment transport by liquid surficial flow: Application to Titan, *Icarus*, *181*, 235–242, doi:10.1016/j.icarus.2005.11.012.

Burr, D. M., R. E. Jacobsen, D. L. Roth, C. B. Phillips, K. L. Mitchell, and D. Viola (2009), Fluvial network analysis on Titan: Evidence for subsurface structures and west-to-east wind flow, southwestern Xanadu, *Geophysical Research Letters*, *36*, 22,203, doi:10.1029/2009GL040909.

Butzer, K. W. (1976), *Geomorphology from the Earth*, Harper & Row, New York.

Caldwell, J., et al. (1992), Titan: Evidence for seasonal change - A comparison of Hubble Space Telescope and Voyager images, *Icarus*, *96*, 1–9, doi:10.1016/0019-1035(92)90053-A.

Campbell, D. B., G. J. Black, L. M. Carter, and S. J. Ostro (2003), Radar evidence for liquid surfaces on Titan, *Science*, *302*, 431–434, doi:10.1126/science.1088969.

Capaccioni, F., A. Coradini, P. Cerroni, and S. Amici (1998), Imaging spectroscopy of Saturn and its satellites: VIMS-V onboard Cassini, *Planetary and Space Science*, *46*, 1263–1276, doi:10.1016/S0032-0633(98)00037-3.

Carr, M. H. (1979), Formation of Martian flood features by release of water from confined aquifers, *Journal of Geophysical Research*, *84*, 2995–3007, doi:10.1029/JB084iB06p02995.

Clark, R. M., and T. L. Roush (1984), Reflectance spectroscopy: Quantitative analysis techniques for remote sensing applications, *Journal of Geophysical Research*, *89*, 6329–6340, doi:10.1029/JB089iB07p06329.

Clark, R. N., T. V. V. King, M. Klejwa, G. A. Swayze, and N. Vergo (1990), High spectral resolution reflectance spectroscopy of minerals, *Journal of Geophysical Research*, *95*, 12,653–12,680, doi:10.1029/JB095iB08p12653.

Clark, R. N., et al. (2006), Detection of widespread aromatic and aliphatic hydrocarbon deposits on Titan's surface observed by Cassini VIMS, in *American Geophysical Union, Fall Meeting*.

Clark, R. N., et al. (2010), Detection and mapping of hydrocarbon deposits on Titan, *Journal of Geophysical Research (Planets)*, *115*(E14), 10,005, doi:10.1029/2009JE003369.

Clarke, D. W., and J. P. Ferris (1997), Chemical evolution on Titan: Comparisons to the prebiotic Earth, *Origins of Life and Evolution of the Biosphere*, *27*, 225–248, doi:10.1023/A:1006582416293.

Collins, G. C. (2005), Relative rates of fluvial bedrock incision on Titan and Earth, *Geophysical Research Letters*, *32*, 22,202, doi:10.1029/2005GL024551.

Combes, M., L. Vapillon, E. Gendron, A. Coustenis, O. Lai, R. Wittemberg, and R. Sirdey (1997), Spatially resolved Images of Titan by means of Adaptive Optics, *Icarus*, *129*, 482–497, doi:10.1006/icar.1997.5772.

Courtin, R. (1982), The spectrum of Titan in the far-infrared and microwave regions, *Icarus*, *51*, 466–475, doi:10.1016/0019-1035(82)90140-3.

Courtin, R., D. Gautier, and C. P. McKay (1995), Titan's thermal emission spectrum: Reanalysis of the Voyager infrared measurements, *Icarus*, *114*(1), 144–162, doi:10.1006/icar.1995.1050.

Coustenis, A. (1991), Titan: Recent developments, *Vistas in Astronomy*, *34*, 11–50, doi:10.1016/0083-6656(91)90018-N.

Coustenis, A. (1995), Titan's atmosphere and surface: parallels and differences with the primitive Earth, *Earth, Moon, and Planets*, *67*, 95–100, doi:10.1007/BF00613295.

Coustenis, A. (2006), Titan and the Cassini-Huygens mission, in *Recent Advances in Astronomy and Astrophysics*, *American Institute of Physics Conference Series*, vol. 848, edited by N. Solomos, pp. 23–40, doi:10.1063/1.2347959.

Coustenis, A., and F. W. Taylor (2008), *Titan - Exploring an Earthlike World*, 2nd ed., World Scientific Publishing Co. Pte. Ltd.

Coustenis, A., E. Lellouch, J. P. Maillard, and C. P. McKay (1995), Titan's surface: Composition and variability from the near-infrared albedo, *Icarus*, *118*, 87–104, doi:10.1006/icar.1995.1179.

Coustenis, A., et al. (2001), Images of Titan at 1.3 and 1.6 $\mu$m with Adaptive Optics at the CFHT, *Icarus*, *154*, 501–515, doi:10.1006/icar.2001.6643.

Coustenis, A., et al. (2009a), TandEM: Titan and Enceladus Mission, *Experimental Astronomy*, *23*, 893–946, doi:10.1007/s10686-008-9103-z.

Coustenis, A., E. Lellouch, B. Sicardy, and H. Roe (2009b), Earth-based perspective and pre-Cassini-Huygens knowledge of Titan, in *Titan from Cassini-Huygens*, edited by R. H. Brown, J.-P. Lebreton, and J. H. Waite, pp. 9–34, Springer.

Cui, J., et al. (2009), Analysis of Titan's neutral upper atmosphere from Cassini Ion Neutral Mass Spectrometer measurements, *Icarus*, *200*, 581–615, doi:10.1016/j.icarus.2008.12.005.

Czechowski, L., and K. Kossacki (2009), Thermal convection in the porous methane-soaked regolith of Titan: Investigation of stability, *Icarus*, *202*, 599–606, doi:10.1016/j.icarus.2009.02.032.

Danielson, R. E., J. J. Caldwell, and D. R. Larach (1973), An inversion in the atmosphere of Titan, *Icarus*, *20*, 437–443, doi:10.1016/0019-1035(73)90016-X.

de Pater, I., M. Ádámkovics, S. Gibbard, H. G. Roe, and C. A. Griffith (2004), Flight through Titan's atmosphere, in *Titan - From Discovery to Encounter*, *ESA Special Publication*, vol. 1278, edited by K. Fletcher, pp. 313–321.

Dermott, S. F., and C. Sagan (1995), Tidal effects of disconnected hydrocarbon seas on Titan, *Nature*, *374*, 238–240, doi:10.1038/374238a0.

Dunlop, M. W., M. K. Dougherty, S. Kellock, and D. J. Southwood (1999), Operation of the dual magnetometer on Cassini: Science performance, *Planetary and Space Science*, *47*, 1389–1405, doi:10.1016/S0032-0633(99)00060-4.

Duxbury, E., and D. Jensen (1994), *VICAR user's guide, Version 3*, http://www-mipl.jpl.nasa.gov/external/vug/vugfinal.html, access Dec-2010.

Elachi, C., et al. (2004), Radar: The Cassini Titan Radar Mapper, *Space Science Reviews*, *115*, 71–110, doi:10.1007/s11214-004-1438-9.

Elachi, C., et al. (2006), Titan Radar Mapper observations from Cassini's T3 fly-by, *Nature*, *441*, 709–713, doi:10.1038/nature04786.

Engel, S., J. I. Lunine, and W. K. Hartmann (1995), Cratering on Titan and implications for Titan's atmospheric history, *Planetary and Space Science*, *43*, 1059–1066, doi:10.1016/0032-0633(95)00044-6.

Eshleman, V. R., G. F. Lindal, and G. L. Tyler (1983), Is Titan wet or dry?, *Science*, *221*, 53–55, doi:10.1126/science.221.4605.53.

Flasar, F. M. (1983), Oceans on Titan?, *Science*, *221*, 55–57, doi:10.1126/science.221.4605.55.

Flasar, F. M., R. E. Samuelson, and B. J. Conrath (1981), Titan's atmosphere: Temperature and dynamics, *Nature*, *292*, 693–698, doi:10.1038/292693a0.

Fortes, A. D., and P. M. Grindrod (2006), Modelling of possible mud volcanism on Titan, *Icarus*, *182*(2), 550–558, doi:10.1016/j.icarus.2005.11.013.

Fortes, A. D., and E. R. Stofan (2005), Clathrate Formation in the Near-Surface Environment of Titan, in *Lunar and Planetary Institute Science Conference Abstracts*, p. 1123.

Fortes, A. D., P. M. Grindrod, S. K. Trickett, and L. Vočadlo (2007), Ammonium sulfate on Titan: Possible origin and role in cryovolcanism, *Icarus*, *188*, 139–153, doi:10.1016/j.icarus.2006.11.002.

Fulchignoni, M., et al. (2002), The characterisation of Titan's atmospheric physical properties by the Huygens Atmospheric Structure Instrument (Hasi), *Space Science Reviews*, *104*, 395–431, doi:10.1023/A:1023688607077.

Gaffey, S. J., L. A. McFadden, D. Nash, and C. M. Pieters (1993), Ultraviolet, visible, and near-infrared reflectance spectroscopy: Laboratory spectra of geologic minerals, in *Remote geochemical analysis: elemental and mineralogical composition (Topics in Remote Sensing)*, edited by C. M. Pieters and P. A. J. Englert, pp. 43–77, Cambridge University Press, doi:10.1016/0016-7037(94)90356-5.

Ghoneim, E., and F. El-Baz (2007), The application of radar topographic data to mapping of a mega-paleodrainage in the eastern Sahara, *Journal of Arid Environments*, *69*, 658–675, doi:10.1016/j.jaridenv.2006.11.018.

Gibbard, S. G., B. Macintosh, D. Gavel, C. E. Max, I. de Pater, A. M. Ghez, E. F. Young, and C. P. McKay (1999), Titan: High-resolution speckle images from the Keck Telescope, *Icarus*, *139*, 189–201, doi:10.1006/icar.1999.6095.

Gillett, F. C. (1975), Further observations of the 8-13 micron spectrum of Titan, *The Astrophysical Journal*, *201*, L41–L43, doi:10.1086/181937.

Gillett, F. C., W. J. Forrest, and K. M. Merrill (1973), 8-13 micron observations of Titan, *The Astrophysical Journal*, *184*, L93–L95, doi:10.1086/181296.

Grasset, O., C. Sotin, and F. Deschamps (2000), On the internal structure and dynamics of Titan, *Planetary and Space Science*, *48*, 617–636, doi:10.1016/S0032-0633(00)00039-8.

Graves, S. D. B., C. P. McKay, C. A. Griffith, F. Ferri, and M. Fulchignoni (2008), Rain and hail can reach the surface of Titan, *Planetary and Space Science*, *56*, 346–357, doi:10.1016/j.pss.2007.11.001.

Griffith, C. A. (1993), Evidence for surface heterogeneity on Titan, *Nature*, *364*, 511–514, doi:10.1038/364511a0.

Griffith, C. A., T. Owen, and R. Wagener (1991), Titan's surface and troposphere, investigated with ground-based, near-infrared observations, *Icarus*, *93*, 362–378, doi:10.1016/0019-1035(91)90219-J.

Griffith, C. A., T. Owen, G. A. Miller, and T. Geballe (1998), Transient clouds in Titan's lower atmosphere, *Nature*, *395*, 575–578, doi:10.1038/26920.

Griffith, C. A., T. Owen, T. R. Geballe, J. Rayner, and P. Rannou (2003), Evidence for the exposure of water ice on Titan's surface, *Science*, *300*, 628–630, doi:10.1126/science.1081897.

Griffith, C. A., et al. (2005), The evolution of Titan's mid-latitude clouds, *Science*, *310*, 474–477, doi:10.1126/science.1117702.

Griffith, C. A., C. P. McKay, and F. Ferri (2008), Titan's tropical storms in an evolving atmosphere, *The Astrophysical Journal*, *687*, L41–L44, doi:10.1086/593117.

Hanel, R., et al. (1981), Infrared observations of the Saturnian System from Voyager 1, *Science*, *212*, 192–200, doi:10.1126/science.212.4491.192.

Hansen, C. J., J. H. Waite, and S. J. Bolton (2009), Titan in the Cassini-Huygens Extended Mission, in *Titan from Cassini-Huygens*, Springer.

Hartle, R. E., et al. (2006), Initial interpretation of Titan plasma interaction as observed by the Cassini plasma spectrometer: Comparisons with Voyager 1, *Planetary and Space Science*, *54*, 1211–1224, doi:10.1016/j.pss.2006.05.029.

Hayes, A., et al. (2008), Hydrocarbon lakes on Titan: Distribution and interaction with a porous regolith, *Geophysical Research Letters*, *35*, L09,204, doi:10.1029/2008GL033409.

Hayes, A., et al. (2010a), Transient surface liquid in Titan's polar regions from Cassini, *Icarus*, *in Press*.

Hayes, A. G., et al. (2010b), Bathymetry and absorptivity of Titan's Ontario Lacus, *Journal of Geophysical Research (Planets)*, *115*, E09,009, doi:10.1029/2009JE003557.

Hendrix, A. R., and C. J. Hansen (2008), Ultraviolet observations of Phoebe from the Cassini UVIS, *Icarus*, *193*, 323–333, doi:10.1016/j.icarus.2007.06.030.

Herschel, J. F. W., Sir (1847), *Results of astronomical observations made during the years 1834, 5, 6, 7, 8, at the Cape of Good Hope; being the completion of a telescopic survey of the whole surface of the visible heavens, commenced in 1825*, Smith, Elder and Co, London.

Heslop, S. E., L. Wilson, H. Pinkerton, and J. W. Head (1989), Dynamics of a confined lava flow on Kilauea volcano, Hawaii, *Bulletin of Volcanology*, *51*, 415–432, doi:10.1007/BF01078809.

Hillier, J. K., et al. (2007), Interplanetary dust detected by the Cassini CDA Chemical Analyser, *Icarus*, *190*, 643–654, doi:10.1016/j.icarus.2007.03.024.

Hourdin, F., O. Talagrand, R. Sadourny, R. Courtin, D. Gautier, and C. P. McKay (1995), Numerical simulation of the general circulation of the atmosphere of Titan, *Icarus*, *117*, 358–374, doi:10.1006/icar.1995.1162.

Howard, A. D., and C. F. McLane III (1988), Erosion of cohesionless sediment by groundwater seepage, *Water Resources Research*, *24*, 1659–1674, doi:10.1029/WR024i010p01659.

Howard, A. D., J. M. Moore, and R. P. Irwin (2005), An intense terminal epoch of widespread fluvial activity on early Mars: 1. Valley network incision and associated deposits, *Journal of Geophysical Research (Planets)*, *110*, E12S14, doi:10.1029/2005JE002459.

Hueso, R., and A. Sánchez-Lavega (2006), Methane storms on Saturn's moon Titan, *Nature*, *442*, 428–431, doi:10.1038/nature04933.

Hunt, G. R. (1977), Spectral signatures of particulate minerals in the visible and near-infrared, *Geophysics*, *42*, 501–513, doi:10.1190/1.1440721.

Hunten, D. M. (1974), The atmosphere of Titan, *Icarus*, *22*, 111–116, doi:10.1016/0019-1035(74)90170-5.

Hunten, D. M., M. G. Tomasko, F. M. Flasar, R. E. Samuelson, D. F. Strobel, and D. J. Stevenson (1984), Titan, in *Saturn*, edited by T. Gehrels and M. S. Matthews, pp. 671–759, The University of Arizona Press, Tucson, Arizona.

Huygens, C. (1659), *Systema Saturnium, sive de causis mirandorum Saturni phaenomenon, et comite ejus planeta novo*, Ex Typographia Adriani Vlacq, Hagae-Comitis; digital edition at http://www.sil.si.edu/DigitalCollections/HST/Huygens/huygens.htm.

Illies, J. (1961), Versuch einer allgemeinen biozönotischen Gliederung der Fliessgewässer, *Internationale Revue der gesamten Hydrobiologie und Hydrographie*, *46*(2), 205–213, doi:10.1002/iroh.19610460205.

Jacob, D. J. (1999), *Introduction to Atmospheric Chemistry*, Princeton University Press.

Janssen, M. A., et al. (2009), Titan's surface at 2.2-cm wavelength imaged by the Cassini RADAR radiometer: Calibration and first results, *Icarus*, *200*(1), 222–239, doi:10.1016/j.icarus.2008.10.017.

Jaumann, R., and G. Neukum (2009), The surface age of Titan, in *Lunar and Planetary Institute Science Conference Abstracts*, vol. 40, p. 1641.

Jaumann, R., et al. (2005), Interior channels in Martian valleys: Constraints on fluvial erosion by measurements of the Mars Express High Resolution Stereo Camera, *Geophysical Research Letters*, *32*, L16,203.

Jaumann, R., et al. (2006), High-resolution CASSINI-VIMS mosaics of Titan and the icy Saturnian satellites, *Planetary and Space Science*, *54*, 1146–1155, doi:10.1016/j.pss.2006.05.034.

Jaumann, R., et al. (2008), Fluvial erosion and post-erosional processes on Titan, *Icarus*, *197*, 526–538, doi:10.1016/j.icarus.2008.06.002.

Jaumann, R., et al. (2009), Geology and surface processes on Titan, in *Titan from Cassini-Huygens*, edited by R. H. Brown, J.-P. Lebreton, and J. H. Waite, pp. 75–140, Springer.

Jaumann, R., A. Nass, D. Tirsch, D. Reiss, and G. Neukum (2010), The western Libya Montes valley system on Mars: Evidence for episodic and multi-genetic erosion events during the Martian history, *Earth and Planetary Science Letters*, *294*, 272–290, doi:10.1016/j.epsl.2009.09.026.

Jennings, D. E., et al. (2009), Titan's surface brightness temperatures, *The Astrophysical Journal*, *691*, L103–L105, doi:10.1088/0004-637X/691/2/L103.

Karkoschka, E., and M. G. Tomasko (2009), Rain and dewdrops on Titan based on in situ imaging, *Icarus*, *199*, 442–448, doi:10.1016/j.icarus.2008.09.020.

Kazeminejad, B., D. H. Atkinson, M. Pérez-Ayúcar, J. Lebreton, and C. Sollazzo (2007), Huygens' entry and descent through Titan's atmosphere - Methodology and results of the trajectory reconstruction, *Planetary and Space Science*, *55*, 1845–1876, doi:10.1016/j.pss.2007.04.013.

Khare, B. N., C. Sagan, E. T. Arakawa, F. Suits, T. A. Callcott, and M. W. Williams (1984), Optical constants of organic tholins produced in a simulated Titanian atmosphere - From soft X-ray to microwave frequencies, *Icarus*, *60*, 127–137, doi:10.1016/0019-1035(84)90142-8.

Kirk, R. L., E. Howington-Kraus, K. L. Mitchell, S. Hensley, B. W. Stiles, and the Cassini RADAR Team (2007), First Stereoscopic Radar Images of Titan, in *Lunar and Planetary Institute Science Conference Abstracts*, vol. 38, p. 1427.

Kleinhans, M. G. (2005), Flow discharge and sediment transport models for estimating a minimum timescale of hydrological activity and channel delta formation on Mars, *Journal of Geophysical Research*, *110*, E12,003, doi:10.1029/2005JE002521.

Knight, J. F., and R. S. Lunetta (2003), An experimental assessment of minimum mapping unit size, *IEEE Transactions on Geoscience and Remote Sensing*, *41*, 2132–2134, doi:10.1109/TGRS.2003.816587.

Kohlhase, C. E., and P. A. Penzo (1977), Voyager Mission description, *Space Science Reviews*, *21*, 77–101, doi:10.1007/BF00200846.

Komar, P. D. (1979), Comparisons of the hydraulics of water flows in Martian outflow channels with flows of similar scale on Earth, *Icarus*, *37*, 156–181, doi:10.1016/0019-1035(79)90123-4.

Komatsu, G. (2007), Rivers in the Solar System: Water is not the only fluid flow on planetary bodies, *Geography Compass*, *1/3*, 480–502, doi:10.1111/j.1749-8198.2007.00029.x.

Komatsu, G., and V. R. Baker (1996), Channels in the Solar System, *Planetary and Space Science*, *44*, 801–815, doi:10.1016/0032-0633(96)00010-4.

Kondratev, K. Y., and N. I. Moskalenko (1985), The atmospheric greenhouse effect and climates on various planets, *Advances in Space Research*, *5*, 37–40, doi:10.1016/0273-1177(85)90239-X.

Kossacki, K. J., and R. D. Lorenz (1996), Hiding Titan's ocean: densification and hydrocarbon storage in an icy regolith, *Planetary and Space Science*, *44*, 1029–1037, doi:10.1016/0032-0633(96)00022-0.

Krupp, N., et al. (2009), Energetic particles in Saturn's magnetosphere during the Cassini Nominal Mission (July 2004 - July 2008), *Planetary and Space Science*, *57*, 1754–1768, doi:10.1016/j.pss.2009.06.010.

Kuiper, G. P. (1944), Titan: A satellite with an atmosphere, *Astrophysical Journal*, *100*, 378–383, doi:10.1086/144679.

Lamb, M. P., A. D. Howard, J. Johnson, K. X. Whipple, W. E. Dietrich, and J. T. Perron (2006), Can springs cut canyons into rock?, *Journal of Geophysical Research (Planets)*, *111*, E07,002, doi:10.1029/2005JE002663.

Lamb, M. P., W. E. Dietrich, S. M. Aciego, D. J. DePaolo, and M. Manga (2008), Formation of Box Canyon, Idaho, by megaflood: Implications for seepage erosion on Earth and Mars, *Science*, *320*, 1067–1070, doi:10.1126/science.1156630.

Langhans, M., R. Jaumann, K. Stephan, R. H. Brown, B. J. Buratti, R. Clark, K. H. Baines, P. D. Nicholson, and R. Lorenz (2010), Spectral properties of fluvial terrain on Titan: An update, in *European Planetary Science Congress Abstracts*, vol. 5, pp. EPSC2010–714.

Langhans, M. H., et al. (2011), Titan's fluvial valleys: Morphology, distribution, and spectral properties, *Planetary and Space Science*, *accepted*.

Lara, L. M., R. D. Lorenz, and R. Rodrigo (1994), Liquids and solids on the surface of Titan: Results of a new photochemical model, *Planetary and Space Science*, *42*, 5–14, doi:10.1016/0032-0633(94)90135-X.

Le Corre, L., et al. (2008), Global distribution of dunes on Titan with VIMS, in *American Geophysical Union, Fall Meeting*, pp. P21A–1312.

Le Corre, L., et al. (2009), Analysis of a cryolava flow-like feature on Titan, *Planetary and Space Science*, *57*, 870–879, doi:10.1016/j.pss.2009.03.005.

Le Gall, A., M. A. Janssen, P. Paillou, R. D. Lorenz, S. D. Wall, and the Cassini RADAR team (2010), Radar-bright channels on Titan, *Icarus*, *207*, 948–958, doi:10.1016/j.icarus.2009.12.027.

Le Mouélic, S., et al. (2008), Mapping and interpretation of Sinlap crater on Titan using Cassini VIMS and RADAR data, *Journal of Geophysical Research (Planets)*, *113*, E04,003, doi:10.1029/2007JE002965.

Le Mouélic, S., et al. (2010), Imaging of Titan in the infrared with Cassini VIMS: Toward homogeneous surface maps, in *Gephysical Research Abstracts EGU General Assembly*, vol. 12, pp. EGU2010–8483.

Lebreton, J., et al. (2005), An overview of the descent and landing of the Huygens probe on Titan, *Nature*, *438*, 758–764, doi:10.1038/nature04347.

Lebreton, J.-P., and D. Matson (2007), The Cassini-Huygens Mission (Part I), *Space Research Today*, *169*, 11–19, doi:10.1016/S1752-9298(07)80035-1.

Lellouch, E., B. Schmitt, A. Coustenis, and J. G. Cuby (2004), Titan's 5-micron lightcurve, *Icarus*, *168*(1), 209–214, doi:10.1016/j.icarus.2003.12.001.

Lemmon, M. T., E. Karkoschka, and M. Tomasko (1993), Titan's rotation - Surface feature observed, *Icarus*, *103*, 329–332, doi:10.1006/icar.1993.1074.

Lemmon, M. T., E. Karkoschka, and M. Tomasko (1995), Titan's rotational light-curve, *Icarus*, *113*, 27–38, doi:10.1006/icar.1995.1003.

Leopold, L. B. (1994), *A view of the river*, Harvard University Press.

Leopold, L. B., M. G. Wolman, and J. P. Miller (1964), *Fluvial processes in geomorphology*, W. H. Freeman & Co Ltd, San Francisco.

Lewis, J. S. (1971), Satellites of the outer planets: Their physical and chemical nature, *Icarus*, *15*, 174–185, doi:10.1016/0019-1035(71)90072-8.

Lillesand, T. M., R. W. Kiefer, and J. W. Chipman (2003), *Remote Sensing and Image Interpretation*, 5th ed., Wiley & Sons, New York.

Lindal, G. F., G. E. Wood, H. B. Hotz, D. N. Sweetnam, V. R. Eshleman, and G. L. Tyler (1983), The atmosphere of Titan: An analysis of the Voyager 1 radio occultation measurements, *Icarus*, *53*, 348–363, doi:10.1016/0019-1035(83)90155-0.

Lopes, R. M. C., et al. (2007a), Cryovolcanic features on Titan's surface as revealed by the Cassini Titan Radar Mapper, *Icarus*, *186*, 395–412, doi:10.1016/j.icarus.2006.09.006.

Lopes, R. M. C., et al. (2007b), The lakes and seas of Titan, *EOS Transactions*, *88*, 569–571, doi:10.1029/2007EO510001.

Lopes, R. M. C., et al. (2010), Distribution and interplay of geologic processes on Titan from Cassini radar data, *Icarus*, *205*, 540–558, doi:10.1016/j.icarus.2009.08.010.

Lorenz, R. D. (1993), The life, death and afterlife of a raindrop on Titan, *Planetary and Space Science*, *41*, 647–655, doi:10.1016/0032-0633(93)90048-7.

Lorenz, R. D. (1994), Crater lakes on Titan: rings, horseshoes and bullseyes, *Planetary and Space Science*, *42*, 1–4, doi:10.1016/0032-0633(94)90134-1.

Lorenz, R. D. (1996), Pillow lava on Titan: expectations and constraints on cryovolcanic processes, *Planetary and Space Science*, *44*, 1021–1028, doi:10.1016/0032-0633(95)00139-5.

Lorenz, R. D. (1997), Impacts and cratering on Titan: a pre-Cassini view, *Planetary and Space Science*, *45*(8), 1009–1019, doi:DOI:10.1016/S0032-0633(97)00085-8.

Lorenz, R. D. (2000), The weather on Titan, *Science*, *290*(5491), 467–468, doi:10.1126/science.290.5491.467.

Lorenz, R. D., and J. I. Lunine (1996), Erosion on Titan: Past and present, *Icarus*, *122*, 79–91, doi:10.1006/icar.1996.0110.

Lorenz, R. D., and J. I. Lunine (1997), Titan's surface reviewed: The nature of bright and dark terrain, *Planetary and Space Science*, *45*, 981–992, doi:10.1016/S0032-0633(97)00087-1.

Lorenz, R. D., and J. I. Lunine (2002), Titan's snowline, *Icarus*, *158*, 557–559, doi:10.1006/icar.2002.6880.

Lorenz, R. D., and J. I. Lunine (2005), Titan's surface before Cassini, *Planetary and Space Science*, *53*, 557–576, doi:10.1016/j.pss.2004.06.004.

Lorenz, R. D., J. I. Lunine, J. A. Grier, and M. A. Fisher (1995), Prediction of aeolian features on planets: Application to Titan paleoclimatology, *Journal of Geophysical Research*, *100*, 26,377–26,386, doi:10.1029/95JE02708.

Lorenz, R. D., C. P. McKay, and J. I. Lunine (1997), Photochemically driven collapse of Titan's atmosphere, *Science*, *275*, 642–644, doi:10.1126/science.275.5300.642.

Lorenz, R. D., et al. (2002), Titan, in *The Future of Solar System Exploration (2003-2013) - First Decadal Study Contributions*, *Astronomical Society of the Pacific Conference Series*, vol. 272, edited by M. V. Sykes, pp. 253–261.

Lorenz, R. D., G. Biolluz, P. Encrenaz, M. A. Janssen, R. D. West, and D. O. Muhleman (2003), Cassini RADAR: Prospects for Titan surface investigations using the microwave radiometer, *Planetary and Space Science*, *51*, 353–364, doi:10.1016/S0032-0633(02)00148-4.

Lorenz, R. D., J. I. Lunine, and W. Zimmerman (2005a), Post-Cassini exploration of Titan: Science goals, instrumentation and mission concepts, *Advances in Space Research*, *36*, 281–285, doi:10.1016/j.asr.2005.03.080.

Lorenz, R. D., C. A. Griffith, J. I. Lunine, C. P. McKay, and N. O. Rennò (2005b), Convective plumes and the scarcity of Titan's clouds, *Geophysical Research Letters*, *32*, L01,201, doi:10.1029/2004GL021415.

Lorenz, R. D., et al. (2006), The sand seas of Titan: Cassini RADAR observations of longitudinal dunes, *Science*, *312*, 724–727, doi:10.1126/science.1123257.

Lorenz, R. D., et al. (2007), Titan's young surface: Initial impact crater survey by Cassini RADAR and model comparison, *Geophysical Research Letters*, *34*, L07,204, doi:10.1029/2006GL028971.

Lorenz, R. D., et al. (2008a), Fluvial channels on Titan: Initial Cassini RADAR observations, *Planetary and Space Science*, *56*, 1132–1144, doi:10.1016/j.pss.2008.02.009.

Lorenz, R. D., et al. (2008b), Titan's inventory of organic surface materials, *Geophysical Research Letters*, *35*, L02,206, doi:10.1029/2007GL032118.

Lorenz, R. D., M. E. Brown, and F. M. Flasar (2009), Seasonal change on Titan, in *Titan from Cassini-Huygens*, edited by R. H. Brown, J.-P. Lebreton, and J. H. Waite, pp. 353–372, Springer.

Louis, H., and K. Fischer (1979), *Allgemeine Geomorphologie*, 4th ed., Walter de Gruyter & Co., Berlin.

Lunine, J., M. Choukroun, D. J. Stevenson, and G. Tobie (2009), The origin and evolution of Titan, in *Titan from Cassini-Huygens*, edited by R. H. Brown, J.-P. Lebreton, and J. H. Waite, pp. 35–59, Springer.

Lunine, J. I. (1990), Titan, *Advances in Space Research*, *10*, 137–144, doi:10.1016/0273-1177(90)90097-J.

Lunine, J. I., and S. K. Atreya (2008), The methane cycle on Titan, *Nature Geoscience*, *1*, 159–164, doi:10.1038/ngeo125.

Lunine, J. I., and R. D. Lorenz (2009), Rivers, lakes, dunes, and rain: Crustal processes in Titan's methane cycle, *Annual Review of Earth and Planetary Sciences*, *37*, 299–320, doi:10.1146/annurev.earth.031208.100142.

Lunine, J. I., and C. P. McKay (1995), Surface-atmosphere interactions on Titan compared with those on the pre-biotic Earth, *Advances in Space Research*, *15*(3), 303–311, doi:10.1016/S0273-1177(99)80101-X.

Lunine, J. I., and D. J. Stevenson (1987), Clathrate and ammonia hydrates at high pressure - Application to the origin of methane on Titan, *Icarus*, *70*, 61–77, doi:10.1016/0019-1035(87)90075-3.

Lunine, J. I., D. J. Stevenson, and Y. L. Yung (1983), Ethane ocean on Titan, *Science*, *222*, 1229–1230, doi:10.1126/science.222.4629.1229.

Lunine, J. I., R. D. Lorenz, and W. K. Hartmann (1998), Some speculations on Titan's past, present and future, *Planetary and Space Science*, *46*, 1099–1107, doi:10.1016/S0032-0633(97)00221-3.

Lunine, J. I., et al. (2008a), Titan's diverse landscapes as evidenced by Cassini RADAR's third and fourth looks at Titan, *Icarus*, *195*, 415–433, doi:10.1016/j.icarus.2007.12.022.

Lunine, J. I., et al. (2008b), Lack of south polar methane lakes on Titan, in *Lunar and Planetary Institute Science Conference Abstracts*, vol. 39, p. 1637.

Malaska, M. (2007), list of putative impact craters on Titan, available online: http://www.unmannedspaceflight.com/index.php?s=3f8648cc8c53a496fa2c9ba8435fd556&showtopic=4724&pid=102728&mode=threaded&start=entry102728.

Malin, M. C., and K. S. Edgett (2000), Evidence for recent groundwater seepage and surface runoff on Mars, *Science*, *288*, 2330–2335, doi:10.1126/science.288.5475.2330.

Mangold, N., C. Quantin, V. Ansan, C. Delacourt, and P. Allemand (2004), Evidence for precipitation on Mars from dendritic valleys in the Valles Marineris area, *Science*, *305*, 78–81, doi:10.1126/science.1097549.

Marcinek, J., and E. Rosenkranz (1996), *Das Wasser der Erde*, 2nd ed., Klett-Perthes Verlag.

McCord, T. B., et al. (2004), Cassini VIMS observations of the Galilean satellites including the VIMS calibration procedure, *Icarus*, *172*, 104–126, doi:10.1016/j.icarus.2004.07.001.

McCord, T. B., et al. (2006), Composition of Titan's surface from Cassini VIMS, *Planetary and Space Science*, *54*, 1524–1539, doi:10.1016/j.pss.2006.06.007.

McCord, T. B., et al. (2008), Titan's surface: Search for spectral diversity and composition using the Cassini VIMS investigation, *Icarus*, *194*, 212–242, doi:10.1016/j.icarus.2007.08.039.

McKay, C. P., and H. D. Smith (2005), Possibilities for methanogenic life in liquid methane on the surface of Titan, *Icarus*, *178*, 274–276, doi:10.1016/j.icarus.2005.05.018.

McKay, C. P., J. B. Pollack, and R. Courtin (1989), The thermal structure of Titan's atmosphere, *Icarus*, *80*, 23–53, doi:10.1016/0019-1035(89)90160-7.

McKay, C. P., S. C. Martin, C. A. Griffith, and R. M. Keller (1997), Temperature lapse rate and methane in Titan's troposphere, *Icarus*, *129*, 498–505, doi:10.1006/icar.1997.5751.

Meier, R., B. A. Smith, T. C. Owen, and R. J. Terrile (2000), The surface of Titan from NICMOS observations with the Hubble Space Telescope, *Icarus*, *145*, 462–473, doi: 10.1006/icar.2000.6360.

Mitchell, J. L., R. T. Pierrehumbert, D. M. W. Frierson, and R. Caballero (2009), The impact of methane thermodynamics on seasonal convection and circulation in a model Titan atmosphere, *Icarus*, *203*, 250–264, doi:10.1016/j.icarus.2009.03.043.

Mitchell, K. L., et al. (2007a), Titan's north polar lakes as observed by Cassini Radar: An update, in *Ices, Oceans, and Fire: Satellites of the Outer Solar System*, p. 6042.

Mitchell, K. L., J. S. Kargel, C. A. Wood, J. Radebaugh, R. M. C. Lopes, J. I. Lunine, E. R. Stofan, R. L. Kirk, and the Cassini Radar Team (2007b), Titan's crater lakes: Caldera vs. karst, in *Lunar and Planetary Institute Science Conference Abstracts*, vol. 38, p. 2064.

Mitri, G., A. P. Showman, J. I. Lunine, and R. D. Lorenz (2007), Hydrocarbon lakes on Titan, *Icarus*, *186*, 385–394, doi:10.1016/j.icarus.2006.09.004.

Mitri, G., A. P. Showman, J. I. Lunine, and R. M. C. Lopes (2008), Resurfacing of Titan by ammonia-water cryomagma, *Icarus*, *196*, 216–224, doi:10.1016/j.icarus.2008.02.024.

Mousis, O., D. Gautier, and A. Coustenis (2002), The D/H ratio in methane in Titan: Origin and history, *Icarus*, *159*, 156–165, doi:10.1006/icar.2002.6930.

Muhleman, D. O., A. W. Grossman, B. J. Butler, and M. A. Slade (1990), Radar reflectivity of Titan, *Science*, *248*, 975–980, doi:10.1126/science.248.4958.975.

Muhleman, D. O., A. W. Grossman, and B. J. Butler (1995), Radar investigations of Mars, Mercury, and Titan, *Annual Review of Earth and Planetary Sciences*, *23*, 337–374, doi:10.1146/annurev.ea.23.050195.002005.

NASA (2009), http://www.jpl.nasa.gov/news/fact_sheets/cassini.pdf, access Nov-2010.

NASA (2010a), http://www.jpl.nasa.gov/news/news.cfm?release=2010-039, access Nov-2010.

NASA (2010b), http://imagine.gsfc.nasa.gov/docs/science/how_l1/light_curves.html, access Nov-2010.

NASA (2010c), http://www.jpl.nasa.gov/news/features.cfm?feature=1723, access Nov-2010.

NASA/JPL (2010), http://saturn.jpl.nasa.gov/science/moons/, access September 2010.

Neish, C. D., R. D. Lorenz, D. P. O'Brien, and the Cassini RADAR team (2006), The potential for prebiotic chemistry in the possible cryovolcanic dome Ganesa Macula on Titan, *International Journal of Astrobiology*, *5*, 57–65, doi:10.1017/S1473550406002898.

Nelson, R. M., et al. (2009), Saturn's Titan: Surface change, ammonia, and implications for atmospheric and tectonic activity, *Icarus*, *199*, 429–441, doi:10.1016/j.icarus.2008.08.013.

Neukum, G. (1983), *Meteoritenbombardement und Datierung planetarer Oberflächen*, 186 pp., Ludwig Maximilians Universität, München, Germany, habilitation dissertation.

Neukum, G., and K. Hiller (1981), Martian ages, *Journal of Geophysical Research*, *86*, 3097–3121, doi:10.1029/JB086iB04p03097.

Neukum, G., A. T. Basilevsky, T. Kneissl, M. G. Chapman, S. van Gasselt, G. Michael, R. Jaumann, H. Hoffmann, and J. K. Lanz (2010), The geologic evolution of Mars: Episodicity of resurfacing events and ages from cratering analysis of image data and correlation with radiometric ages of Martian meteorites, *Earth and Planetary Science Letters*, *294*, 204–222, doi:10.1016/j.epsl.2009.09.006.

Nguyen, M., F. Raulin, P. Coll, S. Derenne, C. Szopa, G. Cernogora, G. Israël, and J.-M. Bernard (2007), Carbon isotopic enrichment in Titan's tholins? Implications for Titan's aerosols, *Planetary and Space Science*, *55*, 2010–2014, doi:10.1016/j.pss.2007.04.010.

Niemann, H. B., et al. (2005), The abundances of constituents of Titan's atmosphere from the GCMS instrument on the Huygens probe, *Nature*, *438*, 779–784, doi:10.1038/nature04122.

Owen, T. (1982), The composition and origin of Titan's atmosphere, *Planetary and Space Science*, *30*, 833–838, doi:10.1016/0032-0633(82)90115-5.

Owen, T. C. (2000), On the origin of Titan's atmosphere, *Planetary and Space Science*, *48*, 747–752, doi:10.1016/S0032-0633(00)00040-4.

Paganelli, F., et al. (2005), Channels and fan-like features on Titan surface imaged by the Cassini RADAR, in *Lunar and Planetary Institute Science Conference Abstracts*, vol. 36, p. 2150.

Paillou, P., M. Crapeau, C. Elachi, S. Wall, and P. Encrenaz (2006), Models of synthetic aperture radar backscattering for bright flows and dark spots on Titan, *Journal of Geophysical Research*, *111*, E11,011, doi:10.1029/2006JE002724.

Perron, J. T., M. P. Lamb, C. D. Koven, I. Y. Fung, E. Yager, and M. Ádámkovics (2006), Valley formation and methane precipitation rates on Titan, *Journal of Geophysical Research (Planets)*, *111*, E11,001, doi:10.1029/2005JE002602.

Perrot, B., and R. Giordani (1998), Cassini Huygens mission: the exploration of the Saturn System. Radio science experiments: Radio Frequency Instrument Subsystem, *Planetary and Space Science*, *46*, 1333–1338, doi:10.1016/S0032-0633(97)00212-2.

Perry, J. E., A. S. McEwen, S. Fussner, E. P. Turtle, R. A. West, C. C. Porco, B. Knowles, D. D. Dawson, and the Cassini ISS Team (2005), Processing ISS images of Titan's surface, in *Lunar and Planetary Institute Science Conference Abstracts*, vol. 36, p. 2312.

Perry, J. E., E. P. Turtle, A. S. McEwen, D. D. Dawson, and C. C. Porco (2007), Cassini ISS observations of Titan's trailing hemisphere, in *Ices, Oceans, and Fire: Satellites of the Outer Solar System*, p. 6064.

Pieri, D. (1976), Distribution of small channels on the Martian surface, *Icarus*, *27*, 25–50, doi:10.1016/0019-1035(76)90182-2.

Porco, C. C., et al. (2004), Cassini Imaging Science: Instrument characteristics and anticipated scientific investigations at Saturn, *Space Science Reviews*, *115*, 363–497, doi:10.1007/s11214-004-1456-7.

Porco, C. C., et al. (2005), Imaging of Titan from the Cassini spacecraft, *Nature*, *434*, 159–168, doi:10.1038/nature03436.

Prospero, J. M., and T. N. Carlson (1972), Vertical and areal distribution of Saharan dust over the western equatorial north atlantic ocean, *Journal of Geophysical Research*, *77*, 5255–5265, doi:10.1029/JC077i027p05255.

Radebaugh, J., R. D. Lorenz, R. L. Kirk, J. I. Lunine, E. R. Stofan, R. M. C. Lopes, S. D. Wall, and the Cassini Radar Team (2007), Mountains on Titan observed by Cassini Radar, *Icarus*, *192*, 77–91, doi:10.1016/j.icarus.2007.06.020.

Radebaugh, J., et al. (2008), Dunes on Titan observed by Cassini Radar, *Icarus*, *194*, 690–703, doi:10.1016/j.icarus.2007.10.015.

Radebaugh, J., et al. (2010), Regional geomorphology and history of Titan's Xanadu province, *Icarus*, *in press*.

Rannou, P., F. Montmessin, F. Hourdin, and S. Lebonnois (2006), The latitudinal distribution of clouds on Titan, *Science*, *311*, 201–205, doi:10.1126/science.1118424.

Raulin, F. (1987), Organic chemistry in the oceans of Titan, *Advances in Space Research*, *7*, 571–581, doi:10.1016/0273-1177(87)90358-9.

Raulin, F., and T. Owen (2002), Organic chemistry and exobiology on Titan, *Space Science Reviews*, *104*, 377–394, doi:10.1023/A:1023636623006.

Richardson, J., R. D. Lorenz, and A. McEwen (2004), Titan's surface and rotation: new results from Voyager 1 images, *Icarus*, *170*, 113–124, doi:10.1016/j.icarus.2004.03.010.

Roda, F., J. Bellot, A. Avila, A. Escarré, J. Pinol, and J. Terradas (1993), Saharan dust and the atmospheric inputs of elements and alkalinity to mediterranean ecosystems, *Water, Air, and Soil Pollution*, *66*, 277–288, doi:10.1007/BF00479851.

Rodriguez, S., P. Paillou, M. Dobrijevic, G. Ruffié, P. Coll, J. M. Bernard, and P. Encrenaz (2003), Impact of aerosols present in Titan's atmosphere on the CASSINI radar experiment, *Icarus*, *164*, 213–227, doi:10.1016/S0019-1035(03)00125-8.

Rodriguez, S., et al. (2006), Cassini/VIMS hyperspectral observations of the Huygens Landing Site on Titan, *Planetary and Space Science*, *54*, 1510–1523, doi:10.1016/j.pss.2006.06.016.

Rodriguez, S., et al. (2009a), Global circulation as the main source of cloud activity on Titan, *Nature*, *459*, 678–682, doi:10.1038/nature08014.

Rodriguez, S., et al. (2009b), Titan's surface mapping with VIMS/Cassini thanks to coupled atmospheric empirical correction and radiative transfer modeling, in *European Planetary Science Congress 2009*, vol. 4, pp. EPSC2009–188.

Roe, H. G., I. de Pater, B. A. Macintosh, and C. P. McKay (2002), Titan's clouds from Gemini and Keck Adaptive Optics imaging, *The Astrophysical Journal*, *581*, 1399–1406, doi:10.1086/344403.

Roe, H. G., M. E. Brown, E. L. Schaller, A. H. Bouchez, and C. A. Trujillo (2005), Geographic control of Titan's mid-latitude clouds, *Science*, *310*, 477–479, doi:10.1126/science.1116760.

Sagan, C., and S. F. Dermott (1982), The tide in the seas of Titan, *Nature*, *300*, 731–733, doi:10.1038/300731a0.

Sagan, C., and B. N. Khare (1979), Tholins: organic chemistry of interstellar grains and gas, *Nature*, *277*, 102–107, doi:10.1038/277102a0.

Sahlin, E. A. U., N. F. Glasser, K. N. Jansson, and M. J. Hambrey (2009), Connectivity analyses of valley patterns indicate preservation of a preglacial fluvial valley system in the Dyfi basin, Wales, in *Proceedings of the Geologists' Association 120*, pp. 114–127, doi:10.1016/j.pgeola.2009.10.001.

Saint-Pé, O., M. Combes, F. Rigaut, M. Tomasko, and M. Fulchignoni (1993), Demonstration of Adaptive Optics for resolved imagery of solar system objects - Preliminary results on Pallas and Titan, *Icarus*, *105*, 263–270, doi:10.1006/icar.1993.1124.

Samuelson, R. E. (1983), Radiative equilibrium model of Titan's atmosphere, *Icarus*, *53*, 364–387, doi:10.1016/0019-1035(83)90156-2.

Samuelson, R. E., and L. A. Mayo (1997), Steady-state model for methane condensation in Titan's troposphere, *Planetary and Space Science*, *45*, 949–958, doi:10.1016/S0032-0633(97)00089-5.

Samuelson, R. E., R. A. Hanel, V. G. Kunde, and W. C. Maguire (1981), Mean molecular weight and hydrogen abundance of Titan's atmosphere, *Nature*, *292*, 688–693, doi: 10.1038/292688a0.

Schaller, E. L., M. E. Brown, H. G. Roe, and A. H. Bouchez (2006), A large cloud outburst at Titan's south pole, *Icarus*, *182*, 224–229, doi:10.1016/j.icarus.2005.12.021.

Schowengerdt, R. A. (1997), *Remote Sensing - Models and methods for image processing*, Academic Press, Second Edition.

Schröder, S. E., and H. U. Keller (2008), The reflectance spectrum of Titan's surface at the Huygens Landing Site determined by the Descent Imager/Spectral Radiometer, *Planetary and Space Science*, *56*, 753–769, doi:10.1016/j.pss.2007.10.011.

Schumm, S. A., K. F. Boyd, C. G. Wolff, and W. J. Spitz (1995), A ground-water sapping landscape in the Florida Panhandle, *Geomorphology*, *12*, 281–297, doi:10.1016/0169-555X(95)00011-S.

Smith, B. A., et al. (1981), Encounter with Saturn - Voyager 1 imaging science results, *Science*, *212*, 163–191, doi:10.1126/science.212.4491.163.

Smith, B. A., et al. (1982), A new look at the Saturn system: The Voyager 2 images, *Science*, *215*, 504–537, doi:10.1126/science.215.4532.504.

Smith, P. H. (1980), The radius of Titan from Pioneer Saturn data, *Journal of Geophysical Research*, *85*, 5943–5947, doi:10.1029/JA085iA11p05943.

Smith, P. H., M. T. Lemmon, R. D. Lorenz, L. A. Sromovsky, J. J. Caldwell, and M. D. Allison (1996), Titan's surface, revealed by HST imaging, *Icarus*, *119*, 336–349, doi: 10.1006/icar.1996.0023.

Soderblom, J. M., et al. (2010a), Geology of the Selk crater region on Titan from Cassini VIMS observations, *Icarus*, *208*, 905–912, doi:10.1016/j.icarus.2010.03.001.

Soderblom, J. M., et al. (2010b), Modeling specular reflections from hydrocarbon lakes on the surface of Titan, *Icarus*, *submitted for publication*.

Soderblom, L. A., et al. (2007a), Correlations between Cassini VIMS spectra and RADAR SAR images: Implications for Titan's surface composition and the character of the Huygens Probe Landing Site, *Planetary and Space Science*, *55*, 2025–2036, doi:10.1016/j.pss.2007.04.014.

Soderblom, L. A., et al. (2007b), Topography and geomorphology of the Huygens Landing Site on Titan, *Planetary and Space Science*, *55*, 2015–2024, doi:10.1016/j.pss.2007.04.015.

Sohl, F., W. D. Sears, and R. D. Lorenz (1995), Tidal dissipation on Titan, *Icarus*, *115*, 278–294, doi:10.1006/icar.1995.1097.

Sotin, C., et al. (2005), Release of volatiles from a possible cryovolcano from near-infrared imaging of Titan, *Nature*, *435*, 786–789, doi:10.1038/nature03596.

Sromovsky, L. A., V. E. Suomi, J. B. Pollack, R. J. Krauss, S. S. Limaye, T. Owen, H. E. Revercomb, and C. Sagan (1981), Implications of Titan's north-south brightness asymmetry, *Nature*, *292*, 698–702, doi:10.1038/292698a0.

Stephan, K., et al. (2009), Mapping products of Titan's surface, in *Titan from Cassini-Huygens*, edited by R. H. Brown, J.-P. Lebreton, and J. H. Waite, pp. 489–510, Springer.

Stephan, K., et al. (2010), Specular reflection on Titan: Liquids in Kraken Mare, *Geophysical Research Letters*, *37*, L07,104, doi:10.1029/2009GL042312.

Stevenson, D. J. (1992), Interior of Titan, in *Symposium on Titan*, *ESA Special Publication*, vol. 338, edited by B. Kaldeich, pp. 29–33.

Stevenson, D. J., and B. E. Potter (1986), Titan's latitudinal temperature distribution and seasonal cycle, *Geophysical Research Letters*, *13*, 93–96, doi:10.1029/GL013i002p00093.

Stiles, B. W., Y. Gim, G. Hamilton, S. Hensley, W. T. K. Johnson, J. Shimada, R. D. West, and P. Callahan (2006), Ground processing of Cassini RADAR imagery of Titan, in *IEEE Conference on Radar*, doi:10.1109/RADAR.2006.1631767.

Stiles, B. W., et al. (2009), Determining Titan surface topography from Cassini SAR data, *Icarus*, *202*, 584–598, doi:10.1016/j.icarus.2009.03.032.

Stofan, E. R., et al. (2006), Mapping of Titan: Results from the first Titan radar passes, *Icarus*, *185*, 443–456, doi:10.1016/j.icarus.2006.07.015.

Stofan, E. R., et al. (2007), The lakes of Titan, *Nature*, *445*, 61–64, doi:10.1038/nature05438.

Strobel, D. F. (1974), The photochemistry of hydrocarbons in the atmosphere of Titan, *Icarus*, *21*, 466–470, doi:10.1016/0019-1035(74)90149-3.

Strobel, D. F. (1982), Chemistry and evolution of Titan's atmosphere, *Planetary and Space Science*, *30*, 839–848, doi:10.1016/0032-0633(82)90116-7.

Thompson, W. R., and S. W. Squyres (1990), Titan and other icy satellites: Dielectric properties of constituent materials and implications for radar sounding, *Icarus*, *86*, 336–354, doi:10.1016/0019-1035(90)90224-W.

Thompson, W. R., J. A. Zollweg, and D. H. Gabis (1992), Vapor-liquid equilibrium thermodynamics of $N_2$+$CH_4$: Model and Titan applications, *Icarus*, *97*, 187–199, doi:10.1016/0019-1035(92)90127-S.

Tobie, G., O. Grasset, J. I. Lunine, A. Mocquet, and C. Sotin (2005), Titan's internal structure inferred from a coupled thermal-orbital model, *Icarus*, *175*, 496–502, doi:10.1016/j.icarus.2004.12.007.

Tobie, G., J. I. Lunine, and C. Sotin (2006), Episodic outgassing as the origin of atmospheric methane on Titan, *Nature*, *440*, 61–64, doi:10.1038/nature04497.

Tokano, T. (2009), Impact of seas/lakes on polar meteorology of Titan: Simulation by a coupled GCM-Sea model, *Icarus*, *204*, 619–636, doi:10.1016/j.icarus.2009.07.032.

Tokano, T., F. M. Neubauer, M. Laube, and C. P. McKay (2001), Three-dimensional modeling of the tropospheric methane cycle on Titan, *Icarus*, *153*, 130–147, doi:10.1006/icar.2001.6659.

Tokano, T., C. P. McKay, F. M. Neubauer, S. K. Atreya, F. Ferri, M. Fulchignoni, and H. B. Niemann (2006), Methane drizzle on Titan, *Nature*, *442*, 432–435, doi:10.1038/nature04948.

Tomasko, M. G. (1980), Preliminary results of polarimetry and photometry of Titan at large phase angles from Pioneer 11, *Journal of Geophysical Research*, *85*, 5937–5942, doi:10.1029/JA085iA11p05937.

Tomasko, M. G., and P. H. Smith (1982), Photometry and polarimetry of Titan: Pioneer 11 observations and their implications for aerosol properties, *Icarus*, *51*, 65–95, doi:10.1016/0019-1035(82)90030-6.

Tomasko, M. G., et al. (2005), Rain, winds and haze during the Huygens probe's descent to Titan's surface, *Nature*, *438*, 765–778, doi:10.1038/nature04126.

Toon, O. B., C. P. McKay, R. Courtin, and T. P. Ackerman (1988), Methane rain on Titan, *Icarus*, *75*, 255–284, doi:10.1016/0019-1035(88)90005-X.

Trafton, L. (1972), On the possible detection of $H_2$ in Titan's atmosphere, *The Astrophysical Journal*, *175*, 285–293, doi:10.1086/151556.

Turtle, E. P., J. E. Perry, A. S. McEwen, A. D. Del Genio, J. Barbara, R. A. West, D. D. Dawson, and C. C. Porco (2009), Cassini imaging of Titan's high-latitude lakes, clouds, and south-polar surface changes, *Geophysical Research Letters*, *36*, L02,204, doi:10.1029/2008GL036186.

Turtle, E. P., J. E. Perry, A. G. Hayes, and A. S. McEwen (2010), Shoreline retreat at Titan's Ontario Lacus and Arrakis Planitia from Cassini Imaging Science Subsystem observations, *Icarus*, *submitted for publication*.

Tyler, G. L., V. R. Eshleman, J. D. Anderson, G. S. Levy, G. F. Lindal, G. E. Wood, and T. A. Croft (1981), Radio science investigations of the Saturn system with Voyager 1 - Preliminary results, *Science*, *212*, 201–206, doi:10.1126/science.212.4491.201.

Vinatier, S., et al. (2007), Vertical abundance profiles of hydrocarbons in Titan's atmosphere at 15°S and 80°N retrieved from Cassini/CIRS spectra, *Icarus*, *188*, 120–138, doi:10.1016/j.icarus.2006.10.031.

von Bertalanffy, L. (1968), *General System Theory*, George Braziller Inc., New York.

Waite, J. H., and C. Niebur (2010), Mission Concept Study - Planetary Science Decadal Survey JPL Team X Titan Lake Probe Study Final Report.

Wall, S., et al. (2010), Active shoreline of Ontario Lacus, Titan: A morphological study of the lake and its surroundings, *Geophysical Research Letters*, *37*, L05,202, doi:10.1029/2009GL041821.

Wang, Z., D. A. Gurnett, T. F. Averkamp, A. M. Persoon, and W. S. Kurth (2006), Characteristics of dust particles detected near Saturn's ring plane with the Cassini Radio and Plasma Wave instrument, *Planetary and Space Science*, *54*, 957–966, doi:10.1016/j.pss.2006.05.015.

Williams, R. M. E., and R. J. Phillips (2001), Morphometric measurements of martian valley networks from Mars Orbiter Laser Altimeter (MOLA) data, *Journal of Geophysical Research (Planets)*, *106*, 23,737–23,752, doi:10.1029/2000JE001409.

Wood, C. A., R. Lorenz, R. Kirk, R. Lopes, K. Mitchell, E. Stofan, and the Cassini RADAR Team (2010), Impact craters on Titan, *Icarus*, *206*, 334–344, doi:10.1016/j.icarus.2009.08.021.

World Meteorological Organization (1994), Guide to hydrological practice, http://www.bom.gov.au/hydro/wr/wmo/guide_to_hydrological_practices/WMOENG.pdf, access Nov-2010.

Wye, L. C., H. A. Zebker, S. J. Ostro, R. D. West, Y. Gim, R. D. Lorenz, and the Cassini Radar Team (2007), Electrical properties of Titan's surface from Cassini RADAR scatterometer measurements, *Icarus*, *188*, 367–385, doi:10.1016/j.icarus.2006.12.008.

Wye, L. C., H. A. Zebker, and R. D. Lorenz (2009), Smoothness of Titan's Ontario Lacus: Constraints from Cassini Radar specular reflection data, *Geophysical Research Letters*, *36*, L16,201, doi:10.1029/2009GL039588.

Yung, Y. N., M. Allen, and J. P. Pinto (1984), Photochemistry of the atmosphere of Titan - Comparison between model and observation, *Astrophysical Journal Supplement Series*, *55*, 465–506, doi:10.1086/190963.

Zarnecki, J. C., et al. (2005), A soft solid surface on Titan as revealed by the Huygens Surface Science Package, *Nature*, *438*, 792–795, doi:10.1038/nature04211.

Zebker, H. A., Y. Gim, P. Callahan, S. Hensley, R. Lorenz, and the Cassini Radar Team (2009), Analysis and interpretation of Cassini Titan radar altimeter echoes, *Icarus*, *200*, 240–255, doi:10.1016/j.icarus.2008.10.023.

Zepp, H. (2008), *Geomorphologie - Grundriss Allgemeine Geographie*, 4th ed., UTB Stuttgart.

# Appendix

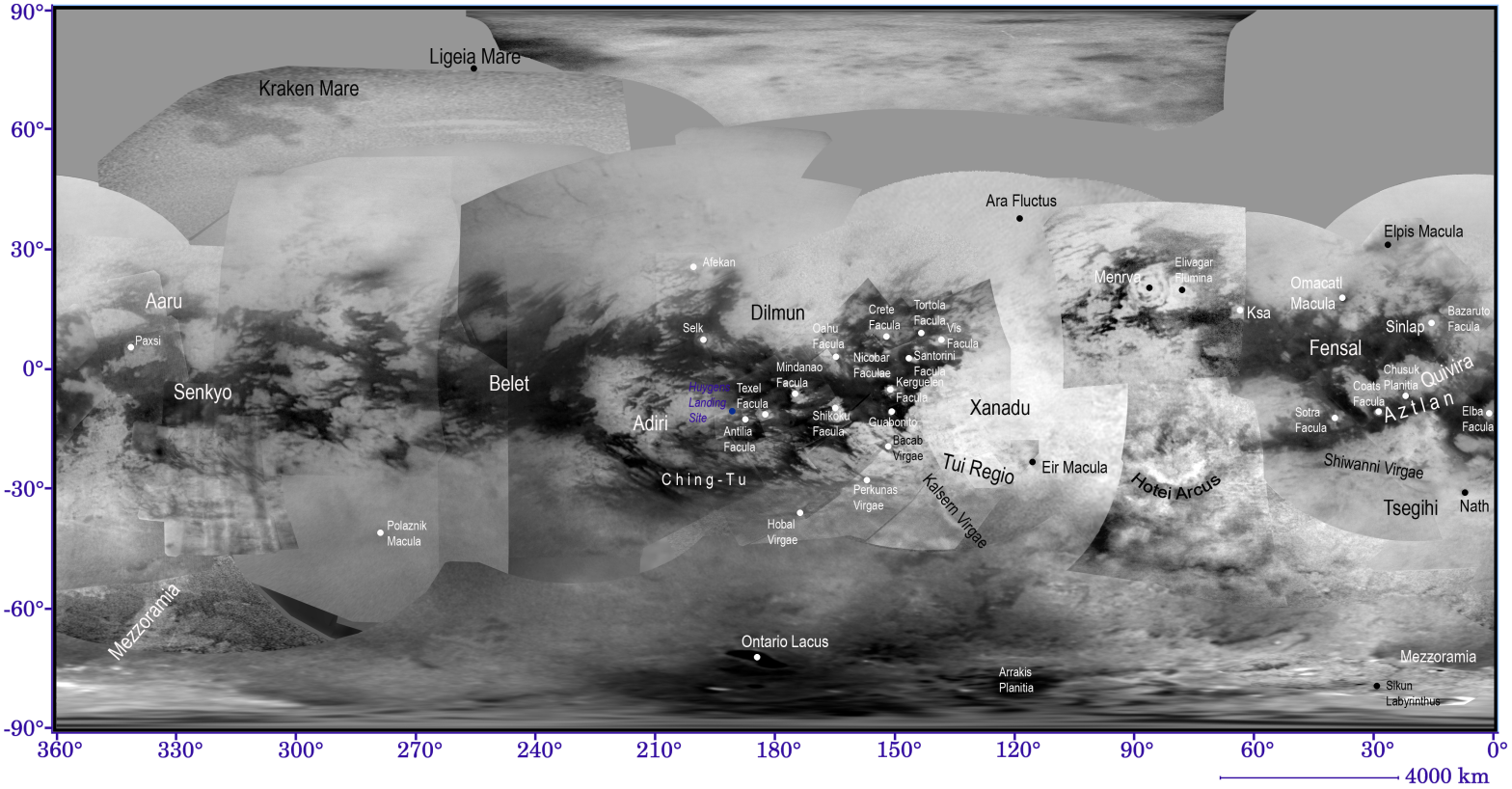


**Figure A.1:** Nomenclature of geologic/albedo features on Titan. Background: ISS-database (Source: http://ciclops.org/maps/maps.php, modified). Simple cylindrical projection, centered at 180°W, 0°N.


**Figure A.2:** Cassini-image database of Titan's lower and mid-latitudes in a simple cylindrical projection. Image is centered at 180°W, 0°N. Radar observations from TA through T57 (October 2004 to June 2009) with ground resolutions between 0.3 and 1.5 km per pixel. Background: VIMS observations (reflectance at 2 µm) from TA through T48 (October 2004 to December 2008) resampled to a ground resolution of 10 km.

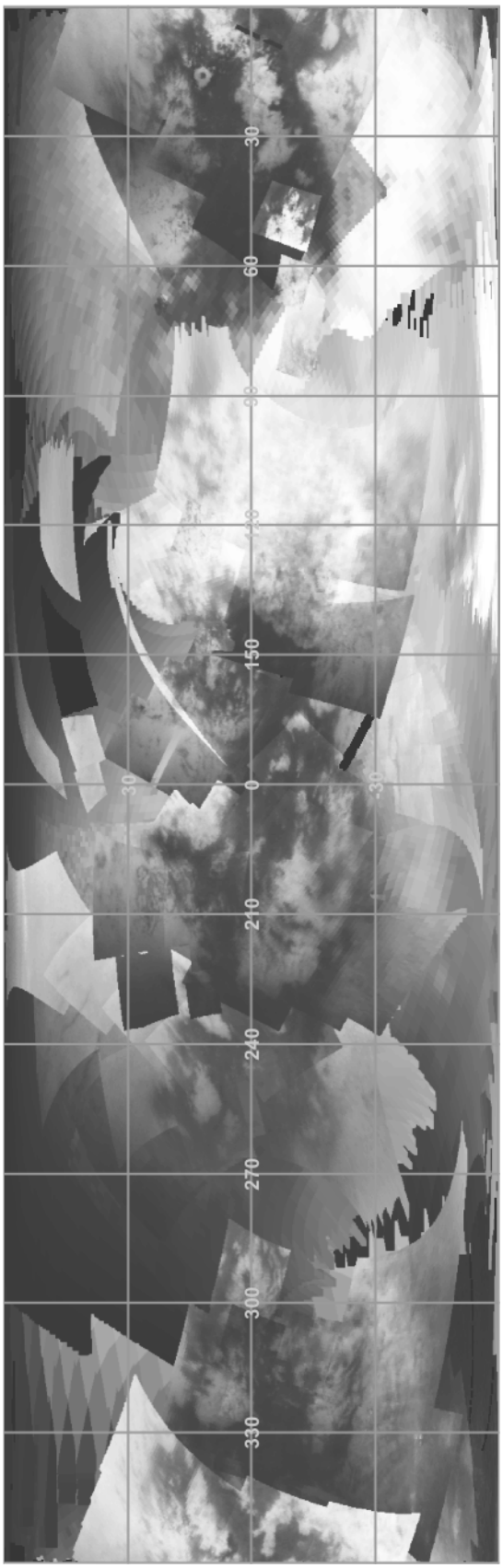


**Figure A.3:** VIMS map of of Titan's lower and mid-latitudes (reflectance at 2 µm). Simple cylindrical projection, centered at 180°W, 0°N. VIMS observations from TA through T48 (October 2004 to December 2008), resampled to a ground resolution of 10 km.

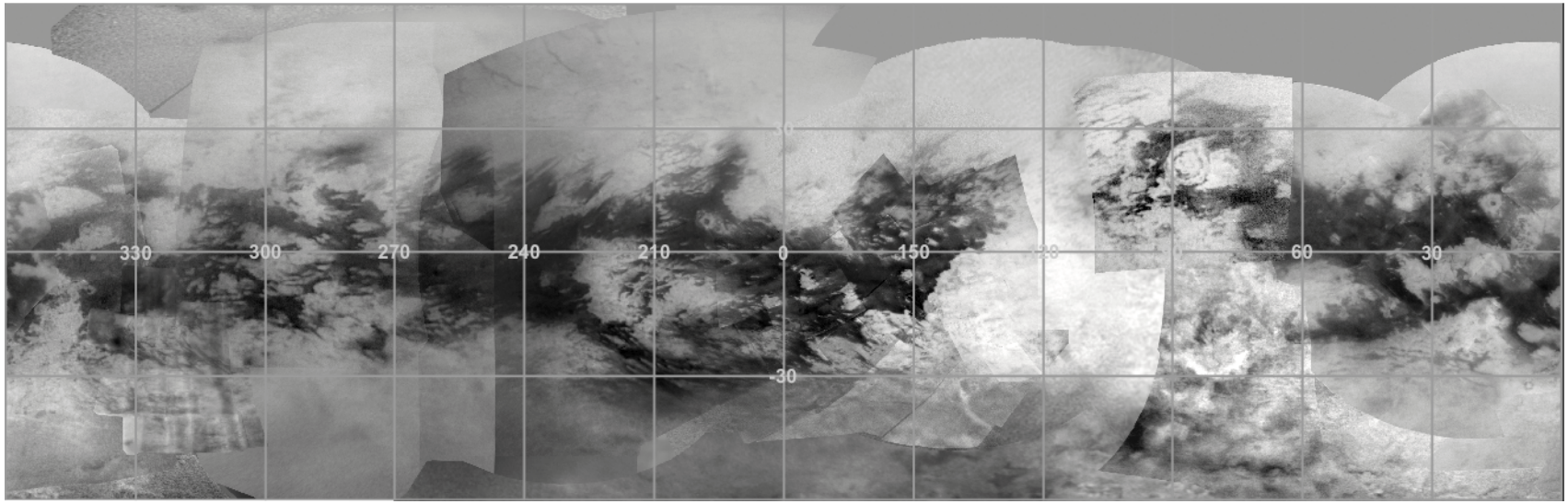


**Figure A.4:** ISS map of Titan's lower and mid-latitudes (reflectance at 938 nm). Simple cylindrical projection, centered at 180°W, 0°N, pixel-scale: 4 km (Courtesy NASA/JPL/Space Science Institute, PIA11149.tif). The center of Titan's leading face is located at 90°W, whereas the position of the sub-Saturnian point is at 0°N, 0°W.

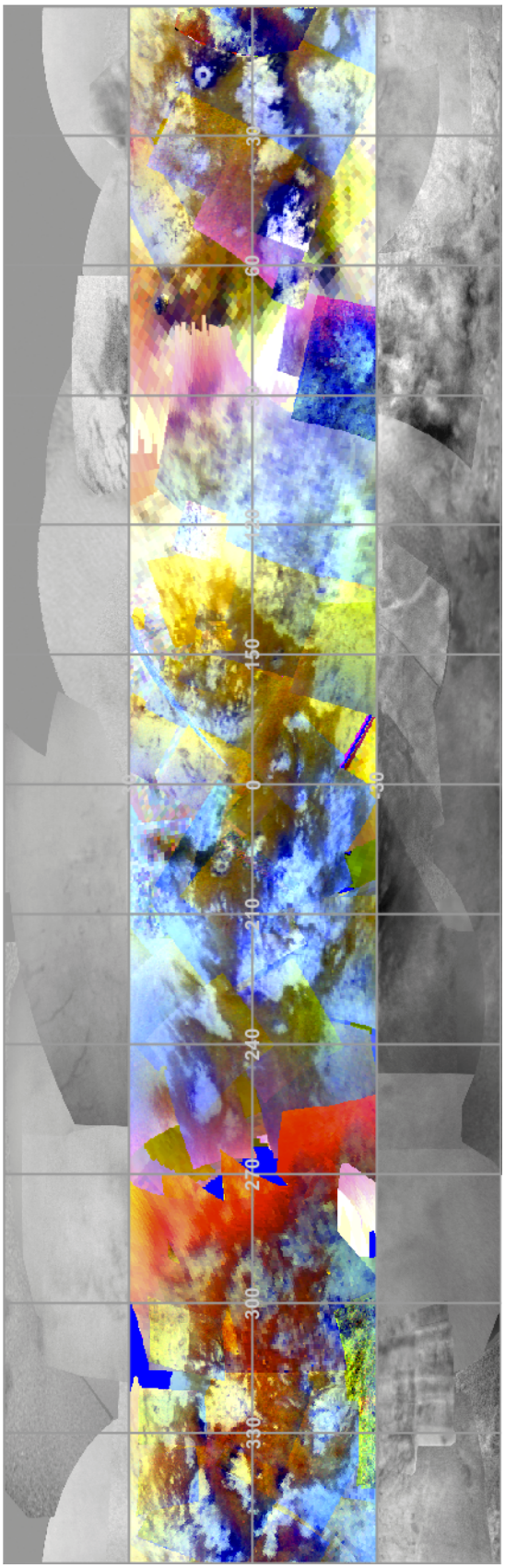


**Figure A.5:** VIMS ratio map of Titan's lower and mid-latitudes (R: 1.59/1.27 µm, G: 2.03/1.27 µm, and B: 1.27/1.08 µm). Simple cylindrical projection, centered at 180°W, 0°N. VIMS observations from TA through T48 (October 2004 to December 2008) resampled to a ground resolution of 10 km.

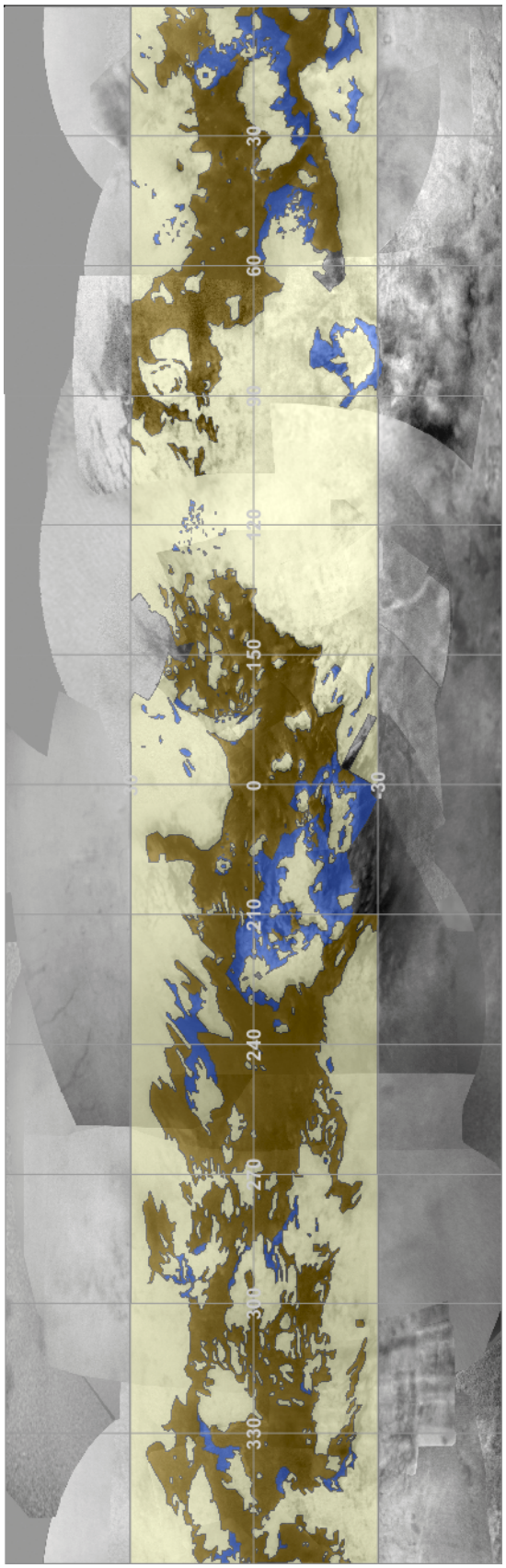


**Figure A.6:** Mapping of spectral surface units of Titan's lower latitudes based on false-color ratio composite (see Figure A.5). Image is centered at 180°W, 0°N.

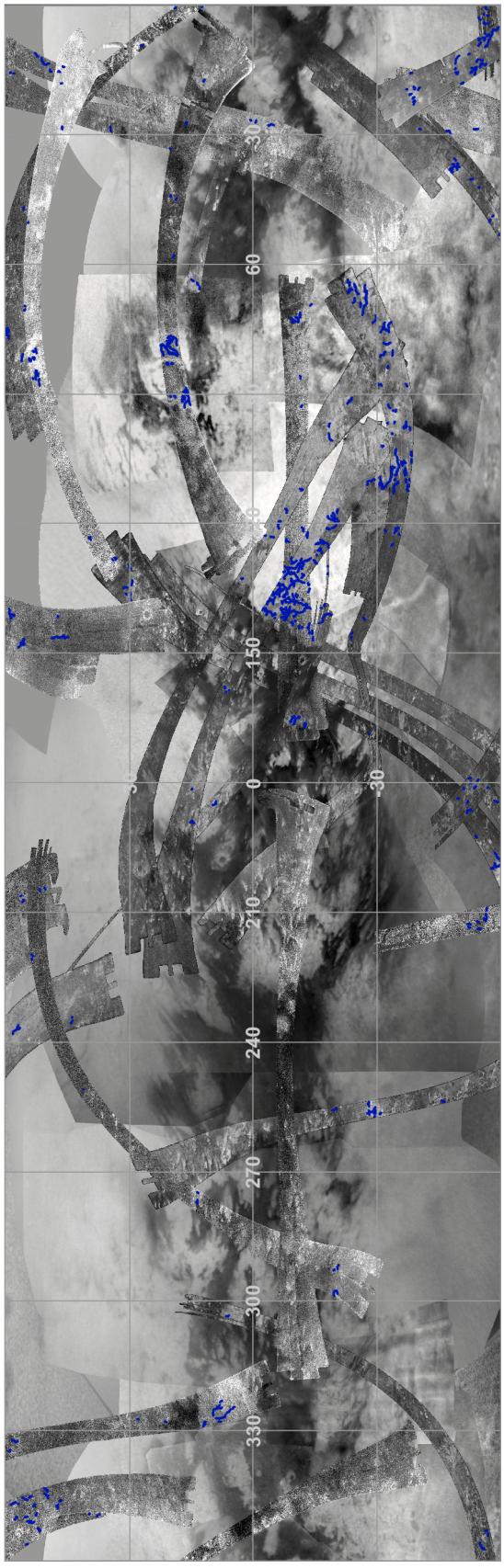


**Figure A.7:** Fluvial valleys (marked in blue) are overlaid on global radar observations and near-infrared ISS map. Simple cylindrical projection of lower and mid-latitudes, enlarged view. Image is centered at 180°W, 0°N.

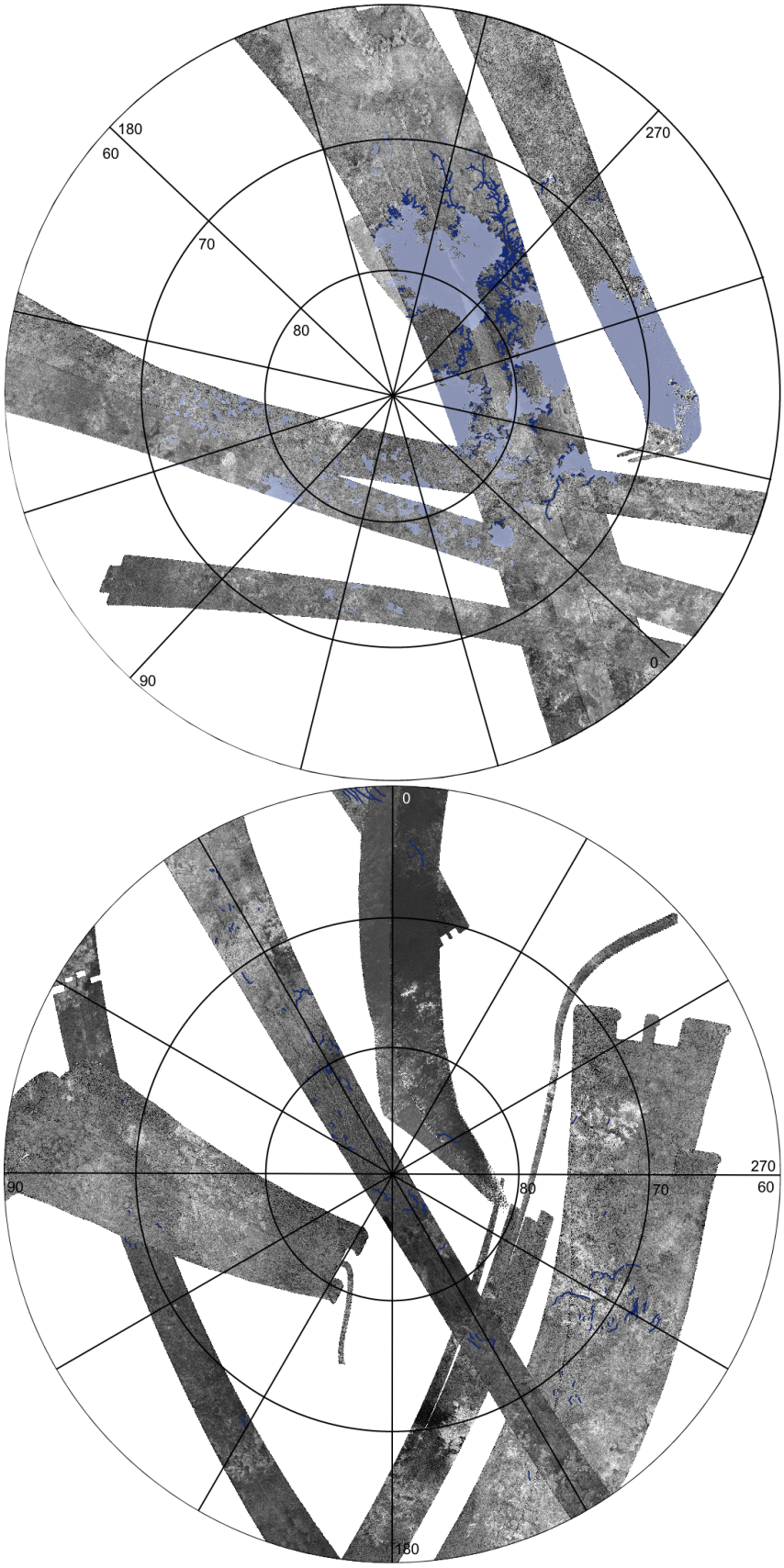


**Figure A.8:** Top: Circular map of Titan's north polar region. Polarstereographic projection of radar swaths T16 (July 22, 2006), T18 (September 23, 2006), T19 (October 9, 2006), T25 (February 22, 2007), T28 (April 10, 2007), and T30 (May 12, 2007). Valleys and lakes are highlighted. Bottom: Circular map of Titan's south polar region. Polarstereographic projection of radar swaths T7 (September 7, 2005), T36 (October 2, 2007), T39 (December 20, 2007), T49 (December 21, 2008), T55 (May 21, 2009), T56 (June 6, 2009), and T57 (June 22, 2009). Valleys are highlighted.

**Table A.1:** Database of fluvial network systems on Titan.

| Longitude | Latitude | Dataset | Date | Type | Length | Width | Stream Order | References |
|---|---|---|---|---|---|---|---|---|
| high southern latitudes | | ISS T0 | Jul 2, 04 | dendritic | >1000 km | 10-20 km | 2nd | Fig. 2 in *Porco et al.* (2005) |
| 80°W | 54°N | radar TA | Oct 26, 04 | fan-like, delta | several tens of km | 0.5-1 km | 1st | Fig. 3A in *Paganelli et al.* (2005), Fig. 2 in *Lorenz et al.* (2008a) |
| 192°W | 10.6°S | DISR | Jan 14, 05 | dendritic | <15 km | <250 m | 4th | e.g. Fig. 5 in *Tomasko et al.* (2005), Fig. 1 in *Perron et al.* (2006), Fig. 8 and Fig. 9 in *Soderblom et al.* (2007b), Fig. 4 in *Jaumann et al.* (2008), Fig. 5.4 this work |
| 192°W | 10.6°S | DISR | Jan 14, 05 | sapping | <10 km | some tens of meters | 2nd to 3rd | Fig. 5 in *Tomasko et al.* (2005), Fig. 8 in *Soderblom et al.* (2007b), Fig. 5.8 this work |
| 77°W | 19°N | radar T3 | Feb 15, 05 | dry | 10-200 km | <10 km | 2nd to 3rd | Fig. 5c in *Stofan et al.* (2006), Fig. 3 in *Lorenz et al.* (2008a), Fig. 5.26c this work |
| 90°W | 16°N | radar T3 | Feb 15, 05 | dendritic | <200 km | <3 km | 2nd to 3rd | Fig. 3 in *Lorenz et al.* (2008a), Fig. 4 in *Burr et al.* (2009) |
| 7°W | 59°S | radar T7 | Sept 07, 05 | dry | <150 km | 1-2 km | braiding | Fig. 6 in *Lorenz et al.* (2008a), Fig. 4 in *Burr et al.* (2009) Fig. 5.30b this work |
| 12°W | 56°S | radar T7 | Sept 07, 05 | elongated | <100 km | <3 km | 2nd | Fig. 5 in *Lorenz et al.* (2008a), Fig. 5.11a this work |
| 6°W | 58°S | radar T7 | Sept 07, 05 | elongated | <100 km | <3 km | 2nd to 3rd | Fig. 5 in *Lorenz et al.* (2008a), Fig. 5.11b this work |
| 138°W | 10°S | radar T13, radar T44 | Apr 30, 06; May 28, 08 | dendritic | <450 km | 300 m to 2.5 km | 6th to 7th | Fig. 7 in *Lorenz et al.* (2008a), Fig. 1 and 2 in *Burr et al.* (2009), Fig. 5.1 and Fig. 5.2 this work |
| 125°W | 10°S | VIMS TB, radar T13 | Dec 13, 04, Apr 30, 06 | dendritic | <300 km | 800 m to 1 km | 2nd to 3rd | Fig. 5 in *Barnes et al.* (2007b) |
| 66°W | 10°S | VIMS T9, radar T13 | Dec 26, 05, Apr 30, 06 | elongated | 50-100 km | 800 - 2000 m | 1st | Fig. 3 and 4 in *Barnes et al.* (2007b) |
| 50°W | 12°S | VIMS T9 | Dec 26, 05 | dendritic | 100-200 km | 800-2000 m | 2nd to 3rd | Fig. 2 in *Barnes et al.* (2007b) |
| 140°W | 8°S | radar T13 | Apr 30, 06 | dendritic | 140 km | 350-1400 m | 2nd | Fig. 2 in *Jaumann et al.* (2008) |
| 347°W | 54°N | radar T16 | Jul 22, 06 | mountain valley | <70 km | <3 km | 2nd | Fig. 5.10, left, this work |
| 143°W | 50°N | radar T16 | Jul 22, 06 | sapping | ∼200 km | <5 km | 2nd | Fig. 5.9 this work |
| 345°W | 75°N | radar T19, radar T25 | Oct 09, 06; Feb 22, 07 | dendritic | ∼100 km | 500-1000 m | 2nd to 3rd | Fig. 8 in *Lorenz et al.* (2008a) |
| 255°W | 75°N | radar T28 | Apr 10, 07 | dendritic | 1200 km | 1400-3000 m | up to 6th | Fig. 2 in *Jaumann et al.* (2008), Fig. 5.26b this work |
| 280°W | 78°N | radar T28 | Apr 10, 07 | dendritic | <200 km | 300 m - 5 km | up to 6th | Fig. 5.3 this work |
| 67°W | 27°S | radar T41 | Feb 22, 08 | dry | ∼350 km | <3 km | 2nd | Fig. 5.7 this work |
| 107°W | 36°S | radar T41 | Feb 22, 08 | mountain valley | some tens of km | <1 km | 1st | Fig. 5.26a this work |
| 120°W | 17°S | radar T44 | May 28, 08 | dry | <180 km | 1-8 km | 1st | Fig. 1b in *Le Gall et al.* (2010), Fig. 5.26d this work |
| 185°W | 72°S | radar T49, radar T57 radar T58 | Dec 21, 08 June 22, 09 July 08, 09 | flooded channel, estuary | several tens of km | 1-3 km | 1st | Fig. 1 in *Wall et al.* (2010) |

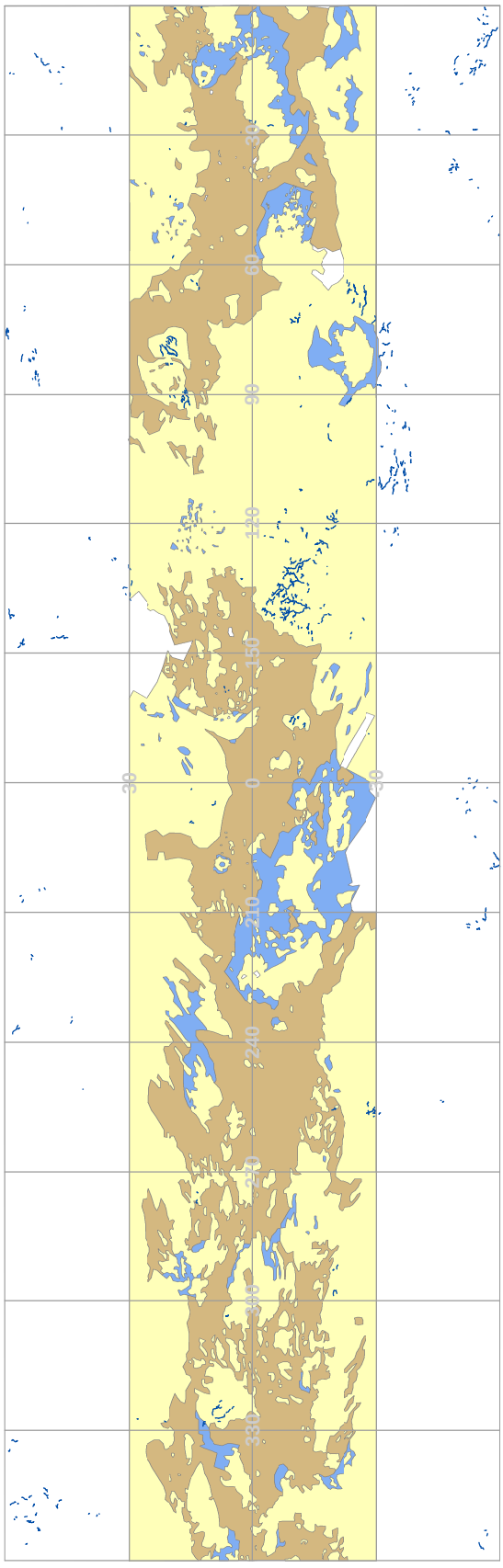


**Figure A.9:** Map of spectral units on Titan with the same coloring as introduced in the text. Fluvial valleys are highlighted in blue. Simple cylindrical projection of Titan's lower and mid-latitudes , enlarged view. Image is centered at 180°W, 0°N.

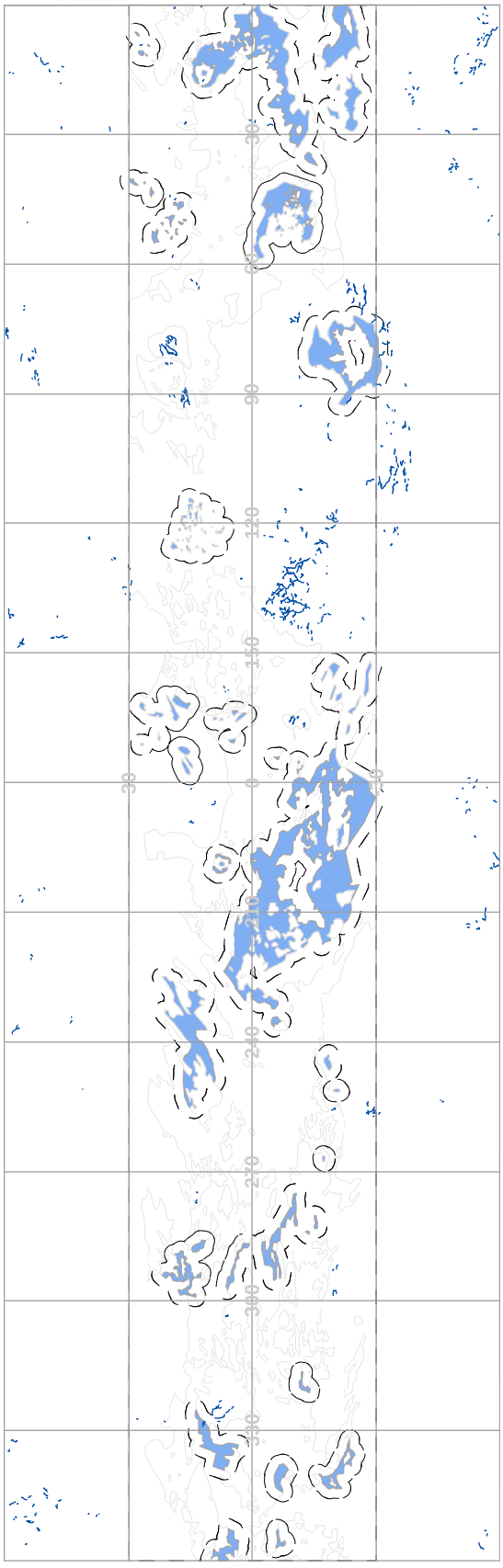


**Figure A.10:** Map of Titan's low and mid-latitudes, simple cylindrical projection, centered at 180°W, 0°N. Blue spectral unit is marked in light blue. Buffer around the blue unit (100 km), indicated by dashed lines. Fluvial valleys are highlighted in blue.

**Figure A.11:** Map of Titan's lower and mid-latitudes, centered at 180°W, 0°N. Craters (red circles) and channels (blue lines) are indicated, enlarged view. Radar coverage is highlighted in gray. The crater inventory is based on crater catalogs in *Malaska* (2007), *Jaumann and Neukum* (2009), and *Wood et al.* (2010). This inventory is complemented by visual mapping of craters of the radar swaths T41 through T57. Blue circles indicate the location of cryovolcanic features based on *Lopes et al.* (2007a) and *Le Corre et al.* (2009).

## Curriculum Vitae

For reasons of data protection, the curriculum vitae is not included in the online version

## Conference Contributions and Publications

Participation in the *'First Workshop of the EARSeL Special Interest Group on Urban Remote Sensing'* (Berlin, March 2006).

### Poster Presentations

M. Langhans, R. Jaumann, K. Stephan, R. H. Brown, B. J. Buratti, R. Clark, K. H. Baines, P. D. Nicholson, and R. D. Lorenz (2008): Analysis of fluvial features at Xanadu-Regio, Titan, observed by Cassini-RADAR and Cassini-VIMS. *European Geosciences Union General Assembly Abstracts*, id. EGU2008-A-07631.

M. Langhans, R. Jaumann, K. Stephan, R. H. Brown, B. J. Buratti, R. Clark, K. H. Baines, P. D. Nicholson, and R. D. Lorenz (2008): Fluvial features on Titan – Cassini VIMS and Cassini RADAR observations. *European Planetary Science Congress Abstracts*, id. EPSC2008-A-00392.

M. Langhans, R. Jaumann, K. Stephan, R. H. Brown, B. J. Buratti, R. Clark, K. H. Baines, P. D. Nicholson, and R. D. Lorenz (2009): Fluvial Valleys on Titan – A Global Perspective. *Lunar and Planetary Science Conference Abstracts*, vol. 40, id. 1681.

### Oral Presentations

M. Langhans, S. van der Linden, A. Damm, and P. Hostert (2007): The influence of bidirectional reflectance in airborne hyperspectral data on Spectral Angle Mapping and Linear Spectral Mixture. *Proceedings of the 5th EARSeL Workshop on Imaging Spectroscopy*.

M. Langhans, R. Jaumann, K. Stephan, R. H. Brown, B. J. Buratti, R. Clark, K. H. Baines, P. D. Nicholson, and R. D. Lorenz (2009): Global distribution of fluvial channels on Titan. *European Geosciences Union General Assembly Abstracts*, id. EGU2009-8539.

M. Langhans, R. Jaumann, K. Stephan, R. H. Brown, B. J. Buratti, R. Clark, K. H. Baines, P. D. Nicholson, and R. D. Lorenz (2009): Morphology of valley systems on Titan - a comparative study. *European Planetary Science Congress Abstracts*, id. EPSC2009-133.

M. Langhans, R. Jaumann, K. Stephan, R. H. Brown, B. J. Buratti, R. Clark, K. H. Baines, P. D. Nicholson, R. D. Lorenz, and C. Sotin (2010): Valley Formation from Methane Convective Storms on Titan. *Lunar and Planetary Science Conference Abstracts*, vol. 41, id. 1533.

M. Langhans, R. Jaumann, K. Stephan, R. H. Brown, B. J. Buratti, R. Clark, K. H. Baines, P. D. Nicholson, and R. D. Lorenz, and C. Sotin (2010): Geologic impact of methane storms on Titan. *European Geosciences Union General Assembly Abstracts*, id. EGU2010-9939.

## Peer-reviewed Publications

R. Jaumann, R. H. Brown, K. Stephan, J. W. Barnes, L. A. Soderblom, C. Sotin, S. Le Mouelic, R. N. Clark, J. Soderblom, B. J. Buratti, R. Wagner, T. B. McCord, S. Rodriguez, K. H. Baines, D. P. Cruikshank, P. D. Nicholson, C. A. Griffith, M. Langhans, R. D. Lorenz (2008): Fluvial erosion and post-erosional processes on Titan. *Icarus* 197 (2), pp. 526-538.

K. Stephan, R. Jaumann, E. Karkoschka, J. W. Barnes, R. Kirk, M. G. Tomasko, E. P. Turtle, L. Le Corre, M. Langhans, S. Le Mouélic, R. Lorenz, and J. Perry (2009): Mapping Products of Titans Surface. In: *Titan from Cassini-Huygens* (Eds.: R. H. Brown, J.-P. Lebreton and J. H. Waite), Springer.

M. Langhans, R. Jaumann, K. Stephan, R. H. Brown, B. J. Buratti, R. N. Clark, K. H. Baines, P. D. Nicholson, R. D. Lorenz, A. Soderblom, J. M. Soderblom, C. Sotin, J. W. Barnes, R. Nelson: Titan's Fluvial Valleys: Morphology, Distribution, and Spectral Properties. *Planetary and Space Science*, accepted (February 2011).